A hybrid method based on a motion database and motion knowledge for the dynamic prediction of task-oriented human motion

DISSERTATION
submitted for the
Degree of Doctor of Philosophy
of the University of Navarra by

Ilaria Pasciuto
under the supervision of
Sergio Ausejo Muñoz and
Juan Tomás Celigüeta Lizarza

Donostia-San Sebastián, June 2013

tecnun
Universidad
de Navarra

UNIVERSITY OF NAVARRA

SCHOOL OF ENGINEERING

DONOSTIA - SAN SEBASTIÁN

A Hybrid Method Based on a Motion Database and Motion Knowledge for the Dynamic Prediction of Task-Oriented Human Motion

DISSERTATION

submitted for the
degree of Doctor of Philosophy
of the University of Navarra by

ILARIA PASCIUTO

under the supervision of

Sergio Ausejo Muñoz
Juan Tomás Celigüeta Lizarza

Donostia-San Sebastián, June 2013

Author: Ilaria Pasciuto
CEIT – Department of Applied Mechanics
Paseo de Manuel Lardizabal, 15
20018 Donostia-San Sebastian – Spain
email: ilariapasciuto@gmail.com

The research described in this book was carried out at CEIT and TECNUN (University of Navarra) in San Sebastian, Spain.

A Manu

Son cosas chiquitas.
No acaban con la pobreza,
no nos sacan del subdesarrollo,
no socializan los medios de producción y de cambio,
no expropian las cuevas de Alí Babá.
Pero quizá desencadenen la alegría de hacer,
y la traduzcan en actos.
Y al fin y al cabo, actuar sobre la realidad
y cambiarla aunque sea un poquito,
es la única manera de probar
que la realidad es transformable.

Eduardo Galeano

AGRADECIMIENTOS

Por más que mis directores me hubieran dicho varias veces que ésta era *mi* tesis, para que me responsabilizara por su desarrollo, toda la ayuda y el apoyo que he recibido a lo largo de estos años hacen que esta tesis sea el resultado del esfuerzo de muchas más personas, a las que quiero agradecer desde estas líneas.

En primer lugar quiero agradecer a mis directores de tesis, Sergio Ausejo y Juan Tomás Celigüeta, por querer que participara en el proyecto DHErgo, por confiar en mí y haberme dedicado tanto tiempo y energía. A Sergio quiero agradecer sobretodo que haya insistido siempre para apuntar más alto y que me haya ayudado a ver los caminos que se abrían a medida que avanzaba esta investigación. A Juanto quiero agradecer especialmente la practicidad con la que me ha ayudado a centrar mis esfuerzos, sus comentarios y correcciones, y la empatía que siempre me ha transmitido, tanto en los éxitos como en los fracasos.

Quiero extender mis agradecimientos también a Ángel Suescun, que me ha mostrado siempre una disponibilidad incondicional para ayudarme a resolver las dudas que me surgían y a interpretar las cuestiones matemáticas más espinosas. Además quiero agradecerle a él y a Juan Flaquer la oportunidad que me brindaron de ser su asistente para las clases de álgebra de la Universidad.

También estoy agradecida por la ayuda que me ha dado Antonio Martín Meizoso en el análisis de la base de datos y en la definición de los índices empleados en la comparación de movimientos. Le agradezco mucho su interés hacia las cuestiones que le planteaba y la disponibilidad que siempre me ha mostrado. Gracias a él y a Eli Viles por aclararme muchos temas de estadística.

Quiero agradecer además a Diego Borro su disponibilidad y sus contribuciones en temas de colisiones. También le agradezco a Carlos Buchart por haberme guiado en mis primeros pasos con NURBS y B-splines.

Muchas gracias a mis compañeros de despacho(s), porque han sido muy buenos compañeros de viaje y me han ayudado tanto en cuestiones

relacionadas con la tesis como en desconectar en los ratos de descanso. Especialmente quiero agradecerle a Yaiza por su alegría y por su amistad dentro y fuera del CEIT y a Alex por todo lo que compartimos, codo a codo, en los primeros tres años de esta aventura.

Muchas gracias también a María Ibarburu, por ayudarme en gestionar las dificultades y el estrés de estos años, y a Juan y las chicas de pintura por hacer descansar mi hemisferio izquierdo y distraerme de la tesis con actividades creativas y divertidas.

Finalmente, quiero agradecer a mi familia italiana y argentina por todo el apoyo y el cariño que siempre me han dado. Gracias de forma especial a mis padres, por creer en mí, apoyarme, y darme las herramientas que me han permitido llegar hasta aquí, y a mi Nonna Anna por su dulzura y por confiar en que lograría todos mis objetivos. No puedo expresar todo el agradecimiento que tengo hacia Emmanuel, por haberme acompañado, querido, animado, apoyado y ayudado durante todos estos años. Esta experiencia fuera de Italia se la debo a él, y a él está dedicada esta tesis.

ABSTRACT

Digital human models are more and more frequently employed in product development processes to take human factors into account since the earliest stages of product design. To simulate the interaction of different user populations with a variety of environments, human motion prediction is a useful tool, as it aims at predicting the motion that a generic subject of a user population would reasonably perform to carry out a specific task in a given environment.

The motivation of the research work presented in this thesis is the improvement of current motion prediction methods in terms of realism and representativeness. On the one hand, dynamics is included in our formulation, in order to yield physically sound predictions and in view of the fact that the forces and torques acting on and within the human body play a relevant role in discomfort perception. On the other, a hybrid approach is followed, combining the advantages of both data-based methods (which rely on actually performed motions for reference) and knowledge-based methods (which rely on the identification of the motion control laws underlying task-oriented motions).

First the method is introduced, and is then applied to the prediction of clutch pedal depression motions. For this purpose, a database of clutch pedal depressions was analysed to gain insight into the subject-related and environment-related features that mostly affect the motion and into the different behavioural patterns that people exhibit carrying out the task.

Both a qualitative and quantitative validation of our motion prediction method are presented. The former consists in comparing the most relevant kinematic and dynamic magnitudes in the motion against actually performed motions; the latter is based on the definition of a novel measure, which represents the realism and the representativeness of the predicted motions, and which is compared to the inherent variability of actually performed motions.

The results obtained show that the proposed motion prediction method is a valid alternative to current methods, when both the physical soundness and the realism of the motion are required in the prediction.

RESUMEN

Los modelos humanos digitales son cada vez más empleados en el desarrollo de nuevos productos, a fin de tener en cuenta la ergonomía del producto desde las primeras fases del diseño. La predicción del movimiento humano es una herramienta útil para simular las interacciones de diferentes poblaciones de usuarios con varios entornos, ya que permite predecir el movimiento que un sujeto genérico de una población de usuarios razonablemente realizaría para llevar a cabo una tarea específica en un entorno dado.

La motivación del trabajo de investigación presentado en esta tesis es mejorar los métodos de predicción actuales en términos de realismo y representatividad. Por una parte, la dinámica se incluye en nuestra formulación a fin de generar movimientos físicamente correctos y puesto que las fuerzas y los pares que actúan en el cuerpo humano desempeñan un papel importante en la percepción del discomfort. Por otra parte, se sigue un enfoque híbrido, que trata de combinar las ventajas de los métodos basados en datos (que emplean movimientos realmente efectuados como referencia) y los métodos basados en el conocimiento (que se basan en la identificación de la ley de control del movimiento que guía la realización de la tarea).

En primer lugar, se presenta un nuevo método de predicción del movimiento y posteriormente se aplica a la predicción de movimientos de pisado de embrague. Con ese objetivo, se ha analizado una base de datos de dichos movimientos para identificar y comprender cuáles son los factores humanos y del entorno que más afectan al movimiento y cuáles son los diferentes patrones de comportamiento empleados por las personas.

Se presenta una validación del método tanto cualitativa como cuantitativa. La cualitativa consiste en la comparación entre el movimiento predicho y los movimientos realmente realizados en términos de las magnitudes cinemáticas y dinámicas más relevantes; la cuantitativa se basa en la definición de una nueva medida, que representa el realismo y la representatividad de los movimientos predichos, y que se compara con la variabilidad inherente a los movimientos reales.

Los resultados obtenidos muestran que el método propuesto es una alternativa válida a los métodos actuales, cuando se requiere que la predicción genere un movimiento físicamente correcto y realista.

CONTENTS

AGRADECIMIENTOS **I**

ABSTRACT **III**

RESUMEN **V**

CONTENTS **VII**

LIST OF FIGURES **XI**

LIST OF TABLES **XXI**

GLOSSARY **XXIII**

CHAPTER 1: INTRODUCTION **1**

1.1 Digital Human Models 2
1.2 Motion Prediction 5
1.3 Motivation 8
1.4 Objectives 10
1.5 Organisation of the Document 12

CHAPTER 2: STATE OF THE ART **15**

2.1 Motion Simulation Methods 15
2.1.1 Mechanics Taxonomy 16
2.1.1.1 Kinematic Simulation 16
2.1.1.2 Dynamic Simulation 21
2.1.1.3 Static Simulation 25
2.1.2 Source of Realism Taxonomy 27
2.1.2.1 Data-based Methods 27
2.1.2.2 Knowledge-based Methods 33
2.1.2.3 Hybrid Methods 40
2.2 Validation Methods 42
2.3 Experimental Data Capture and Analysis 47
2.3.1 Motion Capture 47
2.3.2 Motion Reconstruction 48
2.3.3 Motion Analysis 50
2.3.3.1 Key-Frames 50
2.3.3.2 Strategies and Styles 50
2.3.3.3 Influence of Experimental Parameters 54
2.4 Conclusions 56

CHAPTER 3: HYBRID DYNAMIC MOTION PREDICTION METHOD **61**

3.1 Introduction 61

3.1.1 Approach Outline 62
3.1.2 Digital Human Model 63
3.1.3 Dynamic Formulation Overview 64
3.2 Inputs to the Method 64
3.2.1 Motion Database 64
3.2.2 Prediction Scenario 65
3.3 Reference Motion Selection 66
3.4 Reference Motion Modification 67
3.4.1 Root Pose Modification 67
3.4.2 End-Effector Modification 68
3.4.2.1 Free End-Effector 68
3.4.2.2 Constrained End-Effector 69
3.5 Motion Prediction through Optimisation 70
3.5.1 Design Variables 70
3.5.2 Constraints 73
3.5.2.1 Goal Fulfilment 74
3.5.2.2 Initial and Final Conditions 74
3.5.2.3 Joint Limits 75
3.5.2.4 Collision Avoidance 76
3.5.2.5 Dynamic Balance 76
3.5.3 Objective Function 77
3.5.3.1 Goal Fulfilment 78
3.5.3.2 Data-based Conditions 79
3.5.3.3 Knowledge-based Conditions 80
3.5.4 Formulation of the Optimisation Problem 81
3.5.4.1 Jacobian and Hessian Matrices 81
3.5.4.2 Effect of the Number of Control Points 84
3.6 Output from the Method 85

CHAPTER 4: EXPERIMENTAL DATA ANALYSIS 87

4.1 Experimental Protocol 88
4.2 Adopted Human Model 91
4.3 Motion Reconstruction 93
4.4 Motion Analysis 94
4.4.1 Key-Frame Identification 95
4.4.2 Motion Durations 96
4.4.3 End-Effector Trajectories 100
4.4.4 DoF Profiles 101
4.4.5 Coordination Law 109
4.4.6 Joint Effort Profiles 110
4.4.7 Pedal Stiffness 118
4.4.8 Pedal Friction 119
4.4.9 Pedal Force Direction 120
4.4.10 Foot-Pedal Contact Point 123
4.4.11 Seat Stiffness 125

4.4.12 Behaviours 126
4.5 Structured Database 127

CHAPTER 5: TEST CASE DEFINITION 131
5.1 Prediction Scenarios 131
5.2 Design Variables 133
5.2.1 Number of Control Points 133
5.2.2 Ensured Tolerances 135
5.3 Constraints 137
5.3.1 Goal Fulfilment 137
5.3.2 Initial and Final Conditions 139
5.3.3 Joint Limits 139
5.3.4 Collision Avoidance 140
5.3.5 Dynamic Balance 140
5.4 Objectives 141
5.4.1 Goal Fulfilment 141
5.4.2 Data-based Conditions 142
5.4.3 Knowledge-based Conditions 142
5.5 Contact Models 143
5.5.1 Foot-Pedal Contact Model 143
5.5.1.1 Contact Point 143
5.5.1.2 Stiffness 146
5.5.1.3 Friction 146
5.5.2 Pelvis-Seat Contact Model 147
5.5.2.1 Stiffness 148
5.5.2.2 Damping 150
5.6 Conclusions 155

CHAPTER 6: RESULTS AND VALIDATION 157
6.1 Reference Motion Scenarios 157
6.2 Comparing Kinematic and Dynamic Predictions 159
6.2.1 End-Effector Trajectories 161
6.2.2 DoF Profiles 162
6.2.3 DoF Velocity Profiles 163
6.2.4 Joint Torque Profiles 164
6.2.5 Pelvis-Seat Efforts 167
6.2.6 Conclusions 172
6.3 Comparing Motion Control Laws 172
6.3.1 End-Effector Trajectories 175
6.3.2 DoF Profiles 176
6.3.3 DoF Velocity Profiles 178
6.3.4 Effort Profiles 180
6.3.5 Time-averaged Distance Definition 182
6.3.6 Quantitative Comparison between Motion Control Laws 185
6.4 Comparing Data-based, Knowledge-based and Hybrid Objective Functions 187
6.4.1 End-Effector Trajectories 188

6.4.2 DoF Profiles 190
6.4.3 DoF Velocity Profiles 192
6.4.4 Effort Profiles 194
6.4.5 Quantitative Comparison of the Three Approaches Followed in the Objective Function Definition 197
6.5 Validation 203
6.5.1 The End-Effector TD 204
6.5.2 The DoF Value TD 206
6.5.3 The DoF Velocity TD 207
6.5.4 The Effort TD 208
6.5.5 The Total TD 209
6.5.6 Conclusions 210

CHAPTER 7: CONCLUSIONS AND FUTURE WORKS 213
7.1 Conclusions 213
7.2 Future Work 217

APPENDIX A: PUBLICATIONS 219

REFERENCES 221

LIST OF FIGURES

Figure 1.1: RAMSIS DHMs representing short to tall females and short to tall males (reproduced from http://www.lfe.mw.tum.de/en/research/labs/ramsis). 2
Figure 1.2: Purely skeletal model of the DHM Santos (adapted from (Xiang et al., 2010)) on the left, and musculoskeletal model of the DHM AnyBody (reproduced from www.anybody.aau.dk/?Repository) on the right. 3
Figure 1.3: Interior and exterior model of Santos DHM (adapted from (Yang et al., 2004)). The root joint is shown in colours, and the end-effectors are marked by black rectangles. 4
Figure 1.4: A workspace design application of JACK (a) and Human Builder (b), RAMSIS mannequins inside a car (c), and Santos climbing a ladder (d). Images adapted from http://www.deskeng.com/articles/aaaxns.htm, http://www.uniplm.de/CATIA-Human-Builder-Simulation-89.html, http://www.appliedgroup.com/ramsis, and http://www.engineering.uiowa.edu/~amalek/DHL. 5
Figure 1.5: Due to the kinematic redundancy of the DHM, the end-effector (small black sphere) can reach the target (orange sphere) with different configurations. The large spheres represent the joints of the DHM. 6
Figure 1.6: Different strategies employed to reach the seat belt latch plate: right hand (a), left hand up (b) and left hand down (c). Adapted from (Monnier, 2004). 6
Figure 1.7: DHErgo project, www.dhergo.org. 8
Figure 1.8: Workflow of the DHErgo work package concerned with the development of a motion prediction method. 10
Figure 2.1: Steps characterising experimental capture and analysis. 47
Figure 2.2: Graphical summary of the classification of the main motion simulation methods reviewed in the chapter. The lower triangles contain animation methods and the upper triangles contain prediction methods. 57
Figure 3.1: Flowchart of the proposed hybrid motion prediction method. 62
Figure 3.2: Twelve 5th order uniform basis functions over a normalised time domain. 71
Figure 3.3: Hessian matrices of the objective function adopting different numbers of control points (considering a problem described by 10 DoFs and parameterised with 5th order B-splines). The blue dots represent the non-zero elements of the matrices. 84
Figure 4.1: Overview of the adjustable vehicle mock-up (reproduced from the DHErgo Newsletter n.2). 88
Figure 4.2: Environmental features used to characterise the different configurations of the vehicle mock-up. 89
Figure 4.3: Position of the reflective markers placed on the subjects. 90

Figure 4.4: Graphic representation of the adopted DHM. The active segments are shown in red. The corresponding active joints are reported and present a total of 3 translational and 10 rotational DoFs. 91
Figure 4.5: Velocity of the end-effector (EE) in a clutch pedal depression motion. Both the motion key-frames and the description of the phases in the end-effector's motion are reported 96
Figure 4.6: Box plots of the total motion duration, organised according to the subject groups (a) and the vehicle configurations (b). The red line represents the median, the blue box contains the inter-quartile range (from the 25th to the 75th percentile), and the black whiskers extend from the minimum to the maximum values (outliers are marked with red crosses). The red triangles mark the 95% confidence intervals of the medians. 97
Figure 4.7: Box plots of the relative duration of the reach phase respect to the pedal depression phase (R/D duration), organised according to the subject groups (a) and the vehicle configurations (b) 98
Figure 4.8: Key-frame distribution in the database in a normalised time domain. The average distribution is shown in solid thick black lines and compared to the distribution among the groups (a) and vehicle configurations (b). The coloured solid lines represent the mean of each set and the coloured dashed lines represent the 95% confidence intervals of the means. 99
Figure 4.9: 3D (left) and 2D (right) views of the trajectories followed by the end-effector in the REN3 vehicle configuration. The different colours represent the subject groups performing the motion: YF (magenta), YM (cyan), EF (red) and EM (blue). The yellow circle marks the pedal rest position 100
Figure 4.10: Mean trajectory followed by the end-effector along the 3 axes in the various groups (a1, b1, c1) and vehicle configurations (a2, b2, c2). The dashed lines represent the 95% confidence intervals of the means. The vertical black lines mark the average *StartDepression* and *EndDepression* key-frames 101
Figure 4.11: Movements of the segments in the left leg allowed by the joint DoFs and direction of the medio-lateral (ML), antero-posterior (AP) and infero-superior (IS) axes in each segment of the left leg: thigh, shank and foot. 102
Figure 4.12: Mean joint angle profiles for the hip joint in the various groups (a1, b1, c1) and vehicle configurations (a2, b2, c2). The angles represent the flexion-extension (FE), the abduction-adduction (AA) and the longitudinal rotation (LR) of the hip joint. The dashed lines represent the 95% confidence intervals of the means 103
Figure 4.13: Mean joint angle profiles for the knee joint in the various groups (a1, b1) and vehicle configurations (a2, b2). The angles represent the flexion-extension (FE) and the longitudinal rotation (LR) of the knee joint. The dashed lines represent the 95% confidence intervals of the means. 104
Figure 4.14: Mean joint angle profiles for the ankle joint in the various groups (a1, b1) and vehicle configurations (a2, b2). The angles represent the flexion-extension (FE) and

the longitudinal rotation (LR) of the ankle joint. The dashed lines represent the 95% confidence intervals of the means. 106
Figure 4.15: Mean joint angle profiles for the root joint in the various groups (a1, b1, c1) and vehicle configurations (a2, b2, c2). The angles represent the longitudinal rotation (L-Rot), the lateral tilt (L-Tilt) and the forward tilt (F-Tilt) of the root joint. The dashed lines represent the 95% confidence intervals of the means. 107
Figure 4.16: Mean trajectory followed by the root joint along the 3 axes in the various groups (a1, b1, c1) and vehicle configurations (a2, b2, c2). The dashed lines represent the 95% confidence intervals of the means. 108
Figure 4.17: Mean normalised flexion-extension (FE) DoF profiles at the hip, knee and ankle joints. The dashed lines represent the 95% confidence intervals of the means. The vertical black lines mark the average *StartDepression* and *EndDepression* key-frames. 110
Figure 4.18: Sagittal forces and ML torques acting at the leg joints during the reach phase (a) and sagittal forces acting on the leg segments during the pedal depression (b). Each joint torque in (a) is considered due to the weight of its distal segments, both marked in the same colour. The pedal reaction force (b) can be oriented in different directions. The subscripts F, S and T correspond to the foot, shank and thigh, respectively. 111
Figure 4.19: Mean joint torque profiles at the hip joint in the various groups (a1, b1, c1) and vehicle configurations (a2, b2, c2). The torques are expressed in the medio-lateral (ML), antero-posterior (AP) and infero-superior (IS) axes. The dashed lines represent the 95% confidence intervals of the means. The vertical black lines mark the average *StartDepression* and *EndDepression* key-frames. 112
Figure 4.20: Mean joint torque profiles at the knee joint in the various groups (a1, b1) and vehicle configurations (a2, b2). The torques are expressed in the medio-lateral (ML), and infero-superior (IS) axes. The dashed lines represent the 95% confidence intervals of the means. 113
Figure 4.21: Mean joint torque profiles at the ankle joint in the various groups (a1, b1) and vehicle configurations (a2, b2). The torques are expressed in the medio-lateral (ML) and antero-posterior (AP) axes. The dashed lines represent the 95% confidence intervals of the means. 114
Figure 4.22: Mean forces acting at the root joint in the various groups (a1, b1, c1) and vehicle configurations (a2, b2, c2). The forces are expressed in the global coordinate system. The dashed lines represent the 95% confidence intervals of the means. 116
Figure 4.23: Mean torques acting at the root joint in the various groups (a1, b1, c1) and vehicle configurations (a2, b2, c2). The torques are expressed in the global coordinate system. The dashed lines represent the 95% confidence intervals of the means. 117
Figure 4.24: Geometric characteristics of the pedal: normal (n) and radial (r) directions, initial orientation (θ_0), depression angle (θ), travel length (L) and travel angle (α). .. 118

Figure 4.25: Mean pedal stiffness curves in the various vehicle configurations. The dashed lines represent the 95% confidence intervals of the means. 119
Figure 4.26: Mean values of the radial component of the pedal reaction force respect to its normal component in the various groups (a1, b1) and vehicle configurations (a2, b2). On the left the radial force is plotted against the normal force (a1, a2), whereas on the right the ratio between the radial and normal forces is shown during the pedal depression phase (b1, b2). The dashed lines represent the 95% confidence intervals of the means. 120
Figure 4.27: Orientation of the main forces acting on the leg during the pedal depression. The angle formed by the pedal force and the horizontal axis is marked as α_F, whereas α_{FL} is the angle formed by the pedal force and the leg direction (i.e. line connecting the hip joint and the end-effector). The subscripts F, S and T correspond to the foot, shank and thigh, respectively. 121
Figure 4.28: Box plots of the mean force orientation respect to the horizontal direction (a1, b1) and to the leg direction (a2, b2), organised according to the subject groups (a1, a2) and the vehicle configurations (b1, b2). The red line represents the median, the blue box contains the inter-quartile range (from the 25th to the 75th percentile), and the black whiskers extend from the minimum to the maximum values (outliers are marked with red crosses). The red triangles mark the 95% confidence intervals of the medians. 122
Figure 4.29: Box plots of the position of the end-effector along the foot respect to the foot length, organised according to the subject groups (a) and the vehicle configurations (b) 123
Figure 4.30: Mean local position in the foot during the depression phase of the point in contact with the pedal centre. The positions are reported along the foot antero-posterior (a1, a2), infero-superior (b1, b2) and medio-lateral (c1, c2) axes in the various groups (a1, b1, c1) and vehicle configurations (a2, b2, c2). The dashed lines represent the 95% confidence intervals of the means. 124
Figure 4.31: Environmental features used in the structuring of the database. 129
Figure 5.1: Number of control points required to approximate the DoF profiles within a 5%, 2% and 1% tolerance (represented in red, green and blue, respectively). The black dot represents the median, the coloured box contains the inter-quartile range (from the 25th to the 75th percentile), and the whiskers extend from the minimum to the maximum values (outliers are marked with coloured circles). The black triangles mark the 95% confidence intervals of the medians. 135
Figure 5.2: Average tolerances with which the DoF profiles in the database are approximated by adopting 17 control points for the rotational DoFs and 16 for the translational DoFs. The red line represents the median, the blue box contains the inter-quartile range (from the 25th to the 75th percentile), and the black whiskers extend from the minimum to the maximum values (outliers are marked with red crosses). The red triangles mark the 95% confidence intervals of the medians. 136

Figure 5.3: Average tolerances with which the joint torque profiles in the database are approximated by adopting 17 control points for the rotational DoFs and 16 for the translational DoFs. 137
Figure 5.4: Geometric contact between the left foot and the clutch pedal. 144
Figure 5.5: Mean local position in the foot during the depression phase of the point in contact with the pedal centre, along the foot antero-posterior (a) and infero-superior (b) axes for young females (YF), young males (YM) and elderly males (EM) in the PCA2 vehicle configuration. The dashed lines represent the 95% confidence intervals of the means. 145
Figure 5.6: Mean values of the coefficient relating the radial and the normal forces at the pedal for young females (YF), young males (YM) and elderly males (EM) in the PCA2 vehicle configuration. The dashed lines represent the 95% confidence intervals of the means. 147
Figure 5.7: Geometry of the pelvis-seat interaction in the sagittal plane. 148
Figure 5.8: Forces acting on the pelvis at the beginning of the motion. The point MHP represents the mid hip point. The point CoM represents the centre of mass of the whole upper body and left leg combined, which together weigh *mg*. 149
Figure 5.9: Time-averaged distances (TDs) between the predicted motions and the actually performed motion in the prediction scenario that they seek to resemble. The damping ratio is varied from 0 to 1 with a 0.1 step. 154
Figure 6.1: Trajectories followed by the end-effector in the sagittal plane for young females (YF) employing a similar reference motion (a1, a2) and a dissimilar reference motion (b1, b2) for the kinematic and dynamic predictions. The trajectories are reported along the longitudinal x axis (a1, b1) and the vertical z axis (a2, b2). The blue and red curves, respectively, show the results of the kinematic and the dynamic predictions. The trajectories followed by the end-effector in the reference motions are reported in black. The thin black curves show the mean trajectories μ followed by the end-effector of the YF target population and the thin dashed curves represent their variability $\mu \pm 2\sigma$. The vertical black lines mark the average *StartDepression* and *EndDepression* key-frames of the motions performed by the target population in the prediction environment. 161
Figure 6.2: Flexion-extension profiles for young females (YF) employing a similar reference motion (a1, b1, c1) and a dissimilar reference motion (a2, b2, c2) for the kinematic and dynamic predictions. The blue and red curves, respectively, show the results of the kinematic and the dynamic predictions. The reference DoF profiles are reported in black. 163
Figure 6.3: Forward tilt and translations of the root joint in the sagittal plane for young females (YF) employing a similar reference motion (a1, b1, c1) and a dissimilar reference motion (a2, b2, c2) for the kinematic and dynamic predictions. The blue and red curves, respectively, show the results of the kinematic and the dynamic predictions. The reference DoF profiles are reported in black. 164

Figure 6.4: Flexion-extension velocity profiles for young females (YF) employing a similar reference motion (a1, b1, c1) and a dissimilar reference motion (a2, b2, c2) for the kinematic and dynamic predictions. The blue and red curves, respectively, show the results of the kinematic and the dynamic predictions. The reference DoF velocity profiles are reported in black. 165
Figure 6.5: Forward tilt and translational velocities of the root joint in the sagittal plane for young females (YF) employing a similar reference motion (a1, b1, c1) and a dissimilar reference motion (a2, b2, c2) for the kinematic and dynamic predictions. The blue and red curves, respectively, show the results of the kinematic and the dynamic predictions. The reference DoF velocity profiles are reported in black. 166
Figure 6.6: Joint torque profiles for young females (YF) employing a similar reference motion (a1, b1, c1) and a dissimilar reference motion (a2, b2, c2) for the kinematic and dynamic predictions. The medio-lateral torque profiles are shown at the hip (a1, a2), knee (b1, b2) and ankle (c1, c2) joints. The blue and red curves, respectively, show the results of the kinematic and the dynamic predictions. The reference DoF profiles are reported in black. 167
Figure 6.7: Efforts exerted by the pelvis on the seat for young females (YF) employing a similar reference motion (a1, b1, c1) and a dissimilar reference motion (a2, b2, c2) for the kinematic and dynamic predictions. The efforts in the sagittal plane are reported: forces along the x axis (a1, a2) and z axis (b1, b2) and torque about the global y axis (c1, c2). The results of the kinematic prediction are shown in blue (efforts evaluated through ID) and cyan (efforts expected according to the contact model) whereas the results of the dynamic predictions are shown in red (efforts evaluated through ID) and magenta (efforts expected according to the contact model). The efforts exerted in the reference motion are reported in black.....168
Figure 6.8: Efforts exerted by the pelvis on the seat for young males (YM) employing a similar reference motion (a1, b1, c1) and a dissimilar reference motion (a2, b2, c2) for the kinematic and dynamic predictions. The efforts in the sagittal plane are reported: forces along the x axis (a1, a2) and z axis (b1, b2) and torque about the global y axis (c1, c2). The results of the kinematic prediction are shown in blue (efforts evaluated through ID) and cyan (efforts expected according to the contact model) whereas the results of the dynamic predictions are shown in red (efforts evaluated through ID) and magenta (efforts expected according to the contact model). The efforts exerted in the reference motion are reported in black.....170
Figure 6.9: Forward tilt and translations of the root joint in the sagittal plane for young males (YM) employing a similar reference motion (a1, b1, c1) and a dissimilar reference motion (a2, b2, c2) for the kinematic and dynamic predictions. The blue and red curves, respectively, show the results of the kinematic and the dynamic predictions. The reference DoF profiles are reported in black. 171
Figure 6.10: Trajectories followed by the end-effector in the sagittal plane for young males (YM) following different control laws, employing a similar reference motion (a1, b1)

and a dissimilar reference motion (a2, b2). The blue and red curves, respectively, show the results of employing the DE and the ME performance measures. The result of including the TV and CL conditions are shown in cyan and magenta. The horizontal dotted black line (b2) reports the height of the PCA2 vehicle floor. 175
Figure 6.11: Flexion-extension profiles for young males (YM) following different control laws, employing a similar reference motion (a1, b1, c1) and a dissimilar reference motion (a2, b2, c2). The blue and red curves, respectively, show the results of employing the DE and the ME performance measures. The result of including the TV and CL conditions are shown in cyan and magenta. 177
Figure 6.12: Forward tilt and translations of the root joint in the sagittal plane for young males (YM) following different control laws, employing a similar reference motion (a1, b1, c1) and a dissimilar reference motion (a2, b2, c2). The blue and red curves, respectively, show the results of employing the DE and the ME performance measures. The result of including the TV and CL conditions are shown in cyan and magenta. 178
Figure 6.13: Flexion-extension velocity profiles for young males (YM) following different control laws, employing a similar reference motion (a1, b1, c1) and a dissimilar reference motion (a2, b2, c2). The blue and red curves, respectively, show the results of employing the DE and the ME performance measures. The result of including the TV and CL conditions are shown in cyan and magenta. 179
Figure 6.14: Forward tilt and translational velocities of the root joint in the sagittal plane for young males (YM) following different control laws, employing a similar reference motion (a1, b1, c1) and a dissimilar reference motion (a2, b2, c2). The blue and red curves, respectively, show the results of employing the DE and the ME performance measures. The result of including the TV and CL conditions are shown in cyan and magenta. 180
Figure 6.15: Joint torque profiles for young males (YM) following different control laws, employing a similar reference motion (a1, b1, c1) and a dissimilar reference motion (a2, b2, c2). The medio-lateral torque profiles are shown at the hip (a1, a2), knee (b1, b2) and ankle (c1, c2) joints. The blue and red curves, respectively, show the results of employing the DE and the ME performance measures. The result of including the TV and CL conditions are shown in cyan and magenta. 181
Figure 6.16: Efforts exerted by the pelvis on the seat for young males (YM) following different control laws, employing a similar reference motion (a1, b1, c1) and a dissimilar reference motion (a2, b2, c2). The efforts in the sagittal plane are the forces along the x axis (d1, d2) and z axis (e1, e2) and the torque about the global y axis (f1, f2). The blue and red curves, respectively, show the results of employing the DE and the ME performance measures. The result of including the TV and CL conditions are shown in cyan and magenta. 182
Figure 6.17: Time-averaged distances (TDs) for the three subject groups between the motions performed by the target population and the motions predicted with the

minimum dynamic effort (DE) or minimum mechanical energy (ME) performance measures, combined to the minimum translational velocity (TV) and the flexion-extension coordination law (CL), employing both a similar and a dissimilar reference motion. 185
Figure 6.18: Trajectories followed by the end-effector in the sagittal plane for elderly males (EM) employing a similar reference motion (a1, a2) and a dissimilar reference motion (b1, b2) for the battery of hybrid predictions. The red to blue curves show the results of the data-based to knowledge-based predictions. The trajectories followed by the end-effector in the reference motions are reported in black. The thin black curves show the mean trajectories μ followed by the end-effector of the EM target population and the thin dashed curves represent their variability $\mu \pm 2\sigma$. The vertical black lines mark the average *StartDepression* and *EndDepression* key-frames in the target population. 189
Figure 6.19: Flexion-extension profiles for elderly males (EM) employing a similar reference motion (a1, b1, c1) and a dissimilar reference motion (a2, b2, c2) for the battery of hybrid predictions. The red to blue curves show the results of the data-based to knowledge-based predictions. The reference DoF profiles are reported in black. 190
Figure 6.20: Forward tilt and translations of the root joint in the sagittal plane for elderly males (EM) employing a similar reference motion (a1, b1, c1) and a dissimilar reference motion (a2, b2, c2) for the battery of hybrid predictions. The red to blue curves show the results of the data-based to knowledge-based predictions. The reference DoF profiles are reported in black. 191
Figure 6.21: Flexion-extension velocity profiles for elderly males (EM) employing a similar reference motion (a1, b1, c1) and a dissimilar reference motion (a2, b2, c2) for the battery of hybrid predictions. The red to blue curves show the results of the data-based to knowledge-based predictions. The reference DoF velocity profiles are reported in black. 193
Figure 6.22: Forward tilt and translational velocities of the root joint in the sagittal plane for elderly males (EM) employing a similar reference motion (a1, b1, c1) and a dissimilar reference motion (a2, b2, c2) for the battery of hybrid predictions. The red to blue curves show the results of the data-based to knowledge-based predictions. The reference DoF velocity profiles are reported in black. 194
Figure 6.23: Joint torque profiles for elderly males (EM) employing a similar reference motion (a1, b1, c1) and a dissimilar reference motion (a2, b2, c2) for the battery of hybrid predictions. The medio-lateral torque profiles are shown at the hip (a1, a2), knee (a1, a2) and ankle (c1, c2) joints. The red to blue curves show the results of the data-based to knowledge-based predictions. The efforts in the reference motion are reported in black. 195
Figure 6.24: Efforts exerted by the pelvis on the seat for elderly males (EM) employing a similar reference motion (a1, b1, c1) and a dissimilar reference motion (a2, b2, c2) for

the battery of hybrid predictions. The efforts in the sagittal plane are the forces along the x axis (d1, d2) and z axis (e1, e2) and the torque about the global y axis (f1, f2).The red to blue curves show the results of the data-based to knowledge-based predictions. The efforts in the reference motion are reported in black. 196
Figure 6.25: Time-averaged distances (TDs) for elderly males (EM) between the motions performed by the target population and the motions generated in the battery of hybrid predictions employing a similar reference motion (a, above) and a dissimilar reference motion (b, below). The weight of the knowledge-based objectives ranges from 0 to 1, whereas the weight of the data-based objectives from 1 to 0. 198
Figure 6.26: Time-averaged distances (TDs) for young females (YF) between the motions performed by the target population and the motions generated in the battery of hybrid predictions employing a similar reference motion (a, above) and a dissimilar reference motion (b, below). The weight of the knowledge-based objectives ranges from 0 to 1, whereas the weight of the data-based objectives from 1 to 0. 200
Figure 6.27: Time-averaged distances (TDs) for young males (YM) between the motions performed by the target population and the motions generated in the battery of hybrid predictions employing a similar reference motion (a, above) and a dissimilar reference motion (b, below). The weight of the knowledge-based objectives ranges from 0 to 1, whereas the weight of the data-based objectives from 1 to 0. 201
Figure 6.28: Box plots comparing the time-averaged distance of the end-effector trajectory (TD_T) corresponding to the actually performed motions by the target populations (YF, YM, EM) and the TD_T obtained employing a data-based objective function (a) and two hybrid objective functions: hybrid 0.2-0.8 (b) and hybrid 0.4-0.6 (c). The TDs of the target population are shown in black (a, b, c), the TDs of the data-based objective function in red (a), the TDs of hybrid 0.2-0.8 in green (b) and the TDs of hybrid 0.4-0.6 in blue (c). The boxes contain the inter-quartile range (from the 25th to the 75th percentile), the whiskers extend from the minimum to the maximum values (outliers are marked with crosses), the horizontal line within the boxes represents the median value and the triangles mark the 95% confidence intervals of the median. . 205
Figure 6.29: Box plots comparing the time-averaged distance of the DoF profiles (TD_q) corresponding to the actually performed motions by the target populations (YF, YM, EM) and the TD_q obtained employing a data-based objective function (a) and two hybrid objective functions: hybrid 0.2-0.8 (b) and hybrid 0.4-0.6 (c). The TDs of the target population are shown in black (a, b, c), the TDs of the data-based objective function in red (a), the TDs of hybrid 0.2-0.8 in green (b) and the TDs of hybrid 0.4-0.6 in blue (c). 207
Figure 6.30: Box plots comparing the time-averaged distance of the DoF velocity profiles ($TD_{\dot{q}}$) corresponding to the actually performed motions by the target populations (YF, YM, EM) and the $TD_{\dot{q}}$ obtained employing a data-based objective function (a) and two hybrid objective functions: hybrid 0.2-0.8 (b) and hybrid 0.4-0.6 (c). The TDs of the target population are shown in black (a, b, c), the TDs of the data-based

objective function in red (a), the TDs of hybrid 0.2-0.8 in green (b) and the TDs of hybrid 0.4-0.6 in blue (c).....208
Figure 6.31: Box plots comparing the time-averaged distance of the effort profiles (TD_E) corresponding to the actually performed motions by the target populations (YF, YM, EM) and the TD_E obtained employing a data-based objective function (a) and two hybrid objective functions: hybrid 0.2-0.8 (b) and hybrid 0.4-0.6 (c). The TDs of the target population are shown in black (a, b, c), the TDs of the data-based objective function in red (a), the TDs of hybrid 0.2-0.8 in green (b) and the TDs of hybrid 0.4-0.6 in blue (c).....209
Figure 6.32: Box plots comparing the total time-averaged distance (TD_{TOT}) corresponding to the actually performed motions by the target populations (YF, YM, EM) and the TD_{TOT} obtained employing a data-based objective function (a) and two hybrid objective functions: hybrid 0.2-0.8 (b) and hybrid 0.4-0.6 (c). The TDs of the target population are shown in black (a, b, c), the TDs of the data-based objective function in red (a), the TDs of hybrid 0.2-0.8 in green (b) and the TDs of hybrid 0.4-0.6 in blue (c). 210

LIST OF TABLES

Table 4.1: Characteristics of the groups of subjects who took part in the clutch pedal depression experiments. The values preceding and following the ± symbol represent the mean μ and standard deviation σ, respectively. 88
Table 4.2: Characteristics of the environmental features in the different vehicle configurations shown in Figure 4.2. 90
Table 4.3: Number of motions present in the database performed by each group in each vehicle configuration. 94
Table 4.4: Average value of the key-frames respect to the total duration of the motions. .. 99
Table 4.5: Subject-related features included in the database structuring. The value following the ± symbol represents the standard deviation σ. 128
Table 4.6: Environment-related features included in the database structuring. The value following the ± symbol represents the standard deviation σ. 128
Table 5.1: Characteristics of the target populations and the prediction environment employed in the predictions presented in this work. 132
Table 5.2: Characteristics of the prediction scenarios. 133
Table 5.3: Characteristics of the optimisation problems defined to determine the damping coefficients for the pelvis-seat contact model. 151
Table 6.1: Number of motions performed by each subject in the young female (YF) group in each vehicle configuration. The shaded cells are those corresponding to the prediction subject or the prediction environment. 158
Table 6.2: Characteristics of the reference motion scenarios identified as the most similar to the prediction scenarios. 159
Table 6.3: Characteristics of the reference motion scenarios identified as the most dissimilar to the prediction scenarios. 159
Table 6.4: Characteristics of the optimisation problems defined in the kinematic and the dynamic predictions. 160
Table 6.5: Characteristics of the optimisation problems defined in the predictions to assess the most adequate motion control law for clutch pedal depressions. 174
Table 6.6: Characteristics of the optimisation problems defined to compare data-based, knowledge-based and hybrid objective functions. 188

GLOSSARY

Anatomical planes and axes: planes and axes used to describe positions and orientations in relation to the human body; they are defined in the standard anatomical position shown below.

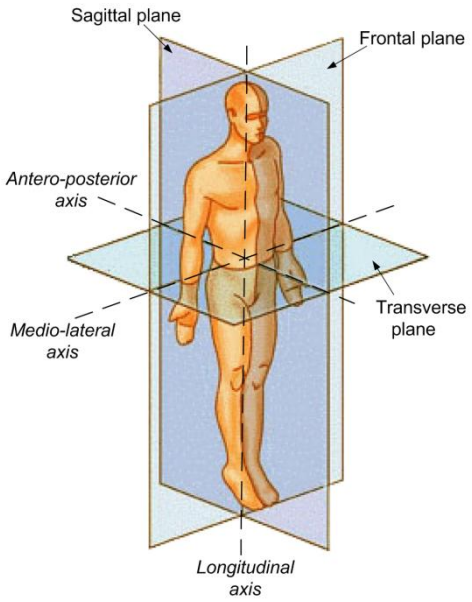

Animation: the process of guiding the DoFs in a model in order to perform a user-defined motion.

Basis functions: a set of linearly independent piecewise polynomials employed in the B-spline parameterisation.

Control points: coefficients of the linear combination of the basis functions employed in the B-spline parameterisation. They constitute the design variables for which the optimisation problem is solved.

Data-based: prediction methods (or conditions included in the prediction) that seek to resemble actually performed motions.

DHM: abbreviation for Digital Human Model.

Distal: further from the pelvis.

End-effector: controlled point in the DHM in charge of fulfilling a specific task in the motion.

Hybrid: a combination of data-based and knowledge-based methods (or conditions included in the prediction).

Key-frames: relevant frames in the motion at which a goal (or sub-goal) is accomplished.

Knowledge-based methods: prediction methods (or conditions included in the prediction) that seek to follow the motion control law that guides actually performed motions.

Motion control law: set of criteria which (more or less consciously) drive the human motion.

Prediction: the process of generating a realistic and representative motion of a generic specimen of the target population.

Prediction environment: the environment employed in the prediction, in which the predicted motion is carried out.

Prediction scenario: the combination of the subject and the environment employed in the prediction.

Prediction subject: the subject employed in the prediction, which represents a generic specimen of the target population.

Proximal: closer to the pelvis.

Reference environment: the environment in which the motion selected as reference was performed.

Reference motion: actually performed motion which is to be resembled in data-based simulations.

Reference scenario: the combination of the subject that performed the reference motion and the environment it was performed in.

Reference subject: the subject that performed the motion selected as reference.

Root joint: joint that connects the root segment to the ground.

Root segment: segment in the DHM that is connected to the ground through the root joint.

Scenario: combination of the subject performing the motion and the environment it is performed in.

Simulation: the process of generating a synthetic motion, which has not actually been performed. Both animation and prediction methods fall into the present definition of simulation.

TD: abbreviation for Time-averaged Distance, it quantifies the resemblance between the predicted motions and the actually performed motions by the target population in the prediction environment.

Target Populations: the groups of users for which a product design is being developed.

WPMV: abbreviation for Within Population Motion Variability, it represents the inherent variability of actually performed motions by a specific population in the prediction environment.

CHAPTER 1

INTRODUCTION

In an expanding, global and competitive economic environment, the concept-to-market time of a new product is required to be as short as possible. Since the 1960's, computer aided design (CAD) technologies have been employed to help the designers of new products increase their productivity and improve the quality of the designs (Narayan, 2008). Shortly after, the first digital models of the human body were developed (Bubb and Fritzsche, 2009) and integrated in virtual designs to assess the performance or the safety of the human-environment interaction.

Since then, digital human models (DHMs) have been more and more employed in product and workplace design (Chaffin, 2007; Duffy, 2009; Monnier et al., 2006), allowing human factors to be taken into account since the earliest phases of the design. As computers evolved into more powerful and capable machines, improved and more sophisticated software applications were developed to represent the interaction between the target customers (or workers) and the designed system. Such applications allow to virtually assess the ergonomics or the safety of the design, thus reducing the physical prototyping process, and consequently the development costs and the concept-to-market time of new products.

In order to study the interaction of the end user and the product, two main features are required by ergonomic evaluation software: a DHM and the motion it is to perform. The DHM must be defined with sufficient accuracy to represent the task being studied and must adapt to the majority of the target users of the product (Figure 1.1). For what concerns the motion of the DHM, certain applications (for instance motion analysis) may

employ actually performed motions, reconstructed in the virtual scene, in order to evaluate the kinematics and dynamics involved in the motion. However, in order to test a new product without resorting to a costly and time-consuming prototype for each change in the design, motion prediction is an interesting and useful tool. In fact, as explained later (Section 1.2), motion prediction is concerned with predicting the motion that representative members of the target users would perform while interacting with the new design. A novel design therefore can be first tested directly in the virtual space, delaying the actual physical prototype to a more final stage of the designing process, thus expediting the designer's work.

Figure 1.1: RAMSIS DHMs representing short to tall females and short to tall males (reproduced from http://www.lfe.mw.tum.de/en/research/labs/ramsis).

In order to help the designer evaluate the future product, the DHM should be able to represent the realistic behaviour of the human interacting with the new environment, not only in terms of anthropometry, but also of motion and discomfort perception.

1.1 DIGITAL HUMAN MODELS

In the study of human motion, DHMs are mathematical descriptions of the human musculoskeletal system, which provide digital representations of the human body inserted into a virtual environment. Several assumptions and simplifications are usually made, which depend on the accuracy with which the DHM must resemble the actual human body. For instance, to study a human motion on the whole, the model may not be very concerned with a detailed description of each articulation, whereas other biomechanical studies (for instance studies focused on the behaviour of a specific joint)

may require a higher level of detail in the representation of the specific part of the human body under examination.

In most studies concerning general human motion, the skeletal system is modelled with a multi-body approach, which is followed also in this work. Multi-body human models can be separated into musculoskeletal and purely skeletal models, according to whether the muscles in the human body are included in the model or not (Figure 1.2). The work presented in this thesis has been developed for purely skeletal models, in which the action of the muscles is represented as an equivalent set of forces and torques acting at the joints in the DHM.

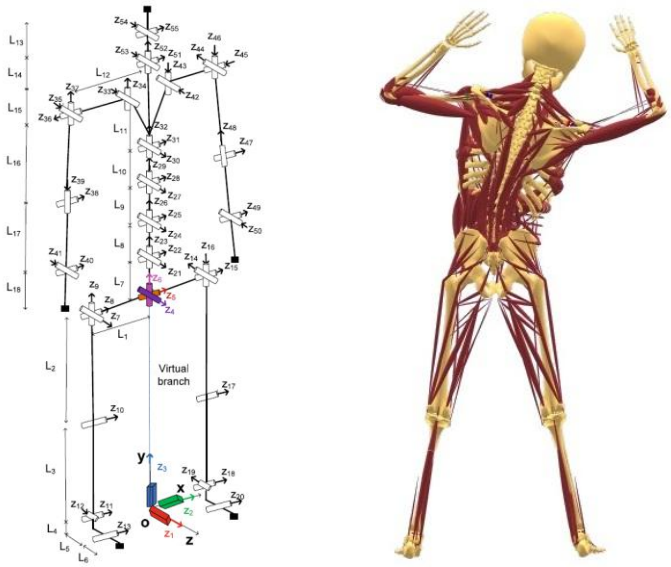

Figure 1.2: Purely skeletal model of the DHM Santos (adapted from (Xiang et al., 2010)) on the left, and musculoskeletal model of the DHM AnyBody (reproduced from www.anybody.aau.dk/?Repository) on the right.

Open chain multi-body DHMs can be represented with a tree structure (Figure 1.3) in which a segment, called root segment, is connected to the ground by a joint, called root joint. Segments which are closer to the root joint are called proximal whereas segments which are further away from the root joint are called distal. The points in the DHM which are in charge of fulfilling the goals in the motion are called end-effectors, and are generally located in the most distal segments of the DHM.

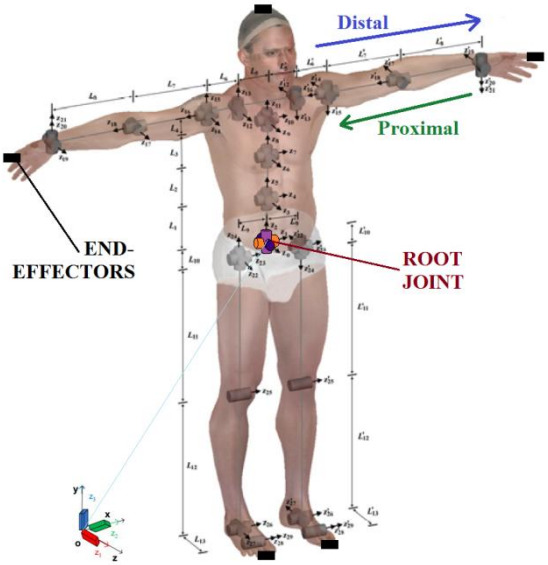

Figure 1.3: Interior and exterior model of Santos DHM (adapted from (Yang et al., 2004)). The root joint is shown in colours, and the end-effectors are marked by black rectangles.

Several DHMs are commercially available in either visualisation software or in complete ergonomic tools (Bubb and Fritzsche, 2009). JACK (Figure 1.4a) is a very common human model which allows to integrate user-defined methods and procedures, visualise them in the virtual space and apply analysis tools for factory workspace planning or vehicle design. Several aerospace and vehicle companies employ JACK, as well as various universities, such as the HUMOSIM Laboratory of the University of Michigan.

Human Builder (Figure 1.4b), originally called SAFEWORK, is a DHM conceived for workplace design in factory planning as well as product design, and is integrated in the CAD software tool CATIA of Dassault Systèmes. Human Builder can be used in conjunction with several modules which allow posture and movement analysis to improve human comfort, performance and safety.

The DHM most commonly employed in vehicle design is RAMSIS (Figure 1.4c), developed by Human Solutions, which is used by more than 75% of all car manufacturers. The anthropometry of the DHM is determined through an international anthropometric database which encompasses percentiles and secular growth models. Several functions are

available to analyse vehicles and vehicle interiors for cars, heavy machinery, buses and aircraft in terms of accessibility, vision, comfort, safety, etc.

The newest development in DHMs is Santos (Figure 1.4d), developed in the Virtual Soldier Research programme by the University of Iowa, which is an anatomically correct human model, with over 100 degrees of freedom (DoFs). Santos is employed in the software application Santos Engine, which allows to predict postures and motions to test equipment design and to assess task performance. Currently research is being carried out to create a musculoskeletal version of Santos, and to develop modules that enhance the software abilities in performance evaluations.

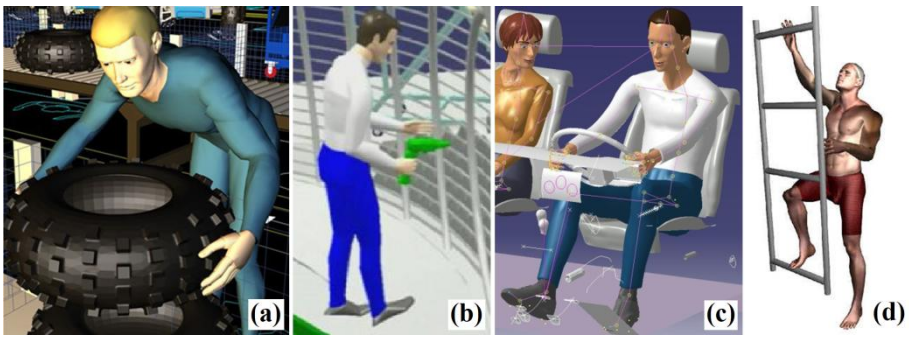

Figure 1.4: A workspace design application of JACK (a) and Human Builder (b), RAMSIS mannequins inside a car (c), and Santos climbing a ladder (d). Images adapted from http://www.deskeng.com/articles/aaaxns.htm, http://www.uniplm.de/CATIA-Human-Builder-Simulation-89.html, http://www.appliedgroup.com/ramsis, and http://www.engineering.uiowa.edu/~amalek/DHL.

1.2 MOTION PREDICTION

For most of the tasks that people carry out, the DHMs representing the human body are kinematically redundant systems, which means that they present more degrees of freedom (DoFs) than those strictly necessary to fulfil the goals in the task. For instance, even the simple task of reaching a close target with a hand does not uniquely define the position of the wrist and elbow joints (Figure 1.5). Therefore, the motion is not completely determined by the goal to be accomplished, and usually there are infinite sets of DoF values which ensure the fulfilment of the task.

Nevertheless, not all the possible motions that accomplish the goal are realistic. Among the infinite sets of DoF values which ensure the fulfilment of the task, only some represent motions that people would actually perform. Actually performed motions can generally be grouped into

strategies and styles, according to the behaviours exhibited by the people performing them.

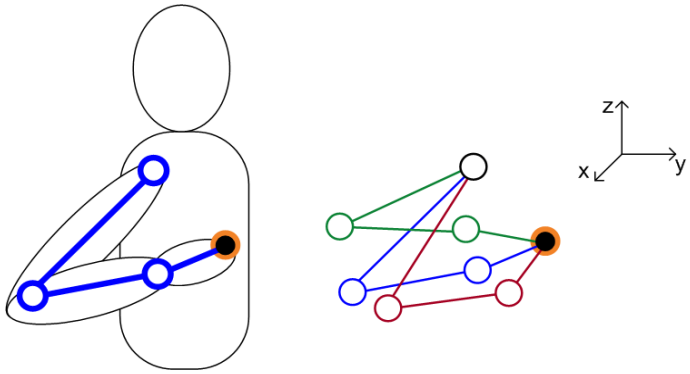

Figure 1.5: Due to the kinematic redundancy of the DHM, the end-effector (small black sphere) can reach the target (orange sphere) with different configurations. The large spheres represent the joints of the DHM.

Strategies are defined when evident differences are observed in the performance. For instance, in seat belt buckling motions, subjects present three different strategies to reach the latch plate (Monnier et al., 2003): some people use their right hand, others use their left from above their shoulder and others use their left from below their shoulder (Figure 1.6). Styles, on the other hand, can be defined as more subtle differences which are generally identified by a more detailed analysis of the motion. Continuing with the seat belt buckling example, styles may be depend for instance on the orientation of the hand reaching the latch plate or on the coordination between the hand and the torso (Monnier, 2004).

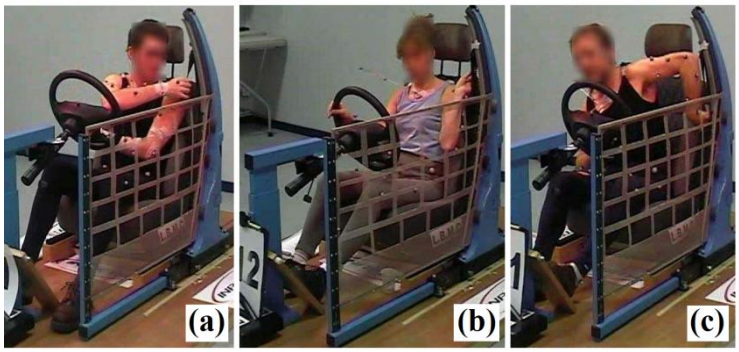

Figure 1.6: Different strategies employed to reach the seat belt latch plate: right hand (a), left hand up (b) and left hand down (c). Adapted from (Monnier, 2004).

The generation of realistic motions and the representation of the variety in behaviour adopted in actually performed motions are the aims and challenges in motion prediction. In this sense, motion prediction is opposed to motion animation. Both animation and prediction are concerned with the generation of motions which have not actually been performed. Defining with the term "simulation" the process of creating a synthetic motion, both animation and prediction methods can be regarded as motion simulation methods. However, the difference between animation and prediction, initially defined by Badler (1993)[1], lies in the goal of the simulation. Animation consists in moving an articulated figure in order to perform the motion expected by the animator. The goal is to produce a motion that *looks* realistic, although it is exaggerated or defies the laws of physics (as it often occurs in cartoon animation). Hence, animation is a suitable tool to be used in videogames or film animation, and is therefore highly concerned with the performance of the algorithm (which in the case of videogames is required to reach real time) and with the simplicity of use of the method (i.e. few parameters to be tuned).

Human motion prediction, on the other hand, is a field concerned with generating the motion that a member of a specific population would reasonably perform to carry out a task in a given environment. The predicted motion, therefore, *must be* realistic, representing actual human behaviour. Additionally, if real subjects perform a task adopting different behaviours, the prediction method should be able to generate realistic representations of all the variety of behaviours actually encountered. The prediction therefore must be both realistic and representative, not focusing on the motion of a specific individual, but reflecting the behaviours of the entire population being predicted, hereinafter referred to as "target population". All the above-mentioned characteristics make motion prediction an interesting and useful tool to be applied in ergonomics, in safety analysis or in motion analysis. The high level of realism and representativeness expected from motion prediction leads the performance of motion prediction algorithms to be of secondary importance.

[1] In (Badler et al., 1993) the term "simulation" refers to what is called "prediction" in this text.

1.3 MOTIVATION

This thesis has been developed initially in the frame of the European project DHErgo (Digital Humans for Ergonomic design of products), in the Seventh Framework Program of the European Commission. The project is led by a European consortium composed by:

- ERT (Europe Recherche Transport) for project coordination and management;
- the following academic research organisations: IFFSTAR (French Institute of Science and Technology for Transport, Development and Networks), CEIT (Centre of Studies and Technical Research of Gipuzkoa), Technical University of Munich and Free University of Brussels;
- the software editors Human Solutions and ESI Group;
- the end-users (car manufacturers) Renault, PCA (Peugeot Citroën) and BMW.

Figure 1.7: DHErgo project, www.dhergo.org.

The aim of the project was to develop more advanced DHM tools for the ergonomic design of products, especially concerning the automotive industry. These tools were required to perform the following tasks:

- evaluation of the motion-induced discomfort;
- prediction of population behaviour (especially including age effects, as elderly people represent an increasing part of the drivers' population);
- prediction of the interaction between the human body and the task-related environment.

The research core of the project was composed by the following work packages:

- collection of anthropometric data to generate more accurate models of the human body;
- motion capture of several subjects representing different target populations, performing vehicle-related tasks;
- dynamic reconstruction of the captured motions to create a motion database;
- development of a novel dynamic motion prediction method, to overcome the limitations of current prediction methods;
- development of discomfort models.

The work carried out in this thesis stems from the aim of the DHErgo project to overcome the limitations of current motion prediction methods. In fact, as detailed later (Chapter 2), the methods employed in motion prediction can be classified according to whether they rely on actually performed motions as a reference in the prediction (data-based methods) or whether the prediction is based on the identification of the motion control law which guides the motion (knowledge-based methods).

The main advantage of data-based methods lies in the intrinsic realism of the reference motion. However, these methods present the drawback of requiring, for each task to be predicted, a large database of motions, among which to select the most adequate reference. Additionally, current data-based motion prediction methods are only kinematic, as they do not take into account the forces and torques acting on and within the DHM.

On the other hand, knowledge-based methods tend to employ dynamic performance measures to represent the motion control law. However, motion control laws are generally difficult to identify, as even simple reaching motions seem to require the combination of several performance measures at once. Their difficulty of conferring realism to the predicted motion is the main drawback of knowledge-based methods.

Therefore, current motion prediction methods seem to require improvement in order to be successfully employed in the ergonomic evaluation of designs. Kinematic predictions may not be sufficient to assess the motion-induced discomfort, as the dynamics involved in the motion seem to play a relevant role in discomfort perception. Additionally, a motion generated through kinematic prediction may not be actually feasible

as the forces and torques required to carry out the motion are not taken into account. Moreover, the extrapolation capabilities of purely data-based predictions may not be satisfactory to allow new products to be tested virtually. On the other hand, purely knowledge-based predictions do not seem to ensure adequate levels of realism to be implemented in ergonomic evaluation tools.

The work package of the DHErgo project dealing with the development of a novel motion prediction method is organised as shown in Figure 1.8.

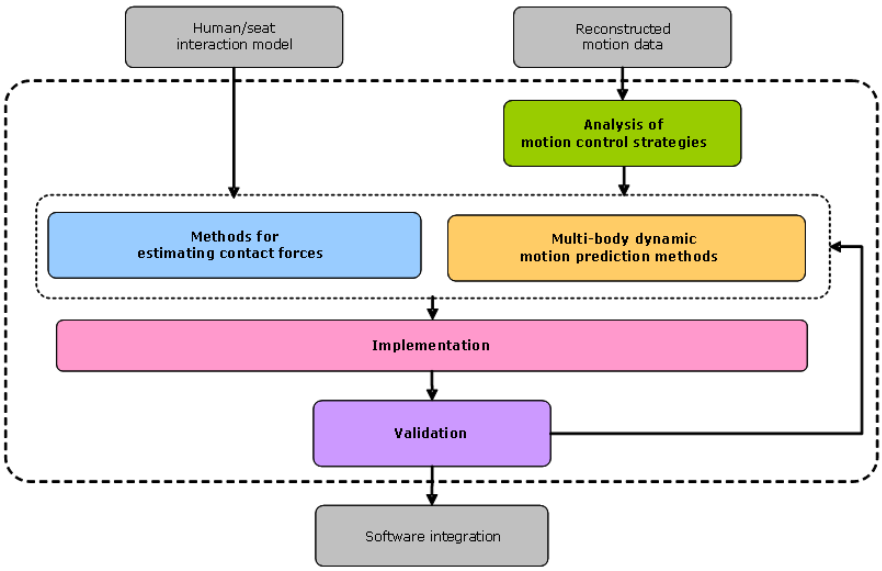

Figure 1.8: Workflow of the DHErgo work package concerned with the development of a motion prediction method.

The work carried out in this thesis follows the workflow presented in Figure 1.8.

1.4 OBJECTIVES

The main purpose of this research work is the development a novel motion prediction method to overcome some of the limitations encountered in the existing methods. This purpose leads to the definition of the following objectives.

- The first objective of this thesis is developing a *dynamic* motion prediction method in order to generate physically sound motions. Moreover, by taking into account the forces and torques acting on and within the human body (which play a relevant role in discomfort perception) the motion-induced discomfort may be assessed more accurately. Additionally, the dynamic *human-environment interaction* must be described and taken into account in the prediction.

- The second objective consists in including both data-based and knowledge-based principles in the prediction method, that is therefore *hybrid* as it combines both data-based and knowledge-based approaches. The purposes of the data-based contribution to the method are to enhance the realism of the prediction through the actually performed reference motion, and to allow to reproduce the variability in behaviour exhibited in actually performed motion. The knowledge-based contribution seeks to reduce the dependency on the goodness of the reference motion and to improve the extrapolation capabilities of the prediction method.

    - The data-based contribution to our motion prediction method requires a *motion database analysis*, in order to identify the most relevant features that affect the kinematics and dynamics of the motion and to structure (i.e. organise) the database consequently. A structured database, in fact, is needed to identify the most adequate reference motion for each motion to be predicted.

    - Additionally, the analysis of the motion database serves the purpose of gaining insight into the motion performance, which is useful in the *motion control law identification* required by the knowledge-based contribution to the method.

- The third objective of this thesis is to develop a method that can be employed for the ergonomic evaluation of product design in industrial development and research. For this purpose, the method is required to be a *general* method, which is not oriented to the prediction of only a specific group of users but that can predict a variety of target populations.

- The fourth objective consists in the *application* of the developed method to the prediction of a specific task, which should contain the most relevant features to test the method. The *clutch pedal depression* in vehicles seems an adequate task to be used as test case: it is a task-

oriented motion in which specific goals must be met, it requires dynamic interaction between the subject and the environment, and nevertheless it remains a relatively simple task. Additionally, the DHErgo project provided us with all the necessary experimental data for this specific task.

- Simple tasks are generally employed as test cases for motion prediction methods, especially for validation purposes, which constitute the fifth objective of the thesis. In fact, to carry out a *qualitative and quantitative validation*, the predicted motions must be compared to motions actually performed in the same conditions as the ones being predicted. Therefore, complex motions do not constitute an appropriate candidate since to carry out the validation it would be necessary to find other subjects that perform the task with exactly the same style throughout the motion, which is difficult to find.

1.5 ORGANISATION OF THE DOCUMENT

The content of this thesis is organised as described hereafter.

The first chapter has introduced the main aspects concerning motion prediction. The motivation for this thesis has been presented and the objectives to be achieved have been set.

Chapter 2 is focused on the review of the state of the art in human motion simulation methods: both animation and prediction methods are included, as they share similar methodologies in the generation of motions which have not actually been performed. The most relevant validation procedures proposed for motion prediction methods are subsequently presented, followed by a section dedicated to experimental data capture and analysis in which the motion analysis methods encountered in the literature are reviewed.

The hybrid dynamic motion prediction method developed in this research work is presented in Chapter 3, which describes the mathematical modelling employed in our optimisation-based method. The inputs and outputs are defined, as well as the main steps composing the prediction algorithm.

Chapter 4 is dedicated to the analysis of a database of experimental motions consisting of clutch pedal depressions. An overview on the

experimental protocol and the reconstruction process open the chapter, which thereafter focuses on the analysis of temporal, kinematic and dynamic features of the motions, which led to the structuring of the database.

The application of the motion prediction method to the clutch pedal depression task is presented in Chapter 5, in which the test case is defined in terms of application of the method to a specific task, target populations definition and description of the contact models employed to represent the human-environment interactions. The results of the prediction and the validation of the method are discussed Chapter 6. A comparison between kinematic and dynamic predictions is then presented, followed by a comparison between motion control laws (in order to assess the most adequate one to represent the task), and by a comparison between data-based, knowledge-based and hybrid approaches. Finally, the hybrid dynamic motion prediction method is validated, qualitatively and quantitatively, against actually performed motions by the target populations.

Chapter 7 presents the conclusions which are drawn from the work presented in the previous chapters and proposes some future research lines.

CHAPTER 2

STATE OF THE ART

This chapter presents a review of the state of the art in the most relevant topics concerning motion prediction, applied to purely skeletal DHMs (see Section 1.1). First a review of the methods adopted in motion simulation is presented (Section 2.1); as will be explained later, both animation and prediction methods are included in the review as they share similar methodologies. The validation procedures encountered in the literature are reported in the following section (Section 2.2). Subsequently, experimental data capture and reconstruction are introduced to review the methods developed in motion analysis (Section 2.3). Finally, the last section presents the conclusions drawn from the review and places the work carried out in this thesis in the current state of the art (Section 2.4).

2.1 MOTION SIMULATION METHODS

The field of motion simulation is vast and the methods developed and employed vary substantially depending on several features. Different taxonomies may be applied to classify existing methods: whether they are animation or prediction methods; if they consider kinematics alone or include dynamics; if they modify existing motions or generate the new motion from scratch; and whether they rely on optimisation or statistical modelling techniques.

All taxonomies are useful to highlight specific aspects of the different formulations. In this review, existing motion simulation methods are presented classifying them according both to the mechanical variables included in the simulation and to the source of realism employed in the

simulation. The reason behind this choice is that both these classifications highlight features of motion simulation methods that are relevant to the context in which this research work has been carried out.

Both animation and motion prediction are included in the review, since the methods developed in both fields present similar features. As mentioned in Section 1.2, the main difference between animation and prediction methods lies in the different goals of the simulation. This mainly affects the required validation process, as will be detailed in Section 2.2.

For what concerns the different procedures adopted to carry out the simulation, both optimisation-based and statistical modelling approaches are presented among the methods reviewed in this chapter. The relevant features of each approach are detailed throughout this section.

A graphical summary of the main simulation methods encountered in the literature, classified according to the considered taxonomies, may be found in Section 2.4.

2.1.1 MECHANICS TAXONOMY

The current methods used to predict human motion can be divided into kinematic, dynamic and static methods. The kinematic methods take into account only the kinematic variables of the motion, such as the joint angle profiles and the positions of the end-effector, i.e. the point in the DHM that is in charge of fulfilling the task. The dynamic methods, on the other hand, include dynamic variables in the prediction, such as external and internal forces. Finally, the static methods are only concerned with the generation of a posture instead of a whole motion and may involve or not the evaluation of forces and torques. As Multon et al. (1999) pointed out, the choice of which formulation to adopt depends on the requirements of the application.

2.1.1.1 Kinematic Simulation

Most of the methods developed to perform kinematic motion simulations are based on inverse kinematics, as opposed to forward kinematics. In motion simulation, forward kinematics (FK) is used to obtain the position $\mathbf{x}$ of the end-effector given the values of the DoFs of the system $\boldsymbol{\theta}$. Inverse kinematics (IK) on the other hand is used to obtain the DoFs of the system $\boldsymbol{\theta}$ given the position $\mathbf{x}$ of the end-effector:

$$\begin{aligned} &\textit{Forward kinematics}: \ \boldsymbol{\theta} \ \rightarrow \ \mathbf{x} = f(\boldsymbol{\theta}) \\ &\textit{Inverse kinematics}: \quad \mathbf{x} \ \rightarrow \ \boldsymbol{\theta} = f(\mathbf{x}) \end{aligned} \tag{2.1}$$

Generally, the DHM is described following a relative coordinates formalism. Hence, the DoFs $\boldsymbol{\theta}$ are the angles and distances between the segments of the multi-body DHM.

Due to the redundancy of DoFs in DHMs (Section 1.2), there are infinite sets of DoF values which allow a specified point in the model to occupy a determined position. Among the infinite sets of DoF values, the most appropriate one must be identified. This process is generally carried out through optimisation: the returned set of DoFs is that which best follows a specific criterion. In motion edition, which represents a wide portion of kinematic simulation methods, an existing motion is available and the optimisation criterion generally seeks to resemble it.

Kinematic simulation methods can be divided into per-frame and per-key methods, according to whether IK is performed at each frame in the motion or only at key-frames, i.e. relevant frames in the motion at which a goal is accomplished. Both per-frame and per-key methods are hereafter described.

Per-frame Methods

In per-frame methods, the position of the end-effector is controlled throughout the motion. However, since an IK problem is defined and solved independently at each frame, the challenge in these methods is that of ensuring a smooth simulated movement.

Monnier et al. (2003) used a per-frame method to perform kinematic predictions of reaching and seat belt buckling motions. To solve the IK problem, the authors adopted the pseudo-inverse method, an iterative method which updates the DoF values $\boldsymbol{\theta}$ to reach the point $\mathbf{x}$:

$$d\boldsymbol{\theta} = \mathbf{J}^{+}\, d\mathbf{x} + \left(\mathbf{I} - \mathbf{J}^{+}\,\mathbf{J}\right) d\boldsymbol{\varphi} \tag{2.2}$$

where $\mathbf{J}$ is the Jacobian matrix defined as:

$$J_{ij} = \frac{\partial x_i}{\partial \theta_j} \tag{2.3}$$

and $\mathbf{J}^{+}$ is its pseudo-inverse.

The increment $d\boldsymbol{\theta}$ is obtained combining two terms. The first term, $\mathbf{J}^{+}d\mathbf{x}$, is in charge of reaching the desired position minimising the joint angle rates $d\boldsymbol{\theta}$. The second term operates in the null space of $\mathbf{J}$, i.e. modifies the joint angles without affecting the end-effector position[2]: Monnier et al. defined the vector of joint angles $d\boldsymbol{\varphi}$ in order to resemble the DoF values of an existing motion, performed in similar conditions to those to be predicted. The motions obtained with this approach seem not to present spikes due to the choice of $d\boldsymbol{\varphi}$.

Other authors chose to explicitly ensure the continuity of the generated motions. Gleicher (2001) presents an animation method in which a low-pass filter is introduced to smoothen the result of the per-frame method. This process however may undo the work done by the per-frame algorithm (i.e. the constraints may no longer be met), so the per-frame simulation and the filtering process are performed iteratively.

On the other hand, the animation method presented by Lee and Shin (1999) avoids discontinuities by using a hierarchical B-spline fitting to approximate the motion obtained with the per-frame method (the main properties of B-spline curves are detailed later in Section 3.5.1). The DoF profiles are fitted with multilevel B-splines, which are a linear combination of B-splines characterised by a different number of control points, yielding a coarse-to-fine hierarchical approximation.

Per-frame methods have also been used in combination with path planning techniques to simulate the motion of an articulated figure carrying out a task while avoiding obstacles in the environment (Pan et al., 2010; Shapiro et al., 2007; Yamane et al., 2004). In (Yamane et al., 2004) and in (Pan et al., 2010), the goal is to generate human-like motions for object manipulation in constrained environments (i.e. in which obstacles are present). The motion of the articulated figure carrying out the task is obtained by adjusting the result of randomised motion planning techniques in order to resemble the motion performed by a real subject in similar conditions. The main difference between the works of Yamane et al. and Pan et al. lies in that the former considers environments with few obstacles while the latter is concerned with simulating motions in highly cluttered areas or tight spaces, in which obstacle avoidance is the primary aim and

[2] Due to the redundancy of DoFs, the null space of $\mathbf{J}$ is not an empty set.

naturalness comes second. Shapiro et al. (2007) on the other hand presented a motion editing method in which a given motion is modified in order to avoid user-defined obstacles in the environment. Similarly to Yamane, the method is better suited for open environments with few obstacles rather than tight spaces.

Per-key Methods

Opposed to per-frame methods, per-key methods apply IK only at relevant frames in the motion (key-frames), at which the end-effector position must be ensured. The time span from one key-frame to the next is called time-period, and during this period the DoF values are obtained by modifying a given motion in order to match the DoF values, obtained through IK, at the key-frames.

Bindiganavale and Badler (1998) retargeted an original motion to a different subject by imposing that between key-frames the new velocities $\dot{\theta}$ of the DoF profiles must be proportional to the velocities in the original motion $\dot{\theta}_0$. For each DoF θ:

$$\dot{\theta}(t) = c_{V1} \cdot \dot{\theta}_0(t) \quad \rightarrow \quad \theta(t) = c_{V1} \cdot \theta_0(t) + c_{V2} \tag{2.4}$$

The coefficients c_{V1} and c_{V2} are obtained by solving a system of equations in which Equation (2.4) is evaluated at the key-frames delimiting the time period, at which both θ_0 and θ are known.

Zhang (2002) compared the velocity proportional (VP) approach, described by Equation (2.4), to an acceleration preserving (AP) approach[3], which imposes to the new motion the same acceleration profiles as the original DoFs θ_0. For each DoF θ:

$$\ddot{\theta}(t) = \ddot{\theta}_0(t) \quad \rightarrow \quad \theta(t) = \theta_0(t) + c_{A1} \cdot t + c_{A2} \tag{2.5}$$

The coefficients c_{A1} and c_{A2} are obtained as in the VP approach. The comparison, applied to the prediction of reaching motions, shows that both approaches generally yield similar results. The main advantage of VP is that

[3] In (Zhang, 2002) the VP approach is called amplitude-proportional and the AP approach is called time-proportional.

it maintains the zero velocities of the end-effector, however if the initial and final values of θ are very similar, numerical problems may arise in the evaluation of the coefficients c_{V1} and c_{V2}, making AP preferable in such cases.

The motion prediction method presented by Park et al. (2004; 2005a) consists in segmenting the DoF profiles of the original motion into increasing, decreasing and stationary periods, separated by boundary points. The new motion must maintain the same sequence of periods (i.e. the velocity of the DoFs must maintain its sign) and in each period the joint angle profiles are obtained by shifting and scaling the original segments. First the postures at key-frames are calculated, solving the IK problem with non-linear programming techniques. The values of the DoFs $\boldsymbol{\theta}$ in the DHM at each key-frame are obtained by solving a constrained optimisation problem, in which $\boldsymbol{\theta}$ must fulfil the end-effector spatial constraints while resembling the posture at the key-frame in an existing motion, performed in similar conditions to those to be predicted, $\boldsymbol{\theta}_O$:

$$\min\left((\boldsymbol{\theta}-\boldsymbol{\theta}_O)^T(\boldsymbol{\theta}-\boldsymbol{\theta}_O)\right) \tag{2.6}$$

The values of the boundary points in between key-frames are obtained minimising the difference between the new DoF velocities $\dot{\boldsymbol{\theta}}$ and the original DoF velocities $\dot{\boldsymbol{\theta}}_O$ in the time period. For each DoF θ:

$$\min \int_0^T \left(\dot{\theta}(t) - \dot{\theta}_O(t)\right)^2 dt \tag{2.7}$$

In the time period in between the boundary points, each DoF is modified through a VP method in order to match the boundary point values calculated through (2.7).

Another per-key motion modification method was proposed by Unuma et al. (1995), which allows to generate new motions by blending existing motions together. The method is applied to the animation of periodical motions, such as walking or running, which are approximated with a truncated Fourier series. Motions are then combined linearly allowing both interpolation and extrapolation: considering for instance that the original motions are a normal walk and a tired walk, motion blending may interpolate a not-so-tired walk or extrapolate a very tired walk.

Finally, Witkin and Popovic (1995) introduced the concept of motion warping in per-key animation methods: not only the DoF profiles are modified, but also the key-frames may be displaced in time.

Respect to per-frame methods, per-key methods present the advantage of being computationally more efficient. However, their main drawback is that they cannot ensure the fulfilment of constraints applied in between the key-frames. This may be problematic for constraints that need to be applied throughout the motion, such as joint limits or the condition that while walking the foot must not penetrate the floor.

Generally, all kinematic simulation methods are computationally less expensive than dynamic methods. However, the conditions to be simulated by kinematic methods are limited as, for instance, they are not able to reasonably predict the motion of lifting a heavier box or the motion of a weaker subject. For such predictions, dynamic variables must be included in the problem.

2.1.1.2 Dynamic Simulation

Dynamic simulation methods generate predictions which take into account factors that actually play a front-stage role in human motion, such as effort, strength or endurance. Not only the joint angle profiles but also the system's internal forces and torques are accounted for. These internal efforts are actually exerted by the muscles in the human body. However, instead of taking into account each muscular force, as is typical in musculoskeletal DHMs (Anderson and Pandy, 2001; Eriksson, 2008; Eriksson and Nordmark, 2011; Kaplan and Heegaard, 2001; Todorov, 2004), in methods employing purely skeletal DHMs it is common to deal with joint torques, which correspond to the resulting action of all the muscles at a joint.

Most of the dynamic simulation methods use inverse dynamics to relate the joint angle profiles (and their time derivatives) to the joint torques. Inverse dynamics is a process opposed to forward dynamics, in a similar way as IK is opposed to FK (Section 2.1.1.1). Forward dynamics (FD) is the process of obtaining the motion (i.e. the DoF profiles $\boldsymbol{\theta}(t)$) given the forces $\mathbf{F}(t)$ and torques $\boldsymbol{\tau}(t)$ that the system is subject to. On the other hand, the starting point of inverse dynamics (ID) is the system DoF profiles $\boldsymbol{\theta}(t)$ and ID consists in obtaining the efforts $\mathbf{F}(t)$ and $\boldsymbol{\tau}(t)$ that generate

the given motion (some of the forces and torques may be given as well: $\hat{\mathbf{F}}(t)$, $\hat{\boldsymbol{\tau}}(t)$).

$$\begin{aligned} &\textit{Forward dynamics}: \ \mathbf{F}, \boldsymbol{\tau} \quad \rightarrow \ \boldsymbol{\theta} = f\left(\mathbf{F}, \boldsymbol{\tau}\right) \\ &\textit{Inverse dynamics}: \quad \boldsymbol{\theta}, \dot{\boldsymbol{\theta}}, \ddot{\boldsymbol{\theta}}, \hat{\mathbf{F}}, \hat{\boldsymbol{\tau}} \ \rightarrow \ \mathbf{F} = f\left(\boldsymbol{\theta}, \dot{\boldsymbol{\theta}}, \ddot{\boldsymbol{\theta}}, \hat{\mathbf{F}}\right) \\ &\qquad\qquad\qquad\qquad\qquad\quad \boldsymbol{\tau} = f\left(\boldsymbol{\theta}, \dot{\boldsymbol{\theta}}, \ddot{\boldsymbol{\theta}}, \hat{\mathbf{F}}, \hat{\boldsymbol{\tau}}\right) \end{aligned} \tag{2.8}$$

When a dynamic simulation is carried out, both the motion and the efforts are unknown (unless ID is performed *a posteriori* on a simulated motion). This means that the approach adopted in simulation methods is neither FD nor ID. However, the relationship between the DoF profiles and the forces and torques must be defined in the method. Adopting the relationship defined following ID is computationally less expensive than the relationship given by FD, since in ID the equations of motion are not integrated (Xiang et al., 2010a).

Including dynamics in the formulation implies that the frames in the motion are related to one another: not only the values $\boldsymbol{\theta}$ of the DoFs, but also their first and second derivatives, $\dot{\boldsymbol{\theta}}$ and $\ddot{\boldsymbol{\theta}}$, appear in the equations of motion. Hence $\mathbf{F}$ and $\boldsymbol{\tau}$ do not depend on three independent sets of variables, but on variables that are related through derivation. This implies that as opposed to kinematics, in which each frame in the motion can be considered independently from the rest, in dynamics the configuration of the system at each instant in time is not independent from the rest of the motion. Nevertheless, it must be mentioned that a per-frame dynamic motion simulation method was proposed (Tak and Ko, 2005): however, the DoFs and their derivatives at each frame are considered as independent variables and the correct relationship between them is restored only as a post-process, smoothing the per-frame results by approximating the DoFs with B-spline curves (Section 3.5.1), similarly to (Lee and Shin, 1999). The method presented by Tak and Ko seeks to include dynamics in an on-line animation tool through control theory, applying iteratively the Kalman filter[4] to each frame, to enforce the constraints to the motion, and a local

[4] The Kalman filter is a control algorithm that estimates the states of a system given its present input measurements and the previously calculated state. In (Tak and Ko, 2005) the measurements are the goals of the constraints evaluated at each frame.

B-spline curve fitting to the current sequence of frames, to restore the correct relationship between the DoFs of the DHM and their derivatives.

To include the relationship between the DoFs and their derivatives in the formulation, Witkin and Kass (1988) introduced a method called spacetime constraints. The motion of an animated figure is simulated solving a constrained optimisation problem in which the vector of design variables contains the values of the DoFs and forces of the system at each frame: considering n DoFs and forces and m frames, the vector of design variables is composed of $n \times m$ elements. The relationship between the variables is established by defining velocities and accelerations in each frame with finite differences and imposing the equations of motion as constraints. The objective function to be minimised is the squared sum of torques across the motion (see Section 2.1.2.2). The method, proposed as an animation tool, is applied to the simulation of a jumping motion performed by a 6 DoFs model of a Luxo lamp. Spacetime constraints have also been applied by Chang et al. (2001) to simulate a manual lifting task in the sagittal plane. The vector of design variables contains the values of the DoFs of the system at every frame and the function to be minimised is the squared sum of torques across the motion, as in (Witkin and Kass, 1988).

Given the extremely large number of variables required by spacetime methods, only simple articulated figures have been used to generate short animation clips. Some authors, however, proposed to simplify either the model (Popovic and Witkin, 1999) or the dynamic constraints (Abe et al., 2006; Liu and Popovic, 2002) in order to apply spacetime methods to more complex characters and motions in motion editing animations. Popovic and Witkin (1999) presented a motion transformation algorithm based on spacetime constraints: a given motion is simplified, adapting it to a simplified articulated figure, and is modified through spacetime constraints. The changes in the simplified figure are then transferred back to the original character. The method is applied to modifying a running and jumping motion by changing the footstep length, gravity, obstacle positions, etc. Liu et al. (2002) and Abe et al. (2006) instead maintained the complexity of the articulated figure but imposed dynamic constraints only to the linear and angular momentum of the figure. Apparently, momentum constraints reflect the aggregate effect of the natural energy storage-and-release of real motions, for instance jumping or running. Motion edition through momentum modification was also employed by Sok et al. (2010), who scale the momentum of the original motion to generate motions such as higher jumps. The new trajectory of the figure's centre of mass (CoM) is

calculated, and the rest of the body is adapted to the new CoM trajectory while considering the constraints imposed to the motion by using IK.

Another way of including the relationship between the DoFs and their derivatives in the formulation is by performing a parameterisation of the DoF profiles. Parameterisations allow to represent the motion with fewer variables than spacetime methods: the motion is assumed to be described by a combination of an independent set of functions and the coefficients of the combination constitute the new set of variables describing the motion. On the one hand the simulation is simplified, as the number of variables is reduced; on the other hand, attention must be paid to the number of constraints that are to be imposed to the motion, which is limited by the variable reduction.

The parameterisation carried out through principal component analysis (PCA) seems to fulfil the requirements of animation methods (Lim et al., 2005; Park and Jo, 2004; Safonova et al., 2004): it drastically reduces the number of variables which describe the motion, significantly decreasing the computational cost of the simulation, while preserving the most relevant features of the motion. The ability of accounting for the majority of the DoF variations during the motion, using such a reduced number of variables, is possible because the principal components of the motion are obtained through the solution of an eigenproblem. PCA considers a matrix $\mathbf{X}$ for each DoF, containing the values that the DoF presents across several experimental motions. A singular value decomposition is performed on each $\mathbf{X}$ and only the first few "modes" (termed principal components) are selected to represent the motion. Depending on the type of motion and on the adequacy of the experimental data, 4 to 7 principal components per DoF were considered sufficient to simulate arm raising and reaching motions (Lim et al., 2005; Park and Jo, 2004), or walking, running and jumping motions (Safonova et al., 2004), once again imposing the minimisation of the squared sum of torques across the motion.

Different parameterisations have been adopted in motion prediction methods, such as in the method presented by Abdel-Malek and Arora (2009), called predictive dynamics. Predictive dynamics is an optimisation-based method in which the design variables are the coefficients of the parameterisation that is performed on the DoFs profiles. A common parameterisation is that of B-splines (described later in Section 3.5.1), which leads the design variables to be the B-spline control points. However Ren et al. (2007) use a Fourier series to parameterise the DoFs profiles in a walking

motion, given the cyclic nature of the movement. Generally in predictive dynamics a set of B-splines is used to parameterise the DoF profiles, and the torque profiles are defined as a function of the DoFs and their derivatives. Nevertheless, Xiang et al. (2010c) adopt a set of B-splines to approximate the DoF profiles, and another set to approximate the torque profiles (i.e. the problem is stated as a function of both the DoF and torque profiles). This way, however, the torques and the DoF values and derivatives are decoupled: the equations of motion relating the two are set as constraints, but these constraints are imposed only at certain frames of the motion, leaving the remaining frames to present incongruousness between kinematics and dynamics. The objective function to be minimised in predictive dynamics is energy related, as detailed later in Section 2.1.2.2. Predictive dynamics has been used to simulate several different motions. Kim et al. (2006; 2007) predicted pulling motions for an upper body DHM with one or two arms respectively. Also running (Chung et al., 2007), lifting (Xiang et al., 2010b) and walking motions (Xiang et al., 2007; Xiang et al., 2011) have been predicted. In these whole body motions the ground reaction forces have also been taken into account: they are applied at the zero moment point (ZMP), and for balance the ZMP must be contained in the support area. To impose balance, Ren et al. (2007) instead limited the tangential ground forces to be balanced by friction.

Respect to kinematic simulations, dynamic simulations allow to generate more physically sound motions, by including balance in the formulation and taking the internal efforts of the human body into account. This way, not only the joint range of motion (RoM) but also the joint maximum torques can be accounted for, producing motions that are more likely to be actually performed by real subjects.

2.1.1.3 Static Simulation

Methods have been developed also to simulate postures of articulated figures. Some of these methods only consider the joint angle values and body positions; others include joint torques and external forces. In this regard, these methods can be seen as special cases of the kinematic and dynamic simulation methods previously described, in which the motion is composed of only one frame.

Static animation methods are also known as postural manipulation methods. Manipulation is the interactive specification of positions and postures for the DHM. It is an animation technique that usually involves

some movement of the figures, but only with the purpose to get them into a desired static posture. A way to manipulate a figure is to control the relative rotation of the segments by adjusting the joint angles using FK, as described in (Multon et al., 1999). However the user more commonly desires to specify the position or orientation of specific points and segments in the figure, and IK is used instead. Zhao and Badler (1994) obtained the posture of an articulated figure specifying spatial goals (positions and orientations). The fulfilment of these goals is included in the objective function of an optimisation problem in order to deal with the case in which all goals cannot be satisfied at once. Different weights can be associated to the goals to reflect their relative importance and different scaling factors can be associated to the DoFs in the figure to reflect their rigidity, improving posture realism. Instead of including the goals of the motion in an objective function, Baerlocher and Boulic (2002; 2004) defined a task-priority formulation. Priorities are associated to each goal, which is fulfilled at its best without affecting the achievement of higher priority goals. This formulation was developed by introducing an Augmented Jacobian matrix, which piles up the Jacobians of all the individual tasks of higher priority, and projecting the IK solution of each task on the null space of its augmented Jacobian, extending the concept stated by Equation (2.2). In the case of an unachievable set of goals, the approach followed by Zhao and Badler (1994) leads to a solution in which no goal is actually accomplished; on the other hand the task-priority formulation ensures the fulfilment of the goal with highest priority. Buss and Kim (2005) introduced a selectively damped least squares method to deal with the IK singularities. A different damping constant is applied to each singular value of the SVD of the Jacobian, effectively reducing oscillations when target positions are out of reach.

For what concerns posture prediction, a kinematic method has been developed by Park et al. (2006). The method is able to obtain the different postures humans are likely to assume in order to reach a target while avoiding collisions with the environment. Of all the postures which achieve the goal, only those in which the DHM does not collide with the obstacles are retrieved. Other posture prediction methods have been developed including dynamic variables. Seitz et al. (2005) developed a force-controlled posture prediction method (FOCOPP) to obtain postures which require minimum joint strain to be maintained under static loads. Finally, predictive dynamics has been adapted to static postures for the upper body by Yang et al. (2004) and Marler et al. (2005).

2.1.2 SOURCE OF REALISM TAXONOMY

Realism may constitute another feature according to which a taxonomy of simulation methods can be carried out: depending on the adopted source of realism, methods can be divided into data-based and knowledge-based methods. Data-based methods rely on experimental data to carry out the simulation, modifying and adapting them in order to fit the conditions to be simulated; whereas knowledge-based methods impose the simulated motion to follow a specific motion control law, i.e. the law which guides actually performed motions. Efforts have recently been made to combine the advantages of both approaches in a hybrid method, described in Section 2.1.2.3.

2.1.2.1 Data-based Methods

The main advantage of data-based methods lies in that they provide the simulation with an intrinsically realistic starting point. The goal of the simulation method is to maintain the realism of actually performed motions during the modification process. The main drawback, however, is that only tasks that are present in the database can be simulated; hence, to consider a new task, additional experimental data must be recorded and analysed, which is a complex and time consuming process.

Data-based methods can be divided according to whether the data are necessary to supply a reference motion to the simulation or whether the methods rely on a statistical analysis of the data.

Methods Based on Reference Motions

Some data-based methods which use a real motion for reference have already been mentioned in Sections 2.1.1.1 and 2.1.1.2. However, in this context, prediction methods must be distinguished from animation methods: as mentioned in Section 1.2, the aim of motion prediction is to generate a motion which is not only realistic, but also representative of the population to be predicted. This is why the motion editing methods used in animation, such as in (Gleicher, 2001; Unuma et al., 1995; Witkin and Popovic, 1995), simply require the availability of a motion of the same kind in order to modify it and generate a new motion. For instance, to obtain the animation of a particular way of running, nothing more than a realistic running motion must first be available. On the other hand, data-based motion prediction requires an entire database of motions in order to predict the motion of a subject belonging to the target population: for instance, to

predict the motion that a subject of specific anthropometric characteristics would perform to fasten a seat belt, motions representing the variety of behaviours actually adopted by similar subjects must be available. Such a database allows the prediction method to answer the question of how *could* a subject belonging to a specific population move, and how *would* they move. Hence, in data-based motion prediction methods, the data provide not only the source of realism but also the source of representativeness for the method.

One of the first data-based motion prediction methods was presented by Monnier et al. (2003) and consists of three steps: constitution of a structured database; reference motion selection; and its modification to meet the constraints for the new motion. The structured database is composed of experimental motions of subjects performing a specific task, which are classified according to the subject's characteristics, the environmental conditions and the descriptors associated to the adopted motion strategy and style. The different strategies and styles observed in motions belonging to the same population characterise the population variability. This variability may then be replicated in the predicted motions, hence representing the variability of the target population as well. This is achieved in the reference motion selection step, as described hereafter. Defining with the term "scenario" the combination of a subject and an environment, the input to generate a motion prediction is the characteristics of the scenario to be predicted. Among the motions composing the database, those carried out in the most similar scenarios to the one to be predicted are retrieved as eligible reference motions. By selecting among them one motion for each adopted strategy and style, a collection of reference motions is generated, which presents the variability encountered in actually performed motions in similar conditions. The prediction can then be carried out with each of the reference motions to replicate the encountered variability or only with the reference which represents the most common observed behaviour (Monnier et al., 2006). The modification process followed by Monnier et al. consists in modifying the end-effector trajectory of the reference motion in order to meet the new targets (adopting a VP or AP modification, Section 2.1.1.1) and in obtaining the DoFs profiles by solving the IK problem with the pseudo-inverse method, as described in Section 2.1.1.1.

The method presented by Park et al. (2004; 2008a), called memory-based motion simulation, is composed of three basic elements, similarly to the method presented by Monnier et al.: motion database, motion finder,

motion modification algorithm. The difference respect to Monnier et al. lies in how the variability in strategies and styles is identified. Monnier et al. identify it manually by analysing the experimental data (as described later in Section 2.3.3.2) and include the information in the structured database. Park et al. on the other hand have the motion finder module retrieve all motions in the database which were performed in similar scenarios to the one to be predicted and then apply an automatic process to identify the different movement techniques (detailed later in Section 2.3.3.2). Another difference between Monnier et al. and Park et al. lies in the motion modification process: the former's modification is per-frame, whereas the latter's is per-key (as described in Section 2.1.1.1).

Park et al. also presented a data-based posture prediction method with collision avoidance (Park et al., 2006), which was mentioned in Section 2.1.1.3. However, the database employed in the method is not constituted by experimental motions: on the contrary, it is a synthetic database, obtained by random postures which respect the joint RoMs and ensure that the projection of the CoM of the DHM lies in the base of support. Finally, of all the postures which achieve the goal, only those in which the DHM does not collide with the obstacles set by the user are retrieved.

The use of a synthetic database reduces one of the greatest drawbacks of data-based motion prediction methods, which is the cumbersome task of generating a large database of human motions that must be performed, captured and analysed. On the other hand though, also the main advantage of data-based methods is reduced, as the realism and representativeness of the database may not be guaranteed.

Methods Based on Statistical Analysis

Motion simulation methods which require data to supply a reference motion to the simulation may or may not need a large database depending on whether they are prediction or animation methods. On the other hand, the methods which use data for statistical analysis always require a large database: how large it must be mostly depends on how noisy and variable the data are.

One of the statistical methods used in motion simulation is functional regression. Functional regression was first presented by Faraway (1997) as a method to build predictive models. It is a statistical modelling technique which relates a smooth functional response $y(t)$ to some known covariates

x by a combination of parameter functions $\beta(t)$ which are to be estimated. The method is applied to the prediction of joint angle profiles in reaching motions: y represents the joint angle profiles and the covariates x are the coordinates of the target location $[c_x; c_y; c_z]$. The aim of the method is to obtain the parameter functions $\beta(t)$ which, multiplied by the covariates, best approximate the $y(t)$ curves in all motions of the database. Using a quadratic model, the joint angle profiles are expressed as:

$$\begin{aligned} y(t) = {} & \beta_0(t) + c_x\beta_x(t) + c_y\beta_y(t) + c_z\beta_z(t) + \\ & + {c_x}^2\beta_{x^2}(t) + {c_y}^2\beta_{y^2}(t) + {c_z}^2\beta_{z^2}(t) + \\ & + c_x c_y\beta_{xy}(t) + c_x c_z\beta_{xz}(t) + c_y c_z\beta_{yz}(t) \end{aligned} \tag{2.9}$$

Once the β functions are obtained by fitting Equation (2.9) to the joint angle profiles y of the database, the same equation is used to predict new y curves, given new target positions. However, the predicted motion may not exactly meet the target: only the joint space (i.e. DoF values) is modified by the method and no constraint on the task space (i.e. end-effector position) is imposed. For this reason, an *a posteriori* rectification is performed (Faraway et al., 1999) using IK, ensuring that the end-effector reaches the target while minimising the angle differences respect to the motion originally predicted through Equation (2.9).

Another way of employing functional regression analysis to carry out a motion prediction, this time without the need of rectifying the final posture, was described by Faraway (2003). The method relies on a different representation of the DHM linkage, introducing the stretch pivot coordinates (SPCs) which ensure that the constraints to achieve the goal in the motion are implicitly satisfied. The number of SPCs needed to describe a kinematic chain matches the degree of redundancy of the chain. SPCs form a linearly independent set and allow to avoid solving an optimisation-based IK problem to ensure that the goal is met: the very same values of the SPCs adopted in an actually performed motion may be used to determine the motion of a new subject performing the task in a new environment while ensuring that the new target is reached. However, rather than adopting the SPCs of a specific motion, Faraway proposes to follow two different paths to seek a greater generality to the predicted motion. One consists in averaging the SPCs of a reduced collection of motions which were performed in conditions similar to those to be predicted. The other

consists in performing a functional regression analysis of the SPCs to generate the predicted motion.

Functional regression has also been used by Faraway et al. (2007) to model and predict end-effector trajectories using Bézier curves. Bézier curves (Piegl and Tiller, 1997) are similar in concept to B-spines, (Section 3.5.1). Cubic Bézier curves are fitted to the trajectories in the database and the control points are obtained imposing maximum similarity between the original data and the Bézier curves. An average response over the complete data set is then generated and used to construct predicted trajectories.

The advantages of performing a functional regression analysis lie in the modelling of the contribution of all the factors which are considered to affect the motion, gaining insight into the effect of each factor (target distance, subject age and gender, etc.). Moreover the method is more rapid than optimisation-based methods. On the other hand, the main weakness of these simulation methods lies in that biomechanical considerations such as joint RoMs or balance conditions are not included. However, unless the conditions to be predicted correspond to large extrapolations from the database, the realism of the predicted motion is supported by the realism of the motions in the database.

Jung and Choe (1996) used a regression model to describe the discomfort associated to a specific posture while holding a certain load. Hip, shoulder, elbow and wrist angles, along with the load imposed by the object to be held, were selected as independent variables. Five different levels were assigned to each variable and volunteers were asked to hold all of the postures, obtained permuting the levels of each variable, and rate their perceived discomfort. A function relating discomfort to the covariates was then determined through regression and new postures were predicted by minimising the obtained discomfort function.

Zhang and Chaffin (2000) presented a method in which motions in a database are fitted with a function which assumes that the change in position of the end-effector is distributed across the joint angles in order to minimise the weighted sum of their displacement. The weights in the sum are obtained imposing maximum resemblance to the motions in the database. A statistical analysis of the weights is then performed to relate their values to certain predictors, which account both for the target position and the subject's anthropometry. Finally, the obtained weights are used to perform novel predictions adopting an IK method, with an accuracy which is similar to the trial-to-trial variability encountered in the database.

Mavrikios et al. (2006) used a statistical design of experiments approach both to evaluate the influence of human anthropometrics on car ingress motions and to predict novel motions. The body height, hip width and spinal flexibility appear to be the most relevant factors that influence the motion, and two levels for each factor are defined to carry out a 2^{n-1} factorial design. A 2^{n-1} factorial design consists in carrying out 2^{n-1} experiments to analyse the influence of n factors on the outcome of the experiments, considering that each of the n factors may assume 2 different levels or values. The authors set the limit between the levels for each factor in order to have approximately 50% of the experiments performed in each factor level. Experiments carried out in the considered permutations of the factor levels are then analysed to determine how each factor affects the joint angle profiles or point trajectories. Regression equations are obtained to relate joint angle profiles and point trajectories to the influence parameters, and are used to predict novel car ingress motions.

Finally, Wang (2002) combined the two data-based methods described in this section: those based on reference motions and those based on statistical analysis. Clutch-pedal operation motions are predicted following a similar modification method as that described in (Monnier et al., 2003). However the reference motion is not selected from the database, but is obtained from the database through statistical regression. A linear functional regression model is used to parameterise the DoFs of the DHM, the end-effector trajectory and its velocity. The covariates are selected as the seat height, the pedal travel length, travel angle and resistance as well as the subject's stature. Once the scenario to be predicted is defined in terms of values of the covariates, the DoFs profiles and end-effector trajectory obtained through the regression equations are used as reference during the simulation. The goals in the motion are fulfilled while resembling the obtained reference motion by solving the IK problem with the pseudo-inverse method described in Section 2.1.1.1. The predictions obtained with a functional-regression-reference are similar to actually performed motions, however adopting a motion from the database as reference seems to yield better results, probably due to the fact that the latter has actually been performed whereas the former is an averaged motion, not a real one. Faraway, on the other hand, seems to believe that predictions which consider averaged motions tend to be superior to the predictions based on a single motion, as averages possess lower variances (Faraway, 2003). However, the comparison performed by Wang appears to raise the

suspicion that the approximation carried out in functional regression might reduce the realism of the motion.

The data-based motion prediction methods described in this section are all kinematic. Although some animation methods reviewed in Section 2.1.1.2 include dynamics in the formulation, data-based dynamic motion prediction methods have not been encountered in the literature.

2.1.2.2 Knowledge-based Methods

As opposed to data-based methods, knowledge-based methods do not rely on a database of captured motions for reference, but aim to conferring realism to the predicted motion through the identification of an appropriate performance measure to be minimised, representing the motion control law that drives the motion.

The main advantage of knowledge-based methods is that they do not require the costly creation of an experimental database. Moreover, they may help to gain insight into the principles underlying human motion patterns: the closer the predicted motions are to actually performed motions, the more adequate the adopted performance will seem to be in representing the motion control law that guides the subjects' motion. On the other hand, the difficulty of identifying an adequate performance measure is the greatest drawback to knowledge-based methods. Moreover, it is reasonable to expect not only that different tasks require different performance measures, but also that different performance measures are associated to the various strategies and styles adopted to carry out each task. In addition, complex tasks (such as vehicle ingress-egress motions) may require different performance measures across the motion, as the various sub-goals of the motion are accomplished. These difficulties explain the reason why current knowledge-based methods are concerned with the prediction of relatively simple motions, such as lifting or walking, and have not yet taken up the challenge of predicting more complex motions or representing the variability of behaviours that people naturally seem to exhibit.

Furthermore, although no database of motions needs to be created for knowledge-based methods, experimental data should anyhow be available: the analysis of real motions may help attain deeper knowledge into the criteria adopted to carry out the considered task, and actually performed motions are necessary to validate the prediction method and the adequacy of the selected performance measure.

Performance Measures

Several performance measures have been proposed and analysed in the literature:

- Joint displacement

  Joint displacement is a purely kinematic performance measure employed in posture prediction (Yang et al., 2004), which minimises the difference between the predicted values of the DoFs q_i and those corresponding to a "neutral" posture q_i^N, defined as a relatively comfortable posture (such as standing with arms at one's sides, according to Abdel-Malek and Arora (2009)).

$$f = \sum_{i=1}^{nDoFs} w_i \left(q_i - q_i^N\right)^2 \tag{2.10}$$

  The sum is weighted through w_i to take into account the different motility of each DoF and to stress the importance of particular joints.

- Discomfort

  The discomfort performance measure described in (Yang et al., 2004) and in (Marler et al., 2005) is a variation of joint displacement: the joint displacement is normalised taking into account the upper q_i^U and lower q_i^L joint limits and penalty functions are added to represent the increase of discomfort as joint values approach their limits. G is the penalty associated to meeting the exact joint limits and QU_i and QL_i are functions which decrease the penalty to zero as the DoFs move away from their upper and lower limits respectively.

$$f = \frac{1}{G} \sum_{i=1}^{nDoFs} \left(w_i \left(\frac{q_i - q_i^N}{q_i^U - q_i^L} \right)^2 + G \cdot QU_i + G \cdot QL_i \right) \tag{2.11}$$

- Delta-potential-energy

  The delta-potential-energy performance measure, also employed in posture prediction (Yang et al., 2004), minimises the change in

potential energy respect to the neutral posture. Considering the system composed by n_M lumped masses:

$$f = \sum_{i=1}^{n_M} (m_i g)^2 * \left(h_i - h_i^N\right)^2 \tag{2.12}$$

where h_i and h_i^N represent the height of the i^{th} lumped mass in the predicted and the neutral posture, respectively. The masses of the segments in the DHM are the inherent weights for the motion of the different segments. However, this cost function only considers joint displacements which produce a vertical movement, hence the horizontal motion is uncontrolled.

- Effort

  The effort performance measure, described in (Abdel-Malek and Arora, 2009), is a variation of the joint displacement applied to motion prediction. The neutral posture is substituted by the initial posture of the motion $\mathbf{q}^{Ini}$, which must be resembled by the DoF values $\mathbf{q}(t)$ throughout the motion.

$$f = \int_{t=0}^{t=T} \left(\sum_{i=1}^{nDoFs} w_i \left(q_i(t) - q_i^{Ini}\right)^2 \right) dt \tag{2.13}$$

- Jerk

  The jerk performance measure consists in minimising the derivative of the acceleration across the motion:

$$f = \int_{t=0}^{t=T} \left(\sum_{i=1}^{nDoFs} \dddot{q}_i^{\,2}(t) \right) dt \tag{2.14}$$

  This condition was introduced by Hogan and Flash (1987) to generate smooth motions and has been used in (Abdel-Malek et al., 2006) to obtain the path to be followed by the hand in a reaching motion, minimising the jerk of the hand's trajectory.

- Dynamic effort

  Dynamic effort is an energy-related performance measure described in (Abdel-Malek and Arora, 2009; Chang et al., 2001; Chung et al., 2007; Xiang et al., 2007; Xiang et al., 2010b; Xiang et

al., 2010c), and adopted also in animation methods, as mentioned earlier in Section 2.1.1.2. The cost function is defined as the integral of squares of all joint torques over time:

$$f = \int_{t=0}^{t=T} \left(\sum_{i=1}^{nDoFs} \tau_i^{\,2}(t) \right) dt \tag{2.15}$$

A variation of Equation (2.15) has been adopted in (Seitz et al., 2005; Xiang et al., 2009; Xiang et al., 2010c; Xiang et al., 2011), and it consists in normalising the joint torques respect to their maximum value:

$$f = \int_{t=0}^{t=T} \left(\sum_{i=1}^{nDoFs} \left(\frac{\tau_i(t)}{|\tau_i|_{Max}} \right)^2 \right) dt \tag{2.16}$$

- Energy

  The mechanical energy expenditure across the motion is the performance measure adopted in (Ren et al., 2007). The mechanical energy is evaluated as the time integral of mechanical power across the motion:

$$f = \int_{t=0}^{t=T} \left(\sum_{i=1}^{nJoints} \left| \boldsymbol{\tau}_i^T(t)\, \boldsymbol{\omega}_i^{Rel}(t) \right| \right) dt \tag{2.17}$$

  where $\boldsymbol{\omega}_i^{Rel}$ is the relative angular velocity between the two segments linked by the i^{th} joint.

  Another formulation to minimise the energy in the motion, encountered in (Kim et al., 2006; Kim et al., 2007), consists in minimising the metabolic energy rather than only the mechanical energy. The metabolic energy is the chemical energy required by the muscles, which is transformed into mechanical energy, heat and basal metabolic energy. Hence, two additional terms appear respect to Equation (2.17): one representing the muscle maintenance heat (expended in proportion to the joint torque), the other the minimum amount of energy needed out to carry out metabolism activity at rest:

$$f = \int_{t=0}^{t=T} \left(\sum_{i=1}^{nJoints} \left| \boldsymbol{\tau}_i^T(t)\, \boldsymbol{\omega}_i^{Rel}(t) \right| + \sum_{i=1}^{nDoFs} h_{mi} \left| \tau_i(t) \right| + \dot{B} \right) dt \tag{2.18}$$

where h_{mi} is the generalised coefficient of the maintenance heat for the i^{th} DoF and $\dot{B}$ is the basal metabolic rate. This cost function is an adaptation of the metabolic energy performance measure proposed by Anderson and Pandy (2001) for musculoskeletal models.

- Dynamic jerk

  Dynamic jerk is defined in (Xiang et al., 2010a) as an alternative to the jerk magnitude: rather than evaluating the acceleration rate, the cost function takes into account the joint torque rate:

$$f = \int_{t=0}^{t=T} \left(\sum_{i=1}^{nDoFs} \dot{\tau}_i^{\,2}(t) \right) dt \tag{2.19}$$

- Stability

  The stability performance measure is generally considered in gait or standing posture simulation. In Xiang et al., 2010b) the stability is defined as the deviation of the zero moment point (ZMP) position from the centre of the support polygon:

$$f = \int_{t=0}^{t=T} \left(\sum_{i=1}^{nb} s_i^{\,2}(t) \right) dt \tag{2.20}$$

  Where *nb* is the number of segments which compose the foot support boundary and s_i is the distance between the ZMP and the i^{th} boundary segment.

Multi-Objective Optimisation

Human motions appear to be guided by more than one performance measure at a time (Dingwell et al., 2010). To deal with the issue that more than one performance measure may have to be taken into account in order to improve the realism of the predicted motion, multi-objective optimisation (MOO) has been applied to knowledge-based motion simulation.

One way of solving MOO problems consists in converting the original multi-objective problem into a single-objective optimisation problem by combining the various performance measures and minimising the combination, a process termed "scalarisation". The performance measures may be combined in different ways, as described in (Marler and Arora, 2004). The most intuitive is probably the weighted sum method, which obtains the cost function F as a weighted sum of the N considered performance measures:

$$F = \sum_{i=1}^{N} w_i f_i \tag{2.21}$$

Another method is called the weighted min-max method and consists in minimising the performance measure which presents the greatest value, hence priority is given to the performance measure which is approximated the least:

$$F = \max_{1 \le i \le N} w_i f_i \tag{2.22}$$

A third method instead, called the weighted global criterion method, minimises the following aggregate function:

$$F = \left(\sum_{i=1}^{N} w_i \left(f_i \right)^p \right)^{1/p} \tag{2.23}$$

The parameter p represents the emphasis that is placed on minimising the objective function with the highest value: when $p = 1$, Equation (2.23) reduces to the weighted sum method; and when $p \to \infty$, it reduces to the weighted min-max method.

Other scalarisation methods are described in (Marler and Arora, 2004), as well as methods which solve MOO problems without scalarisation (termed "vector optimisation" methods). However, the three reported methods are of interest since Yang et al. (2004) compared them to obtain posture predictions combining the following performance measures: joint displacement, discomfort and delta-potential-energy (Equations (2.10), (2.11) and (2.12), respectively). The postures obtained with MOO appear to differ from those obtained with each single-objective optimisation, but on the other hand they are very similar one another. This result may hint that

combining performance measures is more decisive than the way in which they are combined.

MOO has also been used to investigate the most appropriate performance measures (Xiang et al., 2010b). As opposed to the posture prediction in (Yang et al., 2004), in which the weights associated to each performance measure are simply decided and imposed to the simulation (*a priori* articulation of preferences), Xiang et al. carried out several simulations with different weights, in order to assess the importance of each performance measure and obtain the best combination (*a posteriori* articulation of preferences). The method is applied to a lifting task motion prediction in which the considered performance measures are dynamic effort and stability (Equations (2.15) and (2.20), respectively). When only stability is considered, the resulting simulation differs from experimental data much more than when effort is considered as well. By varying the weights of the two performance measures, the authors are able to obtain the set of weights which minimise the error of the simulation respect to experimental data.

When several performance measures are combined, as in MOO, it is useful to transform them so that they all have similar orders of magnitude and all share the same dimension. Different transformation methods are described in (Marler and Arora, 2005) and yield dimensionless functions:

- Lower-bound approach

  The performance measure is normalised respect to the modulus of its minimum value:

$$fn_i = \frac{f_i}{\left|\min f_i\right|} \tag{2.24}$$

  The lower limit of the normalised function fn_i is restricted to –1 (+1 if $\min f_i > 0$) whereas the upper value is unbounded. This method may lead to numerical difficulties if the denominator is close to zero.

- Upper-bound approach

  The performance measure is normalised respect to its maximum value:

$$fn_i = \frac{f_i}{\max f_i} \tag{2.25}$$

The upper limit of the normalised function fn_i is restricted to 1 whereas the lower value is unbounded. Also this method may lead to numerical difficulties if the denominator is close to zero.

- Upper-lower-bound approach

  The normalised performance measure is defined as:

$$fn_i = \frac{f_i - \min f_i}{\max f_i - \min f_i} \tag{2.26}$$

  If $\min f_i$ and $\max f_i$ are determined accurately, the normalised function is restricted between 0 and 1. This method is the most robust transformation method as division by zero is always avoided for any non-constant function.

The advantages of normalising the performance measures can be noticed in simulations with both *a priori* and *a posteriori* articulation of preferences. In the former, normalisation helps setting the weighting parameters more accurately since the weights strictly represent the relative importance that a performance measure should have respect to the others, not having to account for the relative magnitudes of the performance measures. In the latter, normalisation improves the ability to depict the whole feasible set of solutions by systematically varying the weights: when performance measures are not normalised, a single one may dominate the aggregated objective function, clustering the solutions in one area rather than spreading out evenly over the feasible set.

Especially in simulations with *a posteriori* articulation of preferences, a convex combination of performance measures is used, i.e. the set of weights is restricted to sum up to 1. This way the set of weights generating a specific simulation is unique and it is easier to formulate a systematic approach for ensuring an even, consistent sampling of the weight space in terms of the weights' relative values, as in (Xiang et al., 2010b).

2.1.2.3 Hybrid Methods

In parallel to the hybrid prediction method presented in this document, another method has been developed with the aim of combining the

advantages of both data-based and knowledge-based motion prediction methods (Xiang et al., 2012).

The method proposed by Xiang et al., called hybrid predictive dynamics, modifies the knowledge-based framework of predictive dynamics (Abdel-Malek and Arora, 2009; Xiang et al., 2010b; Xiang et al., 2010c) by including the condition that the DoFs in the DHM should resemble experimental values. The adopted parameterisation consists in using B-spline curves to approximate the DoF profiles of an existing motion. The control points of the B-splines constitute the design variables for the optimisation problem, as described in Section 2.1.1.2. The data-based contribution to the method appears as a condition on the values of the control points, which must resemble the values with which the reference motion was approximated. This condition is included as an inequality constraint, and may also appear in the objective function along with the selected performance measure.

It may be argued that the data-based information included in hybrid predictive dynamics is extremely limited for a prediction method, as the experimental data correspond to one single captured motion: not only the different behaviours that people exhibit are not taken into account, but there is no way to assess that the considered motion is actually representative of the motions which may be performed in similar conditions. However, the motivation behind the hybrid predictive dynamics method is to refine the purely knowledge-based predictive dynamics method by including limited experimental data: the aim is to enhance the realism of the prediction without losing the advantage of knowledge-based methods of not requiring the cumbersome generation of a database of captured motions.

Principal component analysis (PCA), introduced in Section 2.1.1.2, may be regarded as a hybrid data- and knowledge-based animation method. On the one hand, the parameterisation carried out by PCA is data-based, since the principal components are extracted from experimental motions. On the other, the PCA simulation method adopted in (Lim et al., 2005; Park and Jo, 2004; Safonova et al., 2004) consists in modifying the contributions of each principal component with the aim of minimising the performance measure of dynamic effort, defined in Equation (2.15). The method, however, is employed only for animation purposes and apparently has not found application in motion prediction methods. This is probably due to the assumption on which PCA is based: that the DoF profiles of the

motion to be simulated may be expressed as a linear combination of the experimental DoF profiles (moreover approximated to the first *k* principal components). Such an assumption may not be acceptable for prediction methods, since it limits the richness of the possible profiles generated.

2.2 VALIDATION METHODS

As mentioned earlier, motion animation and motion prediction have different goals, since the former desires the output to *look* realistic whereas the latter expects the resulting motion to *be* both realistic and representative. It follows that the validation process for both kinds of simulations is different.

Since motion animation is mainly concerned about the looks of the generated motion, the validity of the method is usually assessed by visual inspection: snapshots of key events in the motion are commonly reported in the literature, for instance in (Bindiganavale and Badler, 1998; Chang et al., 2001; Gleicher, 2001; Lee and Shin, 1999; Park and Jo, 2004; Popovic and Witkin, 1999; Safonova et al., 2004; Unuma et al., 1995; Yamane et al., 2004).

Motion prediction, on the other hand, requires a more thorough analysis of the resulting motion, compared to actually performed motions in similar conditions. To validate data-based methods, it is common to compare the predicted motion against motions performed by a sample of the target population, recorded together with the motions that would compose the database, as in (Monnier, 2004; Park et al., 2004; Wang, 2002; Zhang, 2002). In knowledge-based approaches, instead, data are not used in the prediction method and must be collected specifically for validation purposes. Some authors, however, carry out the validation through visual inspection, as in motion animation (Abdel-Malek et al., 2006; Chung et al., 2007; Jung and Choe, 1996; Kim et al., 2006; Kim et al., 2007; Marler et al., 2005; Seitz et al., 2005; Xiang et al., 2010c; Yang et al., 2004).

Other authors compare the results of their prediction method to measured data, representing the measured and predicted magnitudes in the same graph. Usually, not all the variables describing the motion are compared, but only a selection of them, called predictors, is analysed. These predictors are chosen among the variables as those which best characterise and represent the most relevant features of the motions. Examples of selected predictors are the torso, hip, knee and ankle flexion-extension angle

profiles for walking (Ren et al., 2007); the trajectories of two markers, one placed at the acromion (shoulder) and the other at the trochanterion (hip), for vehicle ingress-egress motions (Mavrikios et al., 2006); or the flexion-extension torques at the elbow, shoulder, hip and knee for lifting motions (Chang et al., 2001).

Other authors include a statistical analysis of the available data in their validation, and compare the results of the prediction with the average profiles observed in motions actually performed by subjects belonging to the target population, along with a measure of their variability. The intention is to prove that the predicted motion is contained in the range of natural variability encountered in actually performed motions, i.e. that the probability that the predicted motion could have been performed by a subject of the target population is not very low. This probability decreases with the distance between the predicted motion and the average motion of the target population. For normally distributed data, the probability decreases following a cumulative Gaussian curve. Some authors carry out a qualitative validation (Anderson and Pandy, 2001; Chang et al., 2001; Ren et al., 2007; Xiang et al., 2009; Yang et al., 2007) whereas others perform a quantitative validation (Faraway et al., 2007; Monnier, 2004; Park et al., 2004; Zhang, 2002). Qualitative methods are based on comparing the profiles of selected kinematic and dynamic magnitudes obtained in the prediction against the profiles of actually performed motions in similar conditions. On the other hand, quantitative methods rely on the evaluation of a specific measure. Both qualitative and quantitative validation methods are presented hereafter.

In the validation of the human walking prediction method proposed by Anderson and Pandy (2001), the authors considered the variability of the DoF profiles as an area defined by a standard deviation σ above and below the average profile μ. For normally distributed data, 68.27% of the data lie in the range delimited by $\mu \pm \sigma$. This means that more than 30% of actually performed motions are expected to exceed the $\mu \pm \sigma$ range. Therefore, a motion that exceeds the range only states that its probability of belonging to the target population is below 32.73%: it does not prove the motion to be invalid. A range of $\mu \pm 2\sigma$ might have been more critical in establishing whether the predicted motion may not be reasonably considered as performed by the target population, since only 5% of the motions performed by the target population fall out of that range.

Xiang et al. also carried out a statistical analysis of the motions performed by subjects of the target population, and compared the most relevant DoFs in walking (Xiang et al., 2009; Xiang et al., 2011) and in lifting (Xiang et al., 2010b) to the average profiles of the measured data. However, rather than representing the variability of the population, as in (Anderson and Pandy, 2001), the authors reported the 95% confidence intervals (CIs) for the mean μ. Such CIs delimit an area in which the actual mean of the target population has 95% probability of falling. The thickness of the area depends on how many data were used to evaluate the mean μ: the more data were available, the more exact the mean estimation is and the closer the CIs are to μ. What the CIs for the mean do not represent is the variability of the population: they only indicate how exact the estimated mean μ is. Hence, they are not an appropriate variability measure against which to compare a predicted motion. Nevertheless, if a motion falls in the 95% CIs for the mean, it also belongs to the range delimited by the 95% CIs for the population (i.e. $\mu \pm 2\sigma$ for normally distributed data).

On the other hand, the information provided by the CIs for the mean served the purpose of the posture prediction validation presented by Yang et al. (2007): the validation procedure carried out consists in replicating captured upper body postures by adopting the posture prediction method described in (Yang et al., 2004). The values assumed by the selected predictors in the experimental postures are compared to the predicted values and a linear regression is performed to best fit the experimental-vs.-predicted data. The CIs for the obtained average trend line are used to determine whether the desired slope value of the trend line (unity) is included in the calculated CIs. Moreover, the accuracy of the trend line respect to the data is assessed through the coefficient of determination R^2.

For what concerns quantitative validation methods (Faraway et al., 2007; Monnier, 2004; Park et al., 2004; Zhang, 2002), the measure commonly employed is called time-averaged distance (TD) and quantifies the difference between the predicted and experimental motions:

$$TD = \frac{1}{T}\int_0^T \left\| \mathbf{x}_P(t) - \mathbf{x}_E(t) \right\| dt \tag{2.27}$$

where $\mathbf{x}_P$ represents the value of the predictor $\mathbf{x}$ in the predicted motion and $\mathbf{x}_E$ its value in the actually performed motion. The validation is carried out by comparing the distance between the predicted and an experimental

motion to the distances between actually performed motions in similar conditions, as detailed hereafter.

Both Monnier (2004) and Park et al. (2004) employed TDs to validate their motion prediction methods (described in Sections 2.1.1.1 and 2.1.2.1) applied to seated reaching motions. Simple motions appear to be more apt for validation purposes as they do not present the variety of strategies and styles which characterise more complex motions. To validate a complex motion, in fact, it would be necessary to find at least a subject which performed the motion with exactly the same style during the whole motion, which is highly improbable. Both Monnier and Park et al. selected as predictors the positions of the end-effector and of the upper body joint centres and calculate a TD for each predictor. The TDs are then compared to the inherent variability in repeated reaches, quantified by applying Equation (2.27) to each pair of repeated reaching motions, for each of the selected predictors. The parameters thus obtained are termed within-subject inter-trial motion variability (WIMV) as they refer to reaches towards the same target carried out by the same subject. Park et al. observed that when the target in the reference motion is close to the target in the prediction scenario, the mean TDs are comparable to the mean WIMVs: the accuracy of the prediction is within the natural variability in human motion. However, increasing the distance between targets, the difference between the mean TDs and the mean WIMVs is more significant. Park et al. stated that the TDs are not significantly different from the WIMVs for close reference and prediction targets, and that the differences are significant for further targets, defining the threshold for significance with a p-value of 0.05, i.e. there is less than 5% probability of a WIMV to match or exceed the obtained TD value. Monnier et al. on the other hand carried out the reaching predictions following a slightly modified methodology than the one described in Section 2.1.2.1: the end-effector trajectory in fact is not obtained modifying the reference trajectory but the actual trajectory followed in the experiment is imposed in the prediction. The TDs between the predicted and the actually performed motions are then compared to the WIMVs. Monnier established a threshold to determine whether a predicted motion is to be considered realistic or not: if the calculated TDs do not exceed the WIMVs by more than 10mm, the motion is considered realistic. However, the WIMVs are different for each predictor (the variability increases towards the most distal joints), therefore a relative increment respect to each WIMV may have been more adequate to define a threshold. The results of the validation process lead to state that the prediction of the

most distal joint trajectories is very satisfactory, probably due to the imposition of the actual trajectory for the end-effector, whereas the error in more proximal joint trajectories depends on the distance between the reference and the prediction targets, in agreement with Park et al. While Monnier focused only on seated reaching motions, Park et al. further extended the validation to load-transfer motions. In this case, however, the computed TDs are compared to a different measure of variability, termed between-subject inter-trial motion variability (BIMV), obtained by applying Equation (2.27) to motions performed in the prediction environment by subjects of similar anthropometric characteristics (not the same subject, as for WIMVs). Once again, the mean TDs appear to be comparable to the mean variability measures.

TDs were employed also by Zhang (2002) to assess the validity of the VP and AP modification methods described in Section 2.1.1.1. The motions involved are once again seated reaching motions and the predictors are similar to those selected by Monnier (2004) and Park et al. (2004). The average TDs in the location of the predictors obtained with the VP and AP approaches are compared showing that both approaches yield very similar results as mentioned earlier.

Also Faraway et al. (2007) used TDs to validate the functional regression method used to model and predict end-effector trajectories, comparing the TDs between the predicted and experimental trajectories to the natural WIMVs and BIMVs observed in the experimental data. The error in the trajectory predictions appear to be comparable to the encountered natural variation in human motions.

A common inappropriate practice in validation (Prieto Valiente and Herrantz Tejedor, 2005) is to define a threshold according to which results are considered significant and methods valid: for instance, the p-value limit as in (Park et al., 2004) or the margin to the natural variability introduced in (Monnier, 2004). It is more important to report the actual value of p or of the WIMVs, respectively, rather than to classify the results as significant or not, as a slight crossing of the threshold is considered as unsatisfactory as a large one.

2.3 EXPERIMENTAL DATA CAPTURE AND ANALYSIS

Regardless of whether a prediction method is data-based or knowledge-based, experimental data are always required, either for both the database construction and the validation processes (data-based methods), or for the validation process alone (knowledge-based methods). The captured data must then be reconstructed adopting the same DHM employed in the motion prediction. Finally, the reconstructed motions should be analysed to characterise the temporal features of the motion, to identify the different strategies and styles adopted during the experiments, and/or to assess the influence of experimental parameters on the motions. The analysis of the motions composing the database is necessary in data-based prediction methods, and useful in knowledge-based methods, as it may provide insight into the most adequate performance measures for the considered task.

An overview of the three above-mentioned steps, shown in Figure 2.1 below, is presented in the following sections.

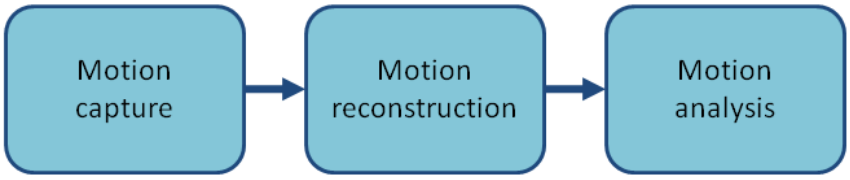

Figure 2.1: Steps characterising experimental capture and analysis.

2.3.1 MOTION CAPTURE

The first step consists in recording the subjects' kinematic and kinetic observable variables involved in the motion.

For what concerns the motion's kinematics, the capture may be based upon several technologies: some rely on the tracking of sensors (markers) located on the subject's skin, whereas others are markerless. Among the sensor tracking technologies, the optoelectronic capture systems are the most commonly employed. In these systems, several cameras simultaneously record reflective or active markers placed on the subject's skin. All the 2D data recorded by each camera are used in stereophotogrammetric methods to generate a 3D trajectory for each marker. The major drawback of optical systems is that the position of a

marker cannot be calculated unless at least two cameras see it. It is quite common that a marker is hidden from a camera, which occurs whenever an object interposes between them (the object may be an element of the environment or the same body of the subject). However, provided at least two cameras see the marker freely, its trajectory can be adequately recorded. The obtained marker trajectories are then used to guide the motion of a DHM. This process is called kinematic motion reconstruction and is described in the following section.

On the other hand, in order to record the motion's kinetic variables, both the environment and the subject may be equipped with appropriate sensors. The environment with which the subject interacts may present measurement devices such as force sensors (Wang et al., 2000), force plates (Robert et al., 2006), or pressure maps (if the pressure distribution over a surface is to be measured). Including kinetic data in the definition of the motion of the DHM is a process called dynamic motion reconstruction and is described in the following section along with the kinematic motion reconstruction.

2.3.2 MOTION RECONSTRUCTION

According to whether the motion of the DHM is to be defined only kinematically or also in dynamic terms, the motion reconstruction process is either kinematic or dynamic.

Kinematic motion reconstruction uses inverse kinematics to obtain, from the captured marker trajectories, the motion of the DHM, which may be described using relative (Lu and O'Connor, 1999) or natural coordinates (Ausejo, 2006; Ausejo et al., 2011). The methods may be divided into local and global methods: the former obtain the motion of each segment in the DHM independently from the others; the latter obtain the motion of all segments at once, considering the constraints imposed by the joints connecting the segments. The reconstruction is usually carried out defining an optimisation problem in which the points representing the markers on the DHM must minimise the difference between their position and the position of the captured markers at each frame in the motion.

The reconstructed motion is an approximate representation of the actually performed motion due to errors deriving from the instrumental measurements and the assumptions made in the definition of the adopted DHM. For what concerns the instrumental errors, their high-frequency content may be eliminated by using low-pass filters on the trajectories of the

captured markers: the characteristic frequencies of captured motions (such as vehicle ingress/egress or gait) are relatively low and signals of above 5-6Hz may generally be considered as noise (Ausejo, 2006). Lower-frequency errors may not be eliminated that easily, such as the skin artefact error, which derives from the assumption that the markers placed on the skin are rigidly connected to the bones. The skin artefact alone may produce errors of up to 4cm, due to the movement of the marker on the skin with respect to the underlying bone (Cappozzo et al., 1996). Errors in the reconstruction are due not only to the marker capture system: the adopted DHM also introduces errors in the reconstruction. To start with, a DHM is an approximation of the complex human musculoskeletal system: the accuracy required in the DHM definition depends on the level of detail expected from the reconstruction; nevertheless some assumptions are always made to create a mathematical model of the human body. Moreover, the DHM must be tailored to the subject it represents and although some anthropometric parameters may be measured (subject weight, body segment lengths, marker positions, etc.), others are usually estimated (joint centre locations, centre of mass locations, moments of inertia, etc.).

For what concerns dynamic motion reconstruction, the kinetic response of the subject is estimated through inverse dynamics, given the measured kinematic and kinetic variables of the motion. Dynamic motion reconstruction can either be a post-process of the kinematic reconstruction (Robert et al., 2006) or the dynamic data can be used to adjust the kinematic reconstruction (Riemer and Hsiao-Wecksler, 2008), seeking to reduce the error it involves. In the first case, ID is performed to obtain the forces and torques acting at the joints in the DHM: the motion of the DHM is defined by the kinematic reconstruction and the external forces it is subject to are obtained through the measurements of the kinetic sensors, appropriately filtered. Robert et al. (2006) filter the results of the kinematic reconstruction before performing ID to avoid high values of accelerations due to the independently reconstructed frames. Riemer and Hsiao-Wecksler (2008), on the other hand, seek to perform a more accurate motion reconstruction considering at once the measurement of the marker positions and of the forces acting on the human body. The reconstruction is carried out by solving an optimisation problem in which the measured forces must be resembled while the position of the markers must match the recorded positions within a specified tolerance, improving the reconstruction of both joint angle and torque profiles.

2.3.3 MOTION ANALYSIS

The analysis of databases of reconstructed motions is very useful both in the generation of a structured database and in the understanding of the human motion and the factors that affect people's performances. The analysis of performed motions can lead to identifying the most relevant frames in the motion (key-frames), establishing the natural variability in behaviour exhibited in the performed motions, and assessing the influence that experimental parameters may present on the motions.

2.3.3.1 Key-Frames

As mentioned earlier, key-frames are defined as the frames at which relevant (or key) events occur in the motion and their identification is important to determine the sub-goals which are set and met in actually performed motions. Key events are usually associated to a specific interaction between the subject and the environment, which may be classified according to whether a collision is established or avoided. The identification of the key-frames may be carried out in several ways: through visual inspection of motion clips, for instance to determine when obstacles are successfully avoided (Chateauroux and Wang, 2010); by analysing the velocity profiles of the end-effector seeking null values, under the assumption that the end-effector only stops for a reason related to the fulfilment of the task (Chateauroux et al., 2011); similarly, by analysing the end-effector acceleration profiles seeking null values, to take into account changes of velocity direction (Bindiganavale and Badler, 1998); or analysing the force sensor measurements to establish when a contact is produced, as the sensor would start reading a non-zero force.

2.3.3.2 Strategies and Styles

A common goal in database analysis is to identify the different behaviours exhibited while carrying out a specific task: for instance, seat belt reaching (Monnier, 2004; Monnier et al., 2003), vehicle ingress or egress (Ait El Menceur et al., 2009; Ait El Menceur et al., 2008; Chateauroux and Wang, 2010; Chateauroux et al., 2011), or lifting motions (Park et al., 2005b). As mentioned earlier (Section 2.1.2.1), the behaviours can be classified according to the adopted strategies or styles. Strategies usually differ one from the other in such a clear way that they may be identified through visual inspection of the motion clips. For instance, Monnier et al. (2004; 2003) report that for seat belt reaching there are three different strategies

according to how the latch plate is reached: with the right hand; with the left hand above the left shoulder; and with the left hand below the left shoulder. On the other hand, motion styles (also referred to as sub-strategies) present more subtle differences, which may become evident analysing the joint angle profiles or point trajectories of the motion. In this regard, Monnier et al. are able to identify several styles depending on the position of the hand on the belt, on whether the torso moves or not, and on the orientation of the hand. Generally, the adopted styles depend on which strategy was adopted in the first place, hence the term "sub-strategy".

The qualitative analysis of the database carried out by Monnier et al. was also adopted by Chateauroux and Wang (2010) to identify the strategies and styles which characterise car egress motions, performed by both young and elderly people. The encountered behaviours are classified into strategies depending on whether the subjects start standing with only the left foot on the ground or whether the pelvis lifts only when both feet are out of the vehicle for support. The age effect is evident in the choice of behaviour, since elderly people tend to seek maximum stability and adopt the second strategy, which is never employed by younger subjects. Key-frames are identified for each strategy, depending on the interactions which occur between the subjects and the environment, and motions are further classified according to the adopted styles (for instance, some subjects tend to bend laterally whereas others rotate the torso). The contacts between the subjects and the environment highlight the support sought by the subjects, which once again reveals differences between young and elderly subjects: the latter tend to rely more often and on more elements of the environment for support.

Chateauroux et al. (2011) also analysed truck cabin egress motions, which are more complex than car egresses as more contacts with the environment are involved and the coordination between the upper and lower limbs plays a relevant role. Two strategies were identified for the lower limbs, similarly to (Chateauroux and Wang, 2010). Additionally, the upper limb motions (how the hands moved along the handles) were classified into four different strategies. The visual identification of the various strategies is supported by contact diagrams, which show how contact forces between the hands and feet of the subjects and the environment are distributed throughout the motion. The contact diagrams prove to be a resourceful aid to understanding how the forces are transferred from one support to the other and how the upper and lower limbs are coordinated.

Both ingress and egress motions were analysed by Ait El Menceur et al. (2008). The authors identified the same strategies described by Chateauroux and Wang (2010), i.e. one foot or two feet, for the egress motions and define similar strategies for the ingress motions as well. However the egress styles defined by Ait El Menceur et al. do not match those of Chateauroux and Wang: the former focus more on the position of the body respect to the vehicle, whereas the latter give more importance to the motion of the trunk. In (Ait El Menceur et al., 2008) not only the age effects are considered, as the motions were performed by both young and elderly subjects, but also the effect of prostheses is taken into account, as some subjects had undergone hip or knee replacement surgery in one or both legs. Analysing the frequency with which each strategy and style is adopted, it appears that elderly subjects prefer multiple supports throughout the motion, in agreement with (Chateauroux and Wang, 2010).

The differences in behaviour of young and elderly people were also studied by Reid et al. (2010), who focused on stair climbing motions. A principal component analysis (PCA), described in Section 2.1.1.2, was performed on the angles, forces and torques at the knee joint for young and elderly subjects respectively, to discover common and singular traits between the two groups. The components which seem to be most affected by the subject's age are generally the first or second principal component, suggesting that the adopted strategies are substantially different. Specifically, the greatest variations are encountered in the dynamic variables, apparently due to a different strategy for load redistribution across the joints adopted by elderly and young subjects.

Alongside the qualitative methods for strategy and style identification, quantitative methods have been proposed, most of them relying on statistical classification techniques. One of these methods was presented by Park et al. (2005b), as mentioned in Section 2.1.2.1. The authors define a quantitative index, called joint contribution vector (JCV), to represent the relative importance of the DoFs in the fulfilment of the considered task, and employ statistical clustering methods to classify the motions according to the values of their JCV. Considering for simplicity that the task goal consists in moving the end-effector along the x axis to reach a determined position, the JCV is a vector, whose length matches the number of DoFs in the DHM, and is defined as follows. Each element of the JCV represents the contribution of the corresponding DoF to the achievement of the task goal along the x axis:

$$JCV_{x\,i} = 100 \frac{C_x^{\,i}}{\sum_{j=1}^{nDoFs} \left| C_x^{\,j} \right|} \tag{2.28}$$

where

$$C_x^{\,i} = \int_{t=0}^{T} \left(x - x^i \right) dt \tag{2.29}$$

C_x^i is the contribution of the i^{th} DoF; x is the trajectory of the end-effector in charge of accomplishing the goal; and x^i is its trajectory if the i^{th} DoF is fixed to zero: the greater the difference in position is, the more important is the effect of the considered DoF on the motion. The contribution C_x^i is then normalised in Equation (2.28) to form the JCV.

If the end-effector moves in a 3D space, Equation (2.28) actually represents the normalised contribution of all joints to the end-effector trajectory along the *x* axis only. In this case, similarly to $\mathbf{JCV}_x$, also $\mathbf{JCV}_y$ and $\mathbf{JCV}_z$ are defined. Combining the vectors, a unique vector is created to characterise each motion: $\mathbf{JCV} = \left[\mathbf{JCV}_x \, \mathbf{JCV}_y \, \mathbf{JCV}_z \right]$. A JCV is calculated for each motion and cluster techniques are adopted to separate the data into *k* clusters, in order to maximise the similarity of JCVs within each cluster and maximise their dissimilarity among clusters. The obtained clusters are assumed to represent the alternative movement techniques, and the method succeeds in identifying stoop and squat lift motions (Park et al., 2005b) and different styles employed in whole-body reaching or load-transferring motions (Park et al., 2008a).

A similar technique was adopted to identify different balance strategies (Park et al., 2008b), through the definition of a balance strategy vector (BSV), which represents the contribution of each DoF to the position of the DHM centre of mass (CoM) in the horizontal plane. In fact, in static conditions, balance is lost when the projection of the DHM centre of mass falls out of the support area of the feet. The BSV is calculated, analogously to the JCV but the contribution C_x^i is defined considering the position of the CoM rather than of the end-effector. The BSV was adopted to identify different balance strategies exhibited in lifting motions. Three strategies were encountered: in one, the greatest contributors to the motion

were the knee and ankle joints; in the second, also the shoulder played a relevant role; and in the third also the hip and elbow seemed to be considerably involved in the motion. Apparently, the subjects were consistent in the choice of the lifting strategy, regardless of the variations in weight, size or position which characterised the object to be lifted.

The JCV was also adopted by Ait El Menceur et al. (2009) to perform a quantitative strategy identification for vehicle ingress motions. The authors defined a 3 based joint contribution vector (3BJCV) which combines three JCV, one for each chain in the model: each of the JCVs represents the contribution to the position of the pelvis of the DoFs in the two lower limb chains and in the head-and-trunk chain, respectively. A clustering technique was applied to the 3BJCV and led to the identification of two main strategies, depending on whether the vehicle is first entered with the right foot or with the pelvis. To further classify the motions, the same kinematic chains were considered, albeit independently: for each chain, the authors analysed the contribution of each DoF in the chain to the position of the chain end-point. The results of this quantitative classification are in agreement with the qualitative analysis of ingress motions performed in (Ait El Menceur et al., 2008): most strategies are identified by both procedures, demonstrating that a good correspondence may be achieved between manual and automatic motion analysis.

2.3.3.3 Influence of Experimental Parameters

Another interesting application of motion analysis is to determine which factors mostly affect the way in which motions are performed. Some factors may be subject-related, such as subject stature or weight, or environment-related, such as object disposition in the environment or specific environmental characteristics (e.g. softer vs. harder or shorter vs. taller chairs in seating motions).

Some of the works presented in Section 2.1.2.1 perform simulations based on a statistical analysis of captured data. The methods seek to determine a regression function which relates kinematic and dynamic variables to a set of controlled parameters, in order to simulate novel motions through the application of the obtained regression function. Therefore, the first part of the method consists in evaluating the effect of several factors on the performed motions. For instance, Faraway (1997) analysed the effect of the target position on the joint angle profiles of reaching motions; Jung and Choe (1996) determined how a lifting posture

and the carried load affect the perceived discomfort of subjects; and Mavrikios et al. (2006) assessed the influence of anthropometric parameters on car ingress motions.

Motion analysis has also been carried out without generating a predictive model for novel motions. Wang et al. (2000) analysed the effect of 4 environmental parameters involved in clutch-pedal operations (seat height, pedal travel length, pedal travel angle and pedal resistance) on the motion performed by three groups of people: short females, average males and tall males. An analysis of variance[5] (ANOVA) was conducted on each group separately and also for all subjects together. The pedal characteristics seem to consistently affect the duration of the foot deceleration phase after the peak velocity during the pedal depression. On the other hand, the seat height apparently has a strong effect on the hip, knee and ankle flexion-extension angles. Attention is paid to the direction of the pedal force, which is not uniquely determined by the geometric configuration of the system due to friction. Although the flexion-extension angles are affected by the seat height, the direction of the pedal force seems to be consistently aligned with the direction defined by hip and the pedal contact point: the friction force exerted on the pedal tends to adapt in order to maintain such a pedal force direction. The authors further investigate whether the force direction is such that the minimal joint torques are required: to this purpose, the posture at the end of pedal travel (corresponding to maximum pedal reaction) is estimated minimising a minimum torque objective function, and the results seem to agree with the experimental data.

Reed et al. (2000) analysed the effect of subject- and environment-specific parameters on the trajectories followed by the feet of truck drivers entering a truck mock-up with two adjustable steps. Both the subject stature and mass were considered, as well as the relative position of the adjustable steps. Cubic Bézier curves were fitted to the foot trajectories and normalised in order to examine the shape of the trajectories independently of the overall extent of the movement. A multivariate analysis of variance (MANOVA) revealed little dependency on the step configurations, whereas the subject-specific parameters were found to mostly affect the shape of the trajectories.

[5] In ANOVA each factor is considered to be independent from the rest. The interaction between factors is taken into account in multivariate analysis of variance (MANOVA).

2.4 CONCLUSIONS

In this chapter some of the main motion simulation methods developed to date have been reviewed, as well as the adopted validation procedures. Subsequently, motion capture and reconstruction techniques have been introduced, in order to explain how motion databases are generated, and motion analysis methods have then been described.

For what concerns motion simulation methods, the review highlighted the advantages and limitations of the current approaches. The following chart (Figure 2.2) summarises the classification of the main motion simulation methods reviewed in Section 2.1.

Kinematic simulation presents the largest variety of developed methods. The reason is that for most animation techniques the modification of the kinematic variables alone provides a wide range of possibilities in the generation of apparently realistic motions. Also in motion prediction, kinematic variables seem sufficient to describe motions in which dynamics does not play a relevant role, for instance motions in which no significant forces characterise the interaction between the DHM and the environment.

The appeal of kinematic methods lies in the relatively low computational cost required to carry out the simulation. On the other hand, tasks in which strength or effort plays a relevant role may not be simulated adequately, let alone predicted. It may be noticed in Figure 2.2 that no dynamic data-based prediction method has been developed, to our best knowledge. Motion edition methods involving dynamics have been developed (Abe et al., 2006; Lim et al., 2005; Liu and Popovic, 2002; Park and Jo, 2004; Popovic and Witkin, 1999; Safonova et al., 2004), but are meant as animation tools: in fact, simplifications which may not be compatible with the goals of motions prediction are adopted in the formulation, in order not to excessively compromise computational efficiency. Dynamics is currently included in motion prediction only in the knowledge-based framework of predictive dynamics (Abdel-Malek and Arora, 2009; Xiang et al., 2010b; Xiang et al., 2010c) and in the more recent hybrid method (Xiang et al., 2012) originated therefrom.

However, the main drawback of knowledge-based methods is the difficulty of identifying the most adequate performance measure to be minimised. Multi-objective optimisation approaches have been adopted (Xiang et al., 2010b; Yang et al., 2004) in order to generate more realistic

predictions, as single performance measures did not seem to be able to adequately represent even simple tasks such as reaching.

Moreover, knowledge-based methods seem concerned only with realism issues, and do not consider the representativeness of the predicted motion: the various strategies and styles which account for the natural variability in human motion are not yet included in the goals of knowledge-based prediction methods. In this sense, data-based methods present an advantage over knowledge-based predictions, since reproducing the variability in behaviour in data-based methods is a relatively simple task: it is enough to change the reference motion and consider one which exhibits a different strategy or style (Park et al., 2008a).

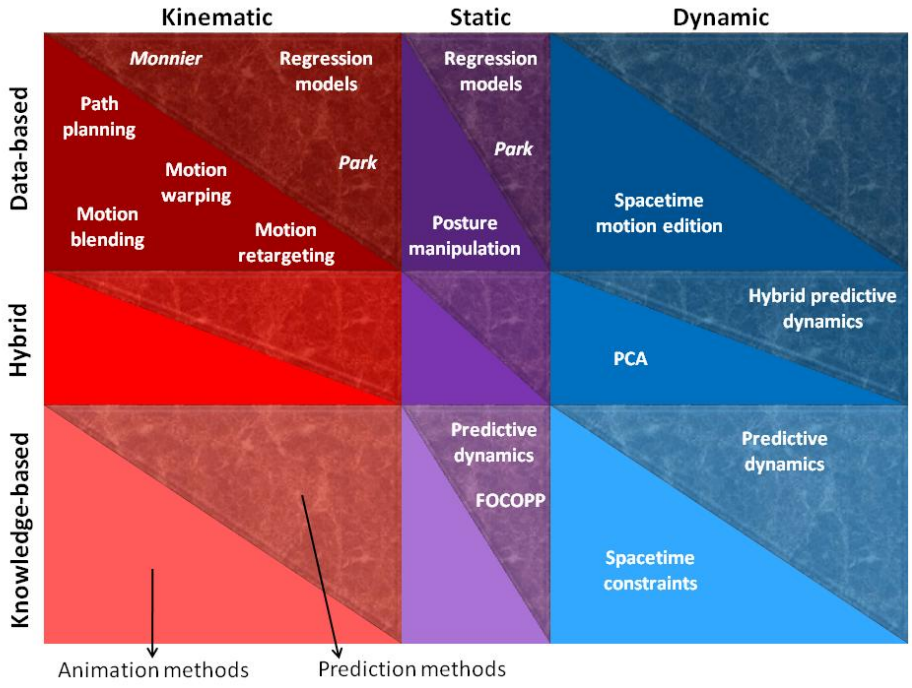

Figure 2.2: Graphical summary of the classification of the main motion simulation methods reviewed in the chapter. The lower triangles contain animation methods and the upper triangles contain prediction methods.

This advantage is paid for by the required cumbersome task of recording, reconstructing and analysing a sufficiently large database of motions, which constitutes the drawback of data-based methods. Additionally, data-based methods may not present adequate extrapolation

capabilities: it was observed in reaching motions (Monnier, 2004; Park et al., 2004) that depending on how close the reference target is to the prediction target, the predicted motion may be considered to belong or not to the range of natural variability of actually performed motions.

The possibility of combining the advantages of both data-based and knowledge-based motion prediction methods has been explored by Xiang et al. (2012) in parallel to the work carried out in this thesis. Xiang's method branches from the predictive dynamics framework and seeks to generate more realistic predictions by included limited data-based information in the method, as detailed before. However, the method lacks a thorough validation procedure, which is carried out by comparing the profiles of selected kinematic predictors in the predicted and the reference motions. Moreover, the representativeness of the reference motion (and hence, of predicted motion too) is not assessed.

Through the review of the state of the art presented in this chapter, the shortcomings of current motion prediction methods justify the motivation and the objectives of the present thesis, stated in Section 1.4. First of all, a dynamic method is required, in order to generate more physically sound motions and to encompass the prediction of motions in which the interaction with the environment involves energy and effort, as most generally occurs in real tasks (Pannetier and Wang, 2012; Wang et al., 2011). Moreover, a hybrid method seems appropriate in order to overcome the extrapolation limitations of purely data-based predictions, and to generate more realistic motions than those resulting from a purely knowledge-based approach. To ensure that the knowledge-based contribution to the hybrid method actually improves the realism of the predicted motion, the identification of the most adequate performance measures should also be addressed.

Hence, a motion database analysis is required both to reveal possible motion patterns which may guide the performance measure identification, and to generate a structured database, necessary to the data-based contribution to the hybrid method. The variability of behaviour exhibited in actually performed motions is also a relevant result of the database analysis and its application is twofold: on the one hand, once the different strategies and styles are identified, they may also be included in the prediction; and on the other, the natural variability of motions constitute an appropriate term of comparison against which to assess the realism of the predicted motions.

Finally, a thorough validation should be carried out to assess the qualities of the method and ensure that it fulfils the realism and representativeness required from a motion prediction method. Although for animation methods a simple validation procedure is generally followed (mainly to determine whether the generated motions look sufficiently realistic), motion prediction methods require a more extensive validation. Both qualitative and quantitative validation methods proposed in the literature have been reviewed in this chapter (Section 2.2). The appeal of a quantitative method lies in the objective comparisons that it allows; on the other hand, the information contained in a unique measure is very compressed and it relies on the goodness of the measure definition. Combining a quantitative measure with a comparison between the kinematic and dynamic profiles of the predicted and actually performed motions may yield a more complete and reliable validation. Therefore, both a quantitative and a qualitative validation is carried out in this work.

CHAPTER 3

HYBRID DYNAMIC MOTION PREDICTION METHOD

This chapter presents the method developed to carry out hybrid dynamic human motion predictions. The first section introduces the method and describes the types of digital human models (DHMs) for which the method was developed, as well as the adopted dynamic formulation. Subsequently, the inputs to the method are presented (Section 3.2), followed by details on the main steps composing the method (Sections 3.3-3.5), and the generated outputs (Section 3.6).

3.1 INTRODUCTION

The two main features of the motion prediction method developed in this work are that the method is both hybrid and dynamic. It is hybrid as it relies on a database of captured motions on the one hand, and on the other it introduces knowledge in the prediction through the definition of the motion control law which is assumed to drive the motion. Moreover, dynamics is included in the prediction both in the definition of the motion control law and in the dynamic balance condition imposed to the DHM while performing the task and interacting with the environment.

The following sections (3.1.1-3.1.3) present an outline of the approach with which the prediction method was developed, detail the characteristics of the DHMs to which the method may be applied, and explain the adopted dynamic formulation.

3.1.1 APPROACH OUTLINE

The developed hybrid dynamic prediction method is composed of three main stages, shown in Figure 3.1, and outlined hereafter.

The first step consists in selecting the reference motion from the available database of captured motions, given the characteristics of the scenario to be predicted (called prediction scenario). As defined earlier (Section 2.1.2.1), a scenario is composed of the subject performing the motion and the environment it is performed in. Once the reference motion is selected, the pose of the root segment (i.e. its position and orientation) and the trajectories followed by the end-effectors of the DHM are modified (Step 2) in order to consider the reference motion in the global position and orientation specified by the prediction scenario and to match the trajectories of the end-effectors required to fulfil the task in the prediction scenario. Finally (Step 3) an optimisation problem, comprising both data-based and knowledge-based approaches, is defined to carry out the prediction.

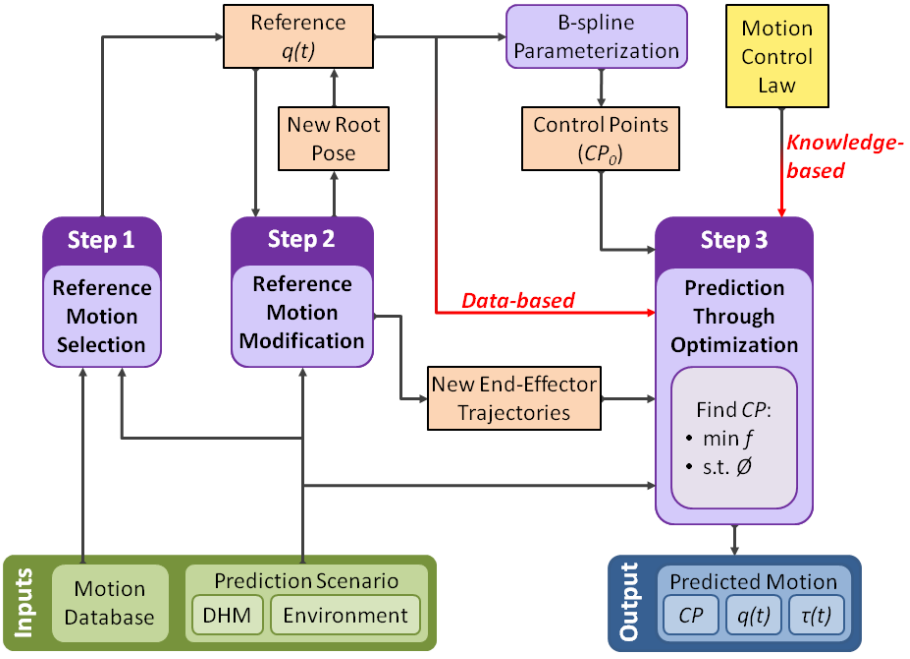

Figure 3.1: Flowchart of the proposed hybrid motion prediction method.

The above-mentioned three steps are inspired by the structure of the kinematic data-based method presented by Monnier et al. (2003). However,

our method differs substantially from Monnier's: not only is it hybrid rather than purely data-based, but dynamics is included in the prediction, requiring a different formulation of the optimisation problem.

3.1.2 DIGITAL HUMAN MODEL

Motion prediction methods require the definition of a human model. Our method expects the same human model to be employed both in the reconstruction process, for the motion database generation, and in the motion predictions. The same DHM is required because the data-based component of the method seeks to generate a predicted motion which is similar to the reference one, and the similarity is imposed to the profiles of the DHM degrees of freedom (DoFs). If the DHMs adopted in the reconstruction and prediction processes were different, it would be difficult to establish a similarity between the motions, as a direct correspondence between DoFs would be missing.

As mentioned in Section 1.1, DHMs are mathematical representations of the human musculoskeletal system. Therefore, in order to define a mathematical model of the human body, some assumption must always be made. In this work, we consider the DHM to be defined as a purely skeletal multi-body model, in which the segments are considered as rigid bodies, connected one another by ideal joints. The adequacy of the rigid body assumption depends on the goals of the study: in this work, we consider that the implications of excluding the soft tissues from the modelling do not affect the validity of the results. On the other hand, the assumption of ideal joints implies that the joints present a fixed centre and fixed axes of rotation. Actually, human articulations behave in a much more complex way, but the variations in rotation centre and axes are considered negligible in this work (along with the joint translations), as we are concerned with the global motion of the human body rather than the behaviour of one specific joint. Therefore, the joints adopted in this work are lower kinematic pairs: rotation, universal and spherical joints are employed to represent the articulations of the human body and a floating joint serves the purpose of defining the global position and orientation of the DHM.

Additionally, the developed motion prediction method requires that the DHM must be described through the relative coordinates formalism. Translational DoFs are represented through the relative position between two points in the model, and rotational DoFs with Euler angles.

3.1.3 DYNAMIC FORMULATION OVERVIEW

Since the method is developed for purely skeletal DHMs, dynamics is described by the forces and torques acting at the joints. These joint efforts are equivalent to the efforts actually exerted by the muscles in the human body and represent the effects at the joints of the muscular activity.

To evaluate the joint forces and torques in the model, we adopt an inverse dynamics formulation, which relates the forces $\mathbf{F}$ and torques $\boldsymbol{\tau}$ at the joints with the values of the DoFs $\mathbf{q}$ and their first and second order time derivatives $\dot{\mathbf{q}}$ and $\ddot{\mathbf{q}}$. Specifically, the efforts $\mathbf{F}$ and $\boldsymbol{\tau}$ are evaluated through the application of the Newton-Euler recursive method (Craig, 2005). The method performs two iterations across the model: the first starts from the root segment and, moving outwards, obtains the kinematics of the segments; the second starts from the distal segments and, moving inwards, obtains the forces and torques at the joints by imposing the dynamic equilibrium of each segment:

$$\forall \text{joint} \quad \begin{cases} \mathbf{F} = \mathbf{F}\left(\mathbf{q}, \dot{\mathbf{q}}, \ddot{\mathbf{q}}, \mathbf{F}_{Ext}\right) \\ \boldsymbol{\tau} = \boldsymbol{\tau}\left(\mathbf{q}, \dot{\mathbf{q}}, \ddot{\mathbf{q}}, \mathbf{F}_{Ext}, \boldsymbol{\tau}_{Ext}\right) \end{cases} \tag{3.1}$$

In order to evaluate the external forces $\mathbf{F}_{Ext}$ and torques $\boldsymbol{\tau}_{Ext}$ acting on the DHM, due to its interaction with the environment, contact models must be defined. Contact models are mathematical approximations of the relationship between the efforts originated in the DHM-environment interaction and the variables which describe the motion of the DHM:

$$\forall \text{externaleffort} \quad \begin{cases} \mathbf{F}_{Ext} = \mathbf{F}_{Ext}\left(\mathbf{q}, \dot{\mathbf{q}}, t\right) \\ \boldsymbol{\tau}_{Ext} = \boldsymbol{\tau}_{Ext}\left(\mathbf{q}, \dot{\mathbf{q}}, t\right) \end{cases} \tag{3.2}$$

3.2 INPUTS TO THE METHOD

Our motion prediction method requires as inputs a motion database and the characteristics of the prediction scenario, which are hereafter described.

3.2.1 MOTION DATABASE

The database required by the method is a collection of reconstructed motions in which a specific task is carried out: the motions are actually performed motions, which are captured and subsequently reconstructed, adopting the same multi-body DHM considered in the prediction.

Once the motions composing the database are reconstructed, the database must be structured so as to be used in the reference motion selection step. Structuring the database consists in analysing the motions, in order to identify their most relevant features, and classifying them accordingly. The features identified and considered for the classification may be related to the subject, the environment or the motion *per se*. For what concerns the subjects, the motions may be classified, for instance, according to the subjects' age, gender, stature and weight. The relevant characteristics of the environment usually depend on the task, but may be the position of the elements with which the subject interacts, their orientation, the presence of obstacles, etc. Finally, the features related to the actual motions may be the variability in behaviour (i.e. adopted strategies and styles) as well as the key-events and corresponding key-frames in motion.

3.2.2 PREDICTION SCENARIO

Along with the motion database, the characteristics of the scenario to be predicted are needed as an input to the method.

The prediction scenario is composed of the DHM performing the motion (characterised by age, gender, anthropometry, etc.) and the environment it is performed in (characterised by target locations, presence of obstacles, geometric and mechanical characteristics of the elements with which the DHM must interact, etc.).

The information that must be provided to characterise the subject to be used in the prediction is:

- subject anthropometry, needed to generate a DHM tailored to the specific subject;
- the values of the subject-related features considered in the structuring of the motion database (e.g. age, gender, stature, etc.), needed in the reference motion selection.

To characterise the prediction environment, the following information is required:

- the values of the environment-related features considered in the structuring of the motion database (e.g. target locations, presence of obstacles, geometry of the environment, etc.), needed in the reference motion selection;

- additional features necessary to fully characterise the environment which had not been considered in the structuring of the database (e.g. mechanical characteristics of the elements with which the DHM must interact, etc).

3.3 REFERENCE MOTION SELECTION

In this step, a motion is selected as reference from the database in order to be resembled in the prediction. Comparing the scenarios in the structured database with the prediction scenario, the most similar one is selected. The similarity between scenarios is assessed through the weighted sum:

$$\forall i = 1 : nMotions \quad \varepsilon_{Similarity_i} = \sum_j w_j \left(\frac{x_{j\,Pred} - x_{j\,Moti}}{\max(x_{j_{DB}}) - \min(x_{j_{DB}})} \right)^2 \tag{3.3}$$

where w_j is a weighting factor which defines the relative importance of each feature and x_j represents the j^{th} feature related to the scenario which was adopted to structure the motions in the database. Specifically, $x_{j\,Pred}$ is the value of the j^{th} feature in the prediction scenario, $x_{j_{Moti}}$ is its value in the i^{th} motion of the database, and $\max(x_{j_{DB}})$ and $\min(x_{j_{DB}})$ are the maximum and minimum values of the j^{th} feature among the motions in the database. Some features are quantitative (such as the subjects' stature), and in this case x_j is directly the value of the feature in the prediction scenario and in the motion database. Instead, in case of qualitative features (such as the subjects' gender), binary values are assigned to x_j (if the feature presents more than two options, discrete levels are adopted to quantify the feature). The difference between features is normalised with an upper-lower bound approach described in Section 2.1.2.2, which represents the range of values of each feature in the database.

If different strategies and styles are present in the database, a motion for each of the exhibited behaviours is retrieved and may be adopted to carry out the prediction. Hence, the motion variability actually exhibited may be represented in the prediction.

Once the reference motion is selected, some of its features may be maintained in the prediction, an assumption that relies on the similarity between the reference and the new scenarios. In this work all temporal characteristics of the reference motion are maintained during the prediction: hence both the duration and the key-frames distribution in the predicted motion are the same as in the reference motion.

On the other hand, other characteristics may require modification, such as the global position and orientation of the DHM or the trajectory followed by the end-effectors. Their modification is described in the following section.

3.4 REFERENCE MOTION MODIFICATION

As mentioned earlier, the motion selected in the previous step is used as reference for the prediction by imposing a resemblance between its DoF profiles and those in the predicted motion. However, the global pose of the DHM root may vary from the reference to the prediction scenario, therefore it must be modified before imposing the resemblance between the reference and prediction DoFs. The modification of the root pose is described hereafter, in Section 3.4.1.

Additionally, since the reference and prediction scenarios generally do not match, the trajectories followed by the end-effectors in the reference motion do not ensure the fulfilment of the task in the prediction environment. Therefore, the end-effector trajectories in the reference motion are modified in order to fit the prediction scenario, as described in Section 3.4.2.

3.4.1 ROOT POSE MODIFICATION

In order to place the DHM of the subject to be predicted in the desired global configuration respect to the prediction environment, the DoFs representing the global position $\mathbf{x}$ and the global orientation $\boldsymbol{\theta}$ of the DHM are modified by adding a constant offset ($\Delta\mathbf{x}$ and $\Delta\boldsymbol{\theta}$, respectively) to the reference DoFs profiles:

$$\begin{aligned} \mathbf{x}_{Mod}(t) &= \mathbf{x}_{Ref}(t) + \Delta\mathbf{x} \\ \boldsymbol{\theta}_{Mod}(t) &= \boldsymbol{\theta}_{Ref}(t) + \Delta\boldsymbol{\theta} \end{aligned} \tag{3.4}$$

The original values of these DoFs ($\mathbf{x}_{Ref}$ and $\boldsymbol{\theta}_{Ref}$) are replaced by the modified values ($\mathbf{x}_{Mod}$ and $\boldsymbol{\theta}_{Mod}$) in the $\mathbf{q}(t)$ vector describing the reference DoF profiles (see Figure 3.1). Therefore, $\mathbf{q}(t)$ now describes the reference motion considering the global position and orientation of the DHM root specified by the prediction scenario.

3.4.2 END-EFFECTOR MODIFICATION

For what concerns the end-effectors, the modification process must ensure the accomplishment of the task in the prediction scenario. Two methods of modification are considered, depending on whether the motion to reach the target is free or constrained by the motion of the environmental elements with which the end-effector interacts. Both modification methods, described in the following sections, rely on the similarity between the reference and prediction scenarios in order to maintain the realism of the reference motion in the modification process.

3.4.2.1 Free End-Effector

When the end-effector's motion is free, the data required to perform the modification are the desired initial and final positions of the end-effector in the predicted motion: the goal is to travel from an initial to a final point following a trajectory which is not constrained. In this work, two modification methods are considered: the velocity proportional (VP) and the acceleration preserving (AP) methods, introduced in Section 2.1.1.1. These methods were proposed by Bindiganavale and Badler (1998) and by Zhang (2002) to modify joint angle profiles. However, Monnier et al. (2003) first applied the methods in the modification of end-effector trajectories, as described hereafter. The VP method imposes that the velocity profile of the end-effector along the modified trajectory $\dot{\mathbf{x}}_{Mod}$ must be proportional to that of the reference motion:

$$\dot{\mathbf{x}}_{Mod}(t) = \mathbf{c}_{V1} \cdot \dot{\mathbf{x}}_{Ref}(t) \quad \rightarrow \quad \mathbf{x}_{Mod}(t) = \mathbf{c}_{V1} \cdot \mathbf{x}_{Ref}(t) + \mathbf{c}_{V2} \tag{3.5}$$

In the AP method, instead, the acceleration profile of the end-effector along the modified trajectory $\ddot{\mathbf{x}}_{Mod}$ is set to be the same as in the reference motion:

$$\ddot{\mathbf{x}}_{Mod}(t) = \ddot{\mathbf{x}}_{Ref}(t) \quad \rightarrow \quad \mathbf{x}_{Mod}(t) = \mathbf{x}_{Ref}(t) + \mathbf{c}_{A1} \cdot t + \mathbf{c}_{A2} \tag{3.6}$$

The vectors of coefficients $\mathbf{c}_{V1}$, $\mathbf{c}_{V2}$ and $\mathbf{c}_{A1}$, $\mathbf{c}_{A2}$ in Equations (3.5) and (3.6) respectively, are obtained by imposing the end-effector's initial and final positions in the reference and prediction motions.

As discussed in Section 2.1.1.1, both methods generally yield very similar results. In this work, however, VP is favoured as it presents the desirable feature of maintaining zero-velocity conditions of the end-effector (which may occur, for instance, when a target is reached). On the other hand, VP fails to generate a reasonable trajectory when the initial and final positions of the end-effector are very close to each other, since numerical problems arise. In this case, AP is applied instead.

3.4.2.2 Constrained End-Effector

When the end-effector interacts with a mobile element of the environment, its trajectory is constrained to follow the motion of the environmental element.

The motion of the environmental element in the prediction scenario may be obtained by modifying its motion in the reference scenario. For this, the initial and final values for each DoF θ_i of the environmental element in both the reference and prediction environment must be known. To obtain the new motion of the environmental element, we use a similar modification to the one applied to the free end-effector in the previous section, with the difference that in this case the modification is applied to the element's DoFs instead of the end-effector's position.

The formulation for the VP modification is:

$$\dot{\boldsymbol{\theta}}_{Mod}(t) = \mathbf{c}_{V1} \cdot \dot{\boldsymbol{\theta}}_{Ref}(t) \quad \rightarrow \quad \boldsymbol{\theta}_{Mod}(t) = \mathbf{c}_{V1} \cdot \boldsymbol{\theta}_{Ref}(t) + \mathbf{c}_{V2} \tag{3.7}$$

If the initial and final values of any of the θ_i are very close to each other, numerical problems may arise in the VP modification. In such cases, the following AP modification is used instead:

$$\ddot{\boldsymbol{\theta}}_{Mod}(t) = \ddot{\boldsymbol{\theta}}_{Ref}(t) \quad \rightarrow \quad \boldsymbol{\theta}_{Mod}(t) = \boldsymbol{\theta}_{Ref}(t) + \mathbf{c}_{A1} \cdot t + \mathbf{c}_{A2} \tag{3.8}$$

Similarly as in Section 3.4.2.1, the vectors of coefficients $\mathbf{c}_{V1}$, $\mathbf{c}_{V2}$ and $\mathbf{c}_{A1}$, $\mathbf{c}_{A2}$ are obtained by imposing the initial and final values for the θ_i DoFs in the reference and prediction environments.

Once the modified motion of the environmental element is obtained, the new trajectory for the end-effector must be calculated. The end-effector must follow the trajectory described by the contact point in the environmental element. The trajectory of the contact point is obtained by applying forward kinematics to the environmental element, which moves according to the $\boldsymbol{\theta}_{Mod}(t)$ values of its DoFs.

3.5 MOTION PREDICTION THROUGH OPTIMISATION

As mentioned earlier, the human body is a highly redundant system, presenting more DoFs than those strictly necessary to carry out most tasks. For this reason, imposing the modified end-effector trajectory is not enough to define the motion of all the bodies in the DHM, since generally infinite sets of values of the DoFs allow its fulfilment.

In this work, a constrained non-linear optimisation problem is defined to carry out the prediction: among the infinite sets of feasible DoF values (which fulfil the constraints to the motion), the set which minimises the specified objective function is obtained. Hence, the objective function must be constructed in order to ensure the realism of the predicted motion.

The aforementioned optimisation problem is solved with non-linear programming techniques and the following three sections describe its main features: the selected design variables (Section 3.5.1), the definition of the constraints to be fulfilled (Section 3.5.2) and the objective function to be minimised (Section 3.5.3). Finally, the optimisation problem is formally formulated (Section 3.5.4).

3.5.1 DESIGN VARIABLES

As the developed motion prediction method is dynamic, the variables required to describe the DHM are the DoF values $\mathbf{q}$ as well as the first and second order time-derivatives of the DoFs, $\dot{\mathbf{q}}$ and $\ddot{\mathbf{q}}$, since they all appear in the equations of motion governing the dynamics of the system (Section 3.1.3). Including the velocities and accelerations in the formulation implies that the value of $\mathbf{q}$ at a frame is related with its values at the previous and following frames. Hence, although kinematic prediction may be carried out one frame at a time, a dynamic prediction must be performed considering the motion as a whole.

Rather than using the DoFs in each frame as design variables, as in spacetime methods (described in Section 2.1.1.2), in this work we chose to parameterise the motion, using a B-spline representation of the DoF profiles. B-splines are chosen over other parameterisations as they allow to fit the most general kind of data while requiring a relatively small number of variables to represent the whole motion.

B-splines curves (Piegl and Tiller, 1997) are defined as a linear combination of independent p^{th} order piecewise polynomial functions N, called basis functions, through coefficients called control points (CPs). The basis functions are a function of the independent variable of the problem (in this case, time t) and are non-zero only in certain intervals. An example of the distribution of basis functions over a normalised time domain is represented in Figure 3.2 below. Any given curve may be approximated multiplying each basis function by a coefficient (i.e. the control point associated to each basis function), hence the name "basis" function.

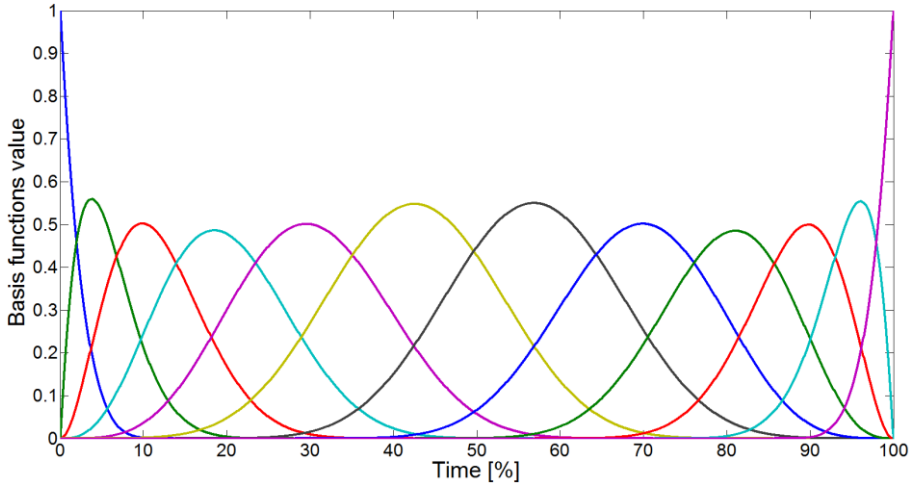

Figure 3.2: Twelve 5th order uniform basis functions over a normalised time domain.

The control points are defined in the dependent variables space (in this case, the DoFs $\mathbf{q}$). Each DoF profile q_i is represented in B-spline form as a combination of nCP_i basis functions:

$$q_i(t) \cong \sum_{j=1}^{nCP_i} N_j^{\,p}(t) CP_{ij} \tag{3.9}$$

where $N_j^{\,p}(t)$ represents the j^{th} basis functions of the nCP_i basis functions considered to represent the DoF q_i; and CP_{ij} represents the j^{th} control point for the DoF q_i, i.e. the coefficient associated to the j^{th} basis function for q_i.

The velocities and accelerations of the DoFs are easily obtained as a linear combination of the time derivatives of the basis functions $\dot{N}_j^{\,p}(t)$ and $\ddot{N}_j^{\,p}(t)$, in which the coefficients of the combination are once more the control points used to represent the DoFs $\mathbf{q}$:

$$\begin{aligned} \dot{q}_i(t) &\cong \sum_{j=1}^{nCP_i} \dot{N}_j^{\,p}(t) CP_{ij} \\ \ddot{q}_i(t) &\cong \sum_{j=1}^{nCP_i} \ddot{N}_j^{\,p}(t) CP_{ij} \end{aligned} \tag{3.10}$$

Moreover, as the external forces and torques acting on the DHM are related to the DoF values and derivatives through the contact models (Section 3.1.3), Equation (3.1) describing the dynamics of the system may be rewritten as:

$$\forall \text{joint} \quad \begin{cases} \mathbf{F} = \mathbf{F}(\mathbf{q}, \dot{\mathbf{q}}, \ddot{\mathbf{q}}, \mathbf{F}_{Ext}) \\ \boldsymbol{\tau} = \boldsymbol{\tau}(\mathbf{q}, \dot{\mathbf{q}}, \ddot{\mathbf{q}}, \mathbf{F}_{Ext}, \boldsymbol{\tau}_{Ext}) \end{cases} \rightarrow \begin{cases} \mathbf{F} = \mathbf{F}(\mathbf{CP}, t) \\ \boldsymbol{\tau} = \boldsymbol{\tau}(\mathbf{CP}, t) \end{cases} \tag{3.11}$$

where $\mathbf{CP}$ is the vector containing the control points which approximate the DoF profiles, obtained in Equation (3.9).

Equation (3.11) states that all the variables describing the dynamics of the system can be expressed in terms of the vector of control points $\mathbf{CP}$, and therefore $\mathbf{CP}$ are chosen to constitute the design variables for which the optimisation problem is solved.

The advantages of using B-spline curves are several: they are a flexible parameterisation, which fits the most general kind of data; they provide local support, given that each basis functions is equal to zero during intervals of the motions; they ensure smoothness and continuity up to the $(p\text{-}1)^{th}$ derivative; and they are able to describe the whole motion with a relatively small number of variables. In fact, B-splines are a common motion parameterisation employed in knowledge-based prediction methods, as described in Section 2.1.1.2.

In this work the assumption is made that the number of CPs which adequately describes the DoF profiles in the reference motion is also suitable to describe the profiles in the predicted motion. This assumption relies on the expected similarity between the reference and predicted motions: not only the reference scenario is the closest to the new one, but resemblance conditions to the reference motion are imposed in the prediction.

To obtain the number of CPs which yield an appropriate representation of the motion, B-splines are adapted to the normalised DoF profiles of the reference motion and the smallest set of CPs which approximates the profiles to a specified tolerance is retrieved. This process is known as global approximation (Piegl and Tiller, 1997).

Given that dynamics involves up to the second order derivative of the DoFs, to guarantee continuity in the accelerations, the basis functions must be at least cubic splines. In this work 5th order splines are adopted to ensure smoothness in accelerations as well.

The control points of the B-splines are the design variables for which the optimisation problem is solved and the set of control points obtained in the global approximation constitutes the initial approximation for the optimisation.

3.5.2 CONSTRAINTS

The equality $\mathbf{\Phi}^{EQ}$ and inequality $\mathbf{\Phi}^{IN}$ constraints that the motion is subject to are of five types, and serve the purpose to: ensure the fulfilment of the task goal; impose initial and final conditions to the motion; respect the natural joint limits, both in terms of range of motion (RoM) and of maximum torques; avoid collisions with obstacles in the environment; and maintain the dynamic balance of the system.

All equality and inequality constraints are normalised following an upper-lower bound approach in order to avoid numerical problems in the computation. Hence, each constraint Φ_i (be it an equality or inequality constraint) is normalised as follows:

$$\Phi_i^{\,N} = \frac{\Phi_i - \Phi_i^{\,Min}}{\Phi_i^{\,Max} - \Phi_i^{\,Min}} \tag{3.12}$$

where Φ_i^N represents the normalised constraint and the superscripts *Min* and *Max* refer to the minimum and maximum values respectively of the quantity Φ_i evaluated in the reference motion.

In the following sections, each constraint type is reported prior to the normalisation procedure, for simplicity in formulation:

3.5.2.1 Goal Fulfilment

To fulfil the goals in the motion, the trajectory $\mathbf{x}$ of the end-effector must match the modified trajectory $\mathbf{x}_{Mod}$ obtained in Step 2 (Section 3.4):

$$t = t^* \in [t_A, t_B] \qquad \mathbf{\Phi}^{EQ}{}_{EndEff\,Traj} = \mathbf{x}(\mathbf{q}) - \mathbf{x}_{Mod}(t) = 0 \tag{3.13}$$

where t_A and t_B are the extremes of the time period during which the end-effector trajectory must be followed exactly.

Moreover, in certain applications, it may be necessary to specify the orientation of the segment containing the end-effector, especially if it is restrained by the environment during the interaction. Given a vector $\mathbf{r}$ belonging to the end-effector segment, the condition that it must follow the orientation of the vector $\mathbf{r}_{Environ}$ is given by:

$$t = t^* \in [t_A, t_B] \qquad \mathbf{\Phi}^{EQ}{}_{EndEff\,Orient} = \mathbf{r}(\mathbf{q}) - \mathbf{r}_{Environ}(t) = 0 \tag{3.14}$$

When the above-mentioned constraints are applied to a period in the motion (i.e. $t_A \neq t_B$), for instance a period during which the DHM interacts with an element of the environment, they are enforced only at specific frames t^* in the period to avoid excessively reducing the number of free control points.

3.5.2.2 Initial and Final Conditions

Conditions may be set to specify the velocity and acceleration conditions at the initial and final frames of the motion, t_0 and t_T respectively.

$$\begin{aligned} t = t_0 \qquad & \mathbf{\Phi}^{EQ}{}_{DoFVel} = \dot{\mathbf{q}}(t) = \dot{\mathbf{q}}_0 \qquad \mathbf{\Phi}^{EQ}{}_{DoFAcc} = \ddot{\mathbf{q}}(t) = \ddot{\mathbf{q}}_0 \\ t = t_T \qquad & \mathbf{\Phi}^{EQ}{}_{DoFVel} = \dot{\mathbf{q}}(t) = \dot{\mathbf{q}}_T \qquad \mathbf{\Phi}^{EQ}{}_{DoFAcc} = \ddot{\mathbf{q}}(t) = \ddot{\mathbf{q}}_T \end{aligned} \tag{3.15}$$

If a motion is to start and end in states of rest, the values of $\dot{\mathbf{q}}_0$, $\ddot{\mathbf{q}}_0$, $\dot{\mathbf{q}}_T$ and $\ddot{\mathbf{q}}_T$ are all set to zero.

Since two conditions are set at each frame t_0 and t_T, the constraints reported in Equation (3.15) reduce by 4 the number of free control points which describe each DoF. Specifically, due to the construction of B-spline curves (Piegl and Tiller, 1997), only one of the first three and one of the last three control points are independent. Therefore the number of control points employed to approximate the DoF profiles must be sufficiently large as to allow Equation (3.15) to be set without excessively reducing the number of free control points in the motion.

3.5.2.3 Joint Limits

To ensure that the predicted motions do not exceed the natural range of motion (RoM) allowed by the human articulations and the maximum torque that the muscular activity can exert, the following inequalities are set:

$$\forall t \in [t_A, t_B] \qquad \begin{aligned} \boldsymbol{\Phi}^{IN}{}_{RoM} &= \mathbf{q}_L - \mathbf{q}(t) \le 0 \\ \boldsymbol{\Phi}^{IN}{}_{RoM} &= \mathbf{q}(t) - \mathbf{q}_U \le 0 \end{aligned} \tag{3.16}$$

$$\forall t \in [t_A, t_B] \qquad \begin{aligned} \boldsymbol{\Phi}^{IN}{}_{\tau} &= \boldsymbol{\tau}_L - \boldsymbol{\tau}(\mathbf{q}, \dot{\mathbf{q}}, \ddot{\mathbf{q}}, t) \le 0 \\ \boldsymbol{\Phi}^{IN}{}_{\tau} &= \boldsymbol{\tau}(\mathbf{q}, \dot{\mathbf{q}}, \ddot{\mathbf{q}}, t) - \boldsymbol{\tau}_U \le 0 \end{aligned} \tag{3.17}$$

Equation (3.16) restricts the values of $\mathbf{q}$ to a range delimited by the DoFs lower and upper limits $\mathbf{q}_L$ and $\mathbf{q}_U$, whereas Equation (3.17) imposes that the torque $\boldsymbol{\tau}$ at each joint must not exceed its maximum limits, denoted with $\boldsymbol{\tau}_L$ and $\boldsymbol{\tau}_U$.

Since inequality constraints do not reduce the number of free control points, Equations (3.16) and (3.17) can be set throughout the specified period of the motion, $[t_A, t_B]$, which may correspond to the whole motion ($t_A = t_0$ and $t_B = t_T$) or to a portion of it.

In this work, the joint limits (both in terms of RoMs and maximum torques) are considered constant and the dependencies that actually exist between the limits of a joint and both the values and velocities of the DoFs (Anderson et al., 2007; Engstler et al., 2011; Guenzkofer et al., 2011) are not taken into account.

Moreover, the DoFs which represent the global position and orientation of the DHM theoretically have no limits in value. However, in this work the global rotations are considered to be contained in a specific

range (for instance [-π, π]) to avoid ambiguities in rotations. For what concerns the global translations, they may be limited too, according to the type of motion and the expected position of the root joint.

3.5.2.4 Collision Avoidance

In this work, a simplified model is considered to take into account the collisions between the DHM and the environment. Obstacles are represented as planes, which forbid the DHM to enter the space beyond the planes. Obstacle avoidance is treated as an inequality constraint set to a specified point in the DHM $\mathbf{x}$: given a vector $\mathbf{n}$, normal to the plane and whose origin $\mathbf{x}_0$ is located on the plane's surface, the condition to be met by the point $\mathbf{x}$ in the DHM is expressed through the scalar product of $\mathbf{n}$ with the vector connecting the point in the DHM with $\mathbf{x}_0$. This scalar product defines the distance between a point and a plane, which must not become negative for penetrations not to occur.

$$\forall t \in [t_A, t_B] \qquad \mathbf{\Phi}^{IN}{}_{Collision} = -(\mathbf{x}(\mathbf{q}) - \mathbf{x}_0(t)) \cdot \mathbf{n} \leq 0 \tag{3.18}$$

Once again, since inequality constraints do not reduce the number of free control points, the constraint can be set throughout the specified period of the motion, $[t_A, t_B]$.

3.5.2.5 Dynamic Balance

To balance the forces and torques in the DHM with the efforts exerted by the environment, the condition of dynamic equilibrium is imposed.

As mentioned in Section 3.1.3, the dynamics of the DHM are evaluated through an inverse dynamics formulation, applying the Newton-Euler recursive method: the efforts at the joints are calculated by imposing the dynamic equilibrium of each segment, starting from the distal ones (Equation (3.1)). Therefore, the dynamic balance of the whole system is ensured by imposing the dynamic equilibrium of the root segment: the sum of all the forces and torques (external, internal and inertial) at the root joint must be zero:

$$t = t^* \in [t_A, t_B] \qquad \mathbf{\Phi}_{FBalance} = \mathbf{F}_{Root}(\mathbf{q}, \dot{\mathbf{q}}, \ddot{\mathbf{q}}, \mathbf{F}_{Ext}) = 0 \tag{3.19}$$

$$t = t^* \in [t_A, t_B] \qquad \mathbf{\Phi}_{MBalance} = \boldsymbol{\tau}_{Root}(\mathbf{q}, \dot{\mathbf{q}}, \ddot{\mathbf{q}}, \mathbf{F}_{Ext}, \boldsymbol{\tau}_{Ext}) = 0 \tag{3.20}$$

where $\mathbf{F}_{Root}$ and $\boldsymbol{\tau}_{Root}$ are obtained by summing all forces and torques, respectively, acting at the root joint.

As mentioned earlier (Section 3.1.3), the external efforts acting on the DHM ($\mathbf{F}_{Ext}$ and $\boldsymbol{\tau}_{Ext}$) are related to the values of the DoFs and their first order time-derivative ($\mathbf{q}$, $\dot{\mathbf{q}}$) through contact models, as stated by Equation (3.2). Such contact models on the one hand allow all dynamic variables to be described in terms of the control points of the B-spline parameterisation of the DoFs (Section 3.5.1), but on the other are only approximations of the complex interactions between humans and the environment. Therefore, to take into account the possible inaccuracies of the employed contact models, the dynamic balance is imposed as an inequality rather than an equality constraint. Tolerances may be specified within which the dynamic balance is considered fulfilled:

$$\forall t \in [t_A, t_B] \qquad \begin{aligned} \boldsymbol{\Phi}^{IN}{}_{FBalance} &= \mathbf{F}_{Root}(\mathbf{q}, \dot{\mathbf{q}}, \ddot{\mathbf{q}}, t) - \boldsymbol{\varepsilon}_F \leq 0 \\ \boldsymbol{\Phi}^{IN}{}_{FBalance} &= -\mathbf{F}_{Root}(\mathbf{q}, \dot{\mathbf{q}}, \ddot{\mathbf{q}}, t) - \boldsymbol{\varepsilon}_F \leq 0 \end{aligned} \tag{3.21}$$

$$\forall t \in [t_A, t_B] \qquad \begin{aligned} \boldsymbol{\Phi}^{IN}{}_{MBalance} &= \boldsymbol{\tau}_{Root}(\mathbf{q}, \dot{\mathbf{q}}, \ddot{\mathbf{q}}, t) - \boldsymbol{\varepsilon}_\tau \leq 0 \\ \boldsymbol{\Phi}^{IN}{}_{MBalance} &= -\boldsymbol{\tau}_{Root}(\mathbf{q}, \dot{\mathbf{q}}, \ddot{\mathbf{q}}, t) - \boldsymbol{\varepsilon}_\tau \leq 0 \end{aligned} \tag{3.22}$$

The tolerances $\boldsymbol{\varepsilon}_F$ and $\boldsymbol{\varepsilon}_\tau$ with which the equilibrium is considered satisfied are chosen according to the accuracy with which the contact model is defined: the unfulfilment of the exact balance is assumed to be due to the approximate nature of the contact model, which is not capable of wholly representing the complex DHM-environment interactions which take place in reality, and not to an inaccuracy of the resulting predicted motion.

Additionally, expressing the balance condition as inequality constraints, Equations (3.21) and (3.22) may be ensured throughout the specified period of the motion, $[t_A, t_B]$.

3.5.3 OBJECTIVE FUNCTION

The objective function represents the criterion that is selected to predict the most realistic motion. In this work a criterion that comprises more than one objective is considered, as several conditions must be included: some related to the fulfilment of the goal, some to the data-based nature of the approach, and others to the knowledge-based nature of the approach. To solve this multi-objective optimisation problem, the objectives are combined in a

single function to be minimised, given by the weighted squared sum of the objectives. In matrix notation, the objective function is given by:

$$f = \frac{1}{2}\boldsymbol{\Psi}^T \mathbf{W} \boldsymbol{\Psi} \tag{3.23}$$

where $\boldsymbol{\Psi}$ is a vector of objectives, in which each function Ψ_i represents an objective at a given instant in time, and $\mathbf{W}$ is a diagonal matrix containing the weights associated to each objective.

In order to combine non-homogeneous objectives, these are normalised using the same upper-lower-bound transformation adopted for the constraints:

$$\Psi_i^N = \frac{\Psi_i - \Psi_i^{Min}}{\Psi_i^{Max} - \Psi_i^{Min}} \tag{3.24}$$

where Ψ_i^N represents the normalised objective and the superscripts *Min* and *Max* refer to the minimum and maximum values respectively of the quantity Ψ_i evaluated in the reference motion. Although the normalised objectives may not be exactly contained in the range [0,1] the values should not exceed the range greatly, given the similarity between the reference and prediction scenarios.

Hence, the objective function is actually evaluated as:

$$f^N = \frac{1}{2}\boldsymbol{\Psi}^{N^T} \mathbf{W}^N \boldsymbol{\Psi}^N \tag{3.25}$$

Normalisation not only reduces the numerical problems that may arise solving a nonlinear optimisation problem, but also allows to use dimensionless weights $\mathbf{W}^N$ which reflect the relative importance of each objective and prevents any single objective from dominating the aggregated function.

As mentioned earlier, the objectives imposed to the predicted motion are of three types and are hereafter reported, for simplicity in formulation, prior to the normalisation procedure.

3.5.3.1 Goal Fulfilment

The condition that the end-effector should follow the modified trajectories (Section 3.4) may be imposed as a constraint (Section 3.5.2.1) or may be

included in the objective function, if the modified trajectory must be resembled rather than matched exactly:

$$\forall t \in [t_A, t_B] \qquad \boldsymbol{\Psi}_{EndEff\,Traj} = \mathbf{x}(\mathbf{q}) - \mathbf{x}_{Mod}(t) \tag{3.26}$$

The same applies to the end-effector segment orientation: when the orientation of the environmental element with which the end-effector is interacting must only be resembled and not matched exactly, the following objective is included:

$$\forall t \in [t_A, t_B] \qquad \boldsymbol{\Psi}_{EndEff\,Orient} = \mathbf{r}(\mathbf{q}) - \mathbf{r}_{Environ}(t) \tag{3.27}$$

Moreover, as mentioned earlier, when a goal fulfilment constraint is applied during a period in the motion, it is enforced only at specific frames (Section 3.5.2.1). To ensure that the modified trajectory is followed (and therefore that the goals in the motion are met) throughout the period, the following condition is included in the objective function:

$$\forall t \in [t_A, t_B] \qquad \boldsymbol{\Psi}_{EndEff\,Traj} = \dot{\mathbf{x}}(\mathbf{q}, \dot{\mathbf{q}}) - \dot{\mathbf{x}}_{Mod}(t) \tag{3.28}$$

The condition is set on the end-effector velocity rather than its position in order to resemble the shape of the modified trajectory $\mathbf{x}_{Mod}$ in between the constraints which affect its value (Equation (3.13)), ensuring a smoother trajectory.

Analogously, to ensure that the end-effector segment orientation follows the orientation of the environmental element it is interacting with, the following condition on the end-effector segment orientation rate is included in the objective function:

$$\forall t \in [t_A, t_B] \qquad \boldsymbol{\Psi}_{EndEff\,Orient} = \dot{\mathbf{r}}(\mathbf{q}, \dot{\mathbf{q}}) - \dot{\mathbf{r}}_{Environ}(t) \tag{3.29}$$

By resembling the orientation rate of the environmental element in between the constraints expressed by Equation (3.14), smooth orientation profiles are ensured.

3.5.3.2 Data-based Conditions

To preserve the realism of the reference motion, conditions are imposed to resemble the DoF values, as in Monnier et al. (2003), and/or to resemble the DoF velocities, as in Park et al. (2004; 2008a).

To resemble the DoF values in the reference motion, the following objective is considered:

$$\forall t \in [t_A, t_B] \qquad \boldsymbol{\Psi}_{DoF} = \mathbf{q}(t) - \mathbf{q}_{Ref}(t) \tag{3.30}$$

To maintain the shape of the DoF profiles in the reference motion, a resemblance condition on the DoF velocities is considered:

$$\forall t \in [t_A, t_B] \qquad \boldsymbol{\Psi}_{DoFVel} = \dot{\mathbf{q}}(t) - \dot{\mathbf{q}}_{Ref}(t) \tag{3.31}$$

In fact, although the values of the DoFs change depending on the subject anthropometry and the geometry of the environment, the shape of the DoF profiles seems to be generally maintained (Park et al., 2004).

3.5.3.3 Knowledge-based Conditions

To introduce knowledge in the prediction, the motion control laws which guide the motion must be identified and represented through a performance measure. Our method is prepared to support any performance measure expressed as a function of the DoF values or derivatives ($\mathbf{q}$, $\dot{\mathbf{q}}$, $\ddot{\mathbf{q}}$):

$$\forall t \in [t_A, t_B] \qquad \boldsymbol{\Psi}_{MotCtrlLaw} = f(\mathbf{q}, \dot{\mathbf{q}}, \ddot{\mathbf{q}}) \tag{3.32}$$

Hereafter, we report two of the most commonly employed dynamic performance measures which have already been implemented: dynamic effort and mechanical energy minimisation.

Dynamic effort is an energy-related performance measure which minimises the squared sum of the joint torques across the motion (Equation (2.15)). Given the form of the objective function f (Equation (3.23)), the dynamic effort objective is defined as:

$$\forall t \in [t_A, t_B] \qquad \boldsymbol{\Psi}_{DynEff} = \boldsymbol{\tau}(\mathbf{q}, \dot{\mathbf{q}}, \ddot{\mathbf{q}}, t) \tag{3.33}$$

where $\boldsymbol{\tau}$ is a vector containing the torques at all the joints of the DHM.

On the other hand, the mechanical energy expenditure is approximated by the Riemann sum of the instantaneous power at the joints with respect to time. The instantaneous power is given by the scalar product of the torques at the joints $\boldsymbol{\tau}$ times the relative angular velocity $\boldsymbol{\omega}^{Rel}$ of the two segments linked by each joint. Therefore, the minimum mechanical energy expenditure is represented by the following objective:

$$\forall t \in [t_A, t_B] \qquad \boldsymbol{\Psi}_{MechEn} = \boldsymbol{\tau}^T(\mathbf{q}, \dot{\mathbf{q}}, \ddot{\mathbf{q}}, t)\boldsymbol{\omega}^{Rel}(\mathbf{q}, \dot{\mathbf{q}})\Delta t \tag{3.34}$$

where Δt is the time interval between two consecutive frames in which the objective is evaluated.

3.5.4 FORMULATION OF THE OPTIMISATION PROBLEM

As mentioned before, the variables which define the system's dynamics are the DoF values $\mathbf{q}$ and their derivatives $\dot{\mathbf{q}}$ and $\ddot{\mathbf{q}}$. However, all these variables depend on the vector of control points $\mathbf{CP}$, as shown in Equations (3.9) and (3.10).

Hence, the optimisation problem can be formulated as:

$$\begin{aligned} \min_{\mathbf{CP}} \quad & f = \frac{1}{2}\boldsymbol{\Psi}^T(\mathbf{CP})\,\mathbf{W}\,\boldsymbol{\Psi}(\mathbf{CP}) \\ \text{s.t.} \quad & \begin{cases} \boldsymbol{\Phi}(\mathbf{CP}) = 0 \\ \boldsymbol{\Phi}^{IN}(\mathbf{CP}) \le 0 \end{cases} \end{aligned} \tag{3.35}$$

3.5.4.1 Jacobian and Hessian Matrices

Given the high nonlinearity of the problem, the Jacobian and Hessian matrices for the objective function and the constraints are evaluated analytically to improve the solver's convergence. Therefore, both the first and second order derivatives of the equations of motion respect to the variables describing the system's dynamics ($\mathbf{q}$, $\dot{\mathbf{q}}$, $\ddot{\mathbf{q}}$) are calculated. Defining Ξ_i as a generic function representing either an objective ($\Xi_i = \Psi_i$) or a constraint ($\Xi_i = \Phi_i$), the following derivatives are calculated:

$$\forall j \quad \frac{\partial \Xi_i}{\partial q_j}, \frac{\partial \Xi_i}{\partial \dot{q}_j}, \frac{\partial \Xi_i}{\partial \ddot{q}_j} \tag{3.36}$$

The derivatives of each function Ξ_i must then be evaluated with respect to the design variables $\mathbf{CP}$. To apply the chain rule, the derivative of the variables respect to the control points must be calculated. Given the definition of the B-spline representation of the variables (Equations (3.9) and (3.10)), their derivatives respect to the control points are obtained as:

$$\forall i,j \quad \frac{\partial q_i}{\partial CP_{ij}} = N_j^{\,p}(t)$$
$$\frac{\partial \dot{q}_i}{\partial CP_{ij}} = \dot{N}_j^{\,p}(t) \tag{3.37}$$
$$\frac{\partial \ddot{q}_i}{\partial CP_{ij}} = \ddot{N}_j^{\,p}(t)$$

where CP_{ij} represents the j^{th} control point used to describe the DoF q_i. The derivatives of q_i respect to any other CP (belonging to the description of another DoF q_k, with $k \neq i$) is zero.

Defining $\mathbf{s}$ as a cumulative vector of variables:

$$\mathbf{s} = [\mathbf{q}, \dot{\mathbf{q}}, \ddot{\mathbf{q}}]^T \tag{3.38}$$

the derivative of the generic function Ξ_i respect to the CPs is calculated as:

$$\forall j \quad \frac{\partial \Xi_i}{\partial CP_j} = \frac{\partial \Xi_i}{\partial s_k}\frac{\partial s_k}{\partial CP_j} \tag{3.39}$$

where the repeated index k implies summation. Denoting with the subscript $\mathbf{s}$ or $\mathbf{CP}$ the derivative respect to $\mathbf{s}$ and $\mathbf{CP}$ respectively, the Jacobian of Ξ_i may be rewritten in matrix form as:

$$\boldsymbol{\Xi}_{\mathbf{CP}i}^T = \boldsymbol{\Xi}_{\mathbf{s}\,i}^T \mathbf{S}_{\mathbf{CP}} \tag{3.40}$$

where $\boldsymbol{\Xi}_{\mathbf{CP}i}^T$ is the i^{th} row of the Jacobian matrix $\boldsymbol{\Xi}_{\mathbf{CP}}$ whose elements are defined by Equation (3.39).

The second derivative is calculated as:

$$\forall j,k \quad \frac{\partial^2 \Xi_i}{\partial CP_j \partial CP_k} = \frac{\partial \Xi_i}{\partial s_m}\left(\frac{\partial \Xi_i}{\partial s_l}\frac{\partial s_l}{\partial CP_j}\right)\frac{\partial s_m}{\partial CP_k} = \frac{\partial^2 \Xi_i}{\partial s_l \partial s_m}\frac{\partial s_l}{\partial CP_j}\frac{\partial s_m}{\partial CP_k} \tag{3.41}$$

Hence, the Hessian of the generic function Ξ_i may be rewritten in matrix notation as:

$$\boldsymbol{\Xi}_{\mathbf{CP}^2\,i} = \mathbf{S}_{\mathbf{CP}}^T\, \boldsymbol{\Xi}_{\mathbf{s}^2\,i}\, \mathbf{S}_{\mathbf{CP}} \tag{3.42}$$

where the squared subscripts denote the variable with respect to which quantities are derived twice.

The derivatives of the constraints are obtained directly from Equations (3.40) and (3.42), whereas the derivatives of the objective function are obtained as:

$$\begin{aligned} f_{\mathbf{CP}} &= \mathbf{\Psi}^T \mathbf{W} \mathbf{\Psi}_{\mathbf{CP}} \\ f_{\mathbf{CP}^2} &= \sum_i w_i \left(\Psi_i \mathbf{\Psi}_{\mathbf{CP}^2 i} + \mathbf{\Psi}_{\mathbf{CP}_i}^T \mathbf{\Psi}_{\mathbf{CP}i} \right) \end{aligned} \tag{3.43}$$

The vectors of constraints $\mathbf{\Phi}$ and objectives $\mathbf{\Psi}$ contain the functions defined in Sections 3.5.2 and 3.5.3 evaluated at several instants in time. At each instant t, the length of the vector of variables $\mathbf{s}$ which affect the dynamics of the system is *3×nDoFs*. On the other hand, the number of control points of a B-spline must be greater than the order of the basis functions: given that accelerations must be at least continuous, this implies *p≥3* and *nCP≥4* for each DoF. Hence, the length of the $\mathbf{CP}$ vector must necessarily be greater than *4×nDoFs*. This implies that the Hessians which appear in Equation (3.42) have different sizes, being the Hessian respect to $\mathbf{CP}$ always larger than the Hessian respect to $\mathbf{s}$. However, the rank of a matrix can never be increased through multiplication, hence the Hessian respect to $\mathbf{CP}$ is always rank deficient. An explanation for this characteristic is that $\mathbf{CP}$ is a vector which represents the totality of the motion, whereas $\mathbf{s}$ only represents a specific instant in time. Due to the local support of B-splines, only a certain number of control points affects the dynamics of a specific instant t of the motion: at t, other control points have no influence at all, leading to zero derivatives.

This characteristic has a strong effect on the objective function f, which must ensure that all variables ($\mathbf{CP}$) be controlled: a necessary condition for this is that the objectives must be evaluated at a minimum number of frames. Given a number *n* of frames (each being represented by a vector of variables $\mathbf{s}$), the number of variables which describe all *n* frames is *n×(3×nDoFs)*. If the size of the $\mathbf{CP}$ vector were greater than this quantity, the evaluation of the objective function at *n* frames would not be sufficient to provide information for each CP, and some CPs would be uncontrolled. Hence we may obtain the minimum number of frames at which the objectives must be evaluated as:

$$n_{Min} = \frac{nCP}{3nDoFs} \tag{3.44}$$

Evaluating the objective function at a number of frames $n > n_{Min}$ however does not guarantee that each CP is controlled. For that, the n frames must be spaced across the period of the motion in order to involve all basis functions in their non-zero interval.

3.5.4.2 Effect of the Number of Control Points

According to the allowed tolerance with which the reference DoF profiles are approximated, the number of control points for each B-spline may range from a minimum value, given by *p+1*, to a maximum value, given by *nFrames-1* (if the number of control points equals the number of data available, the curve no longer approximates but interpolates the data). A larger number of control points on the one hand entails a finer approximation to the reference profiles, and on the other increases the size of the problem. However, due to the particular construction of the basis functions (Piegl and Tiller, 1997), by increasing the number of control points, the intervals during which each basis function is equally zero are longer: each basis function controls a smaller portion of the motion. This implies that by increasing the number of control points in all DoFs, matrices get larger but sparser.

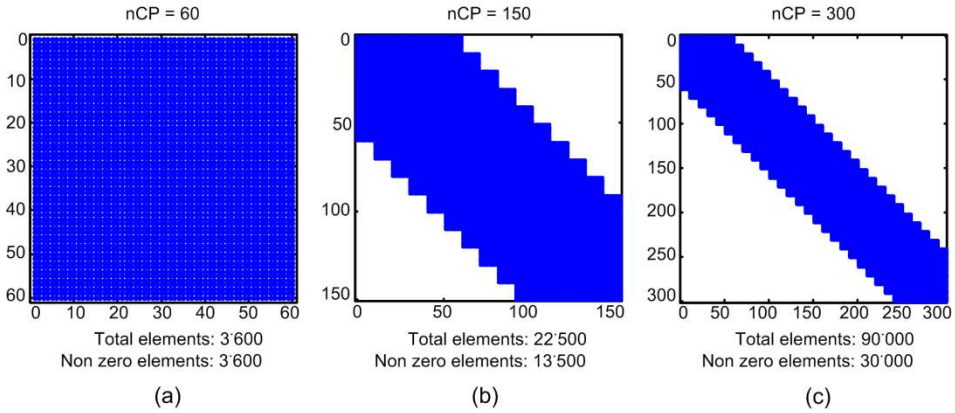

Figure 3.3: Hessian matrices of the objective function adopting different numbers of control points (considering a problem described by 10 DoFs and parameterised with 5th order B-splines). The blue dots represent the non-zero elements of the matrices.

Figure 3.3 shows the effect of the number of CPs on the Hessian matrix of the objective function, considering a problem described by 10 DoFs and parameterised with 5^{th} order B-splines. When the number of control points is close to the minimum, the matrix is relatively small but full (Figure 3.3a corresponds to a case in which the minimum number of CPs is adopted); as it increases (Figure 3.3b, c), the size of the matrix is larger but it becomes more sparse and with a characteristic multi-diagonal shape. Moving towards the right or the bottom of the matrix corresponds to moving across the motion in time: in Figure 3.3b and Figure 3.3c it may be seen how the effect of the first control points (associated to the first basis functions) is nullified while the following control points start affecting the motion.

3.6 OUTPUT FROM THE METHOD

In the previous section, the optimisation problem which is at the core of our motion prediction method was presented. As described earlier (Section 3.5.1), the design variables employed are the control points of the B-spline parameterisation of the DoF profiles. Therefore, the solution to the optimisation problem is given as the values of the design variables (i.e. the control points) which minimise the objective function, subject to the defined equality and inequality constraints.

From the values of the CPs, the DoF profiles and their derivatives are obtained through Equations (3.9) and (3.10) respectively. The external forces and torques acting on the DHM, due to its interaction with the environment, are then evaluated through the contact models (Equation (3.2)). Finally, inverse dynamics is performed to calculate the dynamic variables describing the DHM, i.e. the forces and torques acting at the joints (Equation (3.1)).

CHAPTER 4

EXPERIMENTAL DATA ANALYSIS

As mentioned in the Introduction, the motion prediction method described in Chapter 3 is applied in this work to clutch pedal depression motions. The clutch pedal depression presents the advantage of being a relatively simple task (it may be regarded as a dynamic reaching motion) while containing all the relevant features for testing a dynamic motion prediction method: it is task oriented, it intrinsically requires interaction between the subject and the environment, and the interaction is both kinematic and dynamic as the pedal determines both the motion of the foot and the external forces that the DHM is subject to.

The present chapter describes how a database of clutch pedal depression motions has been generated and analysed. The importance of this process is twofold. On the one hand, a structured database of motions is required as input to our prediction method (Section 3.2.1); for this purpose, the most relevant features in the motions must be identified (such as key-frames, behaviours, or the influence of experimental parameters). On the other hand, the analysis of the database is useful in the validation of the motion prediction method (Section 6.5), as it allows to carry out the comparison of each predicted motion against the most adequate data set.

To constitute the database, motions have been captured following the experimental protocol detailed hereafter (Section 4.1). Subsequently, a DHM is defined (Section 4.2) with which the captured motions are reconstructed (Section 4.3). The database composed of the reconstructed motions is then analysed (Section 4.4). Finally, the features considered in

the structuring of the database for the motion prediction method are presented (Section 4.5).

4.1 EXPERIMENTAL PROTOCOL

The database is constituted by clutch pedal depression motions, recorded at IFSTTAR in the framework of the European Project DHErgo.

Four groups of five healthy subjects were asked to perform the motion in an adjustable vehicle mock-up (shown in Figure 4.1). The characteristics which were considered to describe the groups of subjects recruited for the experiments are detailed in Table 4.1.

Figure 4.1: Overview of the adjustable vehicle mock-up (reproduced from the DHErgo Newsletter n.2).

Group	Description	N	Age [years]	Stature [cm]	BMI [kg/m^2]
YF	Young females	5	21-30	167±3	22.1±1.6
YM	Young males	5	21-34	177±5	22.3±3.0
EF	Elderly females	5	66-72	160±5	24.6±2.6
EM	Elderly males	5	66-78	172±2	27.2±1.2

Table 4.1: Characteristics of the groups of subjects who took part in the clutch pedal depression experiments. The values preceding and following the ± symbol represent the mean μ and standard deviation σ, respectively.

The vehicle mock-up could assume the configuration of six different commercial vehicles from BMW, Peugeot-Citroën and Renault. The features considered to characterise the six environments are depicted in Figure 4.2 and their values are reported in Table 4.2. For what concerns the choice of the global coordinate system, it is located and oriented as shown in Figure 4.2: *x* is the longitudinal axis (positive towards the rear); *z* is the vertical axis (positive upwards); and *y* is the transversal axis, obtained by cross-product (positive towards the right). The origin of the coordinate system was placed to match the H-point[6] of the seat, when it is located in the centre of its longitudinal sliding range (during the experiments, the subjects were free to slide the seat forwards or backwards).

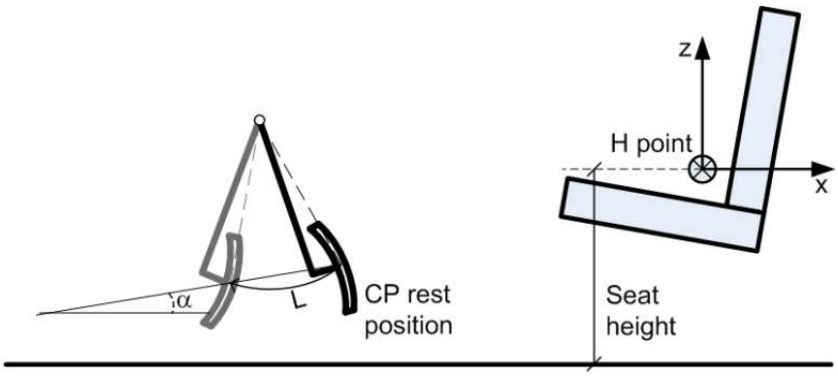

Figure 4.2: Environmental features used to characterise the different configurations of the vehicle mock-up.

The subjects were asked to perform a clutch pedal operation in each vehicle and the motion was repeated 3 times in the vehicle PCA2. Hence, each subject carried out 8 motions, which leads to a total of 160 performed motions. The motion consists in placing both hands on the steering wheel and, starting from the foot rest, reaching and depressing the clutch pedal with the left foot, holding the fully depressed position for 3s, and returning to the foot rest (although only the depression of the pedal is considered in this work).

[6] The H-point is defined as the point in the seat occupied by the mid hip point of a seated male subject of the 50th percentile.

Vehicle	Seat height [mm]	Pedal travel length L [mm]	Pedal travel angle α [deg]	Pedal rest position		
				CPx [mm]	CPy [mm]	CPz [mm]
BMW1	256	140	0	-814	-60	-69
BMW2	247	150	0	-831	-110	-64
BMW4	174	138	0	-816	-120	17
PCA1	355	132	23	-770	-70	-199
PCA2	272	158	8	-766	-80	-130
REN3	360	139	15	-761	-70	-218

Table 4.2: Characteristics of the environmental features in the different vehicle configurations shown in Figure 4.2.

A total of 37 reflective markers (Figure 4.3) were placed on the subject, of which 17 on the pelvis and left leg in order to perform the motion reconstruction, shown in red. Additionally, markers were placed on the fixed environmental elements to establish their position and orientation (such as the seat or the vehicle floor). For what concerns the mobile element of the environment, i.e. the clutch pedal, 8 markers were used to describe its motion during the task.

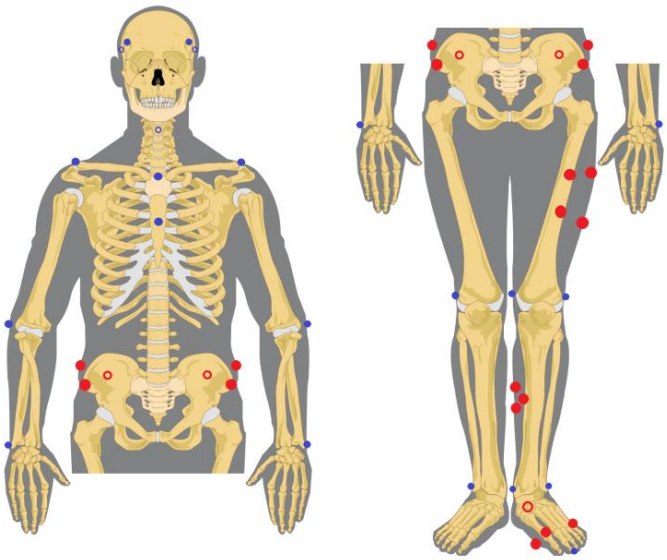

Figure 4.3: Position of the reflective markers placed on the subjects.

Motions were captured using a VICON optoelectronic motion capture system sampling at 100Hz: 10 cameras were employed to record the 3D location of the reflective markers described above.

Dynamic instrumentation was also installed: a 3D TME force sensor was placed on the clutch pedal to record the force applied by the subjects. The contact forces were measured in synchronisation with the motion capture system at 100Hz.

4.2 ADOPTED HUMAN MODEL

To reconstruct the captured motions, a human model is required. To carry out the multi-body reconstruction, a three-dimensional DHM was generated, under the assumptions detailed in Section 3.1.2 and following RAMSIS specifications (Human Solutions GmbH).

Since the clutch pedal depression hardly involves any limbs other than the left leg, we separated the complete RAMSIS DHM into an active and a passive part, shown in Figure 4.4.

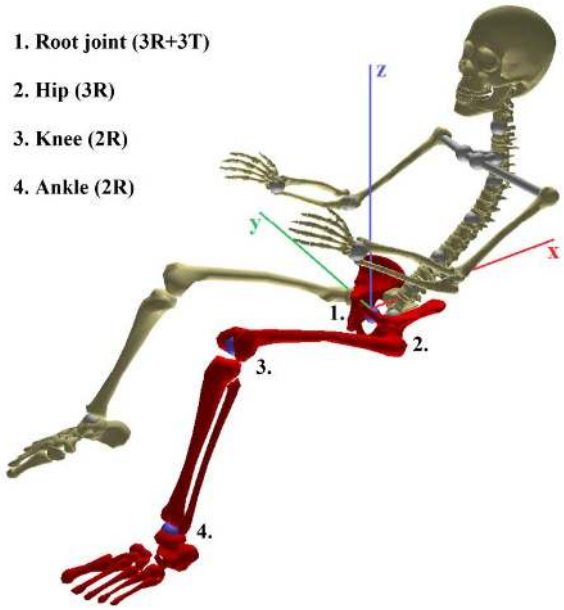

Figure 4.4: Graphic representation of the adopted DHM. The active segments are shown in red. The corresponding active joints are reported and present a total of 3 translational and 10 rotational DoFs.

The active part is a 13 DoF model of the pelvis and left leg, which we described with the relative coordinates formalism (specifically, Euler angles for the rotational DoFs). The rest of the DHM is considered to be fixed in the seated posture shown in the figure, and rigidly connected to the pelvis.

The root joint connects the DHM to the ground, allows all translations and rotations, and specifies the global position and orientation of the DHM. The remaining joints represent the articulations of the human leg: the hip joint is modelled as a spherical joint and both the knee and ankle as universal joints. The knee is assumed to allow flexion-extension movements and rotations about the shank longitudinal axis (see Figure 4.11). Similarly, the ankle allows flexion-extension movements and rotations about the foot longitudinal axis (see Figure 4.11).

For what concerns the inertial properties of the segments, they are considered constant due to the rigid body assumption. Those corresponding to the pelvis and the left leg are estimated employing a method based on anatomical landmarks (Dumas et al., 2007), which are relevant points in the body segments. Moreover, the inertial properties of the upper part of the DHM are taken into account by including them in the pelvis segment: the mass and moments of inertia of the upper body segments are estimated using regression equations based on the subject's anthropometry (Zatsiorsky, 2002), and combined to the pelvis. For what concerns the right leg, the mass and moments of inertia of the upper half of the thigh are estimated analogously (Zatsiorsky, 2002) and included in the pelvis; the inertial properties of the rest of the limb instead are considered negligible as the right leg does not move during the motion and its lower part is assumed to unload its weight directly on the floor.

Finally, a global coordinate system is defined, respect to which the motion of the DHM is described. Its origin is located in the average H-point of the vehicle (considering that the seat may slide forward and backward) and is oriented as shown in Figure 4.2 and Figure 4.4. Additionally, a local coordinate system is defined in each segment of the model. Due to rigid body assumptions, the position of a point belonging to a segment, expressed in the segment's local coordinate system, is constant. Hence, the position that each marker is expected to have in its corresponding segment is constant and is estimated through an anatomical calibration protocol from the global coordinates of markers anatomical landmarks in each body segment.

As mentioned in Section 3.1.2, the DHM defined to carry out the motion reconstruction is also adopted in the motion prediction process.

4.3 MOTION RECONSTRUCTION

Marker-based kinematic motion reconstruction is the process of obtaining the motion of a DHM, in terms of the variables adopted to describe it, given the trajectories of the markers placed on a subject.

To perform the motion reconstruction, the trajectories of the markers were first filtered in order to eliminate high frequency noise. For this purpose, a Butterworth 3rd order filter with a zero-phase lag was employed, with a cut off frequency of 3.5Hz.

The kinematics of the captured motions were reconstructed using the optimal tracking method (OTM) proposed by Ausejo et al. (2006; 2009; 2011). OTM relies on a natural coordinate description of the DHM and solves a constrained non-linear optimisation problem in each frame: the distance between the position of the markers on the DHM and their measured position is minimised while imposing the constraints deriving from the natural coordinates formalism.

If during the motion a marker disappears (it is not visible to at least two cameras), it may lead to discontinuities in the motion: the position of a segment which at first was determined by approximating *n* markers, is now determined by only *n-1*. Hence, the contribution of these *n-1* markers to the segment position changes from one frame to the next, leading to jerky motions. To address this issue, a window was specified within which the trajectory of the missing marker was interpolated from its last known value before disappearance, to its first known value once it reappears.

Once the motion was kinematically reconstructed, inverse dynamics (ID) was applied as a post-process to obtain the forces and torques at the joints. For this purpose the dynamic data recorded by the force sensor was filtered with the same Butterworth filter employed for the marker trajectories. From the kinematic reconstruction, the values of the Euler angles were obtained and a recursive Newton-Euler method was applied to solve the ID problem (Craig, 2005).

4.4 MOTION ANALYSIS

Of the 160 performed motions, only 153 were captured due to technical difficulties. Moreover, only 120 of the 153 motion captures were successful: in the remaining cases, the capture began when the motion had already started. These 33 motions were discarded immediately from the database.

Additionally, the motions performed by two elderly male subjects were eliminated from the database as their body segment parameters were not estimated correctly, leading to an erroneous DHM anthropometry and therefore erroneous motion reconstructions. Also the motions performed by two EF were discarded as the actual experimental conditions did not match the theoretical ones.

Moreover, 10 motions were eliminated from the database as the subjects' left foot started from the vehicle floor rather than the foot rest, affecting the shape of the foot trajectory (see Section 4.4.3). Another 2 motions were discarded since the subjects readjusted the position of the foot on the pedal. Finally, 5 motions were eliminated due to missing markers which led to problems in the reconstruction.

Therefore, the database of clutch pedal motions which we consider in the following analysis is composed of 78 motions, distributed among the groups and vehicle configurations as shown in Table 4.3.

Group	BMW1	BMW2	BMW4	PCA1	PCA2	REN3	Total
YF	4	2	2	4	13	4	29
YM	2	3	2	4	9	3	23
EF	2	0	0	2	2	2	8
EM	2	3	1	2	8	2	18
Total	10	8	5	12	32	11	78

Table 4.3: Number of motions present in the database performed by each group in each vehicle configuration.

The following sections present the results obtained analysing the motion database. Given the purposes of the analysis, stated at the beginning of this chapter, a qualitative approach seemed both sufficient and adequate.

4.4.1 KEY-FRAME IDENTIFICATION

As mentioned earlier, key-frames are frames at which a relevant event occurs in the motion (e.g. a target is reached).

The following key-frames were identified in the pedal depression motion:

- *StartMotion* is the frame at which the motion starts. It is identified as the last frame before the left foot starts moving (the velocity of the foot at *StartMotion* $\|\mathbf{v}\| \cong 0$);
- *StartDepression* is the frame at which the left foot reaches the clutch pedal. It is identified as the first frame at which the force sensor placed on the pedal records a non-zero force: $\|\mathbf{F}\| > 0$;
- *EndDepression* is the frame at which the pedal is fully depressed. It is identified as the frame at which the foot stops moving (the velocity of the foot at *EndDepression* $\|\mathbf{v}\| \cong 0$);
- *EndMotion* is the frame at which the motion ends. The motion is considered to end 0.3s after the *EndDepression* key-frame, after which the subjects hold their final posture.

The aforementioned key-frames are shown in Figure 4.5, which reports the velocity profiles of the end-effector (EE) and the description of the main phases which characterise the 3D motion of the left foot. In this work, the exact point in the left foot which is considered as end-effector is the point in the DHM which reaches the centre of the clutch pedal at the key-frame *StartDepression*.

The shape of the EE velocity (Figure 4.5) presents the typical double hump of clutch pedal depressions(Wang et al., 2000): the foot moves rapidly to the proximity of the pedal, slows down to come into contact with the pedal, moves rapidly again during the depression, and slows down towards the end of the pedal travel. The key-frames *StartMotion*, *EndDepression*, and *EndMotion* are shown in the figure, as their definition is closely related to the motion of the end-effector. On the other hand, for what concerns *StartDepression*, its definition depends on the force values recorded by the pedal sensor. It may be noticed, however, that it marks the beginning of the

second phase of higher velocities for the end-effector, which in fact corresponds to the beginning of the pedal depression.

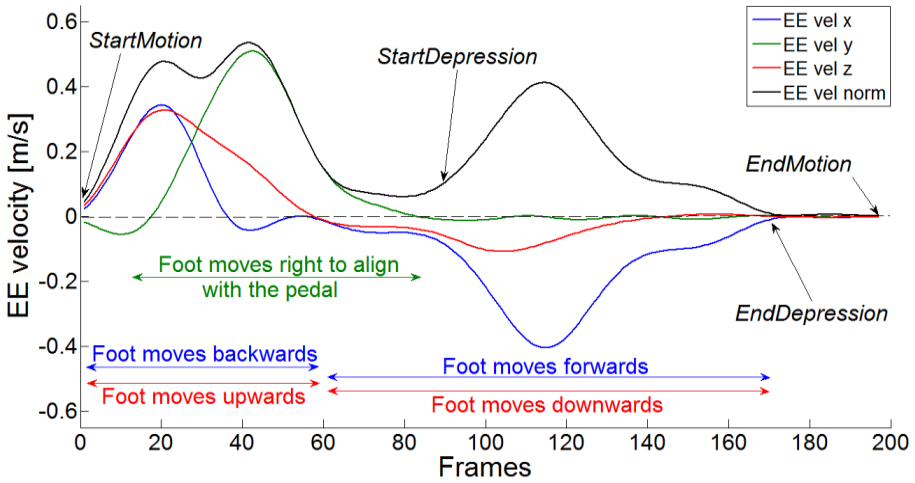

Figure 4.5: Velocity of the end-effector (EE) in a clutch pedal depression motion. Both the motion key-frames and the description of the phases in the end-effector's motion are reported.

4.4.2 MOTION DURATIONS

Once the key-frames for clutch pedal depressions were identified, we analysed the temporal features of the motions composing the database.

First, the overall time employed by the subjects to carry out the task is considered. Figure 4.6 shows box plots of the total time for each group of subjects and for each vehicle configuration. The box plots represent the median for each set of data (the red line in the figures) along with its 95% confidence interval (the red triangles in the figures). The boxes define the inter-quartile range (from the 25th to the 75th percentile) and the whiskers show the maximum and minimum values in each data set (excluding the data considered as outliers, which are marked as red crosses).

What must be noticed is that the confidence intervals (CIs) for the medians depend on the number of samples in each data set. This is true not only for the CIs values (the amplitude of the CIs is inversely proportional to the squared root of the samples), but also for the CIs own confidence intervals: the fewer the motions in a data set, the greater the uncertainty on the accuracy of the CIs. These considerations are relevant especially for the elderly females (EF) group: the motions present in the database performed

by EF are less than half than those performed by the other subject groups (see Table 4.3), hence the CIs for EF are less reliable to be accurate.

To assess whether the subjects' age is a factor which influences the motion duration, we compare the medians of the elderly subjects (EF, EM) with the CIs of the young subjects (YF, EM), and *vice versa* (Figure 4.6a).The reason behind this cross-comparison between medians and CIs is that the aim is to ascertain whether two different data sets may or may not be considered as belonging to the same population. If the median of a data set does not fall within the CIs of another, we may state that the data sets are different (i.e. they belong to different populations) at a 95% confidence level. From the box plots it may be seen that the median of the elderly males (EM) falls within the CIs of the young males (YM), but on the contrary the YM median does not fall within the EM CIs: hence we may conclude that young males tend to carry out the motion in more time than elderly males. Although the same considerations may be applied to the female subjects (YF and EF respectively), the CIs of the EF group present a greater uncertainty than the rest, as explained above. Therefore the claim that age reduces the motion duration remains a speculation for female subjects.

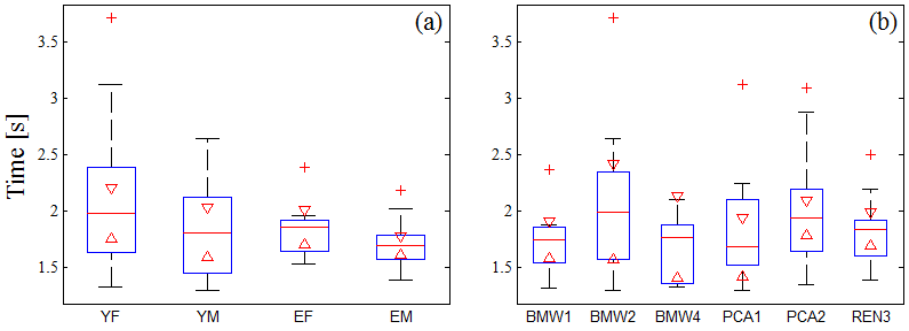

Figure 4.6: Box plots of the total motion duration, organised according to the subject groups (a) and the vehicle configurations (b). The red line represents the median, the blue box contains the inter-quartile range (from the 25th to the 75th percentile), and the black whiskers extend from the minimum to the maximum values (outliers are marked with red crosses). The red triangles mark the 95% confidence intervals of the medians.

Additionally, the motion durations seem to change depending on the vehicle configurations (Figure 4.6b). The CIs for PCA2 are those evaluated with greater accuracy (see Table 4.3) and the medians of BMW1, BMW4, PCA1 and REN3 do not fall within them: hence, the time required in these vehicle configurations is smaller than the time required in PCA2. It may

seem that both PCA2 and BMW2 present longer motion durations, but the CIs for BMW2 do not allow to demonstrate this claim.

Analysing the relative duration of the reach phase respect to the pedal depression phase (R/D duration) shown in Figure 4.7, it may be seen that younger subjects employ almost the same time to reach the pedal as to depress it, in accordance with Wang et al. (2000). Age does not seem to affect the relative duration of the phases for female subjects. On the other hand, the EM subjects, however, employ significantly less time reaching than depressing the pedal respect to YM.

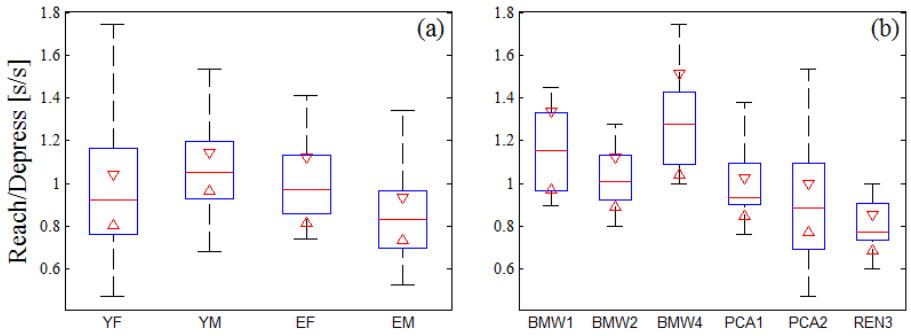

Figure 4.7: Box plots of the relative duration of the reach phase respect to the pedal depression phase (R/D duration), organised according to the subject groups (a) and the vehicle configurations (b).

For what concerns the vehicle configuration, it seems to influence the relative duration of the reach respect to the depression phase strongly. The R/D duration in REN3 is the least among the vehicles, followed by PCA2. Both BMW2 and PCA1 present similar R/D durations, close to the unit value. Finally, BMW1 and BMW4 present similar R/D durations, and require more time reaching than depressing the pedal. Although these differences between vehicle configurations were expected to depend on the relationship between the distance of the pedal rest position from the H-point and the pedal travel length, a clear dependency was not found. However, considering the height from the vehicle floor of the clutch pedal at rest (obtained as the difference between the seat height and the vertical position of the pedal at rest, and reported later in Table 4.6), the R/D durations seem to follow the same distribution: the higher the rest position of the clutch pedal from the floor, the higher the foot must travel from the foot rest, and the longer it takes to reach it.

Finally a normalised time scale was defined, in order to plot and compare the kinematic and dynamic profiles of all the motions. First of all, the key-frames in each motion are expressed as a percentage of the duration of the motion. Subsequently, each time period between key-frames is scaled: this way each key-frame corresponds to the same position in the normalised time scale. The positions assigned to each key-frame are obtained by averaging their percent value across the motions. The average key-frames are reported in Table 4.4 and are shown in Figure 4.8, along with the distribution, among groups (a) and vehicle configurations (b), of their actual values.

Key-frames	Average value
StartMotion	0%
StartDepression	41.27%
EndDepression	84.13%
EndMotion	100%

Table 4.4: Average value of the key-frames respect to the total duration of the motions.

The distance between the average key-frame values and the distribution of their actual values in a specific group or vehicle (Figure 4.8) express how much the time periods in the considered set of motions are stretched or compressed in the normalised time scale.

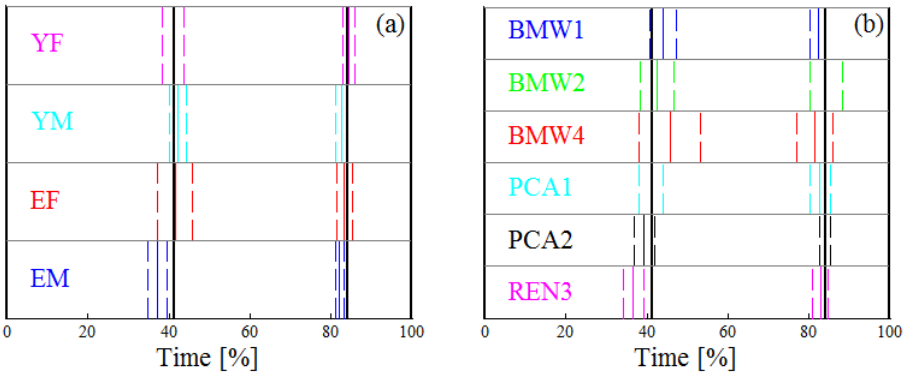

Figure 4.8: Key-frame distribution in the database in a normalised time domain. The average distribution is shown in solid thick black lines and compared to the distribution among the groups (a) and vehicle configurations (b). The coloured solid lines represent the mean of each set and the coloured dashed lines represent the 95% confidence intervals of the means.

The average key-frames are generally very similar to the mean values in each group and vehicle configuration. The only exception is given by the BMW4 vehicle configuration, which is associated to a smaller number of motions, and its mean values are therefore less reliable (the CIs in fact are larger than in the other vehicle configurations).

4.4.3 END-EFFECTOR TRAJECTORIES

As mentioned earlier, some of the reconstructed motions were not included in the database for issues related to the trajectory followed by the end-effector. In Figure 4.9 the 3D trajectories followed by the end-effector (EE) in the REN3 vehicle configuration are shown as example: it may be noticed how one of the trajectories followed by the EE of a YM subject starts from a lower point (i.e. the floor) and presents a different shape from the rest. Therefore, all motions in which the left foot started from the floor have been discarded from the database, as they may lead to erroneous considerations in the analysis.

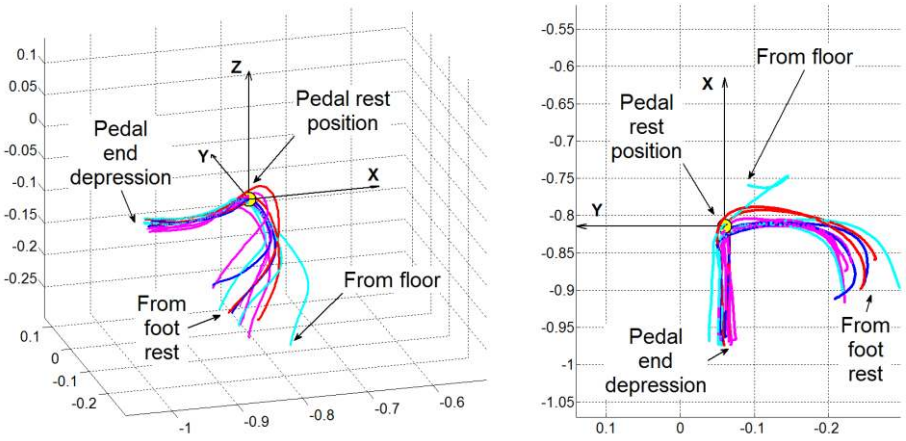

Figure 4.9: 3D (left) and 2D (right) views of the trajectories followed by the end-effector in the REN3 vehicle configuration. The different colours represent the subject groups performing the motion: YF (magenta), YM (cyan), EF (red) and EM (blue). The yellow circle marks the pedal rest position.

The mean trajectory followed by the end-effector (EE) in the database and its 95% CIs are shown in Figure 4.10, according to the subject groups (a1, b1, c1) and vehicle configurations (a2, b2, c2). The vertical black lines mark the average *StartDepression* and *EndDepression* key-frames. As expected, the vehicle configurations appear to strongly affect the EE

trajectory, which depends on where the pedal is located at rest and its travel characteristics. The vehicle configuration seems to govern not only the depression phase (in which the foot is guided by the pedal geometry) but also the reach phase: although the trajectory followed by the end-effector is free, all subjects seem to move in a very similar way from the foot rest to the pedal rest position. The only group-related difference lies in the starting position of the foot on the foot rest (Figure 4.10a1, Time = 0%): females tend to start closer to the seat than males, probably due to their shorter stature.

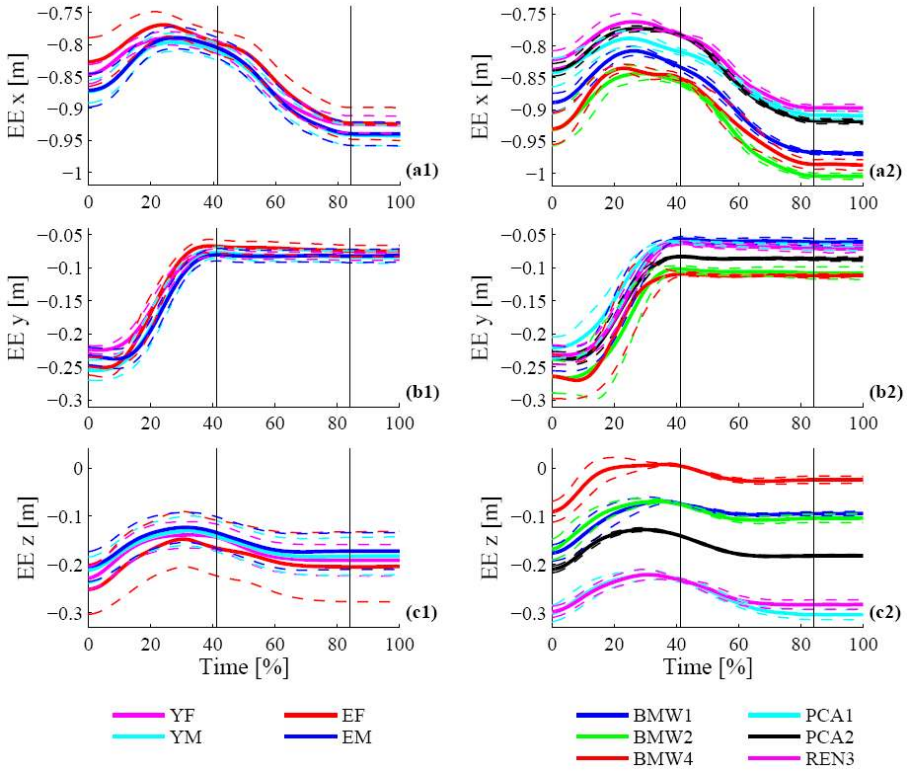

Figure 4.10: Mean trajectory followed by the end-effector along the 3 axes in the various groups (a1, b1, c1) and vehicle configurations (a2, b2, c2). The dashed lines represent the 95% confidence intervals of the means. The vertical black lines mark the average *StartDepression* and *EndDepression* key-frames.

4.4.4 DoF Profiles

In this section we compare the mean DoF profiles (and their CIs) among subject groups and vehicle configurations. From the analysis it is possible to

identify which DoFs are more affected by the group performing the motion and which others depend more on the environment.

As mentioned earlier, the DHM is described with a relative coordinates formalism. Specifically, the rotational DoFs are represented using Euler angles, which are hereafter always reported in their rotation order in the text. The values of the angles are calculated assuming that an upright standing position corresponds to a null value of the angles (Kapandji, 1987), and adopting the following sign criterion: flexion-extension (FE) angles are positive for flexions; abduction-adduction (AA) angles are positive for abductions; and longitudinal rotations (LR) are positive for clockwise rotations respect to the parent segment. The rotations allowed by the DoFs in the left leg are shown in Figure 4.11, along with the following local axes of the thigh, shank and foot segments: medio-lateral axis (ML), antero-posterior (AP) axis, and infero-superior (IS) axis.

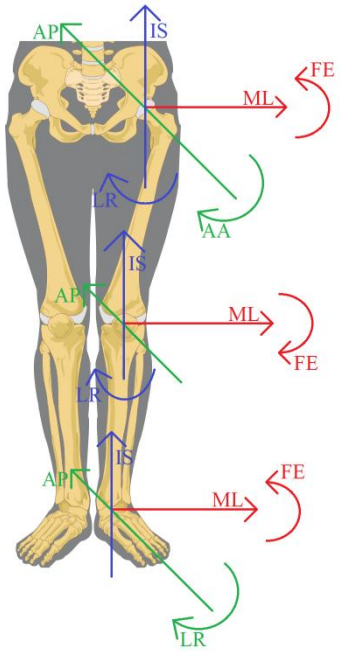

Figure 4.11: Movements of the segments in the left leg allowed by the joint DoFs and direction of the medio-lateral (ML), antero-posterior (AP) and infero-superior (IS) axes in each segment of the left leg: thigh, shank and foot.

For what concerns the hip joint (Figure 4.12), its motion is described by the following rotations: flexion-extension (FE), abduction-adduction

(AA) and longitudinal rotation (LR). Among these, the DoF which mostly governs the clutch pedal depression is the FE DoF, as the motion is mainly carried out in the sagittal plane (see Figure 4.2). The average shape of the FE hip DoF is similar in all sets of data, however its values across the motion differ, and seem to be influenced by the vehicle configuration (Figure 4.12a2) more than by the subject group (Figure 4.12a1). In fact, the average profiles of both PCA1 and REN3 are not contained in the remaining vehicle CIs. This observed difference may be related to the seat height in the vehicle configuration (Table 4.2): in fact, both PCA1 and REN3 present the highest seats, which may reasonably lead to a more extended hip joint, in accordance with Wang et al. (2000).

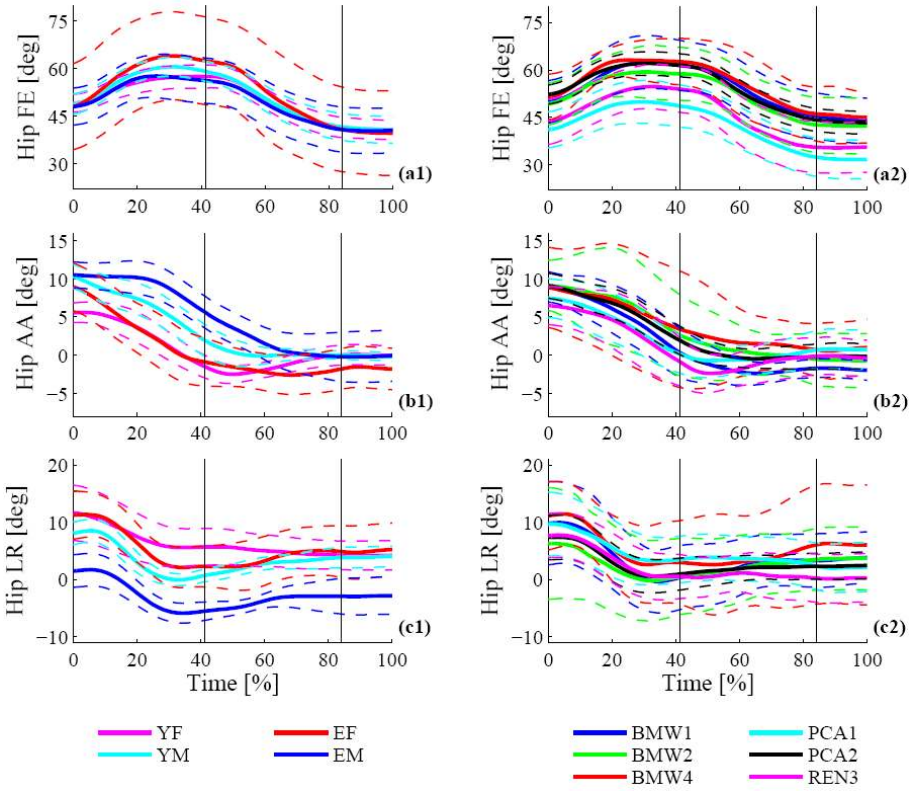

Figure 4.12: Mean joint angle profiles for the hip joint in the various groups (a1, b1, c1) and vehicle configurations (a2, b2, c2). The angles represent the flexion-extension (FE), the abduction-adduction (AA) and the longitudinal rotation (LR) of the hip joint. The dashed lines represent the 95% confidence intervals of the means.

On the other hand, the vehicle configurations seem not to influence as strongly the remaining two hip DoFs, as the CIs of the mean profiles tend to overlap (Figure 4.12b2, c2). Both the AA and the LR DoFs present a smaller effect on the motion in the sagittal plane, and therefore may move more freely without compromising the task fulfilment. In fact, their values seem to depend more on the subject group performing the motion, in accordance with Wang et al. (2000): males tend to abduct the hip more (Figure 4.12b1) and rotate it less (Figure 4.12c1) respect to female subjects, who tend to keep the hip more adducted and rotated inwards, possibly due to cultural upbringing.

The knee joint (Figure 4.13) is described by the following rotations: flexion-extension (FE) and longitudinal rotation (LR). Along with the hip FE, the knee FE plays a relevant role in clutch pedal depression motions and presents a very similar shape in all data sets.

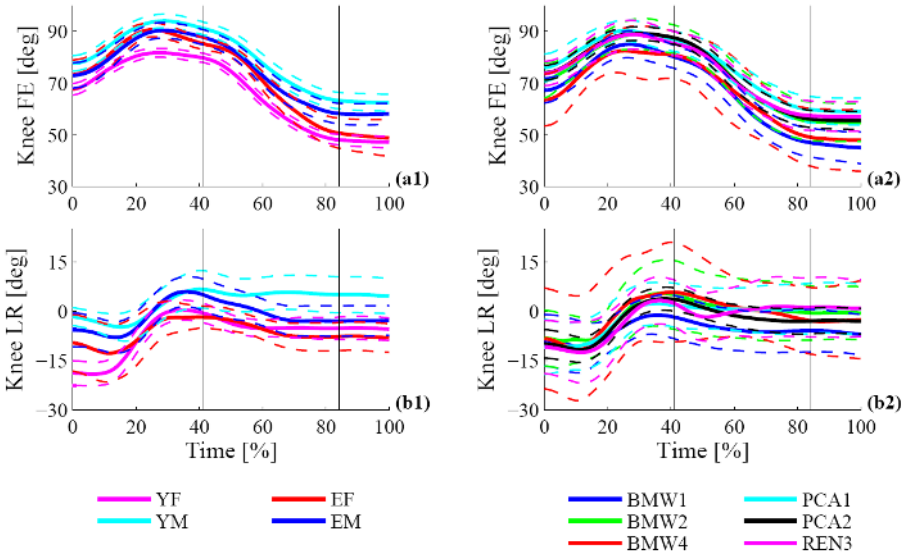

Figure 4.13: Mean joint angle profiles for the knee joint in the various groups (a1, b1) and vehicle configurations (a2, b2). The angles represent the flexion-extension (FE) and the longitudinal rotation (LR) of the knee joint. The dashed lines represent the 95% confidence intervals of the means.

Female subjects however seem to carry out the motion with a more extended knee respect to males (Figure 4.13a1), probably due to their shorter stature. Differences may be noticed also considering the vehicle configurations, as both BMW1 and BMW4 seem to require slightly more

extended knee joints. The clutch pedals in these two vehicles are among those placed further along the longitudinal *x* axis (Table 4.2), which would explain a more extended knee. Nevertheless, subjects tend to flex the knee in BMW2 as much as in the remaining vehicles, although BMW2 presents the furthest clutch pedal. However, the actual longitudinal position of the seat must be taken into account (as reported in Table 4.6): in fact, the seat is placed closer to the pedals in BMW2, reducing the actual distance between the seat and the clutch pedal, and allowing greater knee flexions. Additionally, it may be noticed that only 25% of the motions in BMW2 were performed by females (Table 4.3). This leads to a larger average stature in BMW2 respect to the remaining vehicles, which may account for a more flexed knee.

As in the hip joint, the LR DoF, which does not strongly affect the motion, depends more on the subject groups than the vehicle configurations (Figure 4.13b1), and apparently females twist the knee outwards more than males, compensating the inwards hip rotation mentioned earlier.

The ankle joint is represented, as the knee, by a flexion-extension (FE) and a longitudinal rotation (LR) DoF. Once more, the FE DoF, which acts mainly in the sagittal plane, presents a similar shape in all data sets (Figure 4.14a1, a2). For what concerns the group-related differences, females do not compensate the more extended knee (Figure 4.13a1) with a more flexed ankle. In fact, also the ankle in females is more extended than in males (Figure 4.14a1), reflecting the need for female subjects to extend the leg more in order to reach the pedal, due to their shorter stature. On the other hand, the vehicles do not seem to influence the ankle FE strongly, although at the end of the depression BMW2 presents a more flexed ankle than the rest. This may seem surprising, as Table 4.2 reports that BMW2 is the vehicle with the furthest pedal rest position and of the largest travel lengths. However, this information must be combined once again with the seat longitudinal position chosen by the subjects (as reported in Table 4.6), and the flexion of the ankle may also be explained, as for the knee, with the reduced contribution of female subjects to the BMW2 means.

Similarly to the hip and knee joints, the DoF which less affects the ankle motion in the sagittal plane depends more on the subject group than on the vehicle (Figure 4.14b1, b2): however in this case a gender- or age-related trend is not evident.

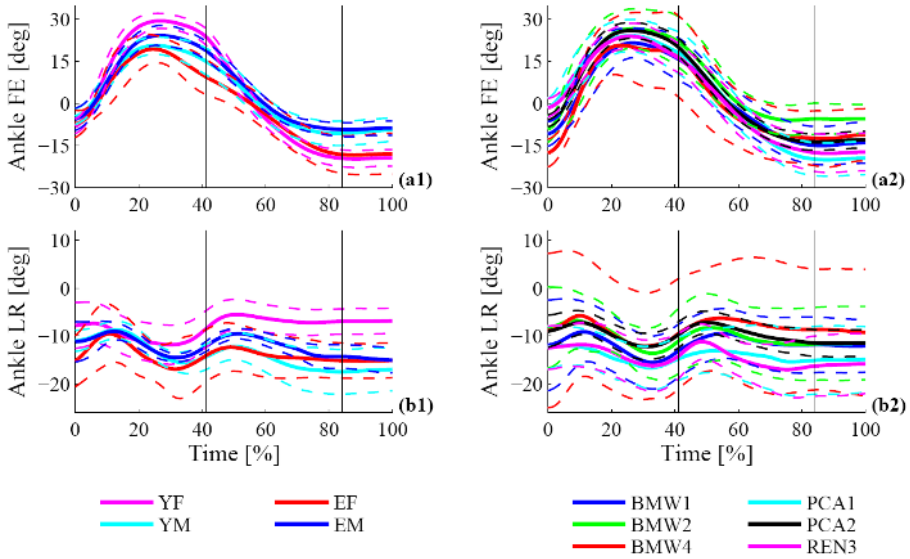

Figure 4.14: Mean joint angle profiles for the ankle joint in the various groups (a1, b1) and vehicle configurations (a2, b2). The angles represent the flexion-extension (FE) and the longitudinal rotation (LR) of the ankle joint. The dashed lines represent the 95% confidence intervals of the means.

Considering the global rotations associated to the root joint (Figure 4.15), these are expressed with Euler angles in the following order and with the following sign criterion: longitudinal rotation about the global *z* axis, positive for clockwise rotations; lateral tilt, positive for tilts towards the right of the DHM; forward tilt, positive for tilts towards the front of the DHM. The pelvis longitudinal rotation (Figure 4.15a1, a2) is modest and the average profiles differ of about 2° both group-wise and vehicle-wise. Such small differences are comparable to the accuracy of the reconstruction, and may be a result of the reconstruction or anthropometric characterisation processes rather than actual group- or vehicle-related issues. Nevertheless, what may be noticed is that all profiles are close to the null rotation, in agreement with a seated posture facing forwards.

Analysing the lateral tilt mean profiles (Figure 4.15b1, b2), the shapes reveal the subjects' tendency to lean to the left while the left foot is travelling from the foot rest to the pedal. In fact, during the reach phase the weight of the left leg is no longer balanced by the floor reaction and generates a torque at the root joint which tilts the pelvis towards the left. On the other hand, during the pedal depression the pelvis returns to a more

symmetric pose respect to the sagittal plane as the pedal reaction increases. In this case neither the subject group nor the vehicle configuration seem to influence the DoF profile, as the mean profiles tend to fall within all the CIs.

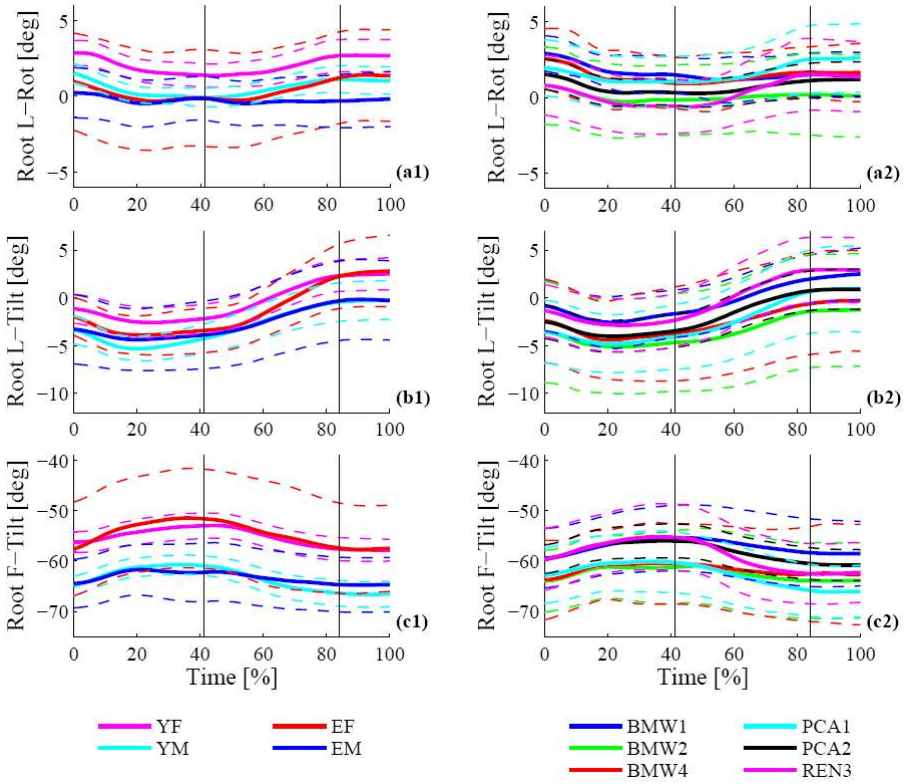

Figure 4.15: Mean joint angle profiles for the root joint in the various groups (a1, b1, c1) and vehicle configurations (a2, b2, c2). The angles represent the longitudinal rotation (L-Rot), the lateral tilt (L-Tilt) and the forward tilt (F-Tilt) of the root joint. The dashed lines represent the 95% confidence intervals of the means.

As for the forward tilt, group-related differences may be noticed (Figure 4.15c1): both male groups (YM, EM) are seated with the pelvis more tilted backwards than the female groups (YF, EF). Given that in the adopted DHM (see Section 4.2) the upper-body is considered to be rigidly connected to the pelvis, the above-mentioned difference in the forward tilt results in female DHMs being seated more upright than male DHMs. However, such differences in seated postures may not be as evident in the actual male and female subjects, as a person's seated posture also depends

on the spinal pose. For what concerns the vehicle configurations, they do not seem to affect the forward tilt as much as the subject group (Figure 4.15c2): in fact, the profiles present less variability among the means than in the group-related comparison.

Finally, the effect of subject groups and vehicle configurations on the translational DoFs is presented (Figure 4.16). These are expressed in the global coordinate system shown in Figure 4.2 and Figure 4.4. For what concerns the position of the pelvis along the *x* axis (Figure 4.16a1, a2), it is strongly related to the subjects' choice in the position of the seat (Table 4.6), which could slide forwards or backwards. This DoF seems to be greatly influenced by the subject group: female subjects (especially EF) tend to slide the seat closer to the front of the vehicle, probably to reach the pedal more easily given their shorter stature. On average, EF subjects tend to sit 5cm closer to the front respect to male subjects.

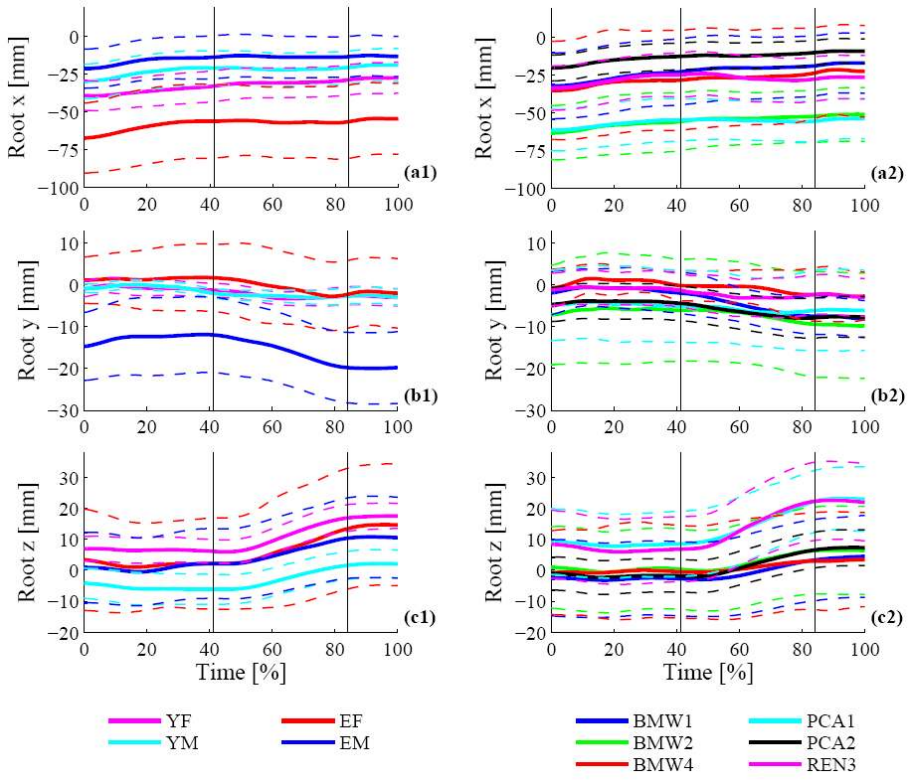

Figure 4.16: Mean trajectory followed by the root joint along the 3 axes in the various groups (a1, b1, c1) and vehicle configurations (a2, b2, c2). The dashed lines represent the 95% confidence intervals of the means.

Also the vehicle configuration seems to affect the position of the seat: in BMW2 and PCA1 subjects tend to sit about 3cm closer to the pedals than in the other vehicles, as confirmed by the seat longitudinal position reported in Table 4.6. In the case of BMW2, the reason seems to be the position of the clutch pedal, which is furthest from the seat than in the other vehicle configurations (Table 4.2). Instead, in the case of PCA1 the reason seems to be related to the initial orientation of the clutch pedal (Table 4.6), which presents a much smaller inclination respect to the horizontal axis: subjects may tend to move closer to the pedal, preparing for a more vertical pedal depression. Finally, it may be noticed that during the motion subjects seem not to change their horizontal position significantly.

For what concerns the vertical position (Figure 4.16c1, c2), the shape of the profiles are all very similar: the pelvis lifts during the depression as the force exerted on the pedal increases. However, the range of vertical movement of the pelvis is in the order of 1cm, which again is comparable to the accuracy of the reconstruction: although the tendency to lift during the pedal depression appears in all sets of data and is physically reasonable, further analyses into the differences between the mean and CI profiles would not be reliable. The same applies to the lateral position of the pelvis (Figure 4.16b1, b2): elderly males (EM) seem to have chosen to sit more towards the left of the seat. Nevertheless it is not possible to ascertain whether this characteristic actually depends on the subject group or on causes related to the definition of the subjects' anthropometric parameters or to the reconstruction process.

4.4.5 COORDINATION LAW

From the analysis of the DoF profiles, it was noticed that the flexion-extension (FE) DoFs, which play the most relevant roles in the motion, present a very similar shape, which does not seem to depend on either the subject group or the vehicle configuration (Figure 4.12a, d; Figure 4.13a, c; Figure 4.14a, c). Hence, the shape of the FE DoF profiles seems determined by the task itself.

Therefore, we analysed the FE profiles of all the motions, normalised considering the minimum and maximum value possessed by the DoFs in each motion, to assess the similarity in profiles. The mean normalised profiles among all motions are shown in Figure 4.17.

The normalised profiles are very similar one another. First of all, they all reach their maximum flexion at around 30% of the motion. Moreover,

the means are almost always included in the each other's CIs. Actually, the hip and knee means always fall inside each other's CIs. The ankle instead is relatively more extended most of the time. However, during the majority of the reach phase, the ankle mean falls within the hip and knee CIs, and although it exceeds their CI range during the depression, it still presents similar values and a strong resemblance to their shape.

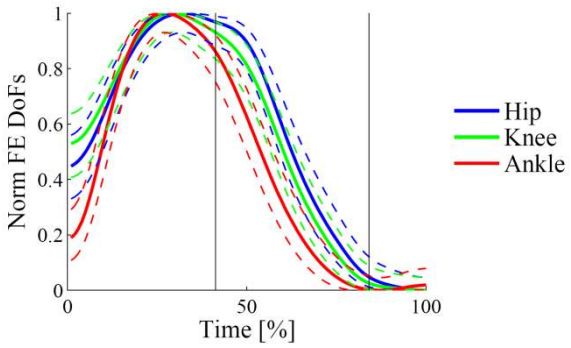

Figure 4.17: Mean normalised flexion-extension (FE) DoF profiles at the hip, knee and ankle joints. The dashed lines represent the 95% confidence intervals of the means. The vertical black lines mark the average *StartDepression* and *EndDepression* key-frames.

Such a close relationship between FE profiles led to the definition of a coordination law for the clutch pedal depression, according to which the FE DoFs move following some kind of synchronicity. This synchronicity is expressed in terms of the normalised FE DoF profiles $\mathbf{q}_n$, which must be similar to one another during the motion:

$$\forall t \quad q_n(Ankle\ FE) \cong q_n(Knee\ FE) \cong q_n(Hip\ FE) \tag{4.1}$$

4.4.6 JOINT EFFORT PROFILES

In this section we analyse the efforts in the DHM at the joints (obtained through ID as mentioned in Section 4.3), defined as the efforts exerted by each segment on the following distal segment, expressed in the local coordinate system of the distal segment. Of the three components for each effort, we present only those which produce work, given the DoFs which characterise each joint. The components are measured along the following axes, shown in Figure 4.11: medio-lateral (ML), antero-posterior (AP), and infero-superior (IS). The same sign criterion defined for the DoFs in Section 4.4.4 is used for the efforts: an effort presents positive values if it is

directed so as to produce motion in the positive direction of the corresponding DoF.

First of all, the torques at the joints in the left leg are analysed. These torques are equivalent to the actual muscular effort required to perform the motions. The components which present greater values are those along the medio-lateral (ML) axes: in fact, they are mainly associated to the motion in the sagittal plane, in which most of the clutch pedal depression is carried out. Figure 4.18 reports the forces which mainly contribute to the ML joint torques during the reach and depression phases: during the former phase, the main contribution to the torques is given by the gravitational forces (Figure 4.18a); whereas during the latter, also the pedal reaction force to its depression plays a front stage role in determining the joint ML torques (Figure 4.18b), and it may be orientated in different directions, as will be explained later (Section 4.4.9).

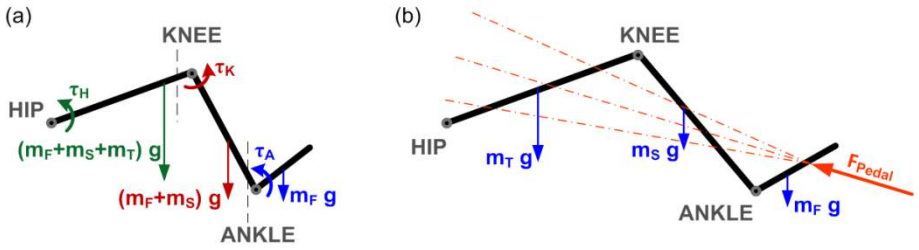

Figure 4.18: Sagittal forces and ML torques acting at the leg joints during the reach phase (a) and sagittal forces acting on the leg segments during the pedal depression (b). Each joint torque in (a) is considered due to the weight of its distal segments, both marked in the same colour. The pedal reaction force (b) can be oriented in different directions. The subscripts F, S and T correspond to the foot, shank and thigh, respectively.

As may be noticed in the following diagrams (Figure 4.19, Figure 4.20 and Figure 4.21), the reach phases all present similar ML torque values, as the gravitational forces acting on the leg are similar in all motions. The pedal depression phase, on the other hand, presents a larger variety of dynamic behaviours, due to the different directions of the pedal reaction force.

For what concerns the hip joint (Figure 4.19), the vehicle configuration seems to affect the ML torque (Figure 4.19a2): the torque required in BMW4 and PCA1 during the pedal depression is smaller and applied in the opposite direction than in the other vehicles (i.e. directed in

the hip extension rather than flexion). In fact, in BMW4 and PCA1 the hip participates actively in the depression, with a torque than seeks to extend the thigh, whereas in the other vehicles, the torque at the hip seeks to maintain the thigh flexed, balancing the leg weight. This difference is related to the direction of the pedal reaction force, discussed later in Section 4.4.9. Clear group-related differences may also be identified (Figure 4.19a1): elderly subjects (EF, EM) tend to load the hip joint more than younger subjects (YF, YM), who end the pedal depression with an almost null ML hip torque (see Section 4.4.9).

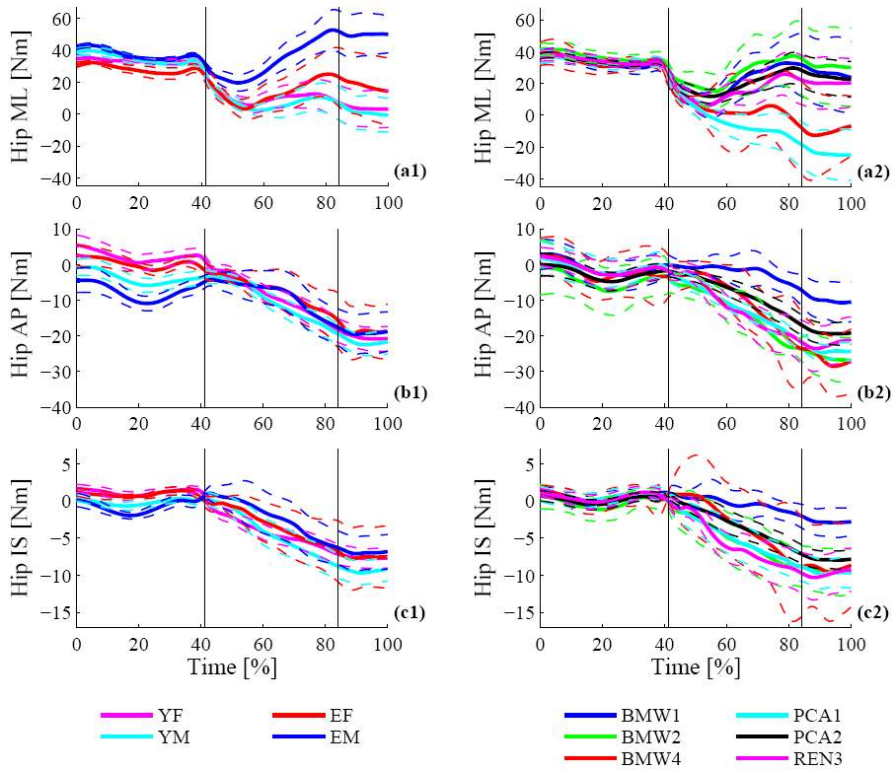

Figure 4.19: Mean joint torque profiles at the hip joint in the various groups (a1, b1, c1) and vehicle configurations (a2, b2, c2). The torques are expressed in the medio-lateral (ML), antero-posterior (AP) and infero-superior (IS) axes. The dashed lines represent the 95% confidence intervals of the means. The vertical black lines mark the average *StartDepression* and *EndDepression* key-frames.

The remaining AP and IS torques at the hip (Figure 4.19b1, b2 and c1, c2, respectively) are smaller and do not seem to be strongly influenced by either the subject or the environment. The only consistent variations

across sets may be observed in the AP torque during the reach phase for the different subject groups (Figure 4.19b1). The differences among sets, however, are small and given the reduced impact of the AP torque on the motion, no further analysis is carried out to assess the group-related influence. What may be noticed is that the inter-group variability is smaller than the inter-vehicle variability in all components, suggesting that the hip torque patterns depend more on the subjects performing the clutch pedal depression than the environmental conditions it is performed in.

The analysis of the knee joint torques (Figure 4.20) reveals dependencies which are similar to those encountered at the hip joint. For what concerns the influence of the vehicle configuration on the medio-lateral (ML) torque (Figure 4.20a2), once again BMW4 and PCA1 present a smaller torque, applied in the opposite direction respect to the other vehicles. In these two vehicle configurations, the hip seems in charge of extending the leg to depress the pedal while the knee maintains its flexion; whereas, in the other vehicles, the hip maintains its flexion while the knee tends to extend during the pedal depression. As for the hip, these differences are related to the direction of the pedal reaction force (Section 4.4.9).

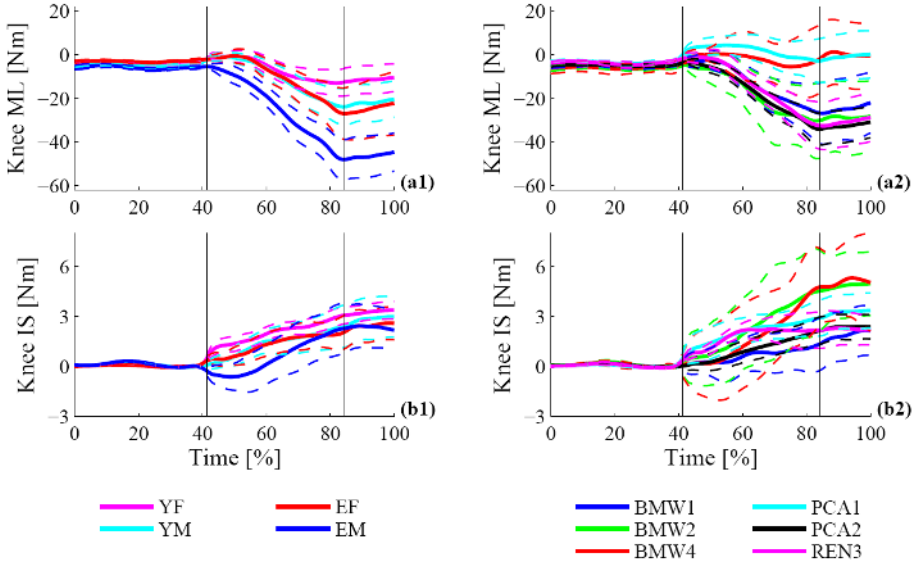

Figure 4.20: Mean joint torque profiles at the knee joint in the various groups (a1, b1) and vehicle configurations (a2, b2). The torques are expressed in the medio-lateral (ML), and infero-superior (IS) axes. The dashed lines represent the 95% confidence intervals of the means.

Once again, group-related differences in the ML torque component are also identifiable (Figure 4.20a1): both elderly groups (EF, EM) tend to load the knee more than the young groups (YF, YM respectively). This difference is clear for male subjects and remains a speculation for females (EF provided fewer motions, hence presenting wider CIs).

Regarding the infero-superior (IS) torque (Figure 4.20b1, b2), it appears during the pedal depression (subjects tend to twist the leg to depress the pedal) and is smaller than the ML torque. As for the hip, it presents smaller variability group-wise, suggesting a group-specific pattern.

Similar considerations apply also for the torque at the ankle joint (Figure 4.21). The inter-group variability is smaller than the inter-vehicle variability, confirming that subject groups tend to behave consistently torque-wise. An inverse trend respect to the hip and knee medio-lateral (ML) torque may be noticed: young subjects (YF, YM) tend to load the ankle more than elderly subjects (EF, EM).

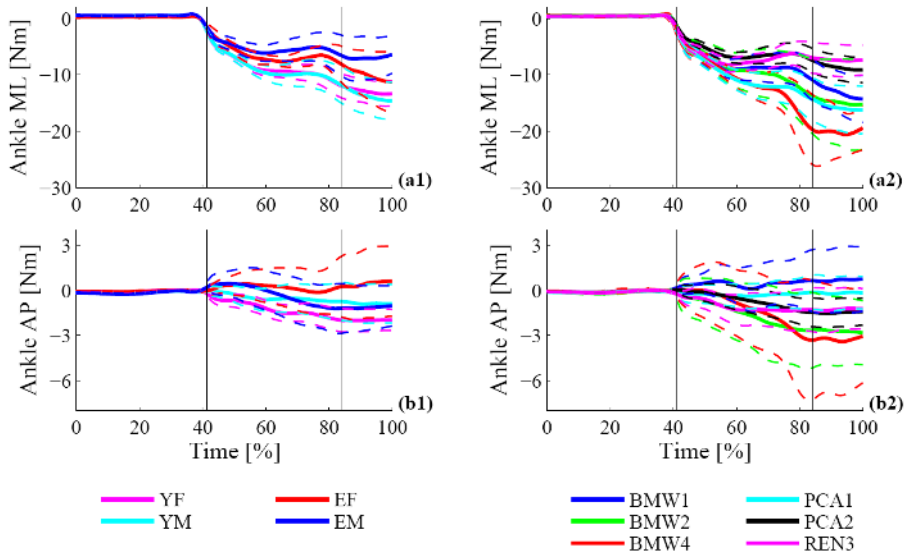

Figure 4.21: Mean joint torque profiles at the ankle joint in the various groups (a1, b1) and vehicle configurations (a2, b2). The torques are expressed in the medio-lateral (ML) and antero-posterior (AP) axes. The dashed lines represent the 95% confidence intervals of the means.

The vehicle configuration also influences the ankle torque, ranging from the reduced torques required in PCA2 and REN3, to the greatest torques of BMW4. These differences seem related to the height of the pedal

rest position from the floor (Table 4.6), which may affect the manner in which subjects perform the depression. For what concerns the antero-posterior (AP) torque, it appears at the ankle during the pedal depression, as subjects tend to twist the foot while depressing the pedal.

For what concerns the efforts acting at the root joint, these are obtained through ID and balanced by the seat reaction. Hence, as opposed to the previous efforts, the forces and torques at the root joint are expressed in the global coordinate system in order to identify more easily the external forces which contribute to each component.

The greatest part of the seat reaction force (Figure 4.22) is applied along the vertical *z* axis to balance the weight of the upper part of the subjects' body. During the reach phase, also the weight of the left leg is unloaded on the seat, whereas during the pedal depression, part of its weight is balanced by the pedal reaction force: the vertical force on the seat is reduced during the depression (Figure 4.22c1, c2).

On the one hand, no significant vehicle-related differences may be encountered (Figure 4.22c2). On the other, however, a very clear trend characterises the group-related seat reaction force profiles (Figure 4.22c1): as expected, the average vertical seat reaction forces follow the average weights of the subject groups, reported in Table 4.5. Regarding the force along the longitudinal *x* axis, it appears during the pedal depression, due to the pedal reaction force (see Section 4.4.7). No group-related differences are noticed (Figure 4.22a1). However, concerning the vehicle configuration (Figure 4.22a2), PCA1 seems to require a more reduced longitudinal seat reaction. This seems directly linked to the pedal travel length and angle (Table 4.1), which are respectively smaller and larger in PCA1 than in the remaining vehicle configurations. On the one hand, a smaller travel length implies a reduced pedal reaction (see Section 4.4.7), and on the other a larger travel angle implies a more vertical reaction (see Section 4.4.9). Finally, the transversal force along the *y* axis (Figure 4.22b1, b2) is smaller and presents no significant group-related or vehicle-related differences.

The torques acting at the root joint are not applied external torques, but the effect of the application point of the seat reaction on the subjects' pelvis and back. It may be seen in fact that the greatest moment values are about the transversal *y* axis (Figure 4.23b1, b2), due to the force components along the longitudinal *x* and vertical *z* axes (Figure 4.22a1, a2 and c1, c2, respectively) and their application point.

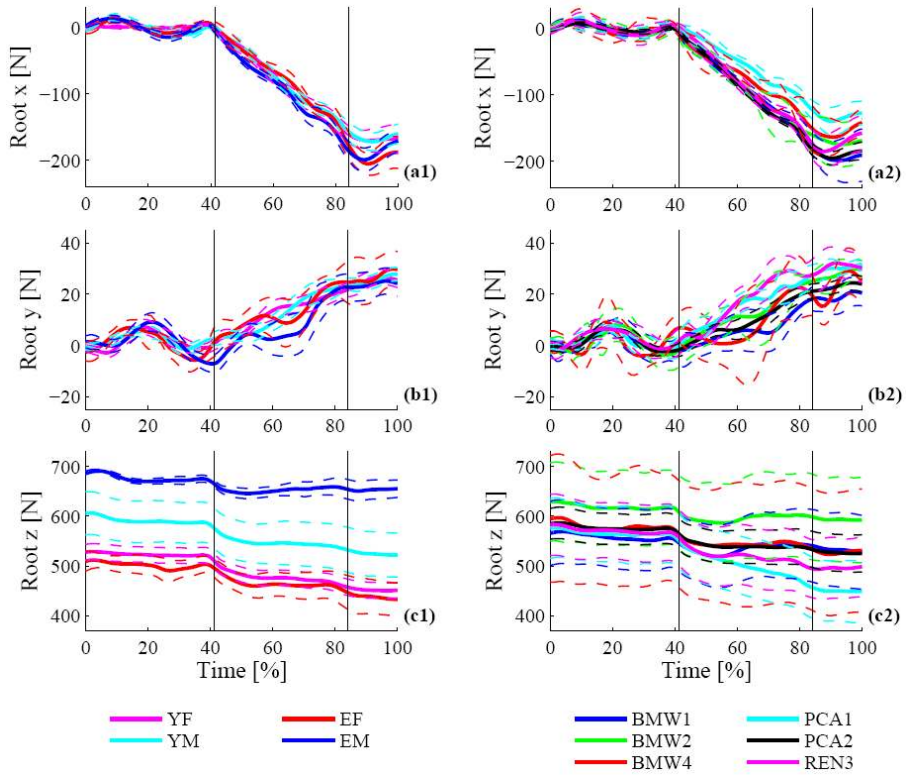

Figure 4.22: Mean forces acting at the root joint in the various groups (a1, b1, c1) and vehicle configurations (a2, b2, c2). The forces are expressed in the global coordinate system. The dashed lines represent the 95% confidence intervals of the means.

During the reach phase, the group-related differences (Figure 4.23b1) follow the same trends encountered in the vertical force component (Figure 4.22c1): male subjects (YM, EM) present a larger torque than females (YF, EF). During the depression, however, age is the most relevant factor and the torque values follow an inverse trend respect to the hip and knee ML torques (Figure 4.19a1 and Figure 4.20a1, respectively): elderly subjects (EF, EM) tend to reduce the torque at the root, as opposed to young subjects (YF, YM). Young subjects, in fact, present a larger torque at the root, which is caused by pushing on the backrest of the seat with the upper part of the back, further away from the pelvis. Apparently young subjects prefer to load their back rather than exerting more effort at the hip and knee joints. On the contrary, elderly subjects tend to avoid back loads, probably because they suffer from back pain is more easily, and prefer loading the hip and knee joints more (see Section 4.4.9). For what concerns the different vehicle

configurations (Figure 4.23b2), during the pedal depression BMW4 and PCA1 seem to require a greater transversal torque at the root, transmitted by the hip joint (Figure 4.19a2).

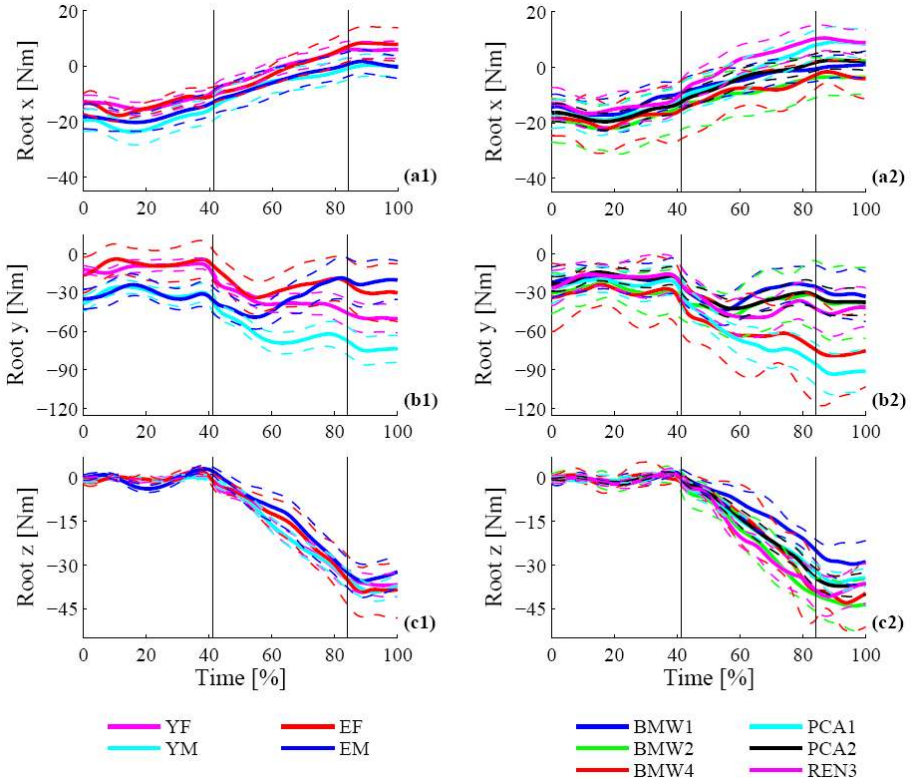

Figure 4.23: Mean torques acting at the root joint in the various groups (a1, b1, c1) and vehicle configurations (a2, b2, c2). The torques are expressed in the global coordinate system. The dashed lines represent the 95% confidence intervals of the means.

The torque about the vertical *z* axis appears during the pedal depression, due to the asymmetric longitudinal load on the feet, and does not seem to present significant group-related or vehicle-related differences. The torque about the *x* axis (Figure 4.23a1) instead is mainly due to the vertical force (the effect of transversal force is negligible) which, given the reduced value of the torque, seems to be applied very close to the root joint in the transversal direction.

Finally, as for all the torques considered in this section, the inter-group variability seems smaller than the inter-vehicle variability, once again

suggesting the existence of a dynamic pattern, which mostly depends on the subject performing the task (their gender, age and weight).

The analysis of the motion dynamics carried out in this section has revealed differences among groups and vehicle configurations that otherwise, with a purely kinematic analysis, would have remained hidden. The most notable group-related result is that elderly people prefer loading the leg joints rather than pushing with their back against the seat (opposed to young subjects). For what concerns the vehicle configuration, two vehicles (BMW4 and PCA1) which did not yield significantly different DoF profiles, tend to require greater torques at the hip and root joints.

4.4.7 PEDAL STIFFNESS

During the pedal depression, the pedal reacts with a force which is tangent to the pedal trajectory (**n** vector in Figure 4.24).

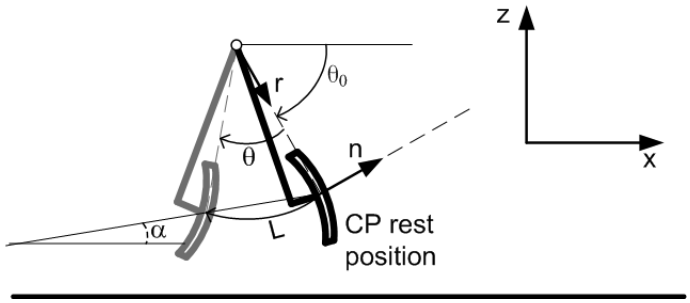

Figure 4.24: Geometric characteristics of the pedal: normal (n) and radial (r) directions, initial orientation (θ_0), depression angle (θ), travel length (L) and travel angle (α).

To characterise this reaction force, a stiffness curve for the pedal in each vehicle configuration was obtained by relating the experimental values of the pedal reaction force along the **n** direction to the pedal depression angle θ, as shown in Figure 4.25. It may be seen that the value of the maximum rotation changes in the vehicle configurations, in accordance with their travel length L, reported in Table 4.2. Moreover, during the central part of the depression, the slope of the curves is very similar in all vehicle configurations: in fact, the stiffness characteristics of the pedal in the vehicle mock-up were not modified in the various vehicle configurations. The last part of the stiffness curves almost present a vertical asymptote, representing the fact that once the pedal has reached its full depression, the depression force may increase but no further rotation is allowed.

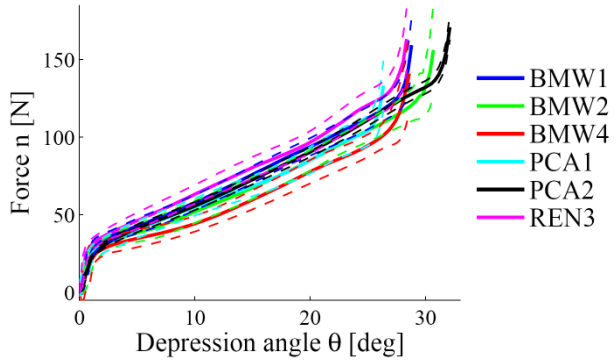

Figure 4.25: Mean pedal stiffness curves in the various vehicle configurations. The dashed lines represent the 95% confidence intervals of the means.

4.4.8 PEDAL FRICTION

Although only the force exerted along the normal direction of the pedal (**n** in Figure 4.24) produces the motion of the pedal, the component of the force along the radial direction **r** may not be null due to friction. In fact, Wang et al. (2000) found that the force exerted on the pedal during its depression presents both normal and radial components. The relationship between the experimental values of the radial and normal forces is discussed in this section.

The relationship between the experimental values of the radial and normal forces is reported in Figure 4.26. The most notable characteristics of the curves in Figure 4.26a1 and a2 is their tendency towards linearity. This implies a constant ratio between the radial and the normal force (Figure 4.26b1, b2).

The subject group seems to affect the radial/normal force ratio: elderly subjects present the lowest ratios whereas young subjects tend to increase the radial force. This group-related characteristic is discussed in detail in the following section, in which the direction of the force exerted on the pedal is analysed.

For what concerns the vehicle configuration, it seems to affect the radial force less than the subject group. However, it may be seen that PCA1 presents the greatest radial/normal force ratio. This characteristic is also discussed in the following section.

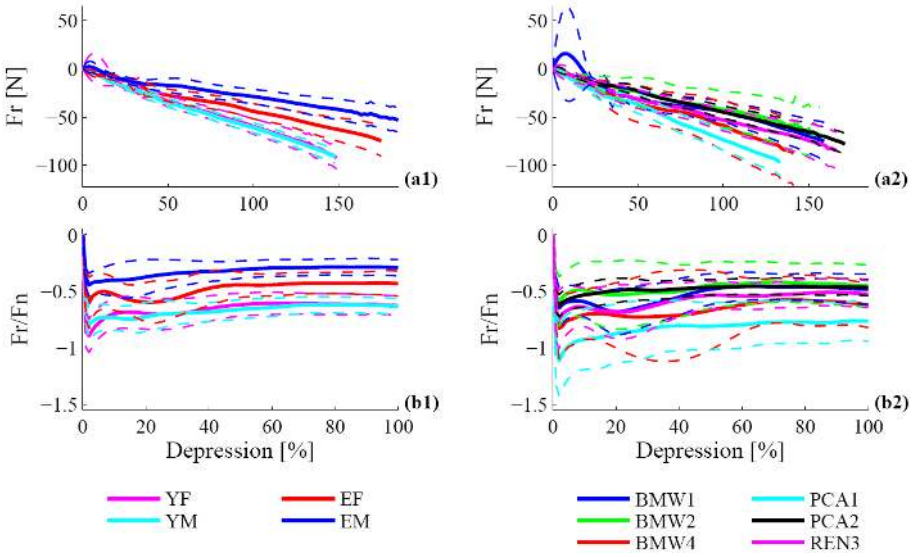

Figure 4.26: Mean values of the radial component of the pedal reaction force respect to its normal component in the various groups (a1, b1) and vehicle configurations (a2, b2). On the left the radial force is plotted against the normal force (a1, a2), whereas on the right the ratio between the radial and normal forces is shown during the pedal depression phase (b1, b2). The dashed lines represent the 95% confidence intervals of the means.

4.4.9 PEDAL FORCE DIRECTION

As discussed in the previous section, the force exerted on the pedal presents a radial component. This component is unnecessary for what concerns the motion of the pedal, but it is nevertheless applied. The effect of the radial force is that of modifying the direction of pedal reaction force, albeit increasing its magnitude. Apparently subjects apply a radial force in order to distribute the torques across the joints in the most convenient manner for them.

To analyse the effect of the radial force, we consider two directions: the direction of the pedal reaction force and the direction of the line which connects the hip joint and the end-effector (called leg direction). Moreover, we define two angles (Figure 4.27): α_F is the angle formed by the pedal force and the horizontal directions, and α_{FL} is the angle which the pedal force forms with the above-mentioned leg direction.

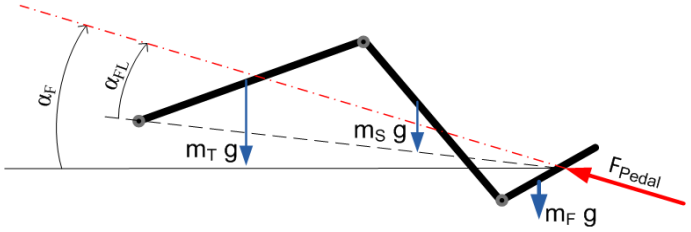

Figure 4.27: Orientation of the main forces acting on the leg during the pedal depression. The angle formed by the pedal force and the horizontal axis is marked as α_F, whereas α_{FL} is the angle formed by the pedal force and the leg direction (i.e. line connecting the hip joint and the end-effector). The subscripts F, S and T correspond to the foot, shank and thigh, respectively.

Since both angles depend on the pedal force direction, we have assessed their dependency on the pedal force magnitude, in order to gain insight into motion patterns. Hence, we have considered the weighted average of the α_F and α_{FL} angles during the depression phase, selecting the magnitudes of the pedal force as weighting factors.

Figure 4.28 reports the weighted mean α_F and α_{FL} angles according to the subject groups and vehicle configurations. Regarding the value of α_F, elderly males (EM) tend to apply a more horizontal force than the remaining groups (Figure 4.28a1). The greater differences, however, seem to be vehicle-related (Figure 4.28b1) and seem to follow the clutch pedal travel angle distribution reported in Table 4.2. The reason is that the travel angle is a measure of the average normal vector $\mathbf{n}$ to the pedal: the greater the angle, the more vertical is the direction of the normal component of the pedal force. Additionally, given the relationship between the radial and normal components of the pedal force (Figure 4.26a2, b2), the radial component contributes to an even greater vertical component of the pedal force. The combination of both the clutch pedal travel angle and the radial pedal force component account for the large mean value of α_F in PCA1 (Figure 4.28b1).

For what concerns the relative pedal force direction respect to the leg direction measured by α_{FL} (Figure 4.28a2, b2), it is considered relevant as it contributes significantly to the ML torque at the hip and root joints. In fact, it may be noticed that elderly subjects (EF, EM) tend to align the pedal force with their leg direction: such behaviour reduces the torque at the hip due to the pedal reaction force, leaving the hip to balance the leg weight as in the reach phase (Figure 4.19a1). On the other hand, low values of α_{FL}

imply a reduced root torque about the *y* transversal axis (Figure 4.23), hence requiring a lower seat reaction torque for balance (i.e. a closer application point to the pelvis in the backrest). On the contrary, young subjects (YF, YM) tend to choose the value of α_{FL} which reduces the hip and knee ML torques, balancing the torque due to the weight of the distal segments (Figure 4.27). According to Wang et al. (2000), the pedal reaction is almost aligned with the leg direction, with an average distance of about 5º. Although all subject groups tend not to strongly misalign the pedal force with their leg direction, the behaviour reported by Wang et al. seems to match the pattern followed only by the elderly people in our database.

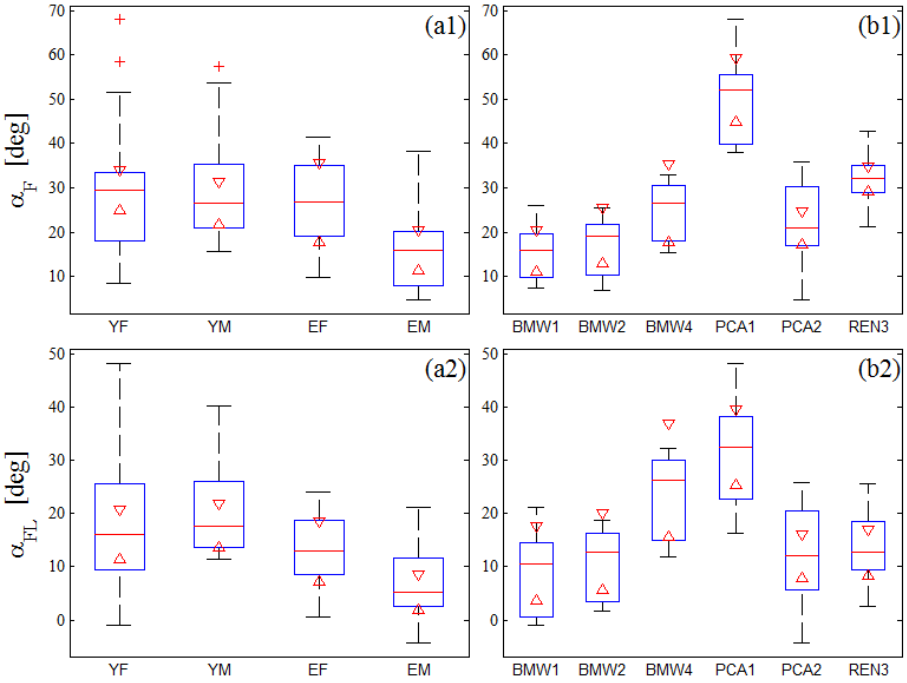

Figure 4.28: Box plots of the mean force orientation respect to the horizontal direction (a1, b1) and to the leg direction (a2, b2), organised according to the subject groups (a1, a2) and the vehicle configurations (b1, b2). The red line represents the median, the blue box contains the inter-quartile range (from the 25th to the 75th percentile), and the black whiskers extend from the minimum to the maximum values (outliers are marked with red crosses). The red triangles mark the 95% confidence intervals of the medians.

Finally, the vehicle-related differences in α_{FL} match the differences in ML torques across the joints, described in Section 4.4.6 The highest α_{FL} angles correspond to the PCA1 and BMW4 vehicle configurations, which

present smaller ML torques at the hip and knee (applied in the opposite direction than in the other vehicles) and larger ML torques at the ankle respect to the other vehicles. It must be noticed that most of the behaviours exhibited in the PCA1 configuration seem to be associated to its large clutch pedal travel angle. However, the similar behaviour exhibited in BMW4 does not seem to be related to the same cause, given the reduced travel angle in BMW4. Nevertheless, the number of motions performed in BMW4 is the smallest among vehicle configurations (Table 4.3), leaving its mean profiles and CIs to be less reliable than the rest.

4.4.10 FOOT-PEDAL CONTACT POINT

For what concerns the point in the foot which reaches the clutch pedal, its position has been analysed to assess how far from the heel it is located along the sole of the shoe. Figure 4.29 reports the mean distance between the end-effector and the heel respect to the foot length, according to the subject groups and vehicle configurations.

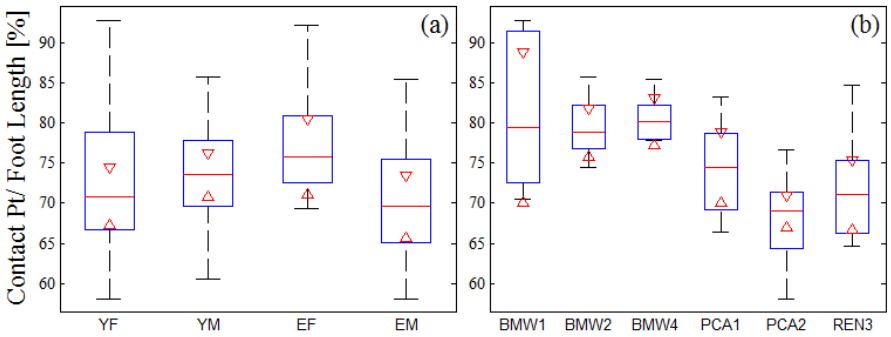

Figure 4.29: Box plots of the position of the end-effector along the foot respect to the foot length, organised according to the subject groups (a) and the vehicle configurations (b).

In the clutch pedal analysis performed by Wang et al. (2000), the contact point was located from the heel at approximately 72% of the shoe length. This value of relative distance along the sole is in agreement with the information obtained from our database (Figure 4.29a), since the CIs of each group contain the mean value encountered by Wang et al.

Considering the vehicle-configurations (Figure 4.29b), significant differences may be seen among the vehicles. Such differences do not seem directly associated to the parameters reported in Table 4.2. However, if we

consider the height of the clutch pedal rest position above the ground (Table 4.6), the relative distance of the end-effector along the sole seems to follow that same distribution. It may be seen that the end-effector is closer to the heel when the pedal is located closer to the ground, probably to avoid collisions between the heel and the ground during the depression.

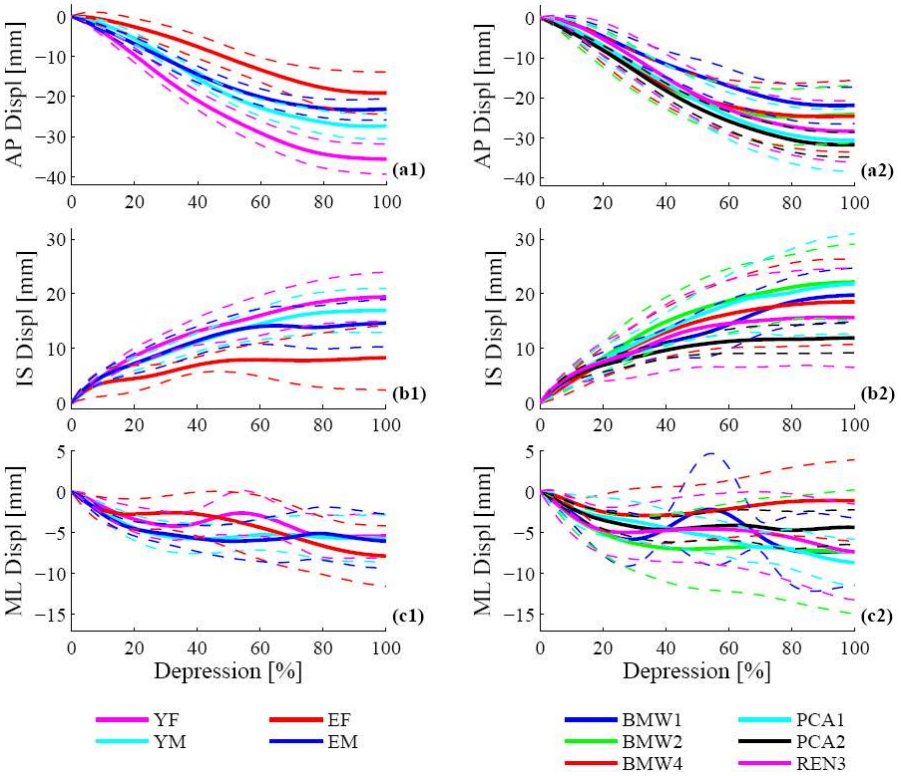

Figure 4.30: Mean local position in the foot during the depression phase of the point in contact with the pedal centre. The positions are reported along the foot antero-posterior (a1, a2), infero-superior (b1, b2) and medio-lateral (c1, c2) axes in the various groups (a1, b1, c1) and vehicle configurations (a2, b2, c2). The dashed lines represent the 95% confidence intervals of the means.

Moreover, it was noted that the foot slides on the pedal during the depression (Figure 4.30). The geometric point in the foot which matches the centre of the pedal slides towards the toes and penetrates into the sole during the pedal depression. Both the displacements along the antero-posterior (Figure 4.30a1, a2) and the infero-superior (Figure 4.30b1, b2) axes depend strongly on the accuracy of the reconstruction as their mean values are limited to about 2 or 3cm. However, both displacements present

clear trends, suggesting a consistency which should not be evident were the displacements due to measurement errors. Nevertheless, the displacement along the medio-lateral (ML) (Figure 4.30c1, c2) axis is even smaller and lacks the general trends observed along the other two axes: hence, the ML displacement is not further investigated.

For what concerns the antero-posterior direction (Figure 4.30a1, a2), the variation of the position of the pedal centre in the foot local coordinate system is explained by the foot sliding along the pedal radial direction. This movement is directly related to the frictional force recorded by the pedal force sensor and analysed in Section 4.4.8.

On the other hand, the position of the pedal centre in the foot local coordinate system along the infero-superior axis (Figure 4.30b1, b2) presents smaller, but nevertheless consistent, displacements. One of the reasons which may explain an infero-superior (IS) displacement is the deformation of the sole in the shoe due to the pressure exerted on the pedal. However, although the sole deformation may account for a part of the IS displacement, it does not seem the only cause. Specifically, the human foot presents a metatarsophalangeal joint which connects the metatarsal bones with the digital rays and mostly allows rotation about the medio-lateral axes. However, in the DHM we adopted, the foot is modelled as a rigid segment, hence metatarsophalangeal rotations are not allowed. Since the point in contact with the pedal centre moves towards the toes, the observed IS displacements (Figure 4.30b1, b2) could be also due to the lack of modelling of the metatarsophalangeal rotations.

4.4.11 SEAT STIFFNESS

The human-environment interaction in clutch pedal depressions is not limited to the pedal element, but involves the seat as well. The geometric and dynamic interaction between the DHM and the pedal allowed to obtain a stiffness curve (Section 4.4.7) and a friction coefficient (Section 4.4.8) to characterise the foot-pedal interaction. For what concerns the pelvis-seat interaction, however, the characterisation is less evident.

In fact, on the one hand, the forces exerted in the sagittal plane by the seat on the pelvis vary significantly across the motion (Figure 4.22). However, on the other, the pelvis does not move enough on the seat in order to determine a stiffness curve as for the pedal. In fact, the variations in position of the pelvis during the motion (Figure 4.16) present the same order of magnitude as the accuracy in the reconstruction.

Therefore, from the analysis of the kinematic and dynamic profiles of the motion database, we are not able to gain sufficient information so as to characterise the interaction between the pelvis and the seat.

4.4.12 BEHAVIOURS

As mentioned earlier, the behaviours exhibited during the motions may be classified into strategies and styles. Strategies are evident differences in the motion which may be identified simply watching the motion being performed (or a video recording). The clutch pedal depression is a straightforward task, which leads to the definition of only one strategy, the one adopted by all the subjects.

Styles, on the other hand, are defined as more subtle differences in the motion, generally identified through the motion analysis. For what concerns the DoF profiles (Section 4.4.4), slight differences associated to the values of the experimental parameters were identified, but generally the kinematic profiles of all motions are very similar to each other. However, the dynamic analysis (Section 4.4.6) revealed two different trends which may be considered as dynamic motion styles:

- Back Load style:
  This style is characterised by a more vertical pedal reaction, which mainly produces two effects. On the one hand, the torques at the hip and knee joint are reduced, as the moment due to the pedal reaction balances the moment due to the leg weight. On the other, to balance the moment at the root joint due to the pedal reaction, the seat reaction at the backrest is applied on the upper part of the subject's back, loading their back.

- Leg Load style:
  This style is characterised by a pedal reaction which is more aligned to the leg direction, i.e. the direction connecting the hip joint with the end-effector. A pedal reaction thus directed generates a small moment about the joints. Therefore, the torques at the hip and knee joints are high, due to the muscular activity required to balance the moment produced by the leg weight. However, the seat reaction must not balance a large torque at the root, hence the seat reaction at the backrest is applied closer to the pelvis, leading to a smaller load on the back.

As mentioned above, the two styles are determined by the pedal reaction direction. This may change due to vehicle-related or group-related causes. On the one hand, the vehicle affects the style selection (Figure 4.28) through the clutch pedal travel angle: a higher travel angle implies a more vertical reaction, hence a tendency towards the Back Load style; a lower travel angle implies a more horizontal reaction, hence a tendency towards the Leg Load style. However, it must be considered that the influence of the vehicle must be combined with the group-related differences in pedal reaction directions (Figure 4.28), which are modified by changing the radial component of the pedal force (Figure 4.26). Young subjects tend to choose the Back Load style, as they prefer to reduce the torque at the joints by loading their back. Elderly subjects instead tend to reduce the load on their back and would rather apply a greater effort across the leg.

Within the same subject group and vehicle configuration, however, no different behaviours were observed, suggesting that the characteristics of the subject and the environment alone establish which of the two styles are adopted.

4.5 STRUCTURED DATABASE

As mentioned in the introduction to this chapter, one of the aims of the database motion analysis is to provide the necessary information to carry out the database structuring. In fact, a structured database is required as input in the motion prediction method described in Chapter 3.

The database structuring consists in characterising the motions with the values of their most relevant features, which are to be taken into account during the prediction process. These features can either be used to select the reference motion (as the features characterising the motion scenario) or they can be passed on from the reference to the predicted motion (as the temporal feature), as described earlier in Section 3.3.

For what concerns the temporal features, each motion is characterised by the values of the key-frames identified in Section 4.4.1. On the other hand, the characterisation of the motion scenarios is carried out through the values of the subject-related and environment-related features which proved to influence the motion, according to the analysis performed in Section 4.4.

Therefore, each motion in the database is characterised by the value of the parameters reported in the following tables. The subject-related features which mostly seem to influence the clutch pedal depression motion

(Table 4.5) are the subjects' gender and age groups, as well as their stature and weight. For what concerns the environment-related features (listed in Table 4.6 and depicted in Figure 4.31), more features than those which were initially employed to characterise the vehicle configurations (Table 4.2) appear to affect the clutch pedal depression motion. In addition to the seat height (S_h), the pedal travel length (L) and angle (α) and the pedal rest position (CP), also the longitudinal position of the seat H-point (Hx), the initial height of the clutch pedal from the vehicle floor (CP_h) and its initial orientation (θ) seem to be relevant features which influence the motion.

Group	Gender	Age	Stature [cm]	Weight [kg]
YF	Females	Young	167±3	61±3
YM	Males	Young	176±5	68±13
EF	Females	Elderly	161±25	50±14
EM	Males	Elderly	171±18	78±1

Table 4.5: Subject-related features included in the database structuring. The value following the ± symbol represents the standard deviation σ.

Vehicle	S_h [mm]	Hx [mm]	CP_h [mm]	L [mm]	α [deg]	θ_0 [deg]	CPx [mm]	CPy [mm]	CPz [mm]
BMW1	256	-5±35	187	140	0	75.7	-814	-60	-69
BMW2	247	-30±32	183	150	0	70.9	-831	-110	-64
BMW4	174	-3±38	191	138	0	69.3	-816	-120	17
PCA1	355	-34±28	156	132	23	47.3	-770	-70	-199
PCA2	272	1±34	142	158	8	64.8	-766	-80	-130
REN3	360	-1±33	142	139	15	59.2	-761	-70	-218

Table 4.6: Environment-related features included in the database structuring. The value following the ± symbol represents the standard deviation σ.

The features reported in Table 4.5 and Table 4.6 are those which are considered in the reference motion selection criterion, described by Equation (3.3). Therefore, in order to select the reference motion, the values of the aforementioned features are required not only for the motions composing the database, but must be specified also for the motion to be predicted (Section 3.2.2).

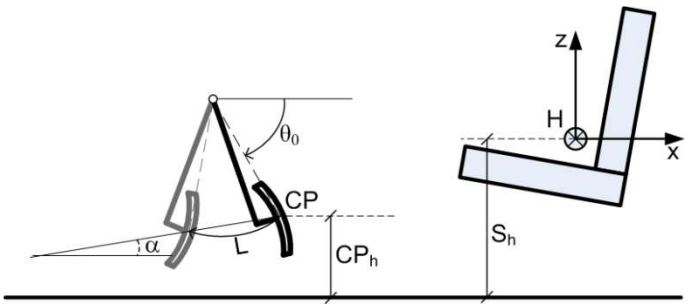

Figure 4.31: Environmental features used in the structuring of the database.

A final remark concerns the two different styles defined in Section 4.4.12, which are not included explicitly in the structuring of the database. The reason is that the choice of the most similar subject and the most similar environment automatically select the adopted style. In fact, as mentioned earlier, the style seems determined by the subject group and the vehicle configuration alone: the same group of subjects in the same environment all carry out the task adopting the same behaviour.

CHAPTER 5

TEST CASE DEFINITION

This chapter describes how the prediction method presented in Chapter 3 is applied to the clutch pedal depression motion, analysed in Chapter 4. First we define the prediction scenarios (Section 5.1), composed by the subjects and the environments employed in the predictions. Subsequently, we detail the optimisation problem to be solved in the prediction of clutch pedal depressions, in terms of the employed design variables (Section 5.2), constraints (Section 5.3) and objectives (Section 5.4). Finally, the description of the contact models, used to evaluate the external forces due to the human-environment interaction, complete the characterisation of the prediction scenarios (Section 5.5).

5.1 PREDICTION SCENARIOS

The definition of the prediction scenarios describes the characteristics of the subjects and the environments employed in the predictions, which are called prediction subjects and prediction environments, respectively. In the context of product design, the prediction subjects represent generic specimens of the target populations for which a product is being designed, and the prediction environments correspond to the new designs which are to be evaluated ergonomically.

The target populations and the prediction environment considered in this work are those reported in Table 5.1: the predictions seek to represent the behaviour of average young females (YF), young males (YM) and elderly males (EM) performing a clutch pedal depression in a specific vehicle configuration (PCA2).

Target Population	Gender	Age	Stature [cm]	Weight [kg]
YF	Female	Young	163±3	61±3
YM	Male	Young	176±5	68±13
EM	Male	Elderly	171±18	78±1

Vehicle	S_h [mm]	Hx [mm]	CP_h [mm]	L [mm]	α [deg]	θ_0 [deg]	CPx [mm]	CPy [mm]	CPz [mm]
PCA2	272	1±34	142	158	8	64.8	-766	-80	-130

Table 5.1: Characteristics of the target populations and the prediction environment employed in the predictions presented in this work.

The reason, for which we specifically consider the vehicle configuration and the populations of Table 5.1, is for validation purposes. In fact, in order to assess the goodness of the predictions obtained with our method, we seek to compare the predicted motions to actually performed motions, carried out in similar conditions to the ones being predicted.

Given the number of available motions performed by each subject group in each vehicle configuration (Table 4.3), we selected PCA2 as prediction environment and the YF, YM and EM groups as target populations, as the greatest number of motions are available in these conditions, leading to a more reliable comparison between predicted and actually performed motions. The group of elderly females (EF) was not selected as target population due to the reduced number of valid motions performed by EF in the PCA2 vehicle, and therefore does not appear in Table 5.1.

For what concerns the specific subjects employed in the predictions, as mentioned earlier, they should represent a generic specimen of the target population. The prediction subjects, therefore, are chosen to represent the average subject of each target population. Rather than averaging the anthropometric measures of each target population sample, the DHMs of the prediction subjects are tailored to represent the experimental subjects which most resemble the average of the target populations.

The characteristics of the prediction scenarios (i.e. the prediction subjects and the prediction environment) considered in this work are reported in Table 5.2.

Subject ID	Gender	Age	Stature [cm]	Weight [kg]
YF_1	Female	30	168.4	58.6
YM_4	Male	21	177.5	79.3
EM_1	Male	72	170.8	76.8

Vehicle	S_h [mm]	Hx [mm]	CP_h [mm]	L [mm]	α [deg]	θ_0 [deg]	CPx [mm]	CPy [mm]	CPz [mm]
PCA2	272	1±34	142	158	8	64.8	-766	-80	-130

Table 5.2: Characteristics of the prediction scenarios.

5.2 DESIGN VARIABLES

As described in Section 3.5.1, our motion prediction method adopts a B-spline parameterisation, which consists in representing the DoF profiles in the motion as a linear combination of a set of linearly independent functions (called basis functions), through a set of coefficients (called control points). The number of control points (and of basis functions) to be employed in the parameterisation depends on the accuracy with which the DoF profiles are to be approximated: the finer the approximation is, the more control points are needed.

Section 5.2.1 hereafter describes the process which was followed to select the number of control points for the parameterisation of clutch pedal depressions, and Section 5.2.2 discusses the tolerances ensured by the selected number of control points.

5.2.1 NUMBER OF CONTROL POINTS

The number of control points, which is required to represent each DoF profile $q(t)$ within a specified tolerance ε, is given by the minimum number of control points which yields parameterised DoF profiles $q^{BS}(t)$ that satisfy the following condition:

$$\forall i = 1 : nDoFs \quad \frac{\sqrt{\sum_{t=0}^{T}\left(q_i(t) - q_i^{BS}(t)\right)^2}}{q_{iMax} - q_{iMin}} \leq \varepsilon \tag{5.1}$$

where $q_i(t)$ represents the i^{th} original DoF profile of the motion; $q_i^{BS}(t)$ represents the i^{th} DoF profile approximated through the B-splines parameterisation employing a specific number of control points; and q_{iMax} and q_{iMin} are respectively the maximum and minimum values of the original DoF profile. The difference between q_{iMax} and q_{iMin} represents the range of values (RoV) of each DoF profile during the motion.

For what specifically concerns the clutch pedal depression motion, the DoFs which characterise the DHM, employed both in the motion reconstruction and prediction processes (Section 4.2), are 13: 10 rotational and 3 translational.

The 13 DoF profiles of each motion in the database have been approximated with a B-spline curve in order to assess the minimum number of control points required by each DoF in each motion. Three different tolerances for the B-spline approximation have been considered, corresponding to 5%, 2% and 1% of the RoV of each DoF in each motion. The resulting number of control points obtained by applying Equation (5.1) in all the motions composing the database, for each DoF and each tolerance ε, is reported in Figure 5.1.

It may be noticed that, as expected, the required number of control points of all DoFs increases when the approximation tolerance is decreased. Moreover, not all DoFs require the same number of control points to achieve the same tolerance. It may be noticed that a greater number of control points is associated to the DoFs that do not play a relevant role in the motion (mostly, the longitudinal rotation DoFs and the translation of the pelvis in the transversal direction). The reason is that the DoFs which are not very relevant to the task accomplishment generally present more irregular profiles, as they are less controlled during the motion and additionally tend to present a more reduced range of values (RoV) respect to more relevant DoFs: hence, any irregularity in the profile shape accounts for a larger percentage of the RoV. Such irregularities are not reflected directly in the figures of Section 4.4.4, as the figures represent the average profiles of the DoFs, and the irregularities in each motion are likely to be compensated in the averaging process by the irregularities in another motion.

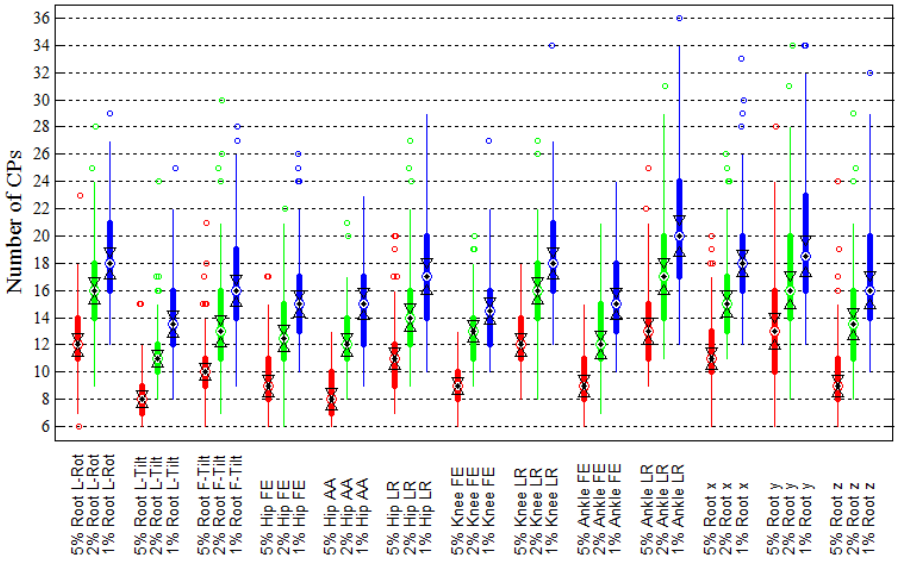

Figure 5.1: Number of control points required to approximate the DoF profiles within a 5%, 2% and 1% tolerance (represented in red, green and blue, respectively). The black dot represents the median, the coloured box contains the inter-quartile range (from the 25th to the 75th percentile), and the whiskers extend from the minimum to the maximum values (outliers are marked with coloured circles). The black triangles mark the 95% confidence intervals of the medians.

To select the number of control points with which to carry out the predictions, we consider the median number of control points which ensure a 2% tolerance in the DoF profiles. To adopt the same number of control points among the rotational DoFs and the same number among the translational DoFs, we select the maximum median value among the rotational and translational DoFs, respectively. Consequently, we consider 17 control points to represent the 10 rotational DoFs in our DHM and 16 for the 3 translational DoFs, which leads to a total of 218 control points.

5.2.2 Ensured Tolerances

The abovementioned number of control points leads to a maximum error of 2% in the B-spline approximation of the DoF profiles in the majority of the motions. However, the average error committed across each motion (employing 17 control points for the rotational DoFs and 16 for the translational DoFs) also seems an interesting quantity to assess how closely the approximation resembles the original DoF profiles.

The average tolerances with which the DoF profiles are approximated by using the selected number of control points are shown in Figure 5.2. It may be noticed that the median values of the tolerances are significantly below 2% and that the selected number of control points actually ensure an even finer approximation for the DoFs which play a more relevant role in the motion (namely, the flexion-extension DoFs at the hip, knee and ankle joints), as they correspond to less than a 0.5% average tolerance in the greatest majority of the motions.

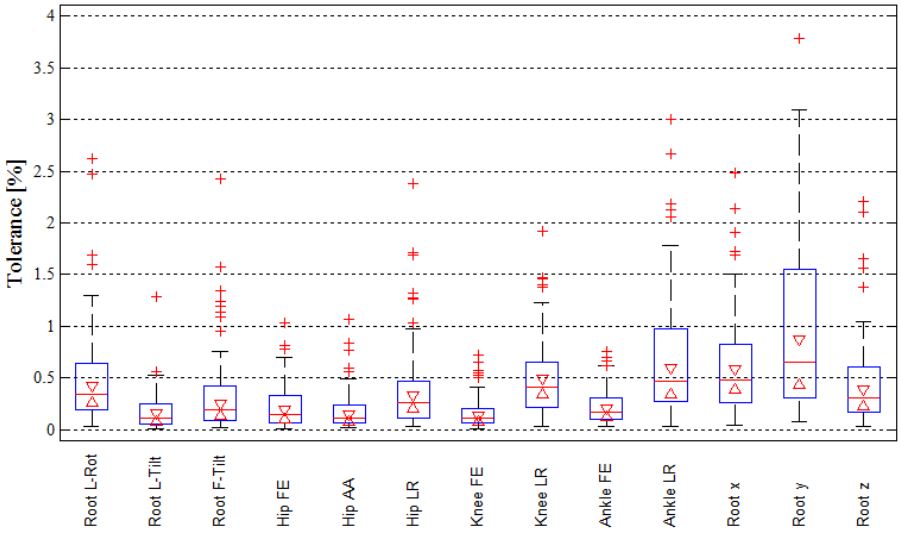

Figure 5.2: Average tolerances with which the DoF profiles in the database are approximated by adopting 17 control points for the rotational DoFs and 16 for the translational DoFs. The red line represents the median, the blue box contains the inter-quartile range (from the 25th to the 75th percentile), and the black whiskers extend from the minimum to the maximum values (outliers are marked with red crosses). The red triangles mark the 95% confidence intervals of the medians.

As mentioned in Section 3.5.1, both the kinematics and dynamics of the predicted motions are represented through the B-spline control points. Therefore, we consider that the tolerance with which the B-spline parameterisation approximates the joint torque profiles should also be assessed. To evaluate the degree of approximation that the selected control points allow for the torques at the joints, a dynamic reconstruction was performed, considering the actually measured external forces and the B-spline approximation of the DoF profiles. The obtained torques are compared to the torques in the original motions, and the average tolerances

with which the B-spline parameterisation approximates the joint torques are shown in Figure 5.3.

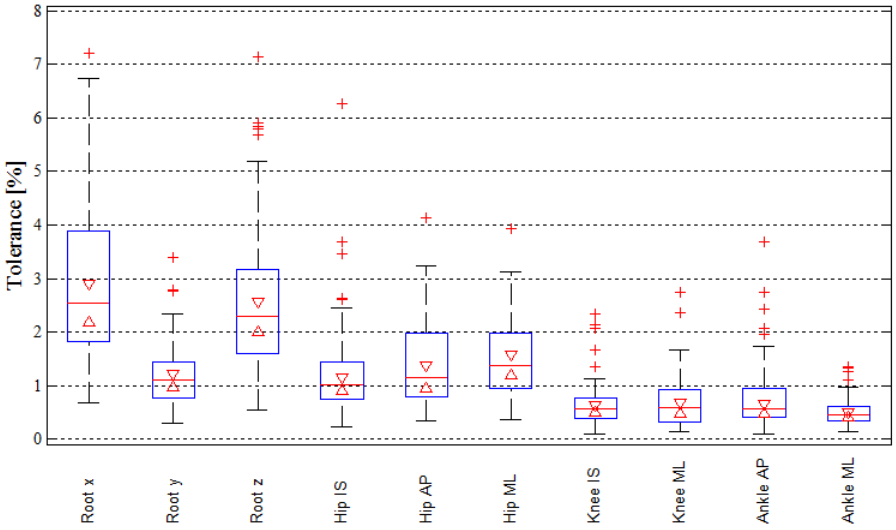

Figure 5.3: Average tolerances with which the joint torque profiles in the database are approximated by adopting 17 control points for the rotational DoFs and 16 for the translational DoFs.

It may be noticed that although the tolerances are greater in the torques than in the DoF profiles, the tolerances in the joint torques achieved through the B-spline approximation are still reduced (the median values are smaller than 3%). Therefore, we consider that the selected number of control points is adequate to represent both the kinematics and dynamics of the clutch pedal depression motions composing the database and thus we employ the above-mentioned 218 control points as design variables for the optimisation problem.

5.3 CONSTRAINTS

In Section 3.5.2 we presented the equality and inequality constraints included in our motion prediction method. The constraints we consider, in the prediction of clutch pedal depression motions, are detailed hereafter.

5.3.1 GOAL FULFILMENT

This equality constraint ensures the fulfilment of the goal in the motion by guiding the motion of the end-effector. In clutch pedal depressions, the

end-effector is considered to be the point in the left foot which reaches the centre of the clutch pedal at the key-frame *StartDepression* (as mentioned in Section 4.4.1).

We consider the trajectory of the end-effector to be constrained to the foot rest at the key-frame *StartMotion* ($t = t_0$) and to the clutch pedal throughout the pedal depression, from key-frame *StartDepression* ($t = t_D$) to key-frame *EndMotion* ($t = t_T$). It must be noticed that we do not guide the motion of the end-effector during the reach phase (we impose the constraint only at t_0 and t_D), allowing any trajectory which starts at the foot rest and ends at the rest position of the clutch pedal in the prediction environment. Thus, the trajectory of the end-effector in the predicted motion during the reach phase is determined by the objective function of the optimisation problem, described later in Section 5.4.

Therefore, the trajectory of the end-effector is guided by:

$$t = t^* \in [t_0, [t_D, t_T]] \qquad \mathbf{\Phi}_{EndEff\,Traj} = \mathbf{x}(\mathbf{q}) - \mathbf{x}_{Mod}(t) = 0 \tag{5.2}$$

where $\mathbf{x}_{Mod}$ is the trajectory that must be followed by the end-effector in order to fulfil the goals in the prediction scenario (see Section 3.4). During the reach phase, the modified trajectory $\mathbf{x}_{Mod}$ is obtained considering a free end-effector (Section 3.4.2.1), by imposing the position of the end-effector on the foot rest at t_0 and on the clutch pedal at t_D in the prediction environment. For what concerns the depression phase, $\mathbf{x}_{Mod}$ is obtained considering a constrained end-effector (Section 3.4.2.2) since the motion of the foot is determined by the geometry of the pedal. Details on the evaluation of the trajectory $\mathbf{x}_{Mod}$ to be followed during the clutch pedal depression phase are given later, when defining the contact model between the foot and the pedal (Section 5.5.1).

As mentioned earlier (Section 3.5.2.1), the constraint is enforced only at specific frames t^* during the depression phase $[t_D, t_T]$, to avoid excessively reducing the number of free control points. Considering the adopted number of control points (Section 5.2), we found that a good compromise between the number of free control points and the task achievement is given by imposing the goal fulfilment constraint at evenly spaced intervals of *N* frames, where $N \cong (t_T - t_D)/5$. A goal fulfilment

objective is defined to ensure that a smooth trajectory is followed throughout the pedal depression (Section 5.4.1).

5.3.2 INITIAL AND FINAL CONDITIONS

We consider the clutch pedal depression motions to start and end in states of rest, therefore we impose:

$$t = t_0 \ , t = t_T \qquad \begin{aligned} \boldsymbol{\Phi}_{DoFVel} &= \dot{\mathbf{q}}(t) = 0 \\ \boldsymbol{\Phi}_{DoFAcc} &= \ddot{\mathbf{q}}(t) = 0 \end{aligned} \tag{5.3}$$

As mentioned earlier (Section 3.5.2.2), these constraints reduce by 4 the number of free control points which describe each DoF. However, the number of control points adopted for clutch pedal depressions to approximate each DoF is sufficiently large to allow the aforementioned constraints to be set while ensuring a sufficient number of free control points for the optimisation. In fact, 13 and 12 control points for the rotational and translational DoFs respectively, ensure an approximation of the DoF profiles with a tolerance less than or equal to 5% (see Figure 5.1).

5.3.3 JOINT LIMITS

As described in Section 3.5.2.3, our method allows to define limits to the DoF values and to the joint torque values, to take into account the RoMs of the articulations and the maximum muscular effort of the human body.

For the prediction of clutch pedal depressions, however, we chose to control only the limit values of the DoFs and not the limit values of the torques. The reason is that the torques exerted in the motion are far from their limits and Equation (3.17) appears to be automatically satisfied. On the other hand, the RoM inequalities seem to be required, as otherwise their limits may be exceeded in the prediction.

Therefore, we restrict the values of the DoFs $\mathbf{q}$ to a range delimited by lower and upper limits ($\mathbf{q}_L$ and $\mathbf{q}_U$) throughout the motion, in order not to exceed the RoM of the articulations:

$$\forall t \in [t_0, t_T] \qquad \begin{aligned} \boldsymbol{\Phi}^{IN}{}_{RoM} &= \mathbf{q}_L - \mathbf{q}(t) \le 0 \\ \boldsymbol{\Phi}^{IN}{}_{RoM} &= \mathbf{q}(t) - \mathbf{q}_U \le 0 \end{aligned} \tag{5.4}$$

The RoM values considered in this work are constant and are those provided in the specifications of the adopted RAMSIS DHM (Section 4.2).

Since each inequality corresponds to two KKT conditions (Arora, 2004), we impose these constraints at evenly spaced intervals of *N* frames in order not to overload the computation. Currently, considering the adopted number of control points (Section 5.2) and the inequalities included in the optimisation problem, we employ $N \cong (t_T - t_0)/10$ for all inequality constraints.

5.3.4 COLLISION AVOIDANCE

Of the collisions which may arise in clutch pedal depression, we only consider the one between the left heel and the vehicle floor, which we consider is the most likely collision to occur.

Denoting with $\mathbf{n}$ the vector normal to the horizontal plane representing the vehicle floor (directed upwards), and whose origin $\mathbf{x}_0$ is located on the surface of the vehicle floor, the trajectory $\mathbf{x}$ followed by the left heel of the DHM must fulfil the following constraint throughout the motion in order to avoid the heel-floor collision:

$$\forall t \in [t_0, t_T] \qquad \mathbf{\Phi}^{IN}{}_{Collision} = -(\mathbf{x}(\mathbf{q}) - \mathbf{x}_0(t)) \cdot \mathbf{n} \leq 0 \tag{5.5}$$

As mentioned earlier (Section 5.3.3), inequalities are currently set at evenly spaced intervals of *N* frames, where $N \cong (t_T - t_0)/10$.

5.3.5 DYNAMIC BALANCE

As described in Section 3.5.2.5, the dynamic balance of the DHM is ensured through an inequality constraint to take into account the approximate nature of the contact models representing the human-environment interaction (the contact models employed to predict clutch pedal depression motions are detailed in Section 5.5).

Therefore, we impose the following condition throughout the motion, at evenly spaced intervals of $N \cong (t_T - t_0)/10$ frames (see Section 5.3.3):

$$\begin{aligned} \forall t \in [t_0, t_T] \qquad & \mathbf{\Phi}^{IN}{}_{FBalance} = \mathbf{F}_{Root}(\mathbf{q}, \dot{\mathbf{q}}, \ddot{\mathbf{q}}) - \boldsymbol{\varepsilon}_F \leq 0 \\ & \mathbf{\Phi}^{IN}{}_{FBalance} = -\mathbf{F}_{Root}(\mathbf{q}, \dot{\mathbf{q}}, \ddot{\mathbf{q}}) - \boldsymbol{\varepsilon}_F \leq 0 \end{aligned} \tag{5.6}$$

$$\forall t \in [t_0, t_T] \qquad \begin{aligned} \boldsymbol{\Phi}^{IN}{}_{MBalance} &= \boldsymbol{\tau}_{Root}(\mathbf{q}, \dot{\mathbf{q}}, \ddot{\mathbf{q}}) - \boldsymbol{\varepsilon}_{\tau} \leq 0 \\ \boldsymbol{\Phi}^{IN}{}_{MBalance} &= -\boldsymbol{\tau}_{Root}(\mathbf{q}, \dot{\mathbf{q}}, \ddot{\mathbf{q}}) - \boldsymbol{\varepsilon}_{\tau} \leq 0 \end{aligned} \tag{5.7}$$

As the clutch pedal motion is carried out mainly in the sagittal plane, we enforce the dynamic balance only along the directions of greatest effort: the *x* and *z* axes for the forces and the *y* axis for the torques.

The tolerances $\boldsymbol{\varepsilon}_F$ and $\boldsymbol{\varepsilon}_{\tau}$ specify the range within which the dynamic balance is considered as fulfilled. In the prediction of clutch pedal depressions, adopting the contact models described later, we set $\boldsymbol{\varepsilon}_F$ to 10% of the weight of the upper part of the body (approximately 40 N), and $\boldsymbol{\varepsilon}_{\tau}$ as the moment produced by $\boldsymbol{\varepsilon}_F$ at a distance equal to the hip width (approximately 15 Nm).

5.4 OBJECTIVES

In Section 3.5.3 we presented the type of objectives included in our motion prediction method. The objectives we consider, in the case of clutch pedal depression motions, are detailed hereafter.

In Section 3.5.4.1, the minimum number of frames at which the objective function must be evaluated has been defined. Ideally, evaluating the objective function at each frame leads the control points to be controlled best; however, the smoothness ensured by the B-spline parameterisation makes a frame-by-frame evaluation unnecessary. Considering the adopted number of control points (Section 5.2), we found that a good compromise between computational cost and accuracy is given by evaluating the objective function at evenly spaced intervals of *N* frames, where $N \cong (t_T - t_0)/50$ (i.e. every 3-7 frames).

5.4.1 GOAL FULFILMENT

As mentioned earlier (Section 5.3.1), the goal fulfilment constraint is applied throughout the clutch pedal depression, but is enforced only at specific frames, to avoid excessively reducing the number of free control points. To ensure that the desired trajectory is followed throughout the depression phase (from t_D to t_T), the following condition is included in the objective function:

$$\forall t \in [t_D, t_T] \qquad \boldsymbol{\Psi}_{EndEff\,Traj} = \dot{\mathbf{x}}(\mathbf{q}, \dot{\mathbf{q}}) - \dot{\mathbf{x}}_{Mod}(t) \tag{5.8}$$

where $\dot{\mathbf{x}}$ is the velocity of the end-effector and $\dot{\mathbf{x}}_{Mod}$ is the time derivative of the modified end-effector trajectory (specified later, in Section 5.5.1.1, for the clutch pedal depression).

The condition is set on the end-effector velocity rather than its position to ensure a smoother trajectory by resembling the shape of the modified trajectory in between the goal fulfilment constraints.

5.4.2 DATA-BASED CONDITIONS

To maintain the realism of the reference motion, a condition is set throughout the motion to resemble the reference DoF velocities $\dot{\mathbf{q}}_{Ref}$ (hence, the shape of the DoF profiles):

$$\forall t \in [t_0, t_T] \qquad \boldsymbol{\Psi}_{DoFVel} = \dot{\mathbf{q}}(t) - \dot{\mathbf{q}}_{Ref}(t) \tag{5.9}$$

The condition is set on the DoF velocities rather than on the DoF values as different scenarios may involve different DoF values, whereas the shape of the DoF profiles is generally maintained (Park et al., 2004).

5.4.3 KNOWLEDGE-BASED CONDITIONS

From the dynamic analysis of the database (Section 4.4.6), it emerged that young and elderly people tend to depress the pedal differently: the former tend to reduce the torques at the joints; whereas the latter tend to reduce the load on their back. It was also noticed that the differences arise from the direction of the force exerted on the clutch pedal, due to the different radial forces exerted on the pedal (Sections 4.4.8 and 4.4.9).

In this work, the different contact behaviours exhibited by young and elderly subjects are represented through the pedal contact model (as described in detail in Section 5.5.1). Therefore, the radial force exerted by the DHM on the pedal is determined by the behaviour *expected* by the DHM: a greater radial force is imposed by the pedal contact model on young people, producing lower joint torques, whereas a lower radial force is imposed on elderly people, yielding lower back loads.

As the age-related behaviours are taken into account by the abovementioned contact model, the aim of the knowledge-based condition is to represent the common goal guiding the motion of all subjects. Energy-

related criteria seems reasonable candidates for clutch pedal depressions, considering the dynamic motion analyses presented in (Wang et al., 2000) and in Chapter 4 of this thesis. According to Wang (2000), the motions appear to be consistent with a minimum energy principle and our findings are that all subjects seem concerned with effort minimisation (joint torques for young subjects and back loads for the elderly).

In order to assess the most adequate energy-related criterion, Section 6.3 of the next chapter presents a comparison between two of the most commonly employed energy-related performance measures (see Section 2.1.2.2): minimum dynamic effort and minimum mechanical energy.

5.5 CONTACT MODELS

To evaluate the efforts exerted by the environmental elements with which the DHM interacts, contact models must be defined. In the case of the clutch pedal depression, the elements with which the DHM interacts are the clutch pedal (described hereafter) and the seat (described in Section 5.5.2).

5.5.1 FOOT-PEDAL CONTACT MODEL

For what concerns the clutch pedal, the information gathered in the motion database analysis (Chapter 4) is taken into account to characterise both the geometric and dynamic interaction between the left foot and the pedal. The following sections describe the geometric (Section 5.5.1.1) and the dynamic characteristics (Sections 5.5.1.2 and 5.5.1.3) of the foot-pedal contact model.

5.5.1.1 Contact Point

As mentioned earlier (Section 5.3.1), the point considered as end-effector for the clutch pedal depression is the point in the left foot which reaches the centre of the clutch pedal at the beginning of the depression. In order to carry out a prediction, the position of the end-effector in the foot local coordinate system must be provided in both the reference and the prediction subject. If no local coordinates are specified, the positions are estimated for each subject group as the point located at the average distance from the heel reported in Figure 4.29, along the line connecting the heel to the toes.

As observed in the motion database analysis, the end-effector does not exactly follow the trajectory of the pedal centre, but slides during the

depression (Section 4.4.10). Therefore, the trajectory $\mathbf{x}_{Mod}$ to be followed by the end-effector during the pedal depression is given by the combination of the trajectory followed by the pedal centre and the sliding of the foot on the pedal.

The clutch pedal is modelled as a rigid body connected to the vehicle by a revolute joint, with its rotation axis aligned to the global *y* axis (Figure 5.4), hence the trajectory of the pedal centre is represented by a circumference arc in the sagittal plane (marked as $\mathbf{x}_{PC}$ in the figure). The trajectory $\mathbf{x}_{PC}$ of the pedal centre is obtained by applying forward kinematics to the clutch pedal:

$$\mathbf{x}_{PC} = \mathbf{x}_{PCR} + \mathbf{R}_{Pedal}(\theta_{Mod})\,{}^{Pedal}\mathbf{x}_{PC}^{PCR} \tag{5.10}$$

where $\mathbf{x}_{PCR}$ is the global position of the pedal centre of rotation; $\mathbf{R}_{Pedal}$ is the matrix describing the rotation of the pedal coordinate system respect to the global coordinate system; $\theta_{Mod}(t)$ is the modified profile of the clutch pedal depression angle, obtained by applying Equations (3.7) and (3.8) to the motion of the clutch pedal; and ${}^{Pedal}\mathbf{x}_{PC}^{PCR}$ is the position of the centre of the pedal (at which the end-effector comes into contact with the pedal) respect to the pedal centre of rotation, measured in the pedal coordinate system.

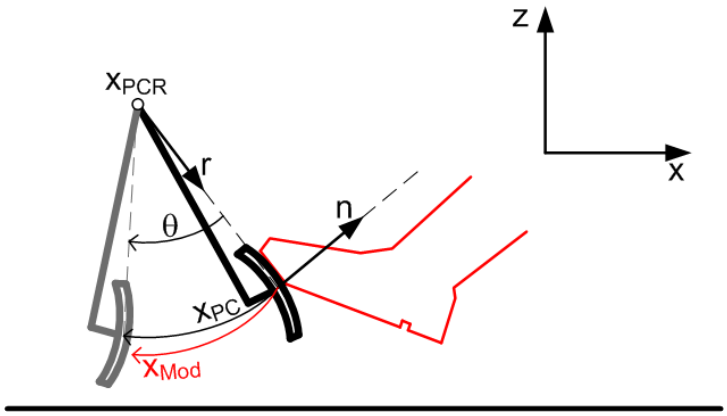

Figure 5.4: Geometric contact between the left foot and the clutch pedal.

The sliding of the foot on the pedal is modelled for each subject group as the average sliding ${}^{Loc}\boldsymbol{\delta}$ along the antero-posterior and infero-superior axes, as reported in Figure 5.5 for the various target populations in the prediction environment (see Table 5.1).

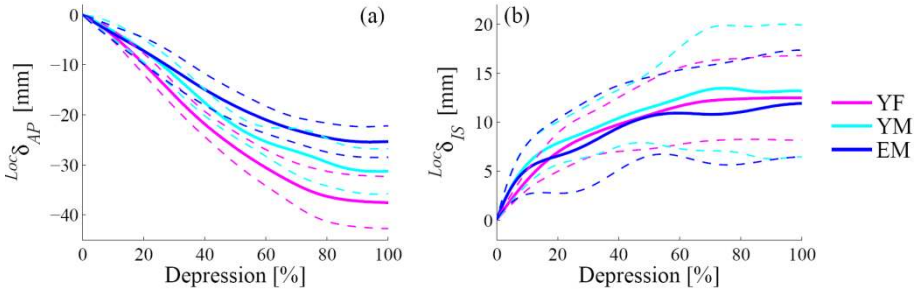

Figure 5.5: Mean local position in the foot during the depression phase of the point in contact with the pedal centre, along the foot antero-posterior (a) and infero-superior (b) axes for young females (YF), young males (YM) and elderly males (EM) in the PCA2 vehicle configuration. The dashed lines represent the 95% confidence intervals of the means.

Since ${}^{Loc}\boldsymbol{\delta}$ depends on the depression angle θ, the final trajectory to be followed by the end-effector is given by:

$$\mathbf{x}_{Mod} = \mathbf{x}_{PC}(\theta) + \mathbf{R}_{Loc}(\mathbf{q})\,{}^{Loc}\boldsymbol{\delta}(\theta) \tag{5.11}$$

where $\mathbf{x}_{Mod}$ is the trajectory which must be followed by the end-effector in the predicted motion; $\mathbf{x}_{PC}$ is the trajectory of the pedal centre, obtained through Equation (5.10); and $\mathbf{R}_{Loc}$ is the rotation matrix between the global coordinate system and the local coordinate system of the foot, in which ${}^{Loc}\boldsymbol{\delta}$ is expressed.

It must be noticed that including the sliding of the foot on the pedal not only changes the trajectory that the end-effector must follow (Equation (5.11)), but also modifies the application point of the pedal reaction on the foot. In fact, the pedal reaction force is considered to be applied at the centre of the pedal, which corresponds to a different point in the foot during the depression due to the sliding. Since the application point of the pedal reaction varies in the foot, also the corresponding moment at the ankle joint varies due to the different lever arm.

5.5.1.2 Stiffness

The reaction force $\mathbf{F_n}$, with which the pedal opposes resistance to its depression, is assumed to be directed as the $\mathbf{n}$ vector in Figure 5.4, tangent to the trajectory followed by the centre of the pedal, and its value is determined by the angular position of the pedal (θ in Figure 5.4) through the pedal stiffness curve $k_{Pedal}(\theta)$.

From the database analysis we obtained the stiffness curves of the pedals in each of the six experimental vehicle configurations (Section 4.4.7, Figure 4.25). Since the prediction environment is chosen to match the PCA2 configuration, its mean stiffness curve is employed to relate the pedal reaction force $\mathbf{F_n}$ to the pedal depression angle θ.

The angular position of the pedal θ depends on the position of the left foot, which in turn depends on the DoF values $\mathbf{q}$ of the DHM. Therefore, the relationship between the pedal reaction force $\mathbf{F_n}$ and the variables describing the motion of the DHM is expressed by the following equation:

$$\mathbf{F_n} = k_{Pedal}(\theta)\theta(\mathbf{q}) \tag{5.12}$$

5.5.1.3 Friction

From the analysis of the motion database, it was noticed that the force which subjects apply on the pedal is not directed as the pedal reaction force $\mathbf{F_n}$ described in the previous section. Additionally, a radial force $\mathbf{F_r}$ is exerted on the pedal, directed as the $\mathbf{r}$ vector in Figure 5.4, although its application does not affect the motion of the pedal. In fact, its aim is that of directing the external force exerted by the pedal so as to reduce the torques at the joints (in young subjects) or the seat reaction torque (in elderly subjects).

The analysis of the relationship between the radial force $\mathbf{F_r}$ and the normal force $\mathbf{F_n}$ (Section 4.4.8), revealed almost a constant ratio between the two (Figure 4.26). Therefore, we consider that the radial force is proportional to the normal force:

$$\mathbf{F}_r = c_F \mathbf{F_n} \tag{5.13}$$

The value of the coefficient c_F is estimated through the curves reported in Figure 5.6, which represent the mean values of the coefficient c_F during the pedal depression for the various target populations in the prediction environment (see Table 5.1).

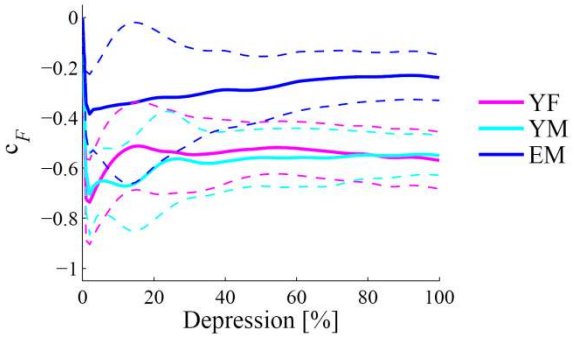

Figure 5.6: Mean values of the coefficient relating the radial and the normal forces at the pedal for young females (YF), young males (YM) and elderly males (EM) in the PCA2 vehicle configuration. The dashed lines represent the 95% confidence intervals of the means.

The value of the coefficient employed in Equation (5.13) is obtained as the approximated median value of the curves reported in Figure 5.6. Therefore, we consider $c_F = -0.6$ for young subjects and $c_F = -0.3$ for elderly males.

5.5.2 PELVIS-SEAT CONTACT MODEL

Contrarily to the foot-pedal interaction, the database analysis did not allow a clear characterisation of the pelvis-seat interaction. In fact, a stiffness curve relating the seat reaction force and the pelvis position was not possible to be determined (Section 4.4.11). Therefore, a different contact model is considered, based on the interference between geometric models representing the seat and the pelvis, respectively. In this work the geometry of the pelvis and the seat are simplified as shown in Figure 5.7.

The geometry of the seat is described by two orthogonal lines in the sagittal plane, which are tilted respect to the global axes. The tilt angles of 64° and 26° were evaluated through the CAD model of the vehicle seat employed in the clutch pedal experiments.

The geometric model of the pelvis is approximated to a rectangle in the sagittal plane and its interference with the seat geometry is represented

by two contacts in the backrest (B1 and B2) and two in the seat cushion (C1 and C2). The contacts are modelled as spring-damper combinations, whose characteristics are described in the following sections.

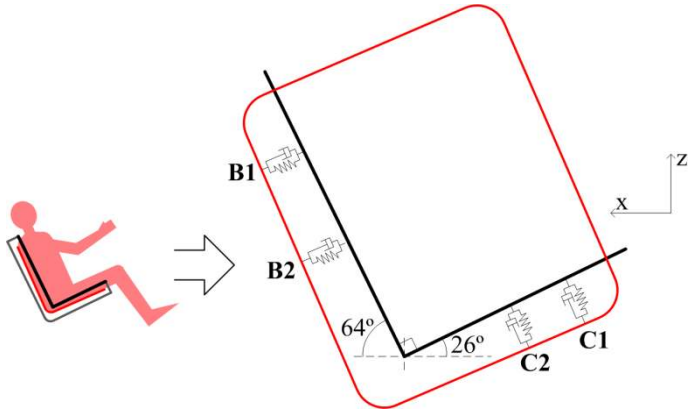

Figure 5.7: Geometry of the pelvis-seat interaction in the sagittal plane.

It may be noticed that only the contacts in the sagittal plane are considered in the characterisation of the pelvis-seat interaction. This simplification is adopted since the clutch pedal depression motion is carried out mainly in the sagittal plane and the balance condition reported in Section 5.3.5 is also limited to the above-mentioned plane. The forces acting in the transversal direction *y* are very small in comparison (Figure 4.22), and are considered to be automatically balanced by the seat.

5.5.2.1 Stiffness

In order to relate the seat reaction force with the interference between the pelvis and seat geometric models, a stiffness curve has to be defined. In general, the pelvis-seat contact is non-linear, due to the different composition of the layers forming the seat and to the combination of soft tissues and bones which compose the human pelvis. However, in clutch pedal operations the position of the pelvis does not present great variability (Figure 4.16). Therefore we assume that in the neighbourhood of the seated pelvis position a linear stiffness curve may be adequate to represent the pelvis-seat coupling.

To determine the stiffness coefficients of the springs reported in Figure 5.7 and the position of the four contacts in the pelvis, we assume that the interference at the beginning of the motion is such as to generate

seat reaction forces which balance the weight of the DHM. As detailed in Section 4.2, the inertial properties of the upper body and of half the right thigh are included in the pelvis segment (the weight of the rest of the right leg is considered to be unloaded directly on the ground). Therefore the weight to be balanced by the seat at the beginning of the motion is given by the weight of the pelvis segment (which accounts for the passive part of the model as well) combined to the weight of the left leg, which is assumed to have just left the ground.

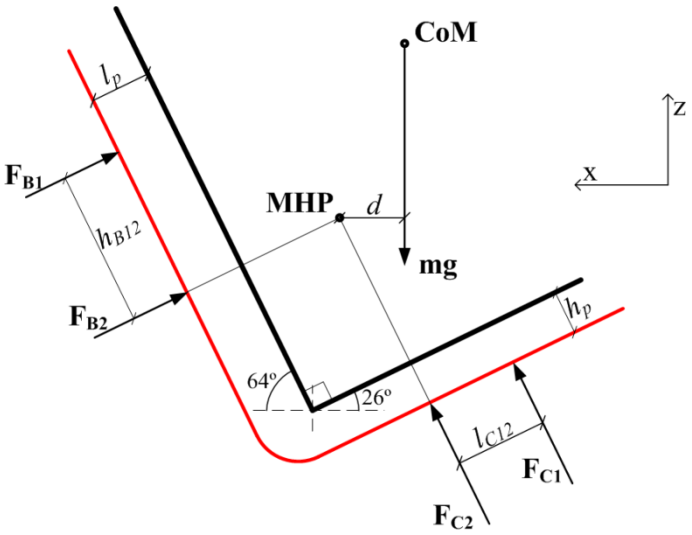

Figure 5.8: Forces acting on the pelvis at the beginning of the motion. The point MHP represents the mid hip point. The point CoM represents the centre of mass of the whole upper body and left leg combined, which together weigh mg.

Some assumptions are required to evaluate the stiffness at each of the four contact points and their position in the pelvis segment. First of all, we consider that the rectangle representing the pelvis is aligned to the seat at the beginning of the motion, as shown in Figure 5.8. Hence, both contacts with the backrest present the same interference (l_p) and both contacts with the cushion also present the same interference (h_p). Additionally, we consider that the stiffness coefficients of the cushion (k_C) and of the backrest (k_B) do not change depending on the position of the contact. Therefore, at the beginning of the motion, the forces exerted at the cushion are the same at both contacts C1 and C2 and that the forces exerted at the backrest are also the same at both contacts B1 and B2. Moreover, we

consider that at the beginning of the motion two seat reaction forces do not produce moment about the mid hip point (MHP).

Under these assumptions, the equations of force and moment balance in the sagittal plane may be written as:

$$\begin{cases} 2F_{C1}\sin(64°) + 2F_{B1}\cos(64°) - mg = 0 \\ 2F_{C1}\cos(64°) - 2F_{B1}\sin(64°) = 0 \\ F_{C1}\,l_{C12} - F_{B1}\,h_{B12} - mgd = 0 \end{cases} \tag{5.14}$$

From the first two equations the values of the forces F_{C1} and F_{B1} are obtained. The forces are related to the backrest k_B and cushion stiffness k_C through the interferences l_p and h_p. To determine the values of these quantities, we set the value of the cushion interference and consider that the backrest is 50% stiffer than the cushion, as reported in Equation (5.15):

$$\begin{aligned} F_{C1} = F_{C2} = k_C\,h_p \quad &\rightarrow \quad h_p = 70mm \quad \rightarrow \quad k_C = F_{C1}/h_p \\ F_{B1} = F_{B2} = k_B\,l_p \quad &\rightarrow \quad k_B = 1.5\,k_C \quad \rightarrow \quad l_p = F_{B1}/k_B \end{aligned} \tag{5.15}$$

The values of the k_C and k_B stiffness coefficients thus obtained are in the order of 5 and 7.5 N/mm respectively. Actual seats seem to be slightly stiffer (Burnett et al., 2004; Wirsching et al., 2011) but a greater stiffness would imply selecting a smaller h_p interference, which would more easily lead to losing contact with the seat during the iterations of the optimisation algorithm.

The third equation in (5.14) imposes the balance of the moments about the mid hip point (MHP) and determines the relationship between the backrest reactions distance and the cushion reactions distance. To determine the position of the contacts B1 and C1 we set the value of the distance between backrest reactions and therefore determine the distance between cushion reactions. We consider B1 to be located in the lower thoracic region, and quantify the distance between MHP and B1 as 40% of the subject back length for young subjects and 30% for elderly males (as they present lower seat torques, see Section 4.4.12).

5.5.2.2 Damping

The damping elements of Figure 5.7 are introduced to include energy dissipation in the contact model, in order to resemble the actual pelvis-seat interaction more closely.

To determine the damping coefficients for the backrest and the cushion, a battery of motion predictions was performed, in which different damping ratios were employed. By choosing the reference scenario to match the prediction scenario, we were able to identify the damping ratio which yielded the closest approximation to the actually performed motion. Specifically, we selected as reference a motion performed by the average male subject (YM_4 in Table 5.2) in the prediction environment.

As the motion to be predicted matches the reference motion, purely data-based predictions were carried out. The optimisation problem to be solved in each prediction is the same: all the constraints detailed in Section 5.3 are imposed and the objective function is composed by the goal fulfilment and the data-based conditions, as reported in Table 5.3. A unit weight is associated to both objectives.

Constraints					Objectives		
Goal Fulfil.	**Init. & Fin.**	**RoMs**	**Collisions**	**Dyn. Balance**	**Goal Fulfil.**	**D-based**	**K-based**
✓	✓	✓	✓	✓	✓	✓	

Table 5.3: Characteristics of the optimisation problems defined to determine the damping coefficients for the pelvis-seat contact model.

The battery of predictions is composed of eleven trials in which the value of the damping ratio ξ was varied progressively. On account of the slight oscillations which are generally perceived when seated in a vehicle, the pelvis-seat damping is assumed to be subcritical. Hence, the damping ratio was varied from 0 (undamped) to 1 (critically damped) with a 0.1 step. Additionally, we considered that the damping coefficient for the cushion c_C is the same at both contacts C1 and C2 and that the damping coefficient for the backrest c_B is also the same at both contacts B1 and B2.

The damping coefficients c_C and c_B are obtained through the definition of the damping ratio ξ :

$$c_C = 2\xi\sqrt{m_C k_C}$$
$$c_B = 2\xi\sqrt{m_B k_B} \tag{5.16}$$

where m_C is the portion of the DHM mass which is balanced by the cushion at the beginning of the motion; m_B is the portion balanced by the backrest; and k_C and k_B are the cushion and backrest stiffness coefficients obtained in the previous section.

In order to compare the results obtained with different damping ratios, we employ time-averaged distances (TDs) to quantify the resemblance between the predictions and the reference motion. Therefore, the damping ratio which yields the closest approximation to the reference motion is determined as the value which gives the smallest TD between the predicted and the reference motion.

TDs were introduced in Section 2.2 and are defined in the literature as the Euclidean norm of the difference between the predicted and the experimental motion, as reported in Equation (2.27). As mentioned earlier (Section 2.2), such TDs have been used for validation purposes in kinematic data-based motion prediction methods, comparing the predicted and experimental positions of the end-effectors and relevant joint centres across the motion. However, since our predictions include dynamics in the formulation, we define a time-averaged distance between motions which takes into account both kinematic and dynamic magnitudes. For this purpose, we consider a global TD (TD_{TOT}) which is defined as a combination of four TDs, representing respectively the time-averaged distance between the predicted and the reference motion in terms of end-effector trajectories (TD_T), DoF values (TD_q), DoF velocities ($TD_{\dot{q}}$) and dynamic efforts (TD_E).

As the clutch pedal depression is carried out mainly in the sagittal plane (and the seat contact model is defined only in this plane), the TDs focus on the n_q most relevant DoFs (n_q=6: three flexion-extensions, root forward tilt and x and z translations), the n_E most relevant efforts (n_E=6: three medio-lateral joint torques and three external efforts acting on the root segment in the sagittal plane) and the two components of the end-effector trajectory in the sagittal plane (along the x and z axes).

In order to deal with comparable TDs and to combine them in the global measure TD_{TOT}, the four aforementioned time-average distances are normalised. The quantities employed to yield dimensionless TDs are the standard deviations $\sigma_{Ref\,T}$, $\sigma_{Ref\,q}$, $\sigma_{Ref\,\dot{q}}$ and $\sigma_{Ref\,E}$, which respectively represent the dispersion from the mean values in the reference motion of the end-effector trajectories, DoF values, DoF velocities and efforts. Equation (5.17) details how each of the above-mentioned TDs is calculated.

$$
\begin{aligned}
TD_T &= \sqrt{\frac{\sum_{t=t_0}^{t_T}\left(\frac{x(t)-x_{Ref}(t)}{\sigma_{Ref\,x}}+\frac{z(t)-z_{Ref}(t)}{\sigma_{Ref\,z}}\right)^2}{2n_t}} \\
TD_q &= \sqrt{\frac{\sum_{i=1}^{n_q}\sum_{t=t_0}^{t_T}\left(\frac{q_i(t)-q_{Ref\,i}(t)}{\sigma_{Ref\,qi}}\right)^2}{n_q n_t}} \\
TD_{\dot{q}} &= \sqrt{\frac{\sum_{i=1}^{n_q}\sum_{t=t_0}^{t_T}\left(\frac{\dot{q}_i(t)-\dot{q}_{Ref\,i}(t)}{\sigma_{Ref\,\dot{q}i}}\right)^2}{n_q n_t}} \\
TD_E &= \sqrt{\frac{\sum_{i=1}^{n_{Eff}}\sum_{t=t_0}^{t_T}\left(\frac{E_i(t)-E_{Ref\,i}(t)}{\sigma_{Ref\,Ei}}\right)^2}{n_E n_t}} \\
TD_{TOT} &= \sqrt{TD_T^{\,2}+TD_q^{\,2}+TD_{\dot{q}}^{\,2}+TD_E^{\,2}}
\end{aligned}
\tag{5.17}
$$

where x and z represent the components of the end-effector trajectory in the predicted motion along the corresponding axes, and x_{Ref} and z_{Ref} represent the same components of the end-effector trajectory in the reference motion; q_i, $\dot{q}_i$ and E_i represent the i^{th} DoF value, DoF velocity and effort (either a force or a torque) in the predicted motion, respectively, and $q_{Ref\,i}$, $\dot{q}_{Ref\,i}$ and $E_{Ref\,i}$ represent the same quantities in the reference motion; $\sigma_{Ref\,x}$, $\sigma_{Ref\,z}$, $\sigma_{Ref\,qi}$, $\sigma_{Ref\,\dot{q}i}$ and $\sigma_{Ref\,Ei}$ respectively represent the standard deviation of the end-effector trajectory along the *x* and *z* axes and

of the i^{th} DoF value, DoF velocity and effort across the reference motion (from t_0 to t_T); n_q is the number of considered DoFs, n_E is the number of considered efforts and n_t is the number of frames in the motion.

Figure 5.9 reports the TDs thus obtained in the battery of predictions. It may be noticed how the small values of $TD_{\dot{q}}$ hardly vary across the trials, due to the data-based objective concerning DoF velocities (Equation (5.9)). Also TD_T presents small values and reduced variability on account of the goal fulfilment constraint (Equation (5.2)) and objective (Equation (5.8)). On the other hand, the TDs concerning the DoF values and the joint torques seem to be reduced for low damping ratios ($\xi \leq 0.4$) and increase for higher damping ratios ($\xi \geq 0.7$). The lowest values of the total TD are obtained in the optimum range of $0.2 \leq \xi \leq 0.4$. Hence, the value 0.3 is selected to represent the pelvis-seat damping ratio in the contact model, as it is the central value in the optimum range.

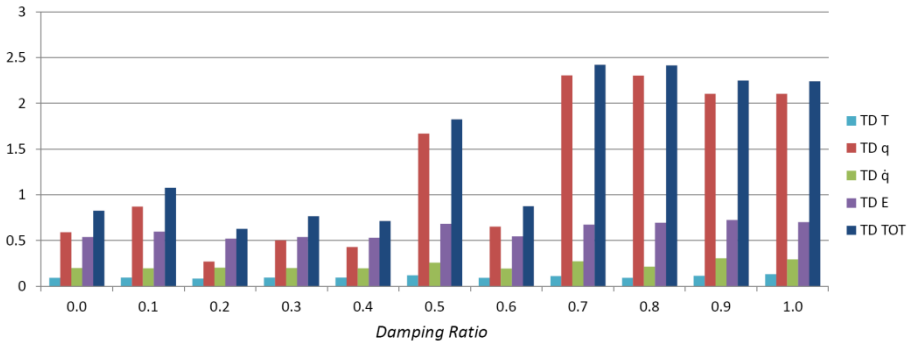

Figure 5.9: Time-averaged distances (TDs) between the predicted motions and the actually performed motion in the prediction scenario that they seek to resemble. The damping ratio is varied from 0 to 1 with a 0.1 step.

Therefore, considering the characterisation of the springs and dampers presented in these sections to represent the seat-pelvis interaction, the seat reaction forces exerted on the pelvis are evaluated throughout the motion as:

$$\begin{aligned} \mathbf{F} &= \sum_{i=1}^{n_{Contacts}} \left(k_i \, \mathbf{p}_i(\mathbf{q}) - c_i \, \mathbf{v}_i(\mathbf{q}, \dot{\mathbf{q}}) \right) \\ \boldsymbol{\tau} &= \sum_{i=1}^{n_{Contacts}} \mathbf{d}_i \times \mathbf{F}_i \end{aligned} \tag{5.18}$$

where $\mathbf{p}_i$ is the interference between the pelvis and the seat at the i^{th} contact; $\mathbf{v}_i$ is the i^{th} interference velocity; k_i and c_i are the stiffness and damping coefficients at the i^{th} contact, which present different values depending on whether the contact is between the pelvis and the cushion or the pelvis and the backrest; and d_i is the lever arm of the i^{th} force respect to the root joint (at which the dynamic balance of Equation (5.7) is imposed).

5.6 CONCLUSIONS

In this chapter we have presented the application of the motion prediction method described in Chapter 3 to the task of clutch pedal depressions. Both the definition of the prediction scenarios and the characteristics of the optimisation problem have been described.

It must be noticed the application of our method to the defined test case always follows a hybrid approach: on the one hand, all predictions rely on the data-based contribution of the reference motion, which determines the temporal features of the predicted motion (Section 3.3) and provides the initial approximation for the optimisation (Section 3.5.1); on the other, knowledge is included in the pedal contact model to reflect the behaviours identified in the database analysis of Chapter 4, imposing a larger or smaller radial force depending on whether a young or elderly subject is being predicted.

The following chapter presents the results of the predictions carried out employing this test case and proceeds to the validation of our motion prediction method.

CHAPTER 6

RESULTS AND VALIDATION

This chapter presents the results of our motion prediction method applied to the test case presented in Chapter 5. First of all, the characteristics of the reference motions employed for each prediction scenario are described (Section 6.1). Subsequently the results of the predictions are presented and discussed in order to compare kinematic and dynamic predictions (Section 6.2), to assess the most adequate motion control law for clutch pedal depressions (Section 6.3), and to compare a data-based, knowledge-based and hybrid objective function (Section 6.4). Throughout these sections, the results of the predictions are compared against the mean profiles of the target populations, which the predictions seek to represent, and their variability.

Finally, a quantitative validation is carried out to verify the realism and the representativeness of our motion prediction method (Section 6.5).

6.1 REFERENCE MOTION SCENARIOS

In order to resemble the conditions in which motion prediction methods are generally applied, we consider that the scenario of the reference motion is constituted by an environment that differs from the prediction environment and by a subject that differs from the prediction subject. Therefore, for each of the prediction scenarios described in Section 5.1, the reference motions are selected among the motions in the database, once the motions performed by the prediction subject and the motions performed by the remaining subjects in the prediction environment are set aside. Hence,

the scenarios selected as reference differ from the prediction scenarios in terms of both subject anthropometry and environment characteristics.

Considering for instance the group of young females, the YF subject whose anthropometry most resembles the average values of the YF group is, as mentioned in Section 5.1, identified by the ID 1 and is therefore employed as prediction subject (see Table 5.2). Consequently, the motions performed by YF_1 are not eligible as reference. Additionally, since PCA2 is the prediction environment, the motions performed in PCA2 are not eligible as reference either. Thus, the reference motion for the prediction of young females must be selected among the motions reported in Table 6.1, excluding the shaded ones, in order to consider as reference a motion performed by a different subject and in a different environment than those defined in the prediction scenario.

YF ID	BMW1	BMW2	BMW4	PCA1	PCA2	REN3
1	•	•		•	•••	•
2	•				••	•
3	•		•	•	•••	•
4	•		•	•	••	•
5		•		•	•••	

Table 6.1: Number of motions performed by each subject in the young female (YF) group in each vehicle configuration. The shaded cells are those corresponding to the prediction subject or the prediction environment.

All the predictions presented in this chapter were carried out twice, adopting two different reference motions. The first reference motion was selected from the database as the motion performed in the most similar scenario to the one to be predicted, thus representing the ideal conditions for a data-based prediction. This reference motion was identified employing the criterion described in Section 3.3: for the reference subject identification, a similar stature to the prediction subject was valued more than a similar weight; for what concerns the reference environment, the initial height of the clutch pedal from the floor, its initial orientation and its travel angle (see Section 4.5) were considered the most relevant features to assess environment similarity.

On the other hand, the second reference motion was selected as the motion performed by each subject group in the most dissimilar scenario, thus representing the extrapolation which may be required from a motion

prediction method. The characteristics of the reference scenarios employed in the predictions are reported in Table 6.2 and Table 6.3.

Subject ID	Gender	Age	Stature [cm]	Weight [kg]
YF_4	Female	21	168.2	57.2
YM_5	Male	34	182.3	78.7
EM_2	Male	78	173.0	77.0

Vehicle	S_h [mm]	Hx [mm]	CP_h [mm]	L [mm]	α [deg]	θ_0 [deg]	CPx [mm]	CPy [mm]	CPz [mm]
REN3	360	-1±33	142	139	15	59.2	-761	-70	-218

Table 6.2: Characteristics of the reference motion scenarios identified as the most similar to the prediction scenarios.

Subject ID	Gender	Age	Stature [cm]	Weight [kg]
YF_5	Female	22	163.2	62.4
YM_3	Male	24	170.0	55.6
EM_3	Male	76	169.5	79.0

Vehicle	S_h [mm]	Hx [mm]	CP_h [mm]	L [mm]	α [deg]	θ_0 [deg]	CPx [mm]	CPy [mm]	CPz [mm]
PCA1	355	-34±28	156	132	23	47.3	-770	-70	-199

Table 6.3: Characteristics of the reference motion scenarios identified as the most dissimilar to the prediction scenarios.

6.2 COMPARING KINEMATIC AND DYNAMIC PREDICTIONS

To compare the results of a kinematic and a dynamic approach, the following predictions were carried out. The three prediction scenarios reported in Table 5.2 were considered and two predictions were performed in each scenario:

- the first is a purely kinematic prediction, in which the DHM forces and torques are calculated *a posteriori* through inverse dynamics (described in Section 3.1.3), employing the contact models described in Section 5.5;
- the second is a dynamic prediction which is identical to the above-mentioned kinematic prediction, and additionally includes the dynamic balance constraint.

The conditions included in the optimisation problems defined in both the kinematic and dynamic predictions are detailed in Table 6.4 (each constraint is described in Section 5.3 and each objective in Section 5.4), and unit weights are associated to each objective.

	Constraints					Objectives		
Prediction	**Goal Fulfilment**	**Initial & Final**	**Joint RoMs**	**Collision Avoidance**	**Dynamic Balance**	**Goal Fulfilment**	**Data-based**	**Knowledge-based**
Kin	✓	✓	✓	✓		✓	✓	
Dyn	✓	✓	✓	✓	✓	✓	✓	

Table 6.4: Characteristics of the optimisation problems defined in the kinematic and the dynamic predictions.

It may be noticed that the knowledge-based objective is not included in the predictions. The reason is that knowledge is generally introduced in terms of a dynamic motion control law, which cannot be adopted in a kinematic approach. Therefore, the kinematic prediction is purely data-based. Since the defined dynamic prediction differs only in the presence of the balance constraint, its objective function is also purely data-based.

All three prediction scenarios reported in Table 5.2 were considered and each prediction was carried out twice, employing the different reference scenarios reported in Table 6.2 and Table 6.3. The results in the various prediction scenarios are similar, and therefore we hereafter present only those corresponding to the group of young females (YF) as example. The considerations that follow are valid also for the young and elderly males.

6.2.1 END-EFFECTOR TRAJECTORIES

The end-effector trajectories followed in the sagittal plane (EEx and EEz) in the kinematic and dynamic predictions are shown in Figure 6.1, along with the mean trajectory μ followed by the target population, its variability (μ±2σ), and the trajectory followed by the end-effector in the reference motions. The vertical black lines in Figure 6.1, and in all the following figures, mark the average *StartDepression* and *EndDepression* key-frames of the motions performed by the target population in the prediction environment. The difference between the reference and predicted trajectories are due to both the different position of the clutch pedal in the vehicles and to the different seat height in the reference and predicted scenarios (the origin of the global coordinate system is placed in the seat H-point, Section 4.2).

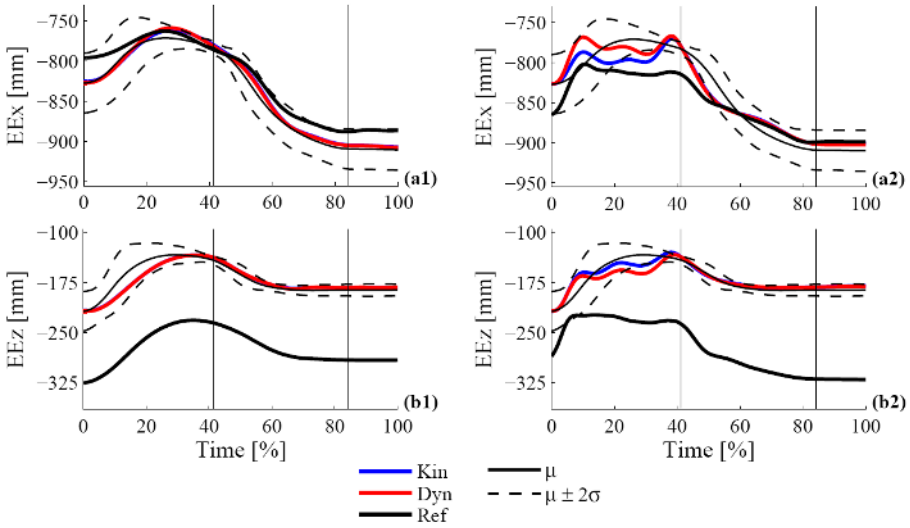

Figure 6.1: Trajectories followed by the end-effector in the sagittal plane for young females (YF) employing a similar reference motion (a1, a2) and a dissimilar reference motion (b1, b2) for the kinematic and dynamic predictions. The trajectories are reported along the longitudinal x axis (a1, b1) and the vertical z axis (a2, b2). The blue and red curves, respectively, show the results of the kinematic and the dynamic predictions. The trajectories followed by the end-effector in the reference motions are reported in black. The thin black curves show the mean trajectories μ followed by the end-effector of the YF target population and the thin dashed curves represent their variability μ±2σ. The vertical black lines mark the average *StartDepression* and *EndDepression* key-frames of the motions performed by the target population in the prediction environment.

It may be seen that the trajectories followed during the pedal depression phase in both the kinematic and dynamic predictions tend to match, due to the goal fulfilment constraint (Equation (5.2)) and objective (Equation (5.8)). Additionally, the predicted trajectories hardly exceed the $\mu \pm 2\sigma$ range of variability of the target population during the depression phase, on account of the goal fulfilment constraint and the adequacy of the modified trajectory to be followed (Equation (5.11)).

For what concerns the reach phase, a similar reference motion seems to yield trajectories that almost match in the kinematic and dynamic predictions, and which also tend to fall within the $\mu \pm 2\sigma$ range of the target population (Figure 6.1a1, b1). However, a dissimilar reference motion may lead to trajectories which differ more in the kinematic and dynamic prediction, and which occasionally exceed the $\mu \pm 2\sigma$ range (Figure 6.1a2, b2)

6.2.2 DoF Profiles

The DoF profiles shown and discussed in this section correspond to the n_q most relevant DoF profiles in clutch pedal depression, which are the DoFs that mostly act in the sagittal plane: namely, the flexion-extension DoFs, the pelvis forward tilt and its longitudinal and vertical translations.

The predicted profiles of the n_q most relevant DoFs, obtained employing a similar and a dissimilar reference motion, are reported in Figure 6.2 and Figure 6.3. The results of both the kinematic and dynamic predictions are shown, as well as the mean profiles μ in the target population, their variability ($\mu \pm 2\sigma$), and the DoF profiles in the reference motions.

It may be noticed that in terms of DoF values, both the kinematic and the dynamic predictions yield similar results, in particular for the flexion-extension DoFs (Figure 6.2). Additionally, the predicted profiles are mostly contained within the $\mu \pm 2\sigma$ range of variability of the target population, especially when a similar reference motion is employed (Figure 6.2a1-c1 and Figure 6.3a1-c1). When a dissimilar reference motion is employed, the predicted profiles occasionally exceed the range of variability of the target population (Figure 6.2b2, Figure 6.3c2).

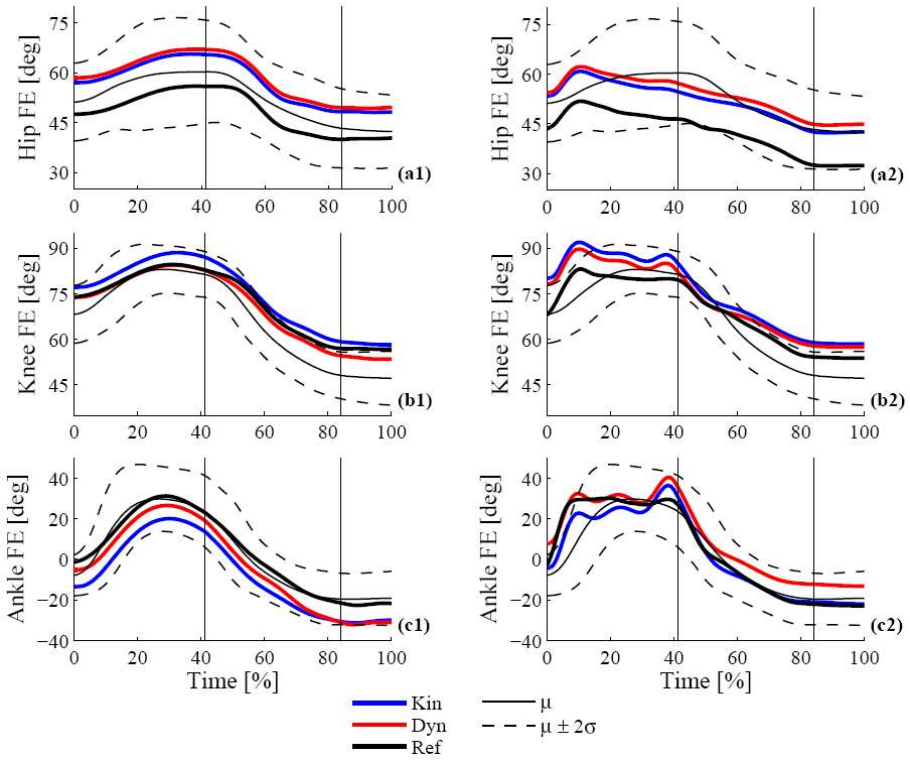

Figure 6.2: Flexion-extension profiles for young females (YF) employing a similar reference motion (a1, b1, c1) and a dissimilar reference motion (a2, b2, c2) for the kinematic and dynamic predictions. The blue and red curves, respectively, show the results of the kinematic and the dynamic predictions. The reference DoF profiles are reported in black.

6.2.3 DoF Velocity Profiles

The shapes of the DoF profiles may be analysed by comparing the values of the DoF velocities across the motion. Figure 6.4 and Figure 6.5 show the predicted velocity profiles corresponding to the n_q most relevant DoFs, obtained employing a similar and a dissimilar reference motion.

The predicted velocity profiles, both in the kinematic and in the dynamic prediction, always follow the reference DoF velocity profiles very closely, which was to be expected given the data-based condition to resemble the reference DoF velocities.

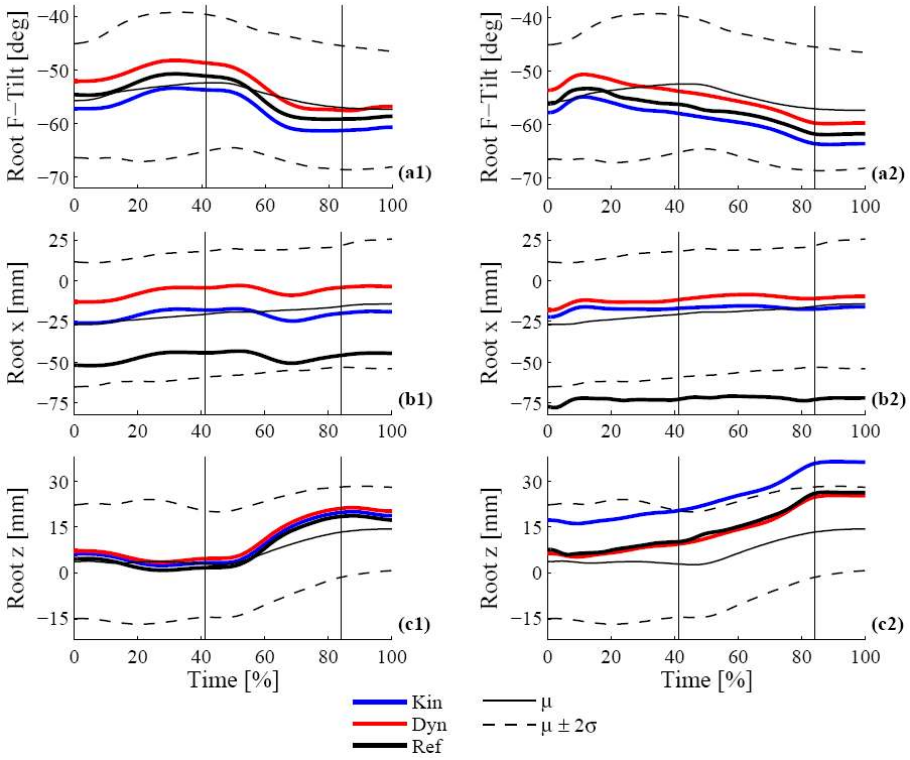

Figure 6.3: Forward tilt and translations of the root joint in the sagittal plane for young females (YF) employing a similar reference motion (a1, b1, c1) and a dissimilar reference motion (a2, b2, c2) for the kinematic and dynamic predictions. The blue and red curves, respectively, show the results of the kinematic and the dynamic predictions. The reference DoF profiles are reported in black.

It may be noticed that the predicted profiles occasionally exceed the $\mu \pm 2\sigma$ range of the target population (for instance, in Figure 6.5b1). This is due to the resemblance of the predicted profiles with the reference profiles, which correspond to motions that do not belong to the target population.

6.2.4 JOINT TORQUE PROFILES

The torque profiles which mostly affect the motion in the sagittal plane are the medio-lateral torques at the joints of the left leg. Their predicted profiles are shown in Figure 6.6, obtained employing a similar and a dissimilar reference motion.

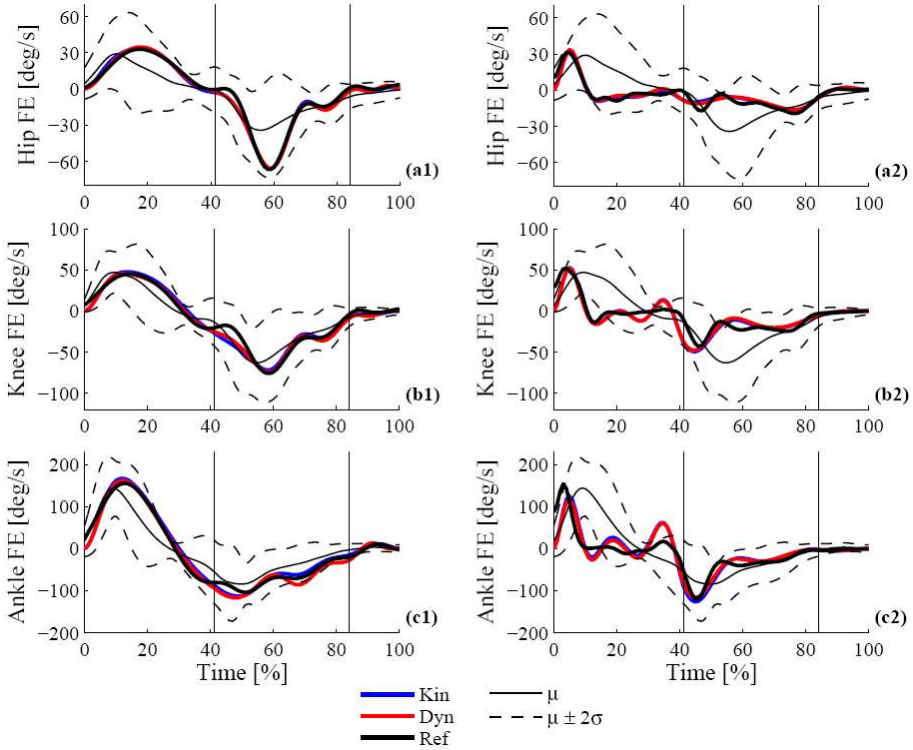

Figure 6.4: Flexion-extension velocity profiles for young females (YF) employing a similar reference motion (a1, b1, c1) and a dissimilar reference motion (a2, b2, c2) for the kinematic and dynamic predictions. The blue and red curves, respectively, show the results of the kinematic and the dynamic predictions. The reference DoF velocity profiles are reported in black.

Once again the results of both the kinematic (with *a posteriori* inverse dynamics) and dynamic predictions are very similar. This is due to both the approach followed to carry out the inverse dynamics calculations and to the forces acting on the DHM. In fact, the employed recursive Newton-Euler approach (Section 3.1.3) evaluates the efforts at the joints from the most distal segments towards the root, and the greatest forces acting on the DHM's left leg (the gravitational force and the pedal reaction force, obtained through the contact model described in Section 5.5.1) are common to both predictions. Given the high similarity in DoF profiles (Figure 6.2), such a resemblance in torque profiles was to be expected.

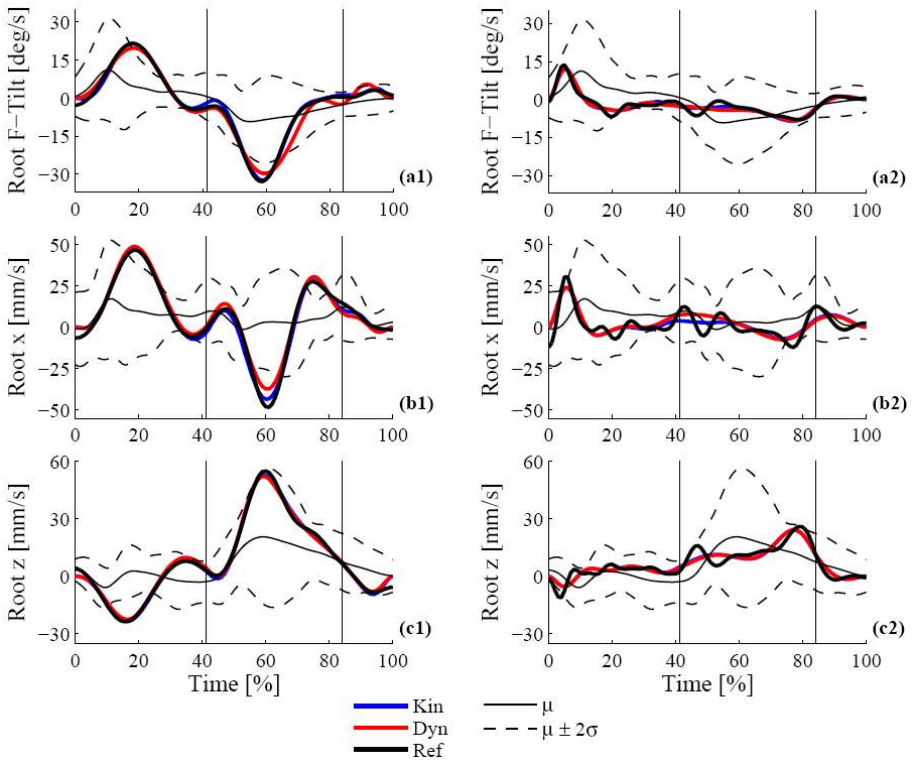

Figure 6.5: Forward tilt and translational velocities of the root joint in the sagittal plane for young females (YF) employing a similar reference motion (a1, b1, c1) and a dissimilar reference motion (a2, b2, c2) for the kinematic and dynamic predictions. The blue and red curves, respectively, show the results of the kinematic and the dynamic predictions. The reference DoF velocity profiles are reported in black.

It may be noticed that the joint torque profiles of the similar reference motion are contained within the range of variability of the target population, on account of the similarities between reference and prediction scenarios. On the other hand, when a dissimilar reference motion is employed, the reference torques present significantly different profiles from the target population.

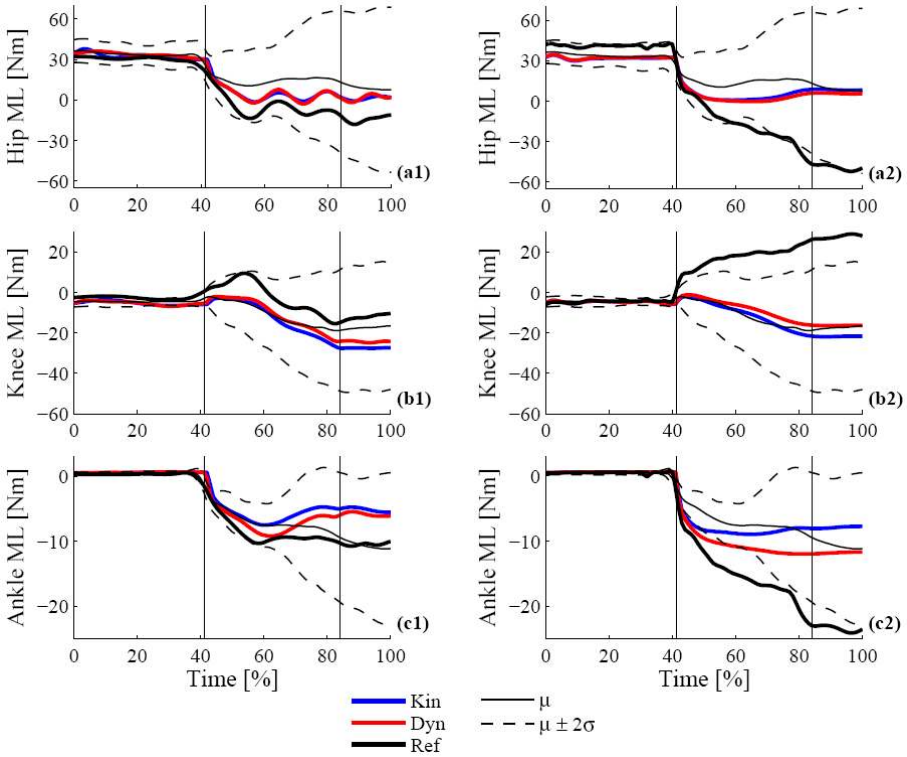

Figure 6.6: Joint torque profiles for young females (YF) employing a similar reference motion (a1, b1, c1) and a dissimilar reference motion (a2, b2, c2) for the kinematic and dynamic predictions. The medio-lateral torque profiles are shown at the hip (a1, a2), knee (b1, b2) and ankle (c1, c2) joints. The blue and red curves, respectively, show the results of the kinematic and the dynamic predictions. The reference DoF profiles are reported in black.

6.2.5 PELVIS-SEAT EFFORTS

The greatest difference between the kinematic and dynamic predictions may be seen analysing the efforts acting on the seat and, therefore, the dynamic balance of the DHM.

Figure 6.7 shows the forces acting on the seat along the global *x* and *z* axes and their resulting moment about the root joint centre. The efforts shown in the figure correspond both to the efforts that the pelvis exerts on the seat according to the inverse dynamics (ID) performed on the predicted motions, and to the efforts that the pelvis is expected to exert according to the employed pelvis-seat contact model (Section 5.5.2). The difference between the two represents the error in the dynamic balance condition.

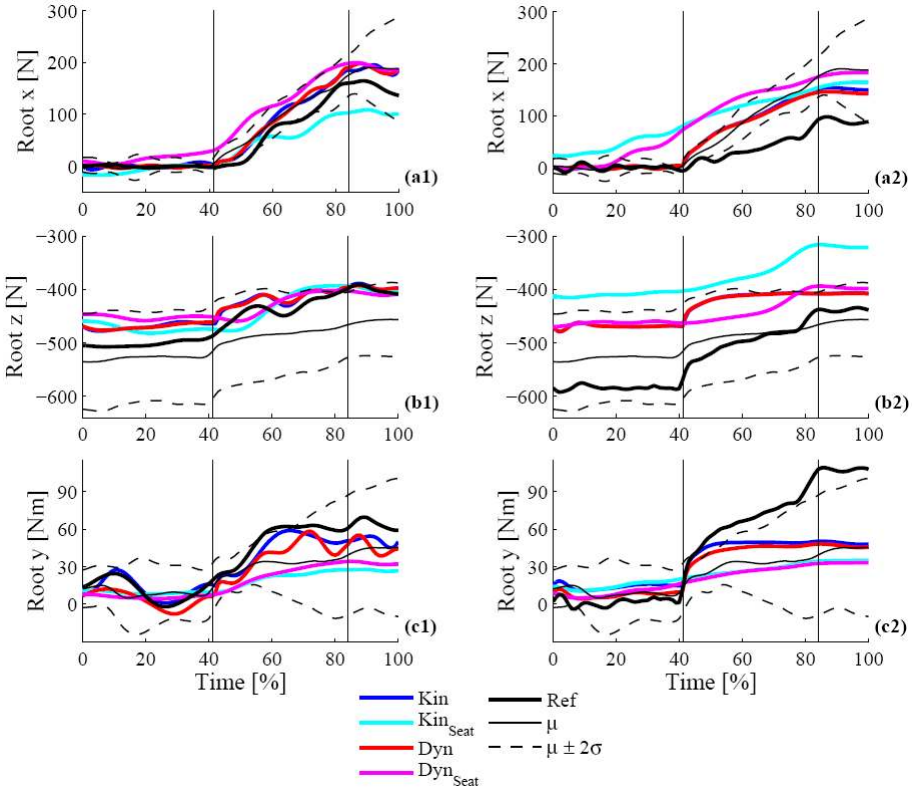

Figure 6.7: Efforts exerted by the pelvis on the seat for young females (YF) employing a similar reference motion (a1, b1, c1) and a dissimilar reference motion (a2, b2, c2) for the kinematic and dynamic predictions. The efforts in the sagittal plane are reported: forces along the x axis (a1, a2) and z axis (b1, b2) and torque about the global y axis (c1, c2). The results of the kinematic prediction are shown in blue (efforts evaluated through ID) and cyan (efforts expected according to the contact model) whereas the results of the dynamic predictions are shown in red (efforts evaluated through ID) and magenta (efforts expected according to the contact model). The efforts exerted in the reference motion are reported in black.

It may be noticed that in the dynamic prediction efforts present similar values. This is due to the balance condition imposed to the motion, which seeks accordance between the efforts obtained through ID and the efforts obtained through the pelvis-seat contact model. The efforts do not match exactly as the balance is imposed through an inequality constraint (Section 5.3.5), but are similar enough to assume that the discrepancy is due to the approximate nature of the pelvis-seat contact model.

Additionally, in most dynamic predictions, both pelvis efforts on the seat (obtained through ID and through the pelvis-seat contact model) hardly exceed the $\mu \pm 2\sigma$ range of the target population. The only exception we encountered is given by the horizontal forces in young females obtained with a dissimilar reference motion (Figure 6.7a2). In this case, the horizontal force according to the pelvis-seat contact model exceeds the $\mu \pm 2\sigma$ range in the central part of the motion, and seems to have anticipated the force values which characterise the depression phase.

For what concerns the kinematic prediction, instead, the discrepancy between the ID efforts and the efforts computed through the pelvis-seat contact model may be significantly large (Figure 6.7b2). The efforts evaluated through ID are once again similar to the dynamic prediction, but the efforts due to the contact model are significantly different. Hence, the dynamic balance is far from being fulfilled.

Such differences may be surprising given the high similarities between the kinematic and dynamic predictions in both the DoF profiles and the efforts evaluated through ID, but are actually the demonstration of the importance of imposing the dynamic balance in the prediction. In fact, if the dynamic balance is not enforced, there is no guarantee that the motion is actually feasible, regardless of whether the DoF and ID profiles are within the $\mu \pm 2\sigma$ range of the target population. For instance, considering the forces exerted along the vertical z axis, it may be seen in Figure 6.7b2 that, according to the contact model, the seat is reacting to a smaller force than the one exerted by the pelvis according to ID. The reason is that in the kinematic prediction the DHM's pelvis is located too high respect to the seat (about 1cm higher than the dynamic prediction, Figure 6.3c2) and therefore is not interfering with the seat geometry as much as needed to balance the weight of the subject.

The predictions carried out employing a similar reference motion (Figure 6.7a1-c1) present a more reduced discrepancy between the forces exerted by the pelvis on the seat. However, this result should not lead to the conclusion that for similar reference motions a kinematic prediction is always sufficient. In fact, in the predictions of both young and elderly males, also a similar reference motion has led to a large discrepancy in pelvis efforts as shown in Figure 6.8 (which depicts the predictions of young males employing a similar and a dissimilar reference motion).

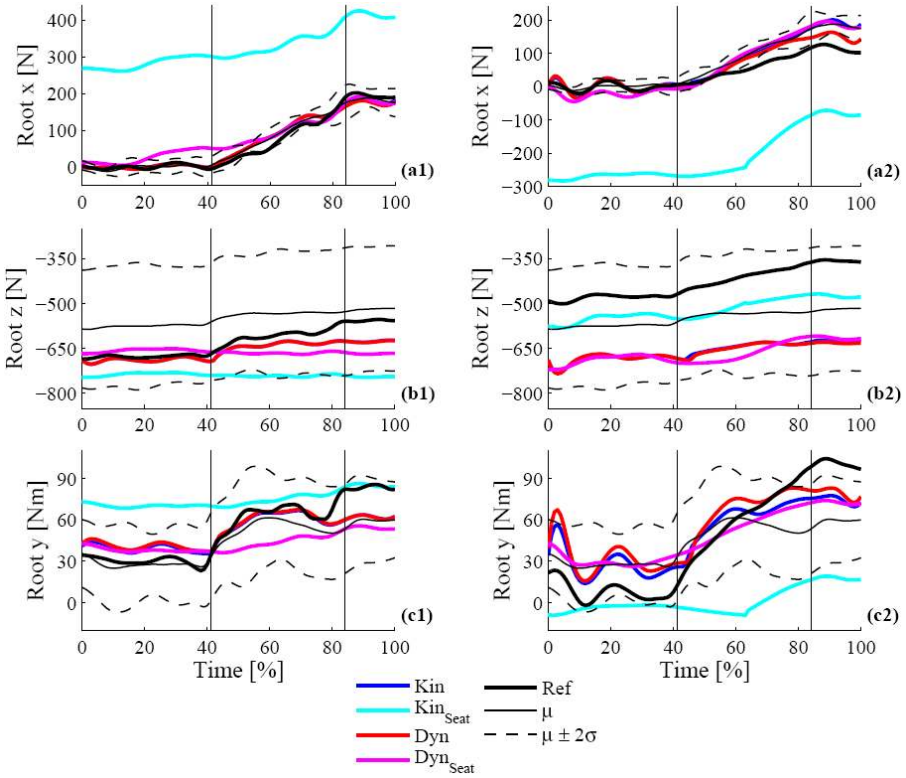

Figure 6.8: Efforts exerted by the pelvis on the seat for young males (YM) employing a similar reference motion (a1, b1, c1) and a dissimilar reference motion (a2, b2, c2) for the kinematic and dynamic predictions. The efforts in the sagittal plane are reported: forces along the x axis (a1, a2) and z axis (b1, b2) and torque about the global y axis (c1, c2). The results of the kinematic prediction are shown in blue (efforts evaluated through ID) and cyan (efforts expected according to the contact model) whereas the results of the dynamic predictions are shown in red (efforts evaluated through ID) and magenta (efforts expected according to the contact model). The efforts exerted in the reference motion are reported in black.

In this case, when a similar reference motion is employed (Figure 6.8a1-c1), the pelvis force along the *x* axis according to the contact model is much larger than the force exerted by the pelvis according to ID. As the DoF velocity profiles are almost identical in both kinematic and dynamic predictions (due to the data-based objective), the reason for the discrepancy between the efforts estimated through the pelvis-seat contact models is to be found in the differences in DoF profiles. Figure 6.9 shows the DoF profiles of the root joint predicted for young males employing both a similar and dissimilar reference motion, and following the kinematic and

dynamic approaches. It may be seen that, for a similar reference motion (Figure 6.9a1-c1), the kinematic prediction places the DHM too far back in the seat (about 1cm further back respect to the dynamic prediction, Figure 6.9b1), which is therefore interfering with the seat geometry more than it should.

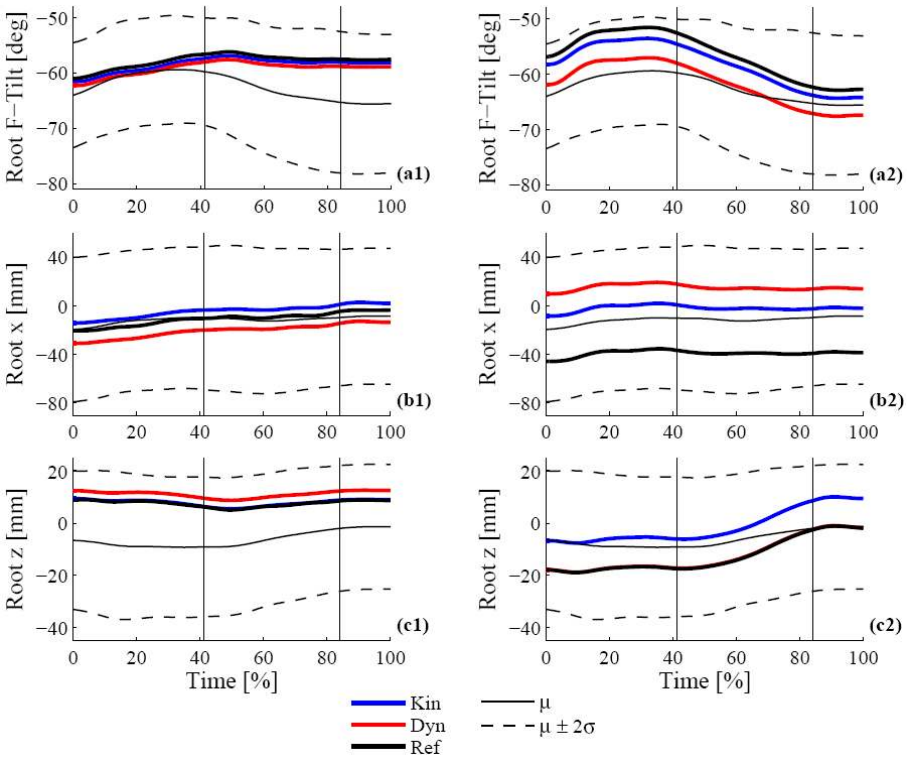

Figure 6.9: Forward tilt and translations of the root joint in the sagittal plane for young males (YM) employing a similar reference motion (a1, b1, c1) and a dissimilar reference motion (a2, b2, c2) for the kinematic and dynamic predictions. The blue and red curves, respectively, show the results of the kinematic and the dynamic predictions. The reference DoF profiles are reported in black.

Additionally, in the predictions of both young and elderly males it has occurred that the resulting seat reaction exerted along the *x* axis, according to the contact model, was directed in the *opposite* direction, pushing the DHM further back (Figure 6.8a2). The reason for the seat reaction to be directed backwards is that the kinematic prediction yields a pelvis which is both tilted and located too forwards. In fact, although the DoF profiles in the kinematic prediction are completely contained within the $\mu \pm 2\sigma$ range of

variability of the target population, the pelvis is tilted about 8º more and located 2cm forward respect to the dynamic prediction (Figure 6.9a2 and b2, respectively), and no interference is being generated with the seat backrest (the only seat reaction is due to the cushion). Therefore, according to the kinematic prediction, the DHM is moving as if it were leaning on the seat, but it actually is not.

6.2.6 CONCLUSIONS

The results presented in this section prove that a kinematic prediction may generate a motion that *looks* natural, but presents no guarantee on the actual feasibility and the physical soundness of the predicted motion.

On the other hand, not only the dynamic prediction yields DoF and joint torque profiles which are mostly contained in the $\mu \pm 2\sigma$ range of the target populations, but both pelvis efforts on the seat (obtained through ID and through the pelvis-seat contact model) in the dynamic prediction generally do not exceed the $\mu \pm 2\sigma$ range of variability. Therefore, we may consider that the defined pelvis-seat contact model (Section 5.5.2) and the tolerances employed in the balance inequality constraints (Section 5.3.5) are sufficiently accurate for the prediction of physically sound clutch pedal depressions.

Finally, some of the predicted profiles are found to occasionally exceed the $\mu \pm 2\sigma$ range of variability encountered in the target populations, especially if the reference and prediction scenarios are not very similar (Figure 6.1a2, b2, Figure 6.2b2 and Figure 6.3c2). This may be due to a limitation of purely data-based methods, which can reasonably predict motions that do not differ significantly from the reference, but which may not be adequate when larger extrapolations are required. Therefore, we seek to include knowledge in the prediction in the form of a motion control law in order to yield more realistic results, which are not bound to the similarity between the reference and prediction scenarios.

6.3 COMPARING MOTION CONTROL LAWS

In order to find the most adequate motion control law to represent clutch pedal depressions, we have compared two of the most common energy-related performance measures: minimum dynamic effort (DE) and minimum mechanical energy (ME).

As mentioned previously (Sections 2.1.2.2 and 3.5.3.3), the DE performance measure minimises the squared sum of the joint torques across the motion, and its corresponding objective Ψ is expressed by:

$$\forall t \in [t_0, t_T] \qquad \boldsymbol{\Psi}_{DE} = \boldsymbol{\tau}(\mathbf{q}, \dot{\mathbf{q}}, \ddot{\mathbf{q}}) \tag{6.1}$$

For what concerns the ME performance measure, approximated through the Riemann sum of the instantaneous power at the joints with respect to time, the corresponding objective Ψ is given by:

$$\forall t \in [t_0, t_T] \qquad \boldsymbol{\Psi}_{ME} = \boldsymbol{\tau}^T(\mathbf{q}, \dot{\mathbf{q}}, \ddot{\mathbf{q}})\boldsymbol{\omega}^{Rel}(\mathbf{q}, \dot{\mathbf{q}})\Delta t \tag{6.2}$$

In order to test both performance measures, purely knowledge-based objectives were employed in the predictions. Once again, all three prediction scenarios reported in Table 5.2 were considered and each prediction was carried out twice, employing different reference motions (Table 6.2 and Table 6.3). In fact, although no data-based objective is employed, the choice of the reference motion may affect the prediction as it determines the temporal features of the predicted motion (Section 3.3) and the initial approximation for the optimisation problem (Section 3.5.1).

By considering only the DE or the ME performance measures, we found that the predicted motions failed to resemble the motions performed by the target population, especially considering the translational velocities of the root segment and the shape of the flexion-extension DoFs (see Figure 6.11 to Figure 6.14). Therefore, additional conditions were considered along with the aforementioned energy-related performance measures. The first condition seeks to minimise the translational velocities (TV) of the root in order to contain the values $\dot{\mathbf{q}}_{Trans}$ within a more realistic range:

$$\forall t \in [t_0, t_T] \qquad \boldsymbol{\Psi}_{TV} = \dot{\mathbf{q}}_{Trans}(t) \tag{6.3}$$

This condition is considered reasonable as the clutch pedal depression is an operation which is carried out in a seated position and in which the pelvis appears to move very slightly (Figure 4.16, Section 4.4.4).

The second additional condition is based on a characteristic of clutch pedal depressions which emerged from the database analysis: the coordination which appears to exist among the hip, knee and ankle flexion-extension DoFs (Section 4.4.5). This coordination law (CL) is set to generate more realistic DoF profiles by imposing that normalised flexion-extension profiles must resemble one another:

$$\forall t \in [t_0, t_T] \qquad \boldsymbol{\Psi}_{CL} = \begin{cases} \dot{q}_{nAnkle}(t) - \dot{q}_{nKnee}(t) \\ \dot{q}_{nKnee}(t) - \dot{q}_{nHip}(t) \\ \dot{q}_{nHip}(t) - \dot{q}_{nAnkle}(t) \end{cases} \tag{6.4}$$

Four different knowledge-based predictions were defined, according to the performance measures considered in each prediction: only DE, only ME, and DE and ME (respectively) combined to the aforementioned TV and CL conditions. The characteristics of the optimisation problem defined in each prediction are detailed in Table 6.5 (the constraints are described in Section 5.3 and the goal-fulfilment objective in Section 5.4.1), and unit weights are associated to each objective.

	Constraints					Objectives					
Prediction	**Goal Fulfil.**	**Init. & Fin.**	**RoMs**	**Collisions**	**Dyn. Balance**	**Goal Fulfil.**	**D-based**	**K-based**			
								Dyn. Eff.	**Mech. En.**	**Trans. Vel.**	**Coord. Law**
DE	✓	✓	✓	✓	✓	✓		✓			
ME	✓	✓	✓	✓	✓	✓			✓		
DE+TV+CL	✓	✓	✓	✓	✓	✓		✓		✓	✓
ME+TV+CL	✓	✓	✓	✓	✓	✓			✓	✓	✓

Table 6.5: Characteristics of the optimisation problems defined in the predictions to assess the most adequate motion control law for clutch pedal depressions.

Although the predictions presented in this section are purely knowledge-based, the choice of the reference motion affects the results of the prediction. In fact, as mentioned earlier, our motion prediction method requires both the temporal features of the motion and the initial approximation for the optimisation problem to be provided by the reference motion. Nevertheless, analogous results are obtained with either reference. Additionally, as similar conclusions may be drawn from the predictions of all three subject groups, we hereafter present as example the kinematic and dynamic profiles corresponding to the group of young males (YM) obtained employing both a similar and a dissimilar reference motion.

6.3.1 END-EFFECTOR TRAJECTORIES

Figure 6.10 reports the end-effector trajectories followed in the sagittal plane, obtained through the four knowledge-based predictions described in Table 6.5, as well as the mean profiles μ in the target population and their variability (μ±2σ). The vertical black lines in Figure 6.10, and in all the following figures, mark the average *StartDepression* and *EndDepression* key-frames of the motions performed by the target population in the prediction environment.

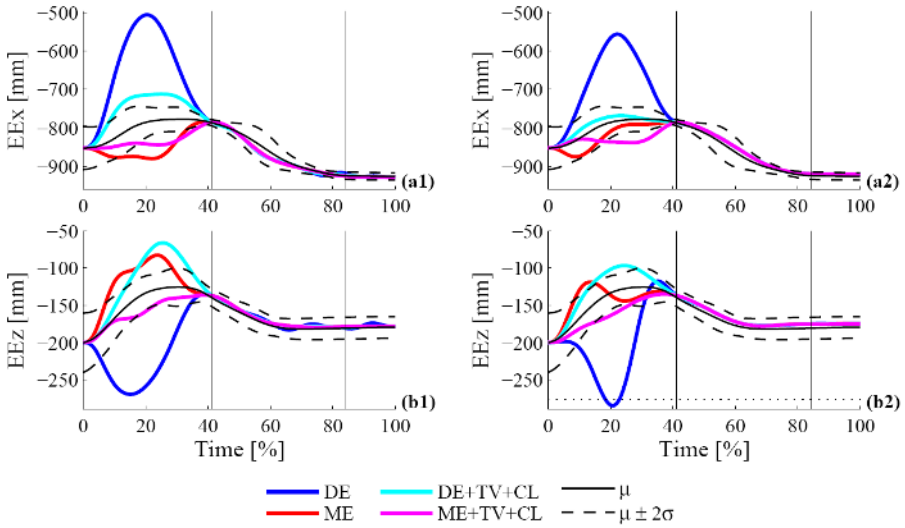

Figure 6.10: Trajectories followed by the end-effector in the sagittal plane for young males (YM) following different control laws, employing a similar reference motion (a1, b1) and a dissimilar reference motion (a2, b2). The blue and red curves, respectively, show the results of employing the DE and the ME performance measures. The result of including the TV and CL conditions are shown in cyan and magenta. The horizontal dotted black line (b2) reports the height of the PCA2 vehicle floor.

The trajectories followed during the pedal depression tend to match, due to the goal fulfilment constraint (Equation (5.2)) and objective (Equation (5.8)), and hardly exceed the μ±2σ range of variability of the target population. During the reach phase, however, the employed motion control law strongly affects the end-effector trajectories.

It may be noticed that the predictions which follows only the DE performance measure yield the trajectories which least resemble the ones followed by the target population: in fact, the left foot is retracted much more (Figure 6.10a1, a2) and is lowered from the foot rest to the vehicle

floor (Figure 6.10b1, b2). In the prediction in which the most dissimilar reference is employed, the end-effector actually reaches the vehicle floor and goes slightly beneath it. The collisions between the end-effector and the floor in fact are not controlled, as they do not seem very probable in actual clutch pedal depressions.

The trajectories followed in the ME predictions are more contained respect to the DE trajectories, but nevertheless tend to exceed the $\mu \pm 2\sigma$ range of variability in the target population.

On the other hand, including the TV and CL conditions improves the results of both the DE and ME predictions as the trajectories resemble more the values and the shape of the trajectories followed by the target population. The DE+TV+CL combination of objectives, however, tend to exceed the $\mu \pm 2\sigma$ range more often than the ME+TV+CL combination. However, the ME+TV+CL combination maintains the foot longer at the initial position along the longitudinal x axis (Figure 6.10a1, a2), respect to the actually performed motions.

6.3.2 DoF Profiles

For what concerns the DoFs in the DHM, the profiles of the n_q most relevant DoFs (which mostly act in the sagittal plane), obtained with the four knowledge-based predictions, are shown in Figure 6.11 and Figure 6.12, along with the mean profiles μ in the target population and their variability ($\mu \pm 2\sigma$).

Similar considerations to those presented discussing the end-effector trajectories can be made: on the one hand, the DE performance measure alone yields the DoF profiles which least resemble actually performed motions. Additionally, the ankle flexion-extension DoF predicted with the DE performance measure, employing a similar reference motion (Figure 6.11c1), slightly exceeds its RoM in between two frames at which RoM inequalities are enforced (Section 5.3.3), close to the *EndDepression* key-frame. The values of the DoF profiles obtained in the ME prediction are generally contained within the $\mu \pm 2\sigma$ range of variability of the target population but present shapes which seem far from resembling the average trend of the target population (see also Section 6.3.3).

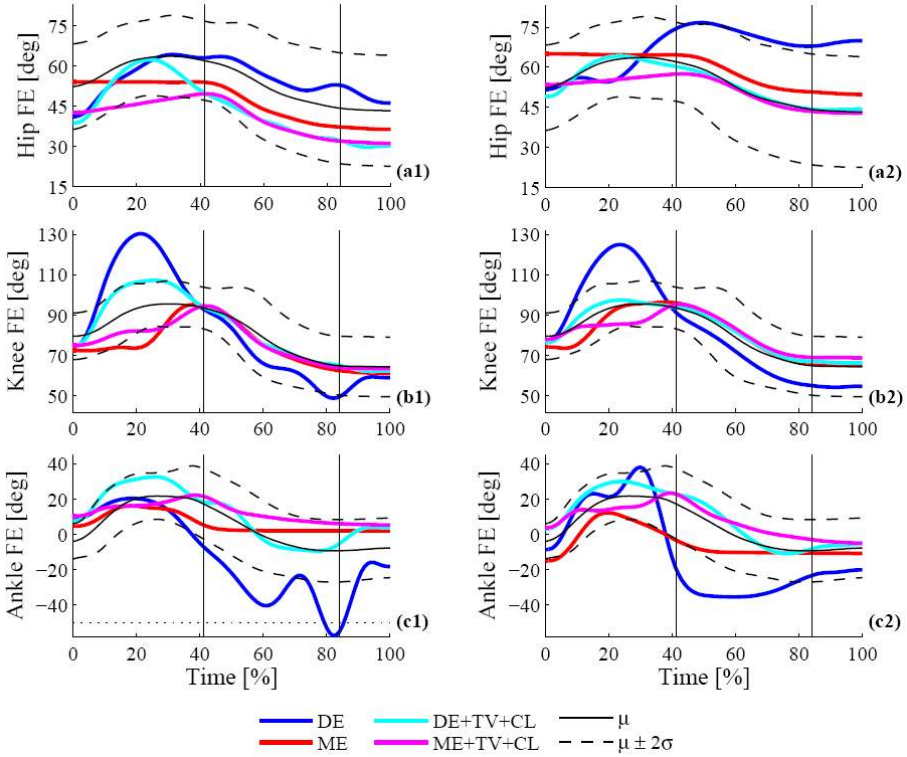

Figure 6.11: Flexion-extension profiles for young males (YM) following different control laws, employing a similar reference motion (a1, b1, c1) and a dissimilar reference motion (a2, b2, c2). The blue and red curves, respectively, show the results of employing the DE and the ME performance measures. The result of including the TV and CL conditions are shown in cyan and magenta.

On the one hand, once again, including the TV and CL conditions improves the results of the predictions, as the predicted profiles are mostly contained within the $\mu \pm 2\sigma$ range of the target population and tend to resemble the shape of the average DoF profiles of the target population more closely, as discussed in detail in the following section. Between the DE+TV+CL and the ME+TV+CL combination, it is unclear which yields the most realistic results as for some DoFs the DE+TV+CL combination seems preferable (e.g. Figure 6.11a2, b2), whereas others seem to be best represented through the ME+TV+CL combination (e.g. Figure 6.11c1, Figure 6.12a1).

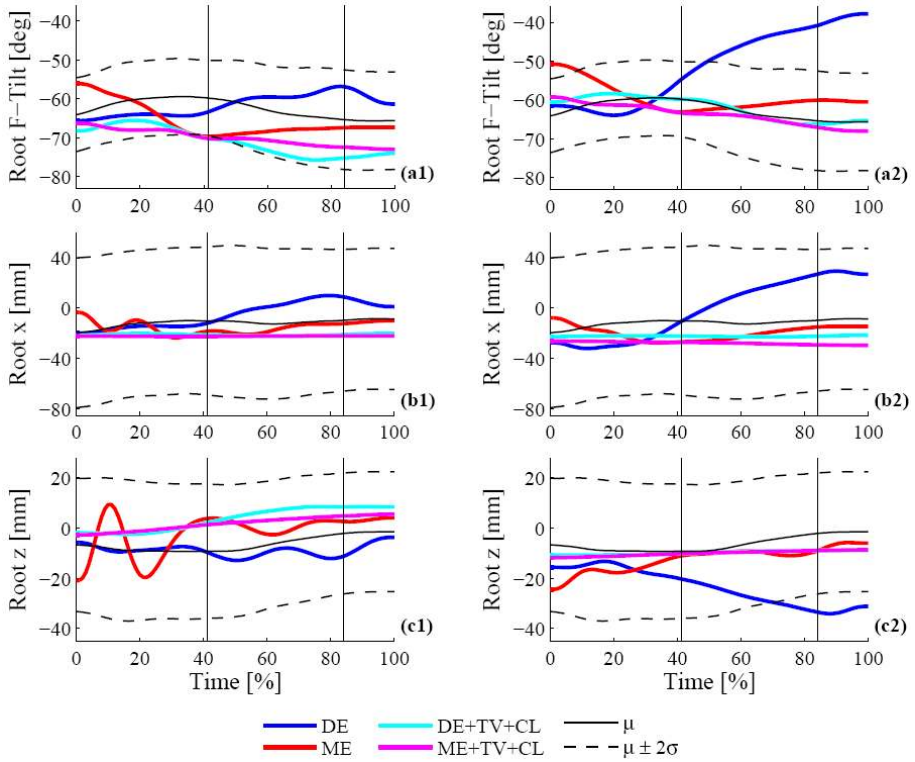

Figure 6.12: Forward tilt and translations of the root joint in the sagittal plane for young males (YM) following different control laws, employing a similar reference motion (a1, b1, c1) and a dissimilar reference motion (a2, b2, c2). The blue and red curves, respectively, show the results of employing the DE and the ME performance measures. The result of including the TV and CL conditions are shown in cyan and magenta.

6.3.3 DoF Velocity Profiles

For what concerns the DoF velocities, and therefore the shape of the DoF profiles, Figure 6.13 and Figure 6.14 show the predicted velocity profiles corresponding to the n_q most relevant DoFs, obtained employing a similar and a dissimilar reference motion. Once again, including the TV and CL conditions yields predicted profiles which resemble the profiles of the target population more closely.

It may be noticed that both DE and ME performance measures alone yield irregular and large translational velocities at the root joint, which are strongly reduced by the TV condition (Figure 6.14b1, b2 and c1, c2). The DE prediction also presents large oscillations in the velocity profiles of the

rotational DoFs, which are also generally reduced through the CL condition (Figure 6.13).

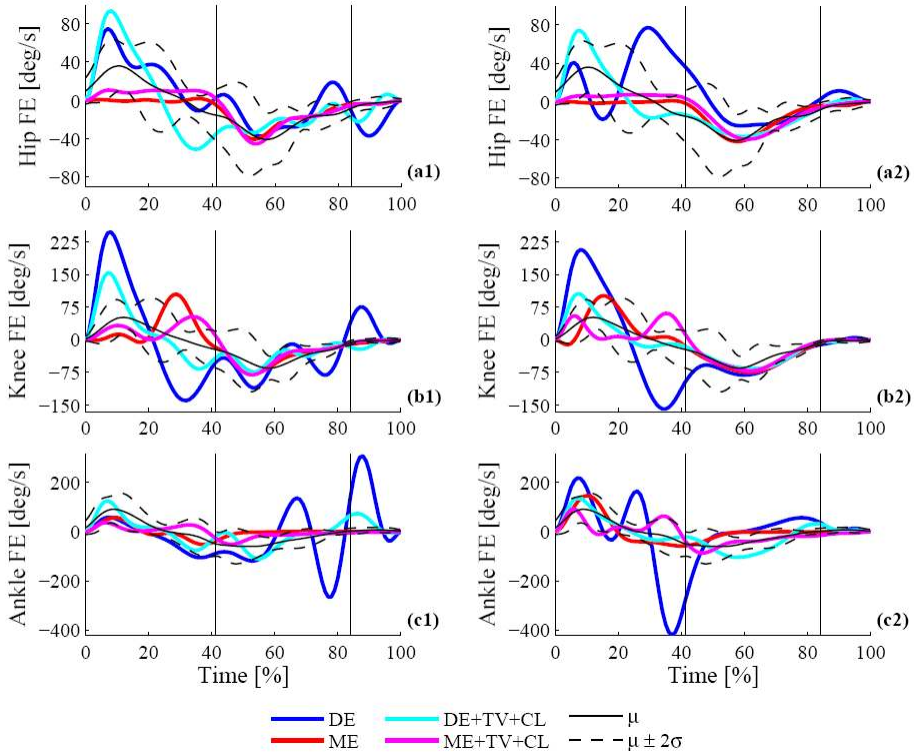

Figure 6.13: Flexion-extension velocity profiles for young males (YM) following different control laws, employing a similar reference motion (a1, b1, c1) and a dissimilar reference motion (a2, b2, c2). The blue and red curves, respectively, show the results of employing the DE and the ME performance measures. The result of including the TV and CL conditions are shown in cyan and magenta.

Nevertheless, the results of the DE+TV+CL combination seem to be outdone by the ME+TV+CL combination, which yield the most realistic DoF velocity profiles, hardly exceeding the $\mu \pm 2\sigma$ variability range of the target population (Figure 6.13).

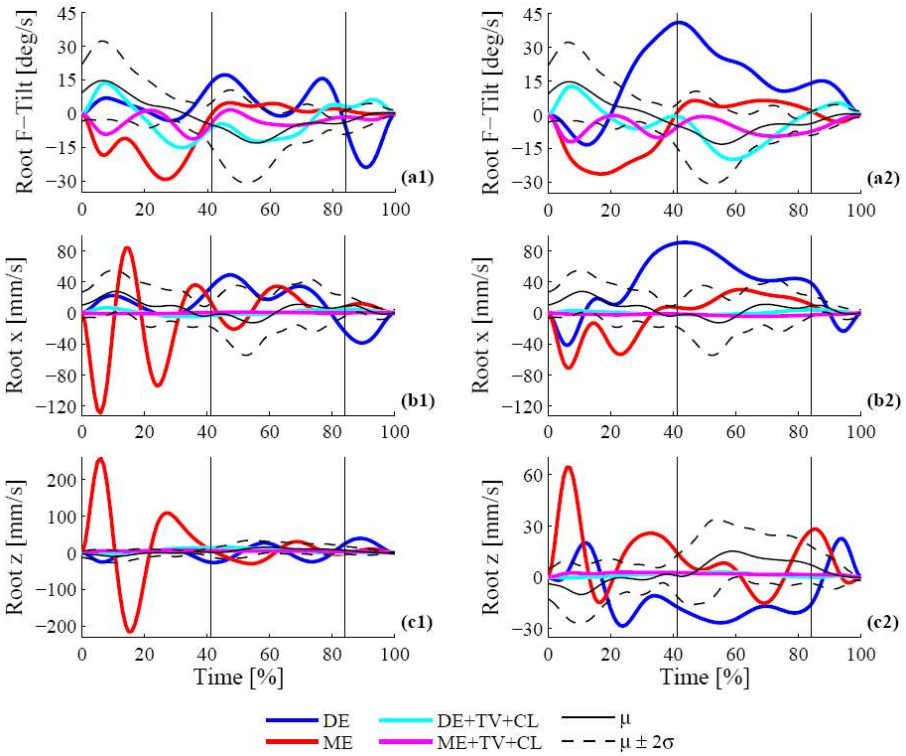

Figure 6.14: Forward tilt and translational velocities of the root joint in the sagittal plane for young males (YM) following different control laws, employing a similar reference motion (a1, b1, c1) and a dissimilar reference motion (a2, b2, c2). The blue and red curves, respectively, show the results of employing the DE and the ME performance measures. The result of including the TV and CL conditions are shown in cyan and magenta.

6.3.4 EFFORT PROFILES

For what concerns the dynamic profiles, Figure 6.15 and Figure 6.16 show the efforts which mostly affect the motion in the sagittal plane (medio-lateral joint torques and efforts exerted by the pelvis on the seat in the sagittal plane) along with the mean profiles μ in the target population and their variability ($\mu \pm 2\sigma$).

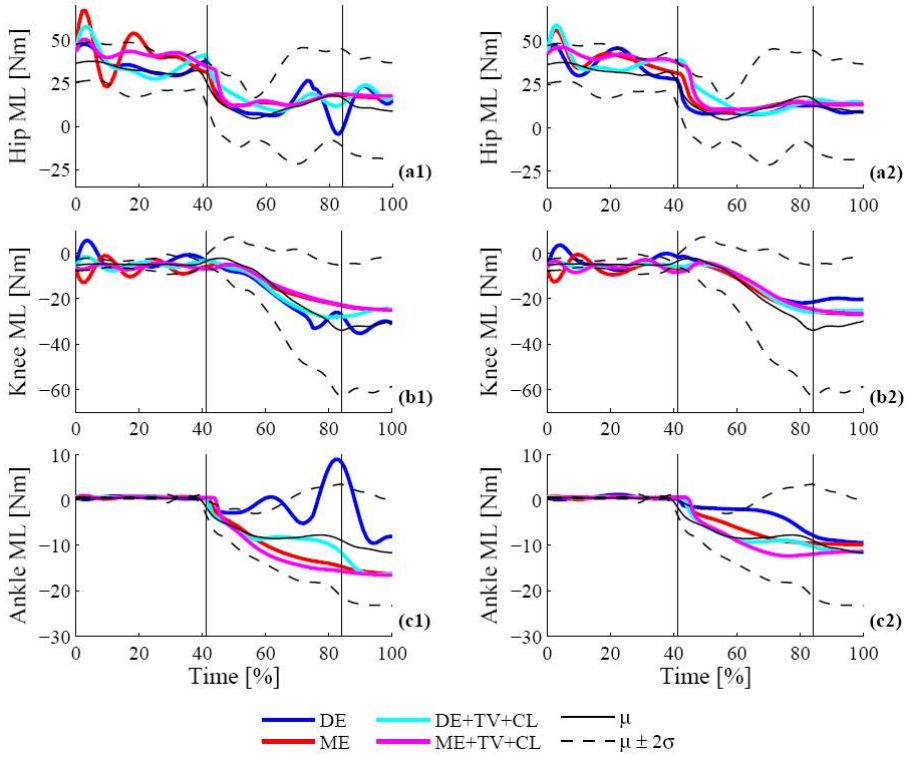

Figure 6.15: Joint torque profiles for young males (YM) following different control laws, employing a similar reference motion (a1, b1, c1) and a dissimilar reference motion (a2, b2, c2). The medio-lateral torque profiles are shown at the hip (a1, a2), knee (b1, b2) and ankle (c1, c2) joints. The blue and red curves, respectively, show the results of employing the DE and the ME performance measures. The result of including the TV and CL conditions are shown in cyan and magenta.

The predictions which employ the DE and ME performance measures alone present strong oscillations or irregular profiles, reflecting the oscillations and irregularities observed in the DoF value and velocity profiles, and yield effort profiles which do not resemble the average profiles in the target population. The results reported in Figure 6.15 and Figure 6.16 show that the values of the forces exerted by the pelvis obtained in the ME prediction significantly exceed the $\mu \pm 2\sigma$ range of the target population in between the frames at which the balance constraint is imposed, leading to highly oscillating and unrealistic force profiles (Figure 6.16a1, b1 and a2). The DE prediction, on the other hand, yields jerky torque profiles at the joints (Figure 6.15a1, c1) and exceeds the $\mu \pm 2\sigma$ range of the torque exerted by the pelvis on the seat (Figure 6.16c2).

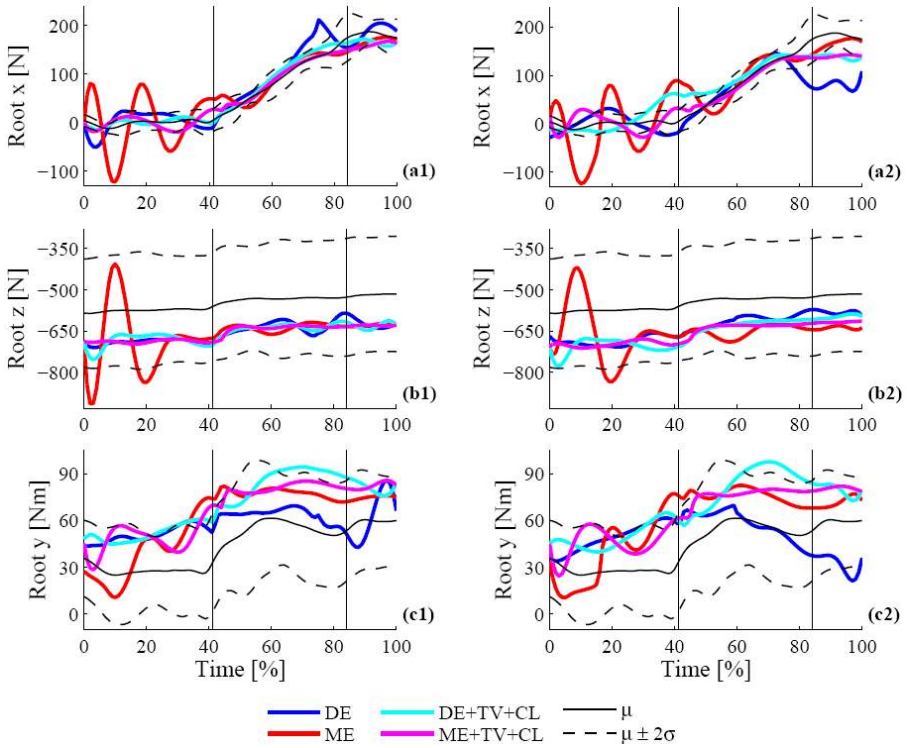

Figure 6.16: Efforts exerted by the pelvis on the seat for young males (YM) following different control laws, employing a similar reference motion (a1, b1, c1) and a dissimilar reference motion (a2, b2, c2). The efforts in the sagittal plane are the forces along the x axis (d1, d2) and z axis (e1, e2) and the torque about the global y axis (f1, f2). The blue and red curves, respectively, show the results of employing the DE and the ME performance measures. The result of including the TV and CL conditions are shown in cyan and magenta.

On the other hand, including the TV and CL conditions seem to improve the realism of both DE and ME performance, yielding effort profiles which tend to resemble the average effort profiles μ of the target population more closely and hardly exceed the $\mu \pm 2\sigma$ range of variability.

6.3.5 TIME-AVERAGED DISTANCE DEFINITION

The results presented above (Figure 6.10-Figure 6.16) show that the DE and ME performance measures alone are not adequate to predict clutch pedal depressions. However, combined with the TV and CL conditions, the predictions yield more satisfactory results, with both kinematic and dynamic profiles mostly contained within the variability of the target population.

In order to assess which of the two knowledge-based combinations (DE+TV+CL and ME+TV+CL) is the most appropriate to represent clutch pedal depressions, a time-averaged distance (TD) is defined to quantitatively compare the results of both combinations. As mentioned in Section 1.2 of the Introduction, the aims of the prediction are to generate a motion which is both realistic and representative of the target population. Under the assumption that the profiles of the target population resemble a normal distribution (no evident reasons have been encountered to suggest a different distribution), the realism and representativeness of the predicted motion require that the predicted profiles should not stray significantly from the target population mean profiles μ. Specifically, realism requires the predicted motion to fall within two standard deviations from the mean, as 95% of actually performed motion are contained within the $\mu \pm 2\sigma$ range. On the other hand, the deviations of a motion from the mean are compensated by opposite deviations of other motions. Hence, representativeness requires the predicted motion to be close to the mean of the target population.

Therefore, we consider that the most desirable prediction is the one which maximises the likelihood between the predicted profiles and the mean profiles of the target population. As the variability of the target population varies across the motion (the $\mu \pm 2\sigma$ curves do not correspond to the mean curve μ shifted vertically), the maximum likelihood is achieved by minimising the normalised Euclidean distance between the predicted profiles and the mean profiles of the target population. The normalised Euclidean distance differs from the standard Euclidean distance as it is normalised by the standard deviation of the target population: the differences between the predicted and mean target profiles, therefore, are related to the variability of the target population across the motion.

As both kinematic and dynamic variables are included in the prediction, we consider a time-averaged distance TD_{TOT} which is given by a combination of four TDs, similarly to the time-averaged distances defined in Section 5.5.2.2. The four TDs represent respectively the time-averaged distance of the predicted end-effector trajectories (TD_T), DoF profiles (TD_q), DoF velocities ($TD_{\dot{q}}$) and dynamic efforts (TD_E) from the corresponding mean profiles of the target population.

As the clutch pedal depression is carried out mainly in the sagittal plane (and the seat contact model is defined only in this plane), the TDs

focus on the n_q most relevant DoFs (flexion-extensions, root forward tilt and x and z translations), the n_E most relevant efforts (medio-lateral joint torques and external efforts acting on the root segment in the sagittal plane), and the two components of the end-effector trajectory in the sagittal plane (along the x and z axes).

Therefore, the time-averaged distances mentioned above are defined by Equation (6.5) as follows:

$$
\begin{aligned}
TD_T &= \sqrt{\frac{\sum_{t=t_0}^{t_T}\left(\frac{x(t)-\mu_x(t)}{\sigma_x(t)}+\frac{z(t)-\mu_z(t)}{\sigma_z(t)}\right)^2}{2\,n_t}} \\
TD_q &= \sqrt{\frac{\sum_{i=1}^{n_q}\sum_{t=t_0}^{t_T}\left(\frac{q_i(t)-\mu_{qi}(t)}{\sigma_{qi}(t)}\right)^2}{n_q\,n_t}} \\
TD_{\dot{q}} &= \sqrt{\frac{\sum_{i=1}^{n_q}\sum_{t=t_0}^{t_T}\left(\frac{\dot{q}_i(t)-\mu_{\dot{q}i}(t)}{\sigma_{\dot{q}i}(t)}\right)^2}{n_q\,n_t}} \\
TD_E &= \sqrt{\frac{\sum_{i=1}^{n_\tau}\sum_{t=t_0}^{t_T}\left(\frac{E_i(t)-\mu_{Ei}(t)}{\sigma_{Ei}(t)}\right)^2}{n_E\,n_t}} \\
TD_{TOT} &= \sqrt{TD_T{}^2+TD_q{}^2+TD_{\dot{q}}{}^2+TD_E{}^2}
\end{aligned}
\tag{6.5}
$$

where x and z represent the components of the end-effector trajectory in the predicted motion along the corresponding axes, and μ_x and μ_z represent the end-effector's mean trajectory followed by the target population along the same axes; q_i, $\dot{q}_i$ and E_i respectively represent the i^{th} DoF value, DoF velocity and effort (either a force or a torque) in the predicted motion, and μ_{qi}, $\mu_{\dot{q}i}$ and μ_{Ei} represent the target population's mean profile for the i^{th} DoF value, DoF velocity and effort; σ_x, σ_z, σ_{qi}, $\sigma_{\dot{q}i}$ and σ_{Ei} respectively represent the target population's standard deviation of the end-effector trajectory along the x and z axes and of the i^{th}

DoF value, DoF velocity and effort; n_q is the number of considered DoFs, n_E is the number of considered efforts and n_t is the number of frames in the motion.

6.3.6 Quantitative Comparison between Motion Control Laws

The TDs described above have been employed to quantitatively compare the results of the predictions carried out with the two combinations of knowledge-based objectives (DE+TV+CL and ME+TV+CL), and assess which of the two yields the most desirable results in all three subject groups, considering both similar and dissimilar reference motions.

The values of the TDs evaluated in each prediction are reported in Figure 6.17. Specifically, the TDs corresponding to the YM predictions presented in the previous sections are represented by the columns above the YM labels. The results of the DE+TV+CL combination are shown in blue, ME+TV+CL in red, and the predictions employing a similar or a dissimilar reference motion are represented with lighter or darker hues, respectively.

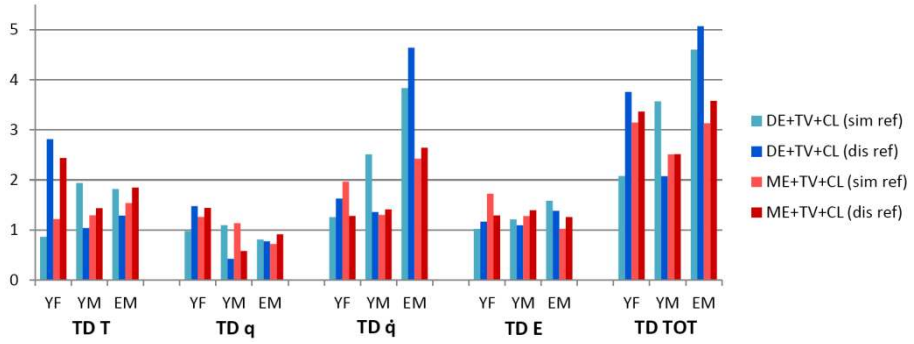

Figure 6.17: Time-averaged distances (TDs) for the three subject groups between the motions performed by the target population and the motions predicted with the minimum dynamic effort (DE) or minimum mechanical energy (ME) performance measures, combined to the minimum translational velocity (TV) and the flexion-extension coordination law (CL), employing both a similar and a dissimilar reference motion.

Analysing the values of the TDs, the following observations may be made. The first is that the choice of the reference motion affects the results of the prediction (see the differences between the light and dark columns in Figure 6.17). In fact, as mentioned earlier, although no data-based

conditions are included in the prediction, the reference motion determines the temporal features of the predicted motion and the initial approximation to the optimisation problem. The choice of the reference motion seems to mostly affect the TDs associated to the end-effector trajectory (TD_T) in the YF group, and the TDs associated to the DoF values (TD_q) in the YM group.

Comparing the two combinations, DE+TV+CL and ME+TV+CL, the former appears to be more sensitive to the choice of the reference motion, as the difference between the light and dark blue columns is generally much larger than the difference between the light and dark red ones. Moreover, employing DE+TV+CL, the choice of a similar or a dissimilar reference motion does not affect the TDs consistently: in fact, in the case of the YF group, a similar reference motion leads to a smaller value of TD_{TOT}, whereas the YM group presents a lower value of TD_{TOT} when a dissimilar motion is employed. Additionally, the DE+TV+CL combination appears to yield very large values of $TD_{\dot{q}}$ in the predictions of the EM group. Employing the ME+TV+CL combination, on the other hand, seems to strongly reduce $TD_{\dot{q}}$, although the values obtained are still larger than in the predictions of younger subjects.

Finally, it can be noticed that, although neither of the two combinations always yields the most realistic and representative results (i.e. the lowest TDs), the ME+TV+CL combination seems to provide, on average, lower TDs than the corresponding DE+TV+CL predictions. Additionally, the ME+TV+CL combination appears to be less sensitive to the choice of the reference motion, which is one of the desirable features we seek in the knowledge-based contribution to our method, as mentioned earlier (Section 6.2.6).

Therefore, we may conclude that the knowledge-based conditions which provide the most satisfying predictions of clutch pedal depressions are the minimum mechanical energy performance measure (ME), combined with the minimisation of the translational DoFs velocity of the root joint (TV) and the flexion-extension coordination law (CL).

6.4 COMPARING DATA-BASED, KNOWLEDGE-BASED AND HYBRID OBJECTIVE FUNCTIONS

As mentioned earlier (Section 5.6), the application of our method to the test case defined in Chapter 5 always follows a hybrid approach: all predictions in fact rely both on the data-based contribution of the reference motion and on the knowledge-based contribution of the different pedal contact models employed for the prediction.

Additionally, data-based and knowledge-based contributions may also appear in the composition of the objective function. As mentioned in Section 5.4.2, the data-based objective consists in resembling the DoF velocities (i.e. the shape of the DoF profiles) of the reference motion. On the other hand, the knowledge-based objective which best seems to represent the motion control law underlying clutch pedal depressions (Section 6.3.6) has been found to be a combination of the mechanical energy performance measure with the coordination law (defined in Section 4.4.5), and the minimisation of the pelvis translational velocity.

The results presented in the two previous sections correspond to the application of either the data-based or the knowledge-based objectives, respectively. These objectives, however, may also be combined in a hybrid objective function, as presented hereafter.

In order to compare the results of data-based, knowledge-based or hybrid objective functions, a battery of predictions was carried out, in which the weights associated to the data-based and knowledge-based objectives were varied progressively.

$$\begin{cases} w_{K-based} = 0:0.1:1 \\ w_{D-based} = 1 - w_{K-based} \end{cases} \tag{6.6}$$

Therefore, the battery of eleven trials, that employ the weights defined in Equation (6.6), ranges from a purely data-based to a purely knowledge-based objective function. Table 6.6 reports the characteristics of the optimisation problem solved to carry out the prediction following the three approaches (the weight associated to the goal fulfilment objective was set to 1 in all trials).

	Constraints					Objectives		
Prediction	**Goal Fulfil.**	**Init. & Fin.**	**RoMs**	**Collisions**	**Dyn. Balance**	**Goal Fulfil.**	**D-based**	**K-based**
D-based	✓	✓	✓	✓	✓	✓	✓	
Hybrid	✓	✓	✓	✓	✓	✓	✓	✓
K-based	✓	✓	✓	✓	✓	✓		✓

Table 6.6: Characteristics of the optimisation problems defined to compare data-based, knowledge-based and hybrid objective functions.

Once again, all three prediction scenarios reported in Table 5.2 were considered and each prediction was carried out twice, employing the different reference scenarios reported in Table 6.2 and Table 6.3. As there are no significant differences among the results in the various prediction scenarios, we hereafter present the kinematic and dynamic profiles corresponding to the group of elderly males (EM) as example.

6.4.1 END-EFFECTOR TRAJECTORIES

The end-effector trajectories followed in the sagittal plane are shown in Figure 6.18, along with the mean trajectory μ followed by the target population, its variability ($\mu \pm 2\sigma$), and the trajectory followed by the end-effector in the reference motions. The vertical black lines in Figure 6.18, and in all the following figures, mark the average *StartDepression* and *EndDepression* key-frames of the motions performed by the target population in the prediction environment. As mentioned in Section 6.2.1, the difference between the reference and predicted trajectories are due to both the different position of the clutch pedal and the different seat height in the reference and prediction environments.

It may be noticed that during the depression phase all the predicted trajectories tend to match, due to the goal fulfilment constraint (Equation (5.2)) and objective (Equation (5.8)), and are contained within the $\mu \pm 2\sigma$ range of variability of the target population.

For what concerns the reach phase, the end-effector trajectory is determined by the data-based and knowledge-based objectives. It may be seen that the trajectory along the vertical axis (Figure 6.18b1, b2) is hardly

affected by the different combination of data-based and knowledge-based objectives, whereas the trajectory along the longitudinal *x* axis (Figure 6.18a1, a2) seems to be more sensitive to the composition of the objective function.

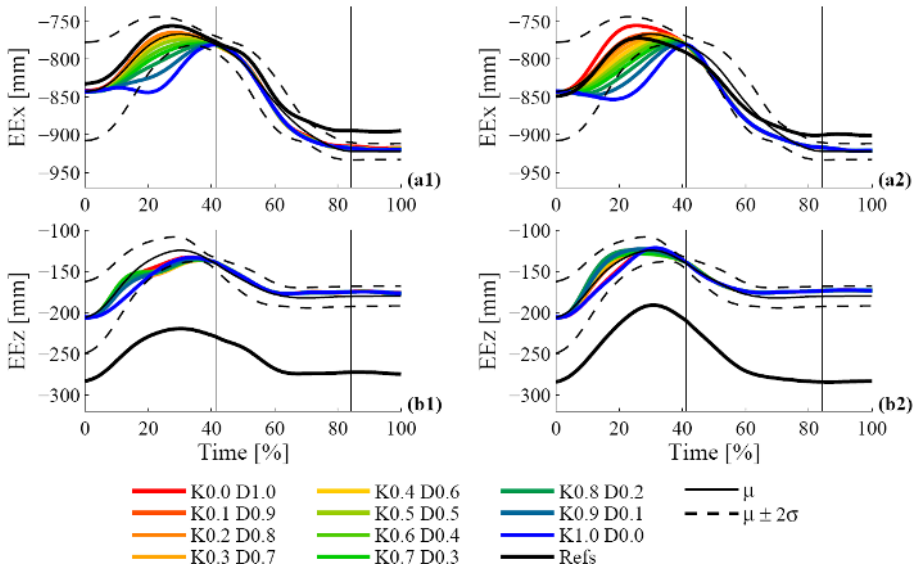

Figure 6.18: Trajectories followed by the end-effector in the sagittal plane for elderly males (EM) employing a similar reference motion (a1, a2) and a dissimilar reference motion (b1, b2) for the battery of hybrid predictions. The red to blue curves show the results of the data-based to knowledge-based predictions. The trajectories followed by the end-effector in the reference motions are reported in black. The thin black curves show the mean trajectories μ followed by the end-effector of the EM target population and the thin dashed curves represent their variability μ±2σ. The vertical black lines mark the average *StartDepression* and *EndDepression* key-frames in the target population.

The trajectories along the *x* axis followed in the purely data-based objective function are contained within the range of variability of the target population, whereas the purely knowledge-based objective function tends to maintain the foot at the same longitudinal position longer and to retract it only enough to reach the clutch pedal (Figure 6.18a1, a2). Nevertheless, the average trajectory of the target population shows that subjects actually tend to retract their foot more before reaching the pedal: in fact, the maximum of the μ curve in Figure 6.18a1 and a2 is reached before the *StartDepression* key-frame.

The pencil of longitudinal trajectories generated in the hybrid battery of predictions tends to vary progressively from the data-based to the knowledge-based trajectory (Figure 6.18a1, a2): a slight knowledge-based contribution generates profiles which greatly resemble the average trajectory of the target population, whereas greater knowledge-based contributions lead to exceeding the target population's range of variability.

6.4.2 DoF Profiles

The DoF profiles discussed in this section once again correspond to the n_q most relevant DoF profiles in clutch pedal depression (which mostly act in the sagittal plane), and are represented in Figure 6.19, employing both a similar and a dissimilar reference motion.

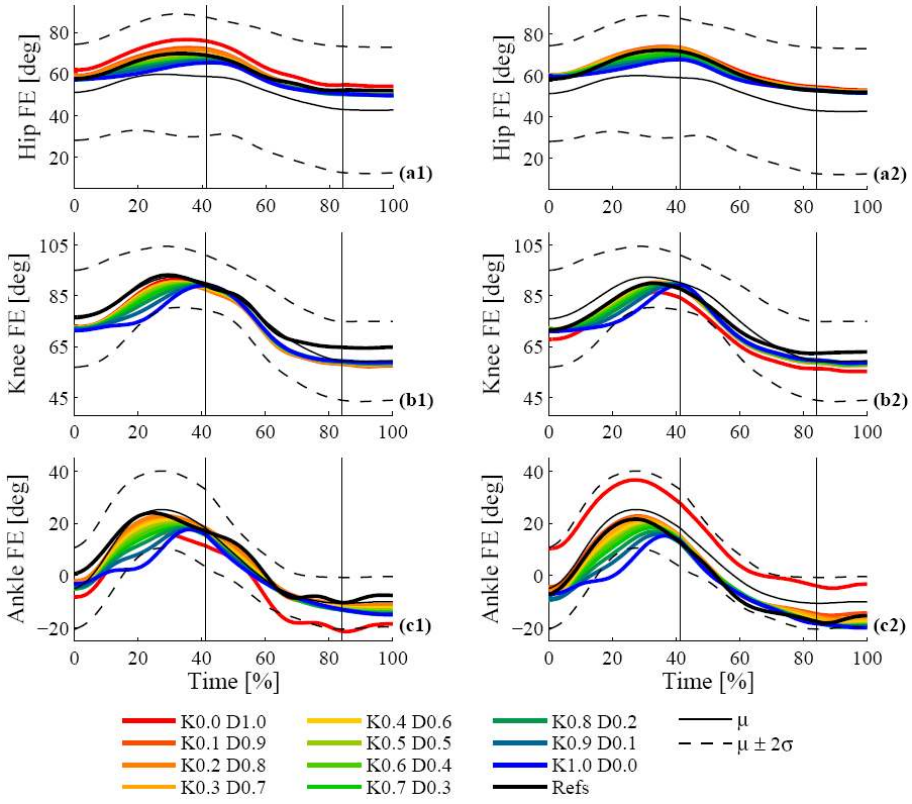

Figure 6.19: Flexion-extension profiles for elderly males (EM) employing a similar reference motion (a1, b1, c1) and a dissimilar reference motion (a2, b2, c2) for the battery of hybrid predictions. The red to blue curves show the results of the data-based to knowledge-based predictions. The reference DoF profiles are reported in black.

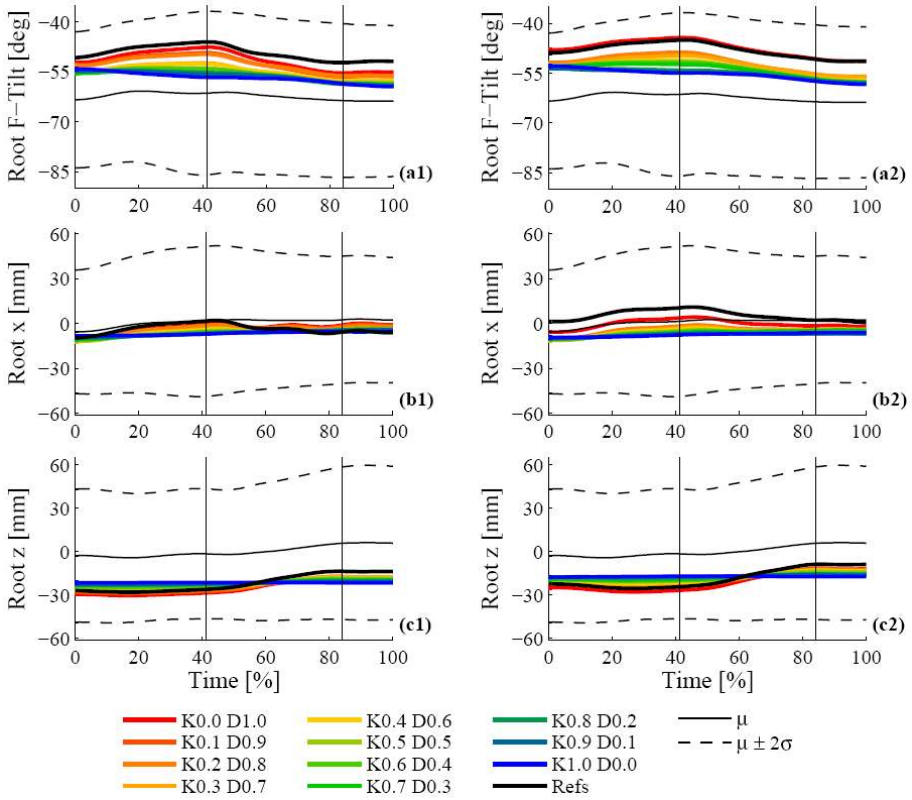

Figure 6.20: Forward tilt and translations of the root joint in the sagittal plane for elderly males (EM) employing a similar reference motion (a1, b1, c1) and a dissimilar reference motion (a2, b2, c2) for the battery of hybrid predictions. The red to blue curves show the results of the data-based to knowledge-based predictions. The reference DoF profiles are reported in black.

The results of the hybrid battery of predictions are shown, as well as the mean profiles μ in the target population, their variability (μ±2σ), and the DoF profiles in the reference motions.

It may be noticed that almost all DoF profiles obtained in the battery of hybrid predictions are contained within the μ±2σ range of variability of the target population. The only exceptions are given at the ankle joint (Figure 6.19c1, c2), as the knowledge-based prediction (shown in blue) leads to a slightly over-extended ankle during the reach phase and the data-based prediction (shown in red) yields a slightly over-extended ankle during the pedal depression when a similar reference motion is employed (Figure 6.19c1).

Additionally, the DoF profiles obtained through the purely knowledge-based objective function are very similar when either reference motion is used, whereas the results of a purely data-based objective function can be very sensitive to the reference motion (see for instance the different data-based predictions of the ankle, Figure 6.19c1 and c2). As mentioned earlier (Section 2.4), data-based predictions employing a dissimilar reference motion are somewhat expected not to yield the most satisfactory results. However, also employing a similar reference motion does not seem to guarantee realistic and representative data-based predictions: a dissimilar reference, in fact, has led to a very flexed ankle throughout the motion (Figure 6.19c2), and a similar reference has yielded a slightly over-extended ankle during the depression phase (Figure 6.19c1).

The hybrid predictions, on the other hand, tend to resemble the mean ankle profile μ of the target population more closely, especially when a slight knowledge-based contribution is employed (shown in orange and yellow), and seem to improve the results obtained through both the data-based and knowledge-based objective functions.

6.4.3 DoF Velocity Profiles

For what concerns the DoF velocities, Figure 6.21 and Figure 6.22 show the predicted profiles corresponding to the n_q most relevant DoFs, obtained employing a similar and a dissimilar reference motion.

Although the knowledge-based condition employed in the predictions is given by the combination of performance measures which yields the most realistic representation of clutch pedal depressions (Section 6.3), the rotational DoF velocity profiles, obtained through purely knowledge-based objective function, exceed the target population's range of variability the most (blue profiles in Figure 6.21 and Figure 6.22a1, a2).

The predictions employing the purely data-based objective function, on the other hand, tend to follow the DoF velocity profiles of the reference motions, due to the objective expressed by Equation (5.9). Since the reference motions do not belong to the motions performed by the target population, the reference profiles (and the profiles in the data-based predictions) may occasionally exceed the $\mu \pm 2\sigma$ range of the target population (e.g. Figure 6.22b2).

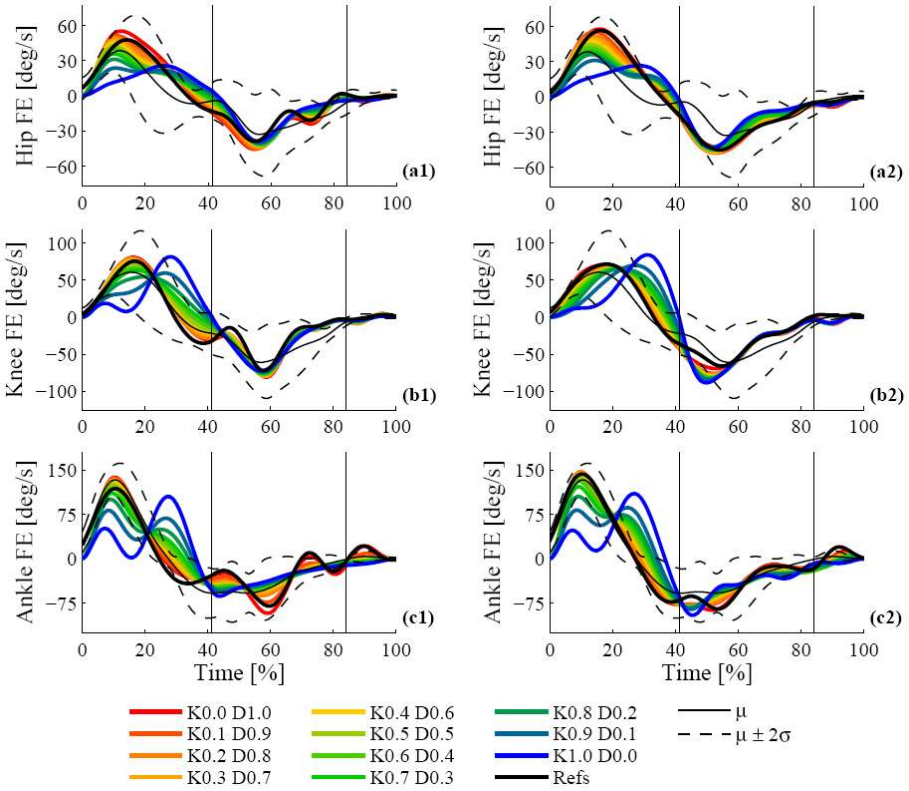

Figure 6.21: Flexion-extension velocity profiles for elderly males (EM) employing a similar reference motion (a1, b1, c1) and a dissimilar reference motion (a2, b2, c2) for the battery of hybrid predictions. The red to blue curves show the results of the data-based to knowledge-based predictions. The reference DoF velocity profiles are reported in black.

Once again, the hybrid predictions which consider a larger data-based contribution and a slighter knowledge-based contribution (shown in orange and yellow) seem to resemble the mean profiles of the target population more closely and are generally contained within its range of variability.

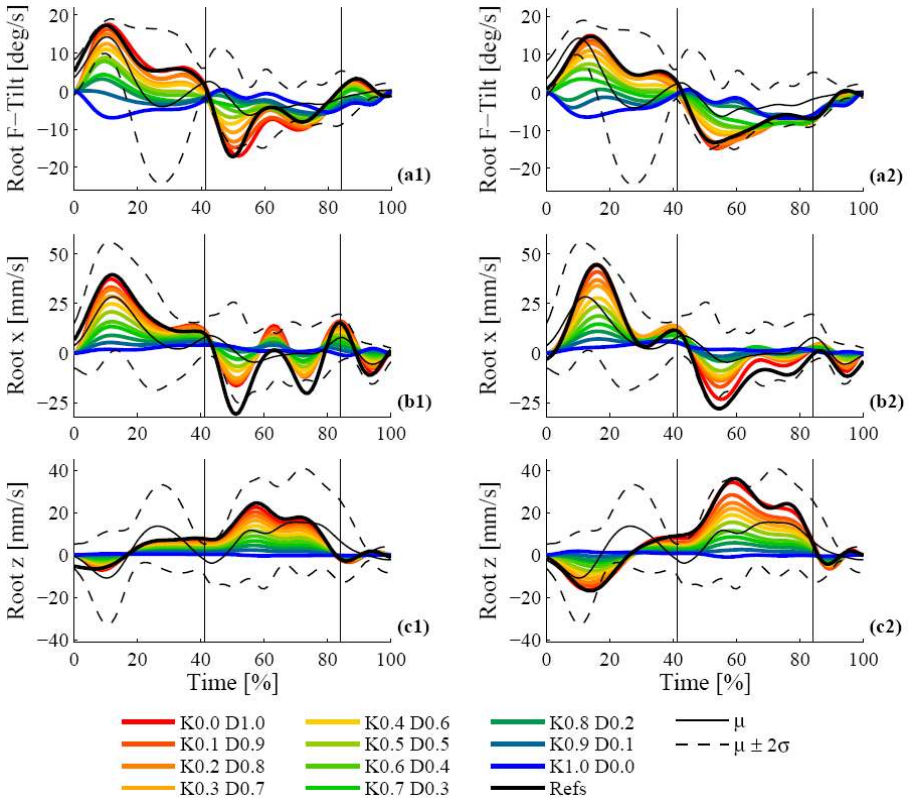

Figure 6.22: Forward tilt and translational velocities of the root joint in the sagittal plane for elderly males (EM) employing a similar reference motion (a1, b1, c1) and a dissimilar reference motion (a2, b2, c2) for the battery of hybrid predictions. The red to blue curves show the results of the data-based to knowledge-based predictions. The reference DoF velocity profiles are reported in black.

6.4.4 EFFORT PROFILES

Figure 6.23 and Figure 6.24 show the efforts which mostly affect the motion in the sagittal plane (medio-lateral joint torques and efforts exerted by the pelvis on the seat in the sagittal plane) obtained in the battery of hybrid predictions, along with the mean profiles μ in the target population, their variability (μ±2σ) and the profiles of the reference motions.

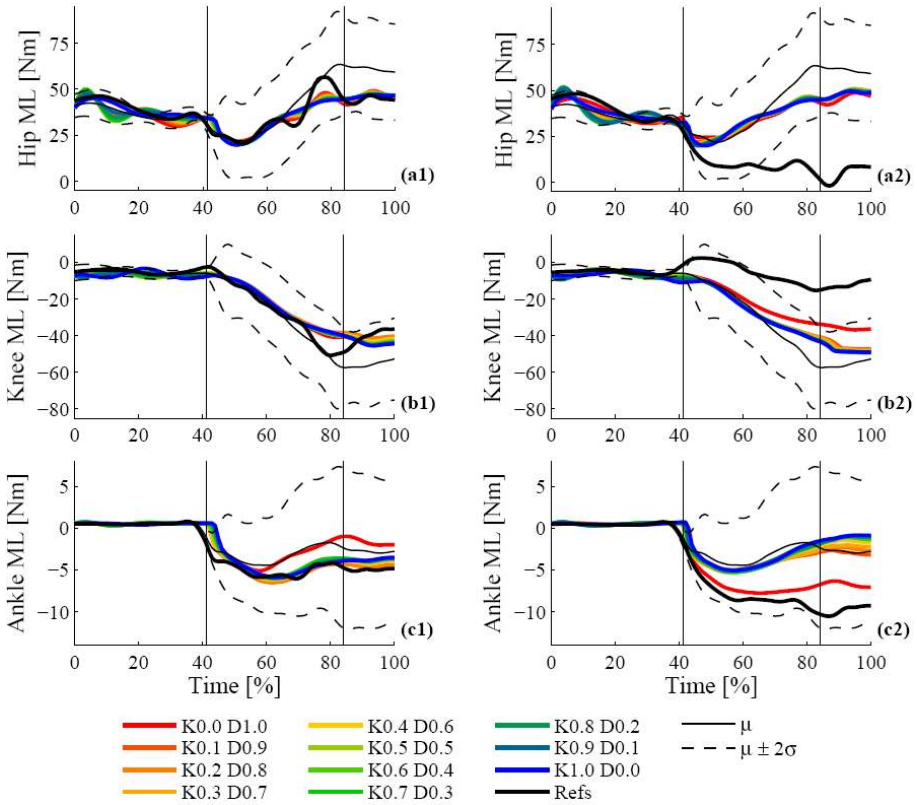

Figure 6.23: Joint torque profiles for elderly males (EM) employing a similar reference motion (a1, b1, c1) and a dissimilar reference motion (a2, b2, c2) for the battery of hybrid predictions. The medio-lateral torque profiles are shown at the hip (a1, a2), knee (a1, a2) and ankle (c1, c2) joints. The red to blue curves show the results of the data-based to knowledge-based predictions. The efforts in the reference motion are reported in black.

It may be noticed that the predicted effort profiles present a much more contained variability depending on the objective function: most profiles are clustered and strongly resemble the mean profiles of the target population (e.g. Figure 6.23a1, b1 and Figure 6.24a2, b2). Occasionally, the data-based objective function yields joint torque profiles which stand out against the rest (Figure 6.23c1, c2 and b2), corresponding to the DoF profiles in which also the data-based prediction is distinct from the remaining hybrid predictions (Figure 6.19 c1, c2 and b2).

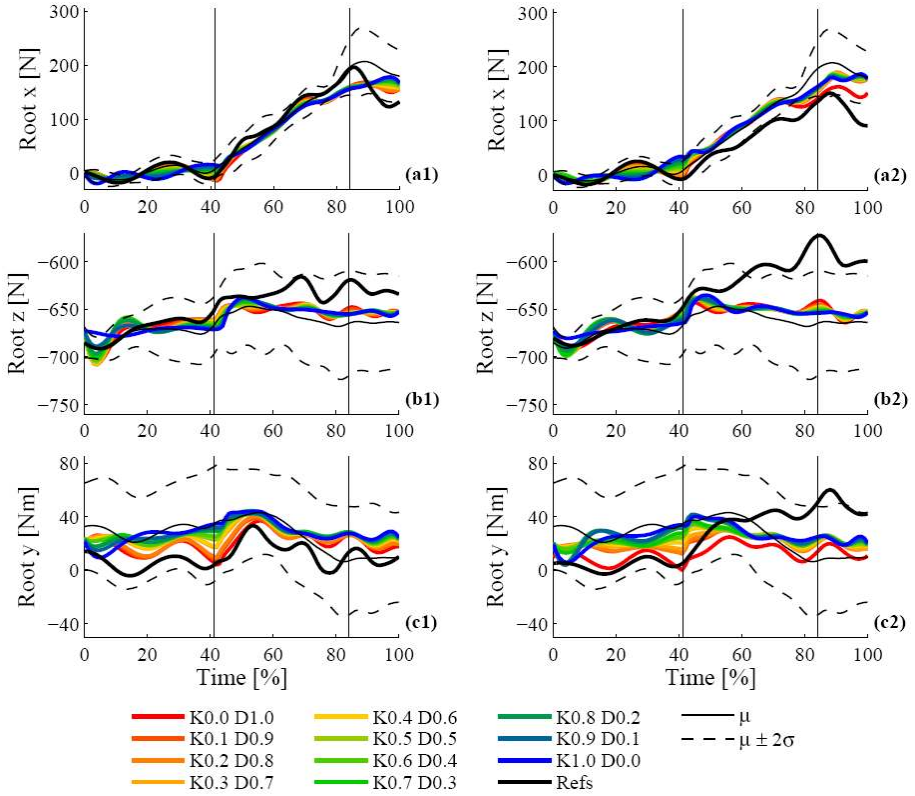

Figure 6.24: Efforts exerted by the pelvis on the seat for elderly males (EM) employing a similar reference motion (a1, b1, c1) and a dissimilar reference motion (a2, b2, c2) for the battery of hybrid predictions. The efforts in the sagittal plane are the forces along the x axis (d1, d2) and z axis (e1, e2) and the torque about the global y axis (f1, f2).The red to blue curves show the results of the data-based to knowledge-based predictions. The efforts in the reference motion are reported in black.

The reason for which most predicted effort profiles do not strongly depend on the composition of the objective function resides in the kind of forces which mainly affect the dynamics of the left leg, which are the gravitational force and the clutch pedal reaction force, obtained through the contact model described in Section 5.5.1. Both these forces are very similar in each predicted motion, and are not linearly dependent on the DoF values and velocities. Therefore, the differences in the kinematic profiles, due to the different objective functions, are generally not reflected in the dynamic profiles.

However, due to the greater mass of the pelvis segment (which accounts for the whole upper part of the DHM as well), the variations in the pelvis forward tilt values (Figure 6.20a1, a2), which modify the position of the pelvis's centre of mass, significantly affect the balance of the pelvis segment. Hence, the torque exerted by the pelvis on the seat (Figure 6.24c1, c2) presents a greater sensitivity to the composition of the objective function.

6.4.5 QUANTITATIVE COMPARISON OF THE THREE APPROACHES FOLLOWED IN THE OBJECTIVE FUNCTION DEFINITION

In order to quantitatively compare the results of the battery of hybrid predictions, and assess the data-based and knowledge-based composition of the objective function that yields the most realistic and representative results, the time-averaged distances (TDs) defined in Section 6.3.5 have been employed. The total time-averaged distance (TD_{TOT}) and the four TDs which comprise it (TD_T, TD_q, $TD_{\dot{q}}$ and TD_E) have been calculated for the batteries of hybrid predictions involving all three subject groups, considering both similar and dissimilar reference motions.

Figure 6.25 reports the TDs evaluated in the hybrid predictions of elderly males (EM), employing a similar and a dissimilar reference motion, which correspond to the predicted profiles shown in the previous sections. It may be noticed that each TD follows a different trend across the data-based to knowledge-based predictions: TD_T, associated to the end-effector trajectories, tends to increase with the knowledge-based contribution to the objective function, and its minimum values correspond to large data-based contributions; TD_q, associated to the DoF values, presents a higher value in the data-based prediction (due to the predictions of the ankle DoF, Figure 6.19c1 and c2) and maintains an almost constant value across the hybrid predictions; $TD_{\dot{q}}$, associated to the DoF velocities, presents a minimum in the hybrid predictions, and increases significantly when a large knowledge-based contribution is employed; and TD_E, associated to the dynamic effort profiles, presents a more irregular behaviour depending on whether a similar or a dissimilar reference motion is employed.

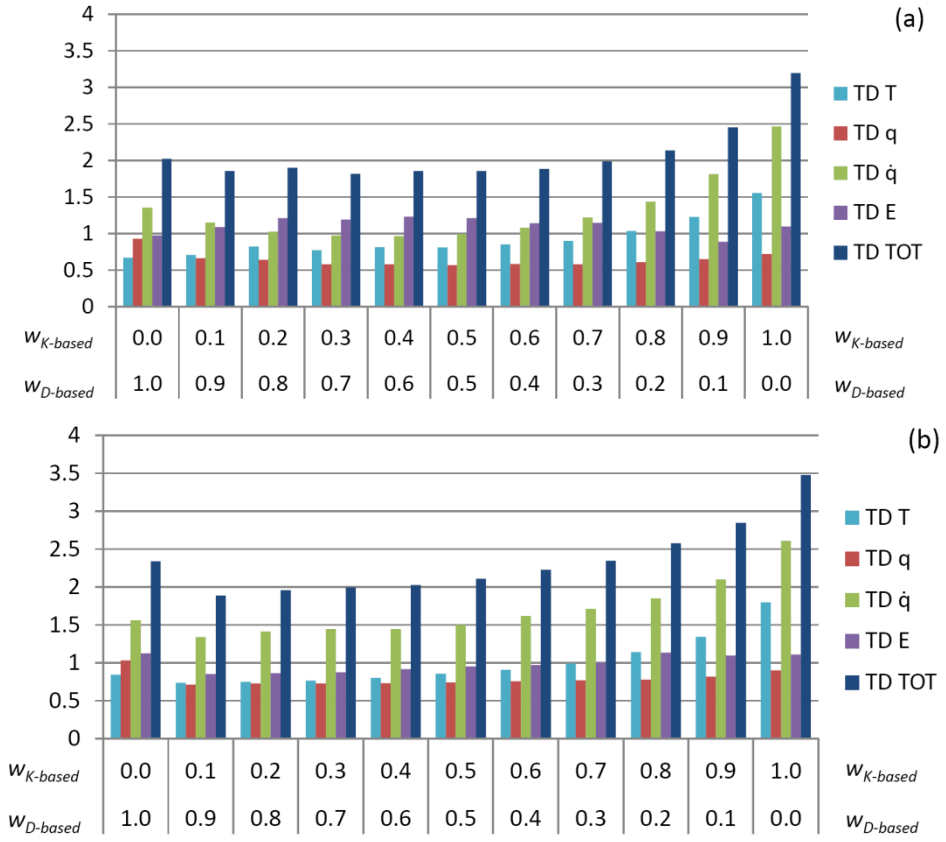

Figure 6.25: Time-averaged distances (TDs) for elderly males (EM) between the motions performed by the target population and the motions generated in the battery of hybrid predictions employing a similar reference motion (a, above) and a dissimilar reference motion (b, below). The weight of the knowledge-based objectives ranges from 0 to 1, whereas the weight of the data-based objectives from 1 to 0.

Finally, TD_{TOT} summarises the contribution of all the above-mentioned TDs. It may be noticed that, regardless of the reference motion, the purely knowledge-based prediction presents the highest values of TD_{TOT}, mostly due to the increase in TD_T and $TD_{\dot{q}}$. In fact, large knowledge-based contributions to the objective function lead to predicted profiles which exceed the $\mu \pm 2\sigma$ range of variability of the target population especially in the reach phase of the motion, in which the motion of the end-effector is not controlled (Figure 6.18a1, a2 and Figure 6.21 and Figure 6.22a1, a2). Therefore, a purely knowledge-based prediction seems to yield

the least realistic and representative results, whereas including an increasing data-based contribution in the prediction progressively reduces the values of TD_{TOT} .

It may be noticed that a hybrid objective function succeeds in reducing the values of TD_{TOT} not only respect to the purely knowledge-based, but also respect to the purely data-based objective function. The improvement brought by including a slight knowledge-based contribution is slighter when a similar reference motion is employed (Figure 6.25a) and more significant when a dissimilar reference is selected (Figure 6.25b). Therefore a hybrid objective function seems to improve the extrapolation capabilities of a purely data-based approach.

Additionally, it may be noticed that when a similar reference motion is employed (Figure 6.25a), the total TD presents an almost constant value for knowledge-based and data-based weights that range in between 0.1-0.6 and 0.9-0.4, respectively. Hence, the optimum sets of weights, which yield the lowest values of TD_{TOT} , are contained within [$w_{K\text{-}based}$=0.1, $w_{D\text{-}based}$=0.9] and [$w_{K\text{-}based}$ =0.6, $w_{D\text{-}based}$ =0.4]. On the other hand, when a dissimilar reference motion is employed (Figure 6.25b), the optimum range of weights, is reduced to approximately [$w_{K\text{-}based}$=0.1, $w_{D\text{-}based}$=0.9] and [$w_{K\text{-}based}$ =0.4, $w_{D\text{-}based}$ =0.6].

However, a hybrid objective function does not always yield the most realistic results, and sometimes the lowest value of TD_{TOT} corresponds to a data-based objective function. It is the case, for instance, of the predictions of young females (YF) carried out employing a dissimilar reference motion (Figure 6.26b). While a hybrid approach seems to slightly improve the data-based results obtained with a similar reference motion (Figure 6.26a), the value of TD_{TOT} corresponding to a dissimilar reference appears to increase following the values of TD_T , associated to the end-effector trajectory. In fact, TD_q and TD_E are almost constant across the battery of hybrid predictions, and the decrease in $TD_{\dot{q}}$, brought by a slight knowledge-based contribution to the objective function, is slighter than the corresponding increase in TD_T .

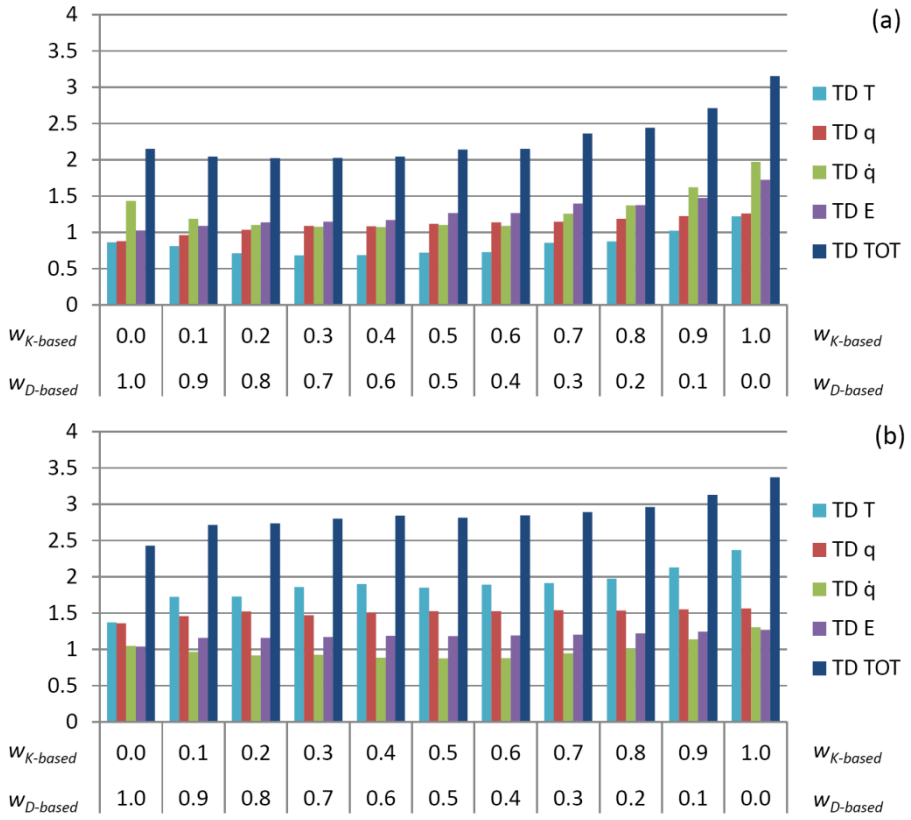

Figure 6.26: Time-averaged distances (TDs) for young females (YF) between the motions performed by the target population and the motions generated in the battery of hybrid predictions employing a similar reference motion (a, above) and a dissimilar reference motion (b, below). The weight of the knowledge-based objectives ranges from 0 to 1, whereas the weight of the data-based objectives from 1 to 0.

The values of TD_T appear to determine the trend of TD_{TOT} also in the case of young males (YM), predicted with a dissimilar reference motion (Figure 6.27b). Although when a similar reference motion is employed (Figure 6.27a) a slight knowledge-based contribution does not seem to deteriorate the goodness of a purely data-based objective function, a dissimilar reference motion tends to produce predictions in which the $\mu \pm 2\sigma$ range of variability of the target population is once again more easily exceeded in terms of end-effector trajectories.

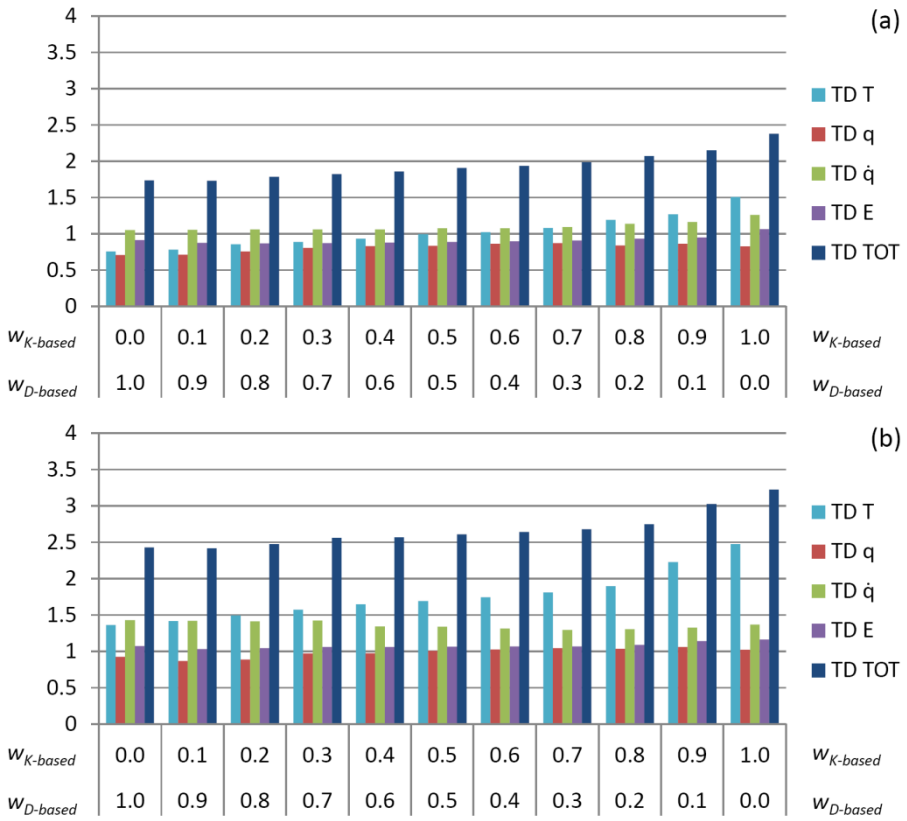

Figure 6.27: Time-averaged distances (TDs) for young males (YM) between the motions performed by the target population and the motions generated in the battery of hybrid predictions employing a similar reference motion (a, above) and a dissimilar reference motion (b, below). The weight of the knowledge-based objectives ranges from 0 to 1, whereas the weight of the data-based objectives from 1 to 0.

Hence, on the one hand, it appears that the knowledge-based contribution may improve the end-effector trajectory of the data-based prediction when the predicted trajectory presents low TDs (approximately, TD_T <1), e.g. Figure 6.25b and Figure 6.26a. However, on the other, when the end-effector trajectory obtained with a data-based objective function does not seem to resemble the trajectories followed by the target population very closely, the knowledge-based contribution is not able to reduce the values of TD_T (e.g. Figure 6.26b and Figure 6.27b).

It must be noticed that applying our prediction method to the clutch pedal depression, we deliberately left uncontrolled the end-effector

trajectory during the reach phase (Section 5.3.1). The reason is that, as mentioned by Wang (2000), the clutch pedal depression is not a motion for which the DHM is a highly redundant system. In fact, considering only the sagittal plane, in which the motion is mainly carried out, the DHM can be simplified to a 3-DoF system, with one rotational DoF at the hip, knee and ankle joints. In such a configuration, establishing the position of the end-effector leaves only one free DoF.

In order to evaluate the effect of different objective functions, it is desirable to consider a larger number of free DoFs, which are to be determined through the minimisation of the objective function. Therefore, only the most essential features of the motion have been enforced in the optimisation problem (Section 5.3), leaving the trajectory followed by the end-effector in the reach phase to be determined as a consequence of the employed objective function. Probably, guiding the end-effector trajectory throughout the motion would lead to smaller values of TD_T (and therefore of TD_{TOT} in the cases in which TD_T appears to determine the global trend of the total TD). The redundancy of the DHM, however, would thus be reduced, consequently reducing the dependency of the predicted motion on the employed objective function.

Considering the results of all the hybrid battery of predictions presented in this section the following conclusions may be drawn. First of all, a purely knowledge-based objective function seems to always yield the largest values of TD_{TOT}, demonstrating the importance of including a data-based contribution to the motion prediction method.

Additionally, a slight knowledge-based contribution to the objective function seems to generally improve the results of employing a purely data-based objective function. The only case in which the smallest value of TD_{TOT} is associated to the purely data-based objective function corresponds to a case in which the trend of TD_{TOT} appears to be determined by the trend of the TD associated to the end-effector trajectory.

Finally, it may be noticed that the improvement provided by a hybrid objective function is not limited to a specific data-based and knowledge-based combination, but rather leads to the identification of an optimum range of weights (larger when a similar reference motion is employed, and more reduced when a dissimilar reference is selected), generally contained

between [$w_{K\text{-}based}$=0.1, $w_{D\text{-}based}$=0.9] and [$w_{K\text{-}based}$ =0.4, $w_{D\text{-}based}$ =0.6]. Thus, our method appears to present a certain robustness to the weights employed in the construction of hybrid objective functions.

6.5 VALIDATION

A qualitative validation of our motion prediction method has been presented in the previous sections (6.2-6.4), discussing the resemblance of the predicted profiles to the mean profiles followed by the target population and their variability. However, a quantitative validation seems necessary in order to thoroughly assess the realism and representativeness of the predicted motions.

The quantitative validation presented in this section was carried out by comparing the time-averaged distances (TDs) of the predicted motions to the TDs of the motions performed by the target population in the prediction environment. For this purpose, the TDs defined in Section 6.3.5 (Equation (6.5)) have also been employed to quantify the natural variability of the actually performed motions. A similar comparison was carried out by Park et al. (2004) and Monnier (2004), who employed the TD described in Section 2.2 not only to evaluate the predicted motions but also to determine the variation of actually performed motions. As mentioned in Section 2.2, Park et al. defined two indices, characterising the within-subject inter-trial motion variability (WIMV), when the motions were performed by the same subject (also employed by Monnier), and the between-subject inter-trial motion variability (BIMV), when the motions were performed by different subjects of similar characteristics. Similarly to the BIMV index, we define a "within population motion variability" (WPMV), employing the TDs defined in Section 6.3.5, to represent the inherent variation of the motions performed by the target population in the prediction environment. By comparing the TDs obtained in the predictions to the WPMVs, we are able to verify whether the predicted motions can or cannot be differentiated from actually performed motions in similar conditions.

Therefore, in order to obtain the values of the WPMVs, the TDs of each of the 13, 9 and 8 motions performed in the PCA2 vehicle by the YF, YM and EM groups, respectively, (see Table 4.3) were evaluated. For what concerns the values of the TDs corresponding to predicted motions, additional predictions to the ones presented in the previous sections were carried out, employing every motion in the database eligible as reference (i.e. performed by a different subject of the same subject group as the prediction

subject, and in a different environment from the prediction environment, see Section 6.1). Hence, 12 different reference motions were employed to predict the YF group in the PCA2 vehicle (see Table 6.1), and analogously 9 and 5 different reference motions were used for the YM and EM groups, respectively.

In the discussion of the results presented in the previous section, it was mentioned that occasionally the purely data-based objective function seems to yield the most realistic and representative predictions, whereas in other cases a slight knowledge-based contribution reduces the value of the total time-averaged distance, TD_{TOT}. Therefore, each of the aforementioned predictions, were carried out three times:

- employing a data-based objective function [$w_{K\text{-}based}$=0.0, $w_{D\text{-}based}$=1.0];
- employing a hybrid objective function, which includes a slight knowledge-based contribution [$w_{K\text{-}based}$=0.2, $w_{D\text{-}based}$=0.8], called "hybrid 0.2-0.8";
- and employing a greater knowledge-based contribution in the hybrid objective function [$w_{K\text{-}based}$=0.4, $w_{D\text{-}based}$=0.6], called "hybrid 0.4-0.6".

The knowledge-based contribution is not increased further as the results presented in Section 6.4 indicate that highly knowledge-based objective functions tend to generate the least realistic motions.

In the following sections, the TDs obtained in the predictions are compared to the WPMVs of the actually performed motions by the target populations in the prediction environment.

6.5.1 THE END-EFFECTOR TD

Figure 6.28 reports the TDs associated to the end-effector trajectory, TD_T, obtained with a data-based prediction (Figure 6.28a) and the two abovementioned hybrid predictions (Figure 6.28b, c), compared to the WPMVs of the target populations in the prediction environment.

It may be noticed that the majority of the predicted motions present values of TD_T which fall within the range of WPMVs observed in actually performed motions. In the case of a purely data-based objective function (Figure 6.28a), the median TD_T of the predictions and the median WPMVs fall within each other's 95% confidence intervals (CIs). Therefore, no

significant difference is observed between the predicted and actual end-effector trajectories.

On the other hand, when a hybrid objective function is employed (Figure 6.28b, c), the differences between the predicted TD_T and the WPMVs are more significant, although similar ranges of values are observed. The effect of the knowledge-based contribution to the objective function appears both in the medians and in the range of values of TD_T. For what concerns the median TDs, they seem to increase in the predictions of young subjects when knowledge is included in the objective function, whereas they are hardly affected in the EM group, which moreover remaining always contained within the 95% CIs of the median WPMV. For what concerns the range of values of TD_T, a wider range of values is contained between the maximum and minimum TD in the YF and EM groups when knowledge is included in the objective function, whereas the range is hardly modified in the prediction of YM subjects. However, a hybrid objective function yields more contained inter-quartile ranges for the TD_T of both YF and YM groups.

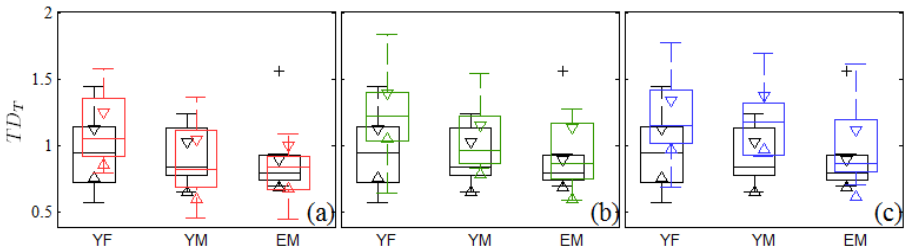

Figure 6.28: Box plots comparing the time-averaged distance of the end-effector trajectory (TD_T) corresponding to the actually performed motions by the target populations (YF, YM, EM) and the TD_T obtained employing a data-based objective function (a) and two hybrid objective functions: hybrid 0.2-0.8 (b) and hybrid 0.4-0.6 (c). The TDs of the target population are shown in black (a, b, c), the TDs of the data-based objective function in red (a), the TDs of hybrid 0.2-0.8 in green (b) and the TDs of hybrid 0.4-0.6 in blue (c). The boxes contain the inter-quartile range (from the 25th to the 75th percentile), the whiskers extend from the minimum to the maximum values (outliers are marked with crosses), the horizontal line within the boxes represents the median value and the triangles mark the 95% confidence intervals of the median.

Therefore, for what concerns the end-effector trajectory, we may conclude that employing a data-based objective function, no significant differences between the predicted TDs and the WMPVs of the target

populations can be observed. The knowledge-based contribution to the objective function, on the other hand, does not seem to improve the realism of the predicted trajectories. However, the range of values of the predicted TDs is always similar to the range of WMPVs.

6.5.2 THE DOF VALUE TD

For what concerns the TDs corresponding to the DoF profiles, Figure 6.29 compares the values of TD_q obtained with the data-based and the hybrid 0.2-0.8 and 0.4-0.6 objective functions against the WPMVs of the target populations in the prediction environment.

It may be noticed once again that the predicted TDs present a similar range of values to the WMPVs. For what concerns the YF group, a hybrid objective function does not seem to improve the prediction of the DoF values, since the median TD_q strays from the median WPMV as the knowledge-based contribution to the objective function increases.

On the other hand, the median value of TD_q for the YM group does not seem to be significantly affected by the composition of the objective function: nevertheless, the inter-quartile range (i.e. the width of the box) is strongly reduced by the knowledge-based contribution, which therefore reduces the dependency of the prediction from the choice of the reference motion.

For what concerns the group of elderly males, the predictions benefit from the hybrid objective function, as the values of the hybrid TD_q are reduced respect to the data-based predictions and the median values of the predicted TDs and of the WPMVs fall within each other's CIs. No significant difference is observed between the hybrid 0.2-0.8 and 0.4-0.6 objective function, therefore combining data-based and knowledge-based objectives seems to be more relevant than their actual degree of combination.

Finally, it may be noticed that a hybrid objective function yields predictions which closely resemble the actually performed motions by the target population in the prediction environment, as the obtained TDs are hardly distinguishable from the WMPVs.

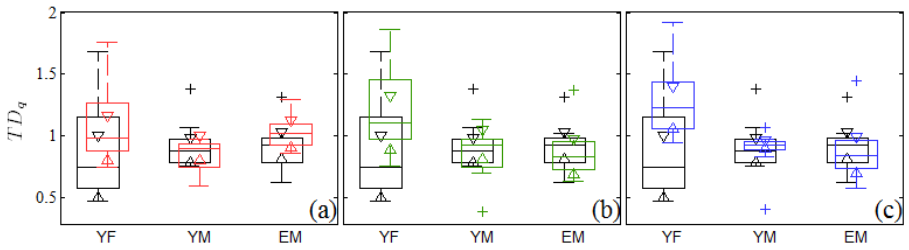

Figure 6.29: Box plots comparing the time-averaged distance of the DoF profiles (TD_q) corresponding to the actually performed motions by the target populations (YF, YM, EM) and the TD_q obtained employing a data-based objective function (a) and two hybrid objective functions: hybrid 0.2-0.8 (b) and hybrid 0.4-0.6 (c). The TDs of the target population are shown in black (a, b, c), the TDs of the data-based objective function in red (a), the TDs of hybrid 0.2-0.8 in green (b) and the TDs of hybrid 0.4-0.6 in blue (c).

6.5.3 THE DOF VELOCITY TD

The TDs associated to the DoF velocities (and therefore to the shape of the DoF profiles) obtained with the hybrid objective functions (Figure 6.30b, c) tend to resemble the WPMV of the target populations much closer respect to the data-based objective (Figure 6.30a).

As the data-based objective seeks the resemblance between the reference and the predicted DoF velocities, the differences between the TDs obtained with the data-based objective and the WPMVs (Figure 6.30a) represent the differences between the motions in the database and the motions which are to be predicted. Such differences, therefore, quantify the extrapolation required in the prediction. As the TDs obtained in the hybrid predictions resemble the WMPVs more closely, the extrapolation capabilities of the method are significantly improved by including knowledge-based conditions in the objective function (Figure 6.30b, c).

The hybrid approach seems to reduce not only the distance between the predicted values of $TD_{\dot{q}}$ and the WPMV, but also the variability of $TD_{\dot{q}}$, reflecting a reduced dependency of the predicted profiles from the choice of the reference motion. Once again, the differences between employing a data-based and a hybrid objective function are greater than between the two hybrid objective functions, showing the robustness of our method with respect to the weights of the hybrid combination in the objective function.

Both YF and YM groups present values of $TD_{\dot{q}}$ which strongly resemble the values of the WPMVs of the target population employing a hybrid objective function. On the other hand, for what concerns the EM group, the knowledge-based combination reduces the variability of $TD_{\dot{q}}$ and limits its greatest values but does not succeed in overlapping the median confidence intervals (CIs) of $TD_{\dot{q}}$ with the CIs of the WPMV.

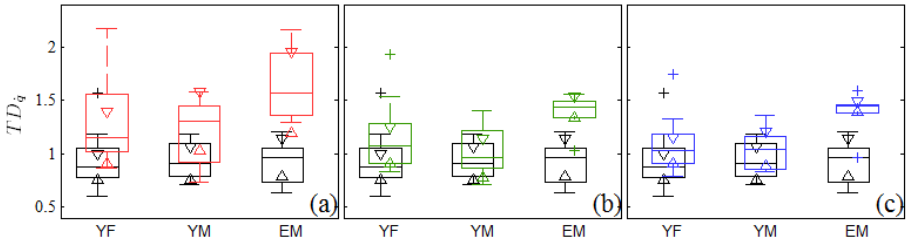

Figure 6.30: Box plots comparing the time-averaged distance of the DoF velocity profiles ($TD_{\dot{q}}$) corresponding to the actually performed motions by the target populations (YF, YM, EM) and the $TD_{\dot{q}}$ obtained employing a data-based objective function (a) and two hybrid objective functions: hybrid 0.2-0.8 (b) and hybrid 0.4-0.6 (c). The TDs of the target population are shown in black (a, b, c), the TDs of the data-based objective function in red (a), the TDs of hybrid 0.2-0.8 in green (b) and the TDs of hybrid 0.4-0.6 in blue (c).

6.5.4 THE EFFORT TD

For what concerns the values of TD_E, associated to the effort profiles, the TDs obtained through a data-based and hybrid objective functions are reported along with the WPMVs of the target populations in Figure 6.31.

In this case, the data-based objective function yields TDs which are more similar to the WPMVs respect to the hybrid objective function, which corresponds to larger values of TD_E. For younger subjects, employing a hybrid objective function affects the predicted efforts more than the actual degree of combination of the data-based and knowledge-based contributions, given their similarities in Figure 6.31b and c, whereas the difference between the predicted TD and the WPMV of the EM group increases consistently with the weight associated to the knowledge-based objective.

Nevertheless, the predicted TD_E are mostly contained within the range of WPMV of the target populations in the prediction environment,

especially for what concerns the younger populations. It must be noticed, however, that fewer motions constitute the target population sample of the EM group (Table 4.3), and therefore its statistical representation is less reliable than the YF and YM groups.

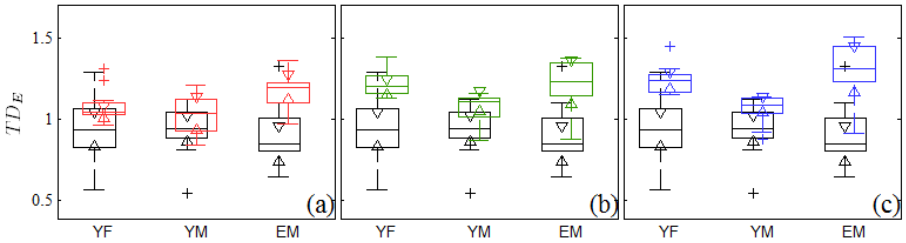

Figure 6.31: Box plots comparing the time-averaged distance of the effort profiles (TD_E) corresponding to the actually performed motions by the target populations (YF, YM, EM) and the TD_E obtained employing a data-based objective function (a) and two hybrid objective functions: hybrid 0.2-0.8 (b) and hybrid 0.4-0.6 (c). The TDs of the target population are shown in black (a, b, c), the TDs of the data-based objective function in red (a), the TDs of hybrid 0.2-0.8 in green (b) and the TDs of hybrid 0.4-0.6 in blue (c).

6.5.5 THE TOTAL TD

Finally, the total TD corresponding to data-based and hybrid objective functions is compared to the total WPMVs of the target population in the prediction environment (Figure 6.32).

For what concerns the YF group, the most realistic predictions are obtained with a data-based objective function, which succeeds in yielding values of TD_{TOT} that are mostly contained in the range of values of the WPMV. On the other hand, when a knowledge-based contribution is employed, the median value of TD_{TOT} increases, but does not seem to be significantly affected by the actual weight associated to the knowledge-based objective (Figure 6.32b, c). Nevertheless, including knowledge in the objective function reduces the range of values of TD_{TOT}, and succeeds in containing its maximum values.

The prediction of YM subjects yields the most satisfying results. A data-based objective function succeeds in generating a median value of TD_{TOT} which almost matches the WMPV, and including a knowledge-based contribution hardly increases the median TD while it significantly reduces

the variability of the values of TD_{TOT}. Therefore, a hybrid objective function succeeds in reducing the dependency of the predicted motion from the selected reference motion.

Finally, for what concerns the EM group, the considered knowledge-based contribution to the objective function does not seem to reduce the dependency of the prediction from the reference motion. However, fewer predictions were carried out in the EM group, due to the smaller number of motions which could be employed as reference (Table 4.3), yielding a less reliable representation of the EM group. Nevertheless, the median TD_{TOT} seems to shift towards lower values employing a slight knowledge-based contribution, and succeeds in resembling the WPMV of the target population more closely than employing a purely data-based objective function.

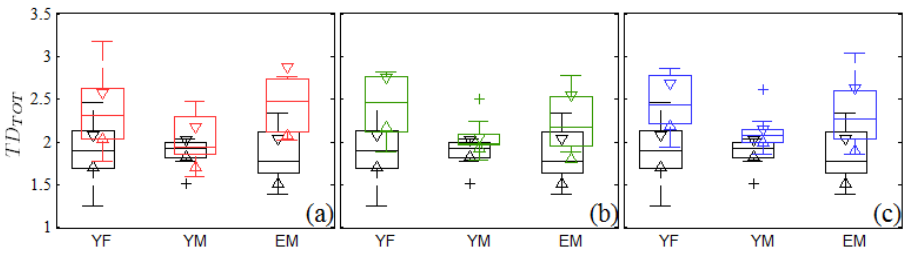

Figure 6.32: Box plots comparing the total time-averaged distance (TD_{TOT}) corresponding to the actually performed motions by the target populations (YF, YM, EM) and the TD_{TOT} obtained employing a data-based objective function (a) and two hybrid objective functions: hybrid 0.2-0.8 (b) and hybrid 0.4-0.6 (c). The TDs of the target population are shown in black (a, b, c), the TDs of the data-based objective function in red (a), the TDs of hybrid 0.2-0.8 in green (b) and the TDs of hybrid 0.4-0.6 in blue (c).

6.5.6 CONCLUSIONS

The results of the quantitative validation presented in the previous sections show that employing both a data-based and a hybrid objective function in our motion prediction method leads to TDs which present a similar range of values to the inherent variability of the target populations in the prediction environment (WPMVs), thus validating the method proposed.

The median value of the total TD in each group (YF, YM, EM) is not significantly affected by the objective function, as the medians in each group mostly fall within their 95% confidence intervals in the data-based,

hybrid 0.2-0.8 and hybrid 0.4-0.6 objective functions. However, the single TDs which compose the total TD do seem to present a stronger dependency on the composition of the objective function: for instance, $TD_{\dot{q}}$, associated to the DoF velocities (and therefore to the shape of the DoF profiles), is significantly improved by the knowledge-based objective; on the other hand, the TD associated to the effort profiles, TD_E, seems to resemble the WPMVs closer when a data-based objective function is employed.

Nevertheless, including a knowledge-based contribution to the objective function consistently reduces the variability of the predicted TDs, especially for what concerns the prediction of young subjects, for which a larger number of reference motions was available. Therefore, employing a hybrid objective function leads to reducing the dependency of the prediction from the reference motion selection, demonstrating a greater robustness to the choice of the reference motion respect to purely data-based objective functions. Additionally, combining data-based and knowledge-based objectives has appeared more decisive than their exact degree of combination, demonstrating a certain robustness also to the weight selection in the composition of the objective function.

CHAPTER 7

CONCLUSIONS AND FUTURE WORKS

The research presented in this thesis has been focused on the development of a novel method for the prediction of task-oriented human motion, in order to overcome some of the limitations encountered in existing motion prediction methods, described in Section 2.4. On the one hand, dynamics is included in the formulation in order to yield physically sound predictions and to take into account the forces and torques acting on and within the human body. On the other hand, a hybrid approach is followed, seeking to combine the advantages of both data-based and knowledge-based methods for human motion prediction.

The main contributions of this research work and the conclusions deriving therefrom are reported in the following section. Subsequently, the future lines of research that may originate from this thesis are presented.

7.1 CONCLUSIONS

As a result of the research work carried out in this thesis, several conclusions have been obtained concerning the analysis and the prediction of human motion, and are presented hereafter.

- We have developed an optimisation-based method for the dynamic prediction of human motion that combines both data-based and knowledge-based approaches.

  - The data-based contributions to the method proposed in this thesis lie in the use of a reference motion and in the definition of a data-based objective. The former determines the temporal features of the predicted motion and provides an initial approximation for the optimisation problem, and the latter seeks to generate a motion that resembles the kinematics of the reference motion. The results obtained have shown that a purely data-based objective function may lead to predicted motions which occasionally exceed the range of variability observed in actually performed motions.
  - The knowledge-based contributions to the method proposed lie in the definition of performance measures, which are included in the objective function and represent the motion control law underlying the motion, and may also appear in the contact models employed to describe the dynamic interaction between the subject and the environment. The results obtained have shown that a purely knowledge-based objective function may generate predicted motions which significantly stray from actually performed motions, and that purely knowledge-based objective functions do not seem able to outperform purely data-based objective functions.
  - In this thesis we propose a combination of data-based and knowledge based objectives in a hybrid objective function. Employing a hybrid objective function has succeeded, especially in the prediction of young male subjects, in reducing the dependency of the predicted motion from the reference motion and in improving the extrapolation capabilities of the data-based objective function.

- Additionally, we have assessed the importance of performing a dynamic prediction.
  - Kinematic predictions have proven to be able to generate apparently realistic motions, but cannot guarantee the actual feasibility of the predicted motion. The results obtained in this thesis prove that the enforcement of the dynamic balance of the DHM is required in order to generate physically sound motions. The feasibility also depends on whether the joint limits are exceeded in the predicted motion: realistic ranges of motion

may be ensured through a kinematic prediction, but in order to control the values of the joint torques, a dynamic prediction is required.

  - Moreover, a dynamic prediction is important for the ergonomic applications of motion prediction methods. In fact, as the forces and torques acting on and within the human body play a relevant role in discomfort perception, dynamic variables must be taken into account in the prediction, in order to then employ the predicted motion in ergonomics analysis tools.

- We have developed a general method, which has proven to be able to predict the behaviour of a variety of populations and is applicable to the prediction of task-related human motion. The different behaviours of the populations can be taken into account both in the data-based contribution to the method (i.e. employing different reference motions) and in the knowledge-based contribution (i.e. employing different performance measures or differently characterising the contact between the DHM and the environment).

- We have applied the motion prediction method presented in this thesis to clutch pedal depressions, predicting the motions of three different populations: average young females, young males and elderly males. The gender-related differences are mostly taken into account in the prediction through the reference motion, whereas the age-related differences strongly appear also in the model employed in the characterisation of the foot-pedal interaction.

- We have analysed a database of 78 valid clutch pedal depressions in order to gain insight into the characteristics of the task-oriented motion and to structure the database for the motion selection step required by our method. The most relevant features, concerning both the subject performing the motion and the environment it is performed in, have been identified and have led to the awareness of the coordination which appears to exist among the flexion-extension DoFs of the left leg. Additionally, two mainly age-related motion styles, associated to the pedal force direction, have been identified: young subjects tend to reduce the torque at the articulations in the left leg, whereas elderly subjects seek to reduce the load on their backs.

- In this thesis we present the results of knowledge-based predictions, performed employing two of the most common energy-related

performance measures: minimum effort and minimum mechanical energy. The resulting prediction of clutch pedal depressions reveals that energy-related performance measures alone do not allow adequate representations of actually performed motions. Therefore we propose the combination of knowledge-based objectives, given by the minimum energy performance measure combined to the coordination law determined through the database analysis and to a minimum translational velocity condition for the pelvis. This combination yields the most realistic knowledge-based predictions. Nevertheless, a greater level of realism appears to be always achieved when data-based objectives are included in the prediction, which demonstrates the difficulty of identifying appropriate motion control laws even for a relatively simple task such as clutch pedal depressions.

- We have performed both a qualitative and a quantitative validation of the method proposed, to assess the realism and the representativeness of the predicted motions.
    - The qualitative validation consists in comparing the predicted kinematic and dynamic profiles to the profiles of real motions, performed in similar conditions to those being predicted. The results of the qualitative validation show that the predicted profiles are generally contained within the natural ranges of variability of actually performed motions by the target populations in the prediction environment.
    - We have defined a new quantitative index (TD_{TOT}) to assess the likelihood between the predicted and the actually performed motions. This index takes into account the time-averaged distance of the predicted profiles respect to the mean profiles of the actually performed motions in terms of end-effector trajectory, DoF profiles value and shape, and efforts exerted by the DHM throughout the motion
    - The definition of TD_{TOT} has led to a new index to represent the inherent variability of actually performed motions, called "within population motion variability" (WPMV).
    - The comparison between the TDs obtained in the predictions and the WPMV show a good correspondence between the range of values of the TDs and the WPMVs, when either a data-based or a hybrid objective function is employed in the

prediction. Nevertheless, including a knowledge-based contribution to the objective function seems to consistently reduce the variability of the predicted TDs, therefore reducing the dependency of the prediction from the reference motion selection. Additionally, combining data-based and knowledge-based objectives appears to be more decisive than their exact degree of combination, demonstrating a certain robustness to the weight selection in the composition of the objective function.

In conclusion, the method proposed in this thesis is able to provide realistic and physically sound predictions of a variety of populations, which carry out the task following different behavioural patterns. The hybrid approach allows a greater flexibility in terms of representing the variability in behaviour exhibited in actually performed motions: in fact the different behaviours can be accounted for both through the data-based condition of resembling the reference motion and through knowledge-based conditions, which may be included either in the form of motion control laws or through the different characterisation of the models describing the human-environment interaction.

7.2 FUTURE WORK

Several lines of research have been identified in this thesis, which can guide future studies.

- By extending the design variables, more features of the motion could be determined through the optimisation problem. For instance, coefficients that relate the timeline in the predicted motion to the timeline in the reference motion could be employed, in order to allow the DHM to perform the predicted motion faster or slower. The external contact forces could also be included in the design variables, in order to determine the efforts exerted by the DHM on the environment through the minimisation of the objective function.

- More accurate RoMs and joint torque limits could be included in the method, taking into account their dependency on the values of the DoFs in the DHM across the motion. Employing more accurate joint limits would allow to generate more realistic predictions when the task to be performed involves DoF values and joint torques which are close to their limits.

- The contact models representing the human-environment interaction could be improved, yielding a more thorough characterisation of the kinetics involved in the motion. For instance, regarding the pelvis-seat interaction, the complexity in the mechanical behaviour of the seat and the human pelvis can be taken into account employing non-linear stiffness and damping coefficients. Additionally, the shape of the seat and human body can be represented more accurately with more complex geometries, thus allowing to determine the load distribution on the DHM due to its contact with the environment.

- It would be interesting to predict longer and more complex motions, involving the whole body. For this purpose the prediction of the motion could be performed one time period at a time, imposing continuity conditions at key-frames. More optimisation problems would be solved, but each would present a smaller number of design variables (i.e. only the control points which affect each specific time period at a time).

- The method could be extended to musculoskeletal DHMs, to analyse the distribution of the muscular efforts in the human body, which are related both to discomfort and injuries. Including muscles in the human model implies that two different redundancies are to be dealt with: in addition to the kinematic redundancy of the skeletal system, a dynamic redundancy is introduced, as the motion of each joint is determined by the interaction of several muscles, which may be activated differently to produce the same motion. Therefore, the optimisation problem presented in this thesis should be reformulated, in order to take into account the dynamic redundancy of the muscular system as well.

- The method could be employed in the ergonomic assessment of new product designs not only in terms of usability, but also in terms of maintenance and manufacturing. Including DHMs in the design process would allow to take human factors into account since the earliest stages of the design of large and complex structures, which require a human operator for assembly/disassembly operations. Therefore, the cost and time of such operations may be reduced while increasing the safety of the manufacturing and maintenance of vehicles, aircraft and large machinery.

APPENDIX A

PUBLICATIONS

The publications generated so far as a result of the research work carried out in this thesis are listed below:

Pasciuto, I., Ausejo, S., Celigüeta, J.T., Suescun, A., Cazón, A., (in press). A comparison between optimisation-based human motion prediction methods: data-based, knowledge-based and hybrid approaches. *Structural and Multidisciplinary Optimization*.

Pasciuto, I., Ausejo, S., Celigüeta, J.T., Suescun, A., Cazón, A., (under review). A hybrid dynamic motion prediction method for multibody digital human models based on a motion database and motion knowledge. *Multibody Systems Dynamics*.

Pasciuto, I., Valero, A., Ausejo, S., Celigüeta, J.T., 2011. A hybrid dynamic motion prediction method with collision detection. *In proceedings of the First Symposium on Digital Human Modeling*. June 14-16, Lyon, France. (Awarded as "Best Oral Presentation").

Pasciuto, I., Valero, A., Ausejo, S., Celigüeta, J.T., 2010. A dynamic motion prediction method based on a motion database and motion knowledge. *In proceedings of the 1st International Conference on Applied Bionics and Biomechanics*. October 14-16, Venice, Italy.

Pasciuto, I., Valero, A., Ausejo, S., Celigüeta, J.T., 2010. Comparación de leyes de control para la predicción dinámica del movimiento humano usando bases de datos. *In proceedings of the XVIII Spanish National Congress on Mechanical Engineering*. November 3-5, Ciudad Real, Spain.

Ausejo, S., Valero, A., Pasciuto, I., Celigüeta, J.T., Suescun, A., Cazón, A., 2011. Reconstrucción y predicción del movimiento humano. *In proceedings of the I Meeting of the Spanish Chapter of the European Society of Biomechanics (ESB)*. November 10, Zaragoza, Spain.

Valero, A., Pasciuto, I., Ausejo, S., Celigüeta, J.T., 2010. Comparación de dos métodos globales de reconstrucción del movimiento basados en coordenadas naturales y relativas. *In proceedings of the XVIII Spanish National Congress on Mechanical Engineering*. November 3-5, Ciudad Real, Spain.

REFERENCES

Abdel-Malek, K., Arora, J., 2009. Physics-based digital human modeling: predictive dynamics. In: Duffy,V.G. (Eds.), Handbook of Digital Human Modeling. CRC Press- Taylor & Francis Group, Boca Raton, Florida, USA, pp. 5.1-5.33.

Abdel-Malek, K., Mi, Z., Yang, J., Nebel, K., 2006. Optimization-based trajectory planning of the human upper body. Robotica 24 (6), 683-696.

Abe, Y., Liu, C.K., Popovic, Z., 2006. Momentum-based parameterization of dynamic character motion. In Proceedings of the Eurographics/ACM SIGGRAPH Symposium on Computer Animation. Los Angeles, California, USA.

Ait El Menceur, M.O., Pudlo, P., Gorce, P., Lepoutre, F.X., 2009. An automatic procedure for identifying alternative automobile ingress movements in young and elderly populations with or without prostheses. International Journal of Industrial Ergonomics 39 (6), 966-980.

Ait El Menceur, M.O., Pudlo, P., Gorce, P., Thévenon, A., Lepoutre, F., 2008. Alternative movement identification in the automobile ingress and egress for young and elderly population with or without prostheses. International Journal of Industrial Ergonomics 38 (11-12), 1078-1087.

Anderson, D.E., Madigan, M.L., Nussbaum, M.A., 2007. Maximum voluntary joint torque as a function of joint angle and angular velocity: model development and application to the lower limb. Journal of Biomechanics 40 (14), 3105-3113.

Anderson, F.C., Pandy, M.G., 2001. Dynamic optimization of human walking. Journal of Biomechanical Engineering 123, 381.

Arora, J., 2004. Introduction to Optimum Design. Elsevier Academic Press.

Ausejo, S., 2006. A new robust motion reconstruction method based on optimisation with redundant constraints and natural coordinates. PhD thesis, University of Navarra, San Sebastian.

Ausejo, S., Suescun, A., Celigüeta, J.T., 2011. An optimization method for overdetermined kinematic problems formulated with natural coordinates. Multibody System Dynamics 26, 397-410.

Ausejo, S., Wang, X., 2009. Motion capture and reconstruction. In: Duffy,V.G. (Eds.), Handbook of Digital Human Modeling. CRC Press-Taylor & Francis Group, Boca Raton, Florida, USA, pp. 38.1-38.13.

Badler, N.I., Phillips, C.B., Webber, B.L., 1993. Simulating Humans: Computer Graphics, Animation and Control. Oxford University Press.

Baerlocher, P., Boulic, R., 2004. An inverse kinematic architecture enforcing an arbitrary number of strict priority levels. The Visual Computer 20 (6), 402-417.

Baerlocher, P., Boulic, R., 2002. Task-priority formulations for the kinematic control of highly redundant articulated structures. In Proceedings of the Intelligent Robots and Systems, 1998. Proceedings., 1998 IEEE/RSJ International Conference on.

Bindiganavale, R., Badler, N.I., 1998. Motion abstraction and mapping with spatial constraints. Motion abstraction and mapping with spatial constraints. Modelling and Motion Capture Techniques for Virtual Environments. Springer, Berlin / Heidelberg, pp. 70-82.

Bubb, H., Fritzsche, F., 2009. A scientific perspective of digital human models: past, present, and future. In: Duffy,V.G. (Eds.), Handbook of Digital Human Modeling. CRC Press-Taylor & Francis Group, Boca Raton, Florida, USA, pp. 3.1-3.30.

Burnett, R., Carter, J., Roberts, V., Myers, B., 2004. The influence of seatback characteristics on cervical injury risk in severe rear impacts. Accident analysis and prevention 36 (4), 591-601.

Buss, S., Kim, J., 2005. Selectively damped least squares for inverse kinematics. Journal of Graphics, GPU, & Game Tools 10 (3), 37-49.

Cappozzo, A., Catani, F., Leardini, A., Benedetti, M.G., Della Croce, U., 1996. Position and orientation in space of bones during movement: experimental artefacts. Clinical Biomechanics 11 (2), 90-100.

Chaffin, D.B., 2007. Human motion simulation for vehicle and workplace design. Human Factors and Ergonomics in Manufacturing & Service Industries 17 (5), 475-484.

Chang, C.C., Brown, D.R., Bloswick, D.S., Hsiang, S.M., 2001. Biomechanical simulation of manual lifting using spacetime optimization. Journal of Biomechanics 34 (4), 527-532.

Chateauroux, E., Monnier, M., Wang, X., Roybin, C., 2011. Strategy analysis of truck cabin egress motion. In Proceedings of the First International Symposium on Digital Human Modeling. June 14-16,2011, Lyon, France.

Chateauroux, E., Wang, X., 2010. Car egress analysis of younger and older drivers for motion simulation. Applied Ergonomics 42 (1), 169-177.

Chung, H., Xiang, Y., Mathai, A., Rahmatalla, S., Kim, J., Marler, T., Beck, S., Yang, J., Arora, J.S., Abdel-Malek, K., 2007. A robust formulation for prediction of human running. In Proceedings of the 2007 Digital Human Modeling for Design and Engineering Symposium. Seattle, Washington, USA.

Craig, J.J., 2005. Introduction to Robotics: Mechanics and Control. Pearson Prentice Hall.

Dingwell, J.B., John, J., Cusumano, J.P., 2010. Do humans optimally exploit redundancy to control step variability in walking? PLoS computational biology 6 (7), 1.

Duffy,V.G., (Eds.), 2009. Handbook of Digital Human Modeling. CRC Press-Taylor & Francis Group.Boca Raton, Florida, USA. ISBN 978-0805856460.

Dumas, R., Cheze, L., Verriest, J., 2007. Adjustments to McConville et al. and Young et al. body segment inertial parameters. Journal of Biomechanics 40 (3), 543-553.

Engstler, F., Guenzkofer, F., Bubb, H., Bengler, K., 2011. Lower limb joint range of motion considering inter-joint dependencies. In Proceedings of the First International Symposium on Digital Human Modeling. June 14-16,2011, Lyon, France.

Eriksson, A., 2008. Optimization in target movement simulations. Computer Methods in Applied Mechanics and Engineering 197 (49), 4207-4215.

Eriksson, A., Nordmark, A., 2011. Activation dynamics in the optimization of targeted movements. Computers & Structures 89 (11), 968-976.

Faraway, J.J., 2003. Data-based motion prediction. SAE transactions 112 (7), 722-732.

Faraway, J.J., 1997. Regression analysis for a functional response. Technometrics, 254-261.

Faraway, J.J., Reed, M.P., Wang, J., 2007. Modelling three-dimensional trajectories by using Bézier curves with application to hand motion. Journal of the Royal Statistical Society: Series C (Applied Statistics) 56 (5), 571-585.

Faraway, J.J., Zhang, X., Chaffin, D.B., 1999. Rectifying postures reconstructed from joint angles to meet constraints. Journal of Biomechanics 32.

Gleicher, M., 2001. Comparing constraint-based motion editing methods. Graphical Models 63, 107-134.

Guenzkofer, F., Engstler, F., Bubb, H., Bengler, K., 2011. Joint torque modeling of knee extension and flexion. In Proceedings of the Third International Conference, ICDHM 2011, Held as a Part of HCI International 2011. July 2011, Orlando, USA.

Hogan, N., Flash, T., 1987. Moving gracefully: quantitative theories of motor coordination. Trends in neurosciences 10 (4), 170-174.

Jung, E.S., Choe, J., 1996. Human reach posture prediction based on psychophysical discomfort. International Journal of Industrial Ergonomics 18 (2), 173-179.

Kapandji, I.A., 1987. The Physiology of the Joints, Vol. 2. Churchill Livingstone.

Kaplan, M.L., Heegaard, J.H., 2001. Predictive algorithms for neuromuscular control of human locomotion. Journal of Biomechanics 34, 1077–1083.

Kim, J.H., Abdel-Malek, K., Yang, J., Marler, R.T., 2006. Prediction and analysis of human motion dynamics performing various tasks. International Journal of Human Factors Modelling and Simulation 1 (1), 69-94.

Kim, J.H., Abdel-Malek, K., Yang, J., Nebel, K., 2007. Dual-arm dynamic motion simulation and prediction of joint constraint loads using optimization.

Lee, J., Shin, S.Y., 1999. A hierarchical approach to interactive motion editing for human-like figures. In Proceedings of the Proceedings of the 26th Annual Conference on Computer Graphics and Interactive Techniques.

Lim, B., Ra, S., Park, F.C., 2005. Movement primitives, principal component analysis, and the efficient generation of natural motions. In Proceedings of the Proceedings of IEEE International Conference on Robotics and Automation.

Liu, C.K., Popovic, Z., 2002. Synthesis of complex dynamic character motion from simple animations. In Proceedings of the ACM Transactions on Graphics (TOG).

Lu, T.W., O'Connor, J.J., 1999. Bone position estimation from skin marker co-ordinates using global optimisation with joint constraints. Journal of Biomechanics 32, 129-134.

Marler, T.R., Arora, J.S., 2005. Function-transformation methods for multi-objective optimization. Engineering Optimization 37 (6), 551-570.

Marler, T.R., Arora, J.S., 2004. Survey of multi-objective optimization methods for engineering. Structural and multidisciplinary optimization 26 (6), 369-395.

Marler, T., Rahmatalla, S., Shanahan, M., Abdel-Malek, K., 2005. A new discomfort function for optimization-based posture prediction. SAE Technical Paper 2005-01-2680.

Mavrikios, D., Karabatsou, V., Alexopoulos, K., Pappas, M., Gogos, P., Chryssolouris, G., 2006. An approach to human motion analysis and modelling. International Journal of Industrial Ergonomics 36 (11), 979-989.

Monnier, G., 2004. Simulation de mouvements humains complexes et prédiction de l'inconfort associé. Institut national des sciences appliquées de Lyon, Ecole Centrale de Lyon.

Monnier, G., Renard, F., Chameroy, A., Wang, X., Trasbot, J., 2006. A motion simulation approach integrated into a design engineering process. In Proceedings of the SAE International Conference and Exposition of Digital Human Modelling for Design and Engineering. July 4-6, Lyon, France.

Monnier, G., Wang, X., Verriest, J.P., Goujon, S., 2003. Simulation of complex and specific task-orientated movements - application to the automotive seat belt reaching. In Proceedings of the SAE International Conference and Exposition of

Digital Human Modeling for Design and Engineering. 17-19 June, Montreal, Canada.

Multon, F., France, L., Cani-Gascuel, M., Debunne, G., 1999. Computer animation of human walking: a survey. The journal of visualization and computer animation 10 (1), 39-54.

Narayan, L., 2008. Computer Aided Design and Manufacturing. PHI Learning Pvt. Ltd.

Pan, J., Zhang, L., Lin, M.C., Manocha, D., 2010. A hybrid approach for simulating human motion in constrained environments. Computer Animation and Virtual Worlds 21 (3-4), 137-149.

Pannetier, R., Wang, X., 2012. Development of objective discomfort evaluation indicators for a task-oriented motion using less constrained motion concept: application to automotive pedal clutching task. Work: A Journal of Prevention, Assessment and Rehabilitation 41, 1461-1465.

Park, F.C., Jo, K., 2004. Movement primitives and principal component analysis. Advances in Robot Kinematics, J.Lenarcic and C.Galletti, Eds., Kluwer.

Park, W., Chaffin, D.B., Martin, B.J., 2004. Toward memory-based human motion simulation: development and validation of a motion modification algorithm. IEEE Transaction on System, Man and Cybernetics – Part A: Systems and Humans 34 (3), 376-386.

Park, W., Chaffin, D.B., Martin, B.J., Faraway, J.J., 2005a. A computer algorithm for representing spatial–temporal structure of human motion and a motion generalization method. Journal of Biomechanics 38 (11), 2321-2329.

Park, W., Chaffin, D.B., Martin, B.J., Yoon, J., 2008a. Memory-based human motion simulation for computer-aided ergonomic design. Systems, Man and Cybernetics, Part A: Systems and Humans, IEEE Transactions on 38 (3), 513-527.

Park, W., Martin, B.J., Choe, S., Chaffin, D.B., Reed, M.P., 2005b. Representing and identifying alternative movement techniques for goal-directed manual tasks. Journal of Biomechanics 38 (3), 519-527.

Park, W., Singh, D.P., Huston, R.L., Song, S., 2008b. A quantitative method for representing balance strategies of goal-directed human motions. Computers in biology and medicine 38 (10), 1094-1102.

Park, W., Singh, D.P., Martin, B.J., 2006. A memory-based model for planning target reach postures in the presence of obstructions. Ergonomics 49 (15), 1565-1580.

Piegl, L.A., Tiller, W., 1997. The NURBS Book. Springer Verlag.

Popovic, Z., Witkin, A., 1999. Physically based motion transformation. In Proceedings of the ACM SIGGRAPH 99, Computer Graphics Proceedings.

Prieto Valiente, L., Herrantz Tejedor, I., 2005. ¿Qué Significa Estadísticamente Significativo? Ediciones Diaz de Santos, Spain.

Reed, M.P., Manary, M.A., Flannagan, C.A.C., Schneider, L.W., 2000. Comparison of methods for predicting automobile driver posture. SAE transactions 109 (6), 2279-2290.

Reid, S.R., Graham, R.B., Costigan, P.A., 2010. Differentiation of young and older adult stair climbing gait using principal component analysis. Gait & posture 31 (2), 197-203.

Ren, L., Jones, R.K., Howard, D., 2007. Predictive modelling of human walking over a complete gait cycle. Journal of Biomechanics 40 (7), 1567-1574.

Riemer, R., Hsiao-Wecksler, E.T., 2008. Improving joint torque calculations: Optimization-based inverse dynamics to reduce the effect of motion errors. Journal of Biomechanics 41 (7), 1503-1509.

Robert, T., Chèze, L., Dumas, R., Verriest, J.P., 2006. Joint forces and moments calculation for a 3D whole body model during complex movement.

Safonova, A., Hodgins, J.K., Pollard, N.S., 2004. Synthesizing physically realistic human motion in low-dimensional, behavior-specific spaces. In Proceedings of the ACM Transactions on Graphics.

Seitz, T., Recluta, D., Zimmermann, A., Wirsching, H.J., 2005. FOCOPP- An approach for a human posture prediction model using internal/external forces and discomfort. In Proceedings of the Proceedings of Digital Human Modeling for Design and Engineering Symposium. June 14-16, Iowa City, IA, USA.

Shapiro, A., Kallmann, M., Faloutsos, P., 2007. Interactive motion correction and object manipulation. In Proceedings of the Symposium on Interactive 3D Graphics and Games.

Sok, K.W., Yamane, K., Lee, J., Hodgins, J., 2010. Editing dynamic human motions via momentum and force. In Proceedings of the Proceedings of the 2010 ACM SIGGRAPH/Eurographics Symposium on Computer Animation. Madrid, Spain.

Tak, S., Ko, H., 2005. A phisically-based motion retargeting filter. In Proceedings of the ACM Transactions on Graphics.

Todorov, E., 2004. Optimality principles in sensorimotor control. Nature neuroscience 7 (9), 907-915.

Unuma, M., Anjyo, K., Takeuchi, R., 1995. Fourier principles for emotion-based human figure animation. In Proceedings of the Proceedings of the 22nd Annual Conference on Computer Graphics and Interactive Techniques.

Wang, X., Pannetier, R., Burra, N.K., Numa, J., 2011. A biomechanical approach for evaluating motion related discomfort: illustration by an application to pedal clutching movement. A biomechanical approach for evaluating motion related discomfort: illustration by an application to pedal clutching movement. Digital Human Modeling. Springer, pp. 210-219.

Wang, X., 2002. Prediction of lower-limb movements of clutch pedal operation from an existing motion database. In Proceedings of the Proceedings of the 5th SAE Digital Human Modelling Conference. Munich, Germany.

Wang, X., Verriest, J.P., Lebreton-Gadegbeku, B., Tessier, Y., Trasbot, J., 2000. Experimental investigation and biomechanical analysis of lower limb movements for clutch pedal operation. Ergonomics 43 (9), 1405-1429.

Wirsching, H.J., Tomp, C., Wiedemann, J., 2011. A new practical approach for measuring and simulating human-seat interactions. In Proceedings of the First International Symposium on Digital Human Modeling. June 14-16,2011, Lyon, France.

Witkin, A., Kass, M., 1988. Spacetime constraints. In Proceedings of the SIGGRAPH 88 Conference Proceedings. August 1988, .

Witkin, A., Popovic, Z., 1995. Motion warping. In Proceedings of the SIGGRAPH 95 Conference Proceedings. August 2008, .

Xiang, Y., Arora, J.S., Abdel-Malek, K., 2012. Hybrid predictive dynamics: a new approach to simulate human motion. Multibody System Dynamics 28 (3), 199-224.

Xiang, Y., Arora, J.S., Abdel-Malek, K., 2011. Optimization-based prediction of asymmetric human gait. Journal of Biomechanics 44 (4), 683-693.

Xiang, Y., Arora, J.S., Abdel-Malek, K., 2010a. Physics-based modeling and simulation of human walking: a review of optimization-based and other approaches. Structural and Multidisciplinary Optimization 42 (1), 1-23.

Xiang, Y., Arora, J.S., Rahmatalla, S., Abdel-Malek, K., 2009. Optimization-based dynamic human walking prediction: One step formulation. International Journal for Numerical Methods in Engineering 79 (6), 667-695.

Xiang, Y., Arora, J.S., Rahmatalla, S., Marler, T., Bhatt, R., Abdel-Malek, K., 2010b. Human lifting simulation using a multi-objective optimization approach. Multibody System Dynamics 23 (4), 431-451.

Xiang, Y., Chung, H., Mathai, A., Rahmatalla, S., Kim, J., Marler, T., Beck, S., Yang, J., Arora, J.S., Abdel-Malek, K., 2007. Optimization-based dynamic human walking prediction. Optimization 1, 2489.

Xiang, Y., Chung, H., Kim, J.H., Bhatt, R., Rahmatalla, S., Yang, J., Marler, T.R., Arora, J.S., Abdel-Malek, K., 2010c. Predictive dynamics: an optimization-based novel approach for human motion simulation. Structural and Multidisciplinary Optimization 41 (3), 465-479.

Yamane, K., Kuffner, J.J., Hodgins, J.K., 2004. Synthesizing animations of human manipulation tasks. In Proceedings of the ACM Transactions on Graphics.

Yang, J., Marler, R.T., Kim, H.J., Arora, J.S., Abdel-Malek, K., 2004. Multi-objective optimization for upper body posture prediction. In Proceedings of the 10th AIAA/ISSMO Multidisciplinary Analysis and Optimization Conference. Alvany, New York, EEUU.

Yang, J., Rahmatalla, S., Marler, T.R., Abdel-Malek, K., Harrison, C., 2007. Validation of predicted posture for the virtual human Santos TM. Digital Human Modeling, 500-510.

Zatsiorsky, V.M., 2002. Kinetics of Human Motion. Human Kinetics Publishers, ISBN 0-7360-3778-0.

Zhang, X., 2002. Deformation of angle profiles in forward kinematics for nullifying end-point offset while preserving movement properties. Journal of Biomechanical Engineering 124, 490-495.

Zhang, X., Chaffin, D.B., 2000. A three-dimensional dynamic posture prediction model for simulating in-vehicle seated reaching movements: development and validation. Ergonomics 43 (9), 1314-1330.

Zhao, J., Badler, N.I., 1994. Inverse kinematics positioning using nonlinear programming for highly articulated figures. ACM Transactions on Graphics 13 (4), 313-336.